Decoupling processes in block-and-ash flows: field evidence and analogue modelling.

A thesis submitted in partial fulfilment

of the requirements for the degree of

Doctor of Philosophy in

Hazard and Disaster Management

Elke Hanenkamp

University of Canterbury

New Zealand

May 2011

Abstract

Pyroclastic density currents are among the most dangerous hazards during explosive volcanic eruptions, typically having catastrophic and lasting impacts on society, infrastructure, and landscape evolution of the area. After the eruption of Unzen volcano, Japan, in 1991, during which 43 people were killed when pyroclastic surges unexpectedly separated from the parental flows, the possibility of decoupling in block-and-ash flows and the potential hazard of this was recognized. In the following years, decoupling has been documented at several composite volcanoes, but still not enough is known about the mechanics of pyroclastic currents, which allow the detachment of ash cloud surges. In this thesis, several processes thought to initiate decoupling in pyroclastic currents, such as entrainment of substrate at the flow base or of air at the flow front, elutriation of fines into the upper ash cloud surge or simple gravity segregation, are investigated. These mechanisms lead to increased non-uniformity and stratification, which is a prerequisite for the onset of decoupling in small-volume block-and-ash flows. Other mechanisms such as topographic control over block-and-ash flow dynamics are also considered, with examples confirming the importance of topographic influence for flow stratification and decoupling in block-and-ash flows. Detailed field studies at Tarawera Volcano, New Zealand, have provided comprehensive descriptions of the distribution and sedimentology of block-and-ash flow deposits emplaced during the Kaharoa eruptive episode in AD 1314 ± 12, and these confirm the importance of changes in topography on flow dynamics. Topographic variations causes channeling, blocking and deceleration of the basal flow parts at Tarawera Volcano, while the upper flow parts are unconfined and decoupled, leading to detached ash cloud surge deposits beyond the limits of the main block-and-ash flow deposits. Interaction of the advancing flow with the substrate resulted in dynamic interaction. Deformation features and erosion gullies confirm the highly erosive nature of the flows. Laboratory-scaled simulations of aqueous glycerol solutions and glass particulate currents are used as quantitative semi-guides for pyroclastic flow behaviour, with special regard to decoupling caused by irregular topographies.

Acknowledgements

This thesis would not have been realized without the help of many hands. First, I would like to thank my principal supervisor Tim Davies for the encouragement and advice I received during the course of this project – without his support it would have not been possible to pursue my studies in New Zealand. Vielen Dank, Tim!

My co-supervisor Jim Cole was always there with a helping hand and time to listen to my ideas and my problems. Thank you very much for your advice, support and your help to keep this project on time.

Thank you to the incredible technical team: Rob Spiers (who is bursting with inspired ideas), Chris Grimshaw, Matt Cockcroft, Vanessa Tappenden, Cathy Higgins, and Kerry Swanson. Without their help and interesting ideas, it would have been hard to realize my analogue experiments.

I am grateful to colleagues around the globe who have shared their knowledge and ideas: Ian Nairn, Steve Self, Shinji Takarada, Geraint Owen, Michael Sheridan, Sylvain Charbonnier, Shane Cronin, Ceinwen Scutter, Gert Lube and Colin Wilson. And many thanks to volcanologists in the Department of Geological Sciences at the University of Canterbury, Darren Graveley and Ben Kennedy, their discussion helped a lot in pushing my project along.

I would like to send my thanks to my parents in Germany, without their understanding and support, I wouldn't have come to New Zealand to pursue my Doctorate.

And many many thanks to my friends and colleagues in the department, who have made my time here so enjoyable. Thank you for lettimg me part of a big and cheerful family.

Permission to access the forests surrounding Tarawera Volcano was granted from Hancock Forest Management, Kaingaroa Timberland Management Limited and the Maori Investment House Kawerau which allowed fieldwork around Tarawera Volcano. Thank you for your help and interest in my studies.

This project was funded by a three-year International Doctoral Scholarship from the University of Canterbury and additional support from the Department of Geological Sciences to allow a three-month extension of my studies. Field work was supported by the University of Canterbury, Department of Geological Sciences Mason Trust.

Table of contents

LIST OF FIGURES

LIST OF TABLES

Introduction

Objectives and Motivation – Thesis outline – Terminology

Decoupling processes in block-and-ash flows

Introduction and Thesis Outline

Objectives and motivation

Pyroclastic density currents are among the most dangerous hazards around volcanoes; the loss of life and the devastation of infrastructure have been widely documented (e.g. Ui et al., 1999; Loughlin et al., 2002; Charbonnier and Gertisser, 2008). As volcanoes are part of the natural environment, interactions between humans and volcanoes are inevitable; during the last 200 years more than 200,000 deaths have been recorded related to volcanic eruptions (Tanguy et al., 1998). Furthermore, communities around volcanoes are getting bigger, increasing their vulnerability to the dangers accompanying explosive eruptions (Tilling, 2005). Chances of survival are rare when facing pyroclastic density currents characterized by extreme temperatures (up to 900°C) and high velocities (< 300km/h).

During the last few decades, studies of pyroclastic density currents and their deposits have revealed insight into flow rheologies and deposit architecture (e.g. Druitt, 1998; Freundt and Bursik, 2001, Branney and Kokelaar, 2002, and references therein), leading to recognition of previously unidentified flow behaviour, such as the development and detachment of surges from pyroclastic currents. Decoupled surges travel independently, typically unconfined by topography, hence posing a greater threat to surrounding communities than anticipated (e.g. Ui et al., 1999; Bourdier and Abdurachman, 2001).

Few studies exist to date that specifically explore decoupling behaviour in block-and-ash flows. After the eruption of Unzen Volcano, Japan (1990-1995), where decoupling in block-and-ash flows led to the death of 43 people, Fisher (1995) published a hazard assessment of this phenomenon, providing a short overview of possible factors initiating the separation of surges from the rest of the flow. Fisher

(1995) acknowledged the influence of rough topography for the initiation of decoupling processes in pyroclastic currents, but emphasized the need for a quantification of the relation of topographic features and dispersal patterns of pyroclastic flows and surges.

In this study, decoupling processes are reviewed for selected case studies with regard to topographic influence, and possible interaction mechanisms between pyroclastic currents and the landscape are presented. The results are supplemented by findings of detailed field studies in New Zealand and analogue modelling of decoupling behaviour in (particulate) density currents. What determines whether or not block-and-ash flows interact with pre-existing topography and how the various types of interaction influence decoupling is a vital question for understanding block-and-ash flow dynamics and for hazard zone delineation.

Thesis Outline

Since the first acknowledged documentation of an explosive eruption by Pliny the Younger (www.eyewitnesstohistory.com) and the description of pyroclastic density currents at Mont Pelée in 1902 (Lacroix, 1904), studies of historical deposits and actual eruptions over the last three centuries have contributed to our knowledge of the dynamics of pyroclastic currents and their hazard potential. However, despite extensive documentation of past events, our understanding of the mechanics of pyroclastic density currents has been limited by confusing terminologies and classifications as well as ambiguous interpretations.

A detailed overview of pyroclastic current classifications is presented in **Chapter 1**, to illustrate the terminology and classification problems identified in the previous paragraph. Comparison of several classifications and extraction of key descriptions led to a refined classification that has been chosen to distinguish individual pyroclastic flows and surges and their deposits at Tarawera Volcano, New Zealand, especially with regard to classification of block-and-ash flows, also known as nuées ardentes.

A striking feature of block-and-ash flows is an often unexpectedly large and destructive ash-cloud surge, generated from the advancing flow, which can travel at high velocities and devastate everything in its path. The detachment of ash cloud surges from block-and-ash flows has been acknowledged for several eruptive events worldwide, e.g. Unzen Volcano (Japan), Merapi Volcano (Indonesia) and Soufriére Hills Volcano (Montserrat), but still not enough is known about the separation of the individual flow parts, especially with regard to influential factors, such as turbulence, gravity segregation or topography. **Chapter 2** compiles an overview of processes that can directly or indirectly initiate decoupling in pyroclastic density currents. Several examples of decoupling are presented and compared to topographic influence for the onset of decoupling.

Detailed field studies at Tarawera Volcano in New Zealand led to a detailed description of the block-and-ash flow deposits generated from the collapse of at least two of the lava domes during the Kaharoa eruptive episode in AD 1314±12, and these descriptions are presented in **Chapter 3**. Parts of Ruawahia and Wahanga Domes collapsed in the later stages of the eruptive episode, depositing two large block-and-ash flow fans, one to the northeast and another to the south of the volcano. Samples were taken from proximal to distal regions of these fans; granulometry and mapping allowed the determination of transport and depositional behaviour of the block-and-ash flows to the south and northeast of the volcano.

The discovery of sediment deformation structures in block-and-ash flows at Tarawera Volcano, confirm the dynamic interaction of the advancing block-and-ash flows with the underlying substrate, and allow discussion about their generation, which is presented in **Chapter 4**. In addition, theories for the emplacement of the block-and-ash flows and associated ash cloud surges are proposed and discussed with implications for possible decoupling in the southern block-and-ash flows at Tarawera Volcano.

The focus of this thesis is to enhance our understanding of how transport properties and flow behaviour of pyroclastic density currents are affected by the interaction with pre-existing topography, specifically with regard to decoupling processes.

Unfortunately, very few direct observations exist of pyroclastic current interactions with suberial valleys and canyons or barriers, because of the highly dangerous nature of these currents. High velocities and extreme temperatures in combination with impressive billowing ash clouds make measurements difficult to obtain. To overcome this problem, reduced-scale laboratory experiments were used to study the interaction of (particulate) density currents with obstacles in the flow path. **Chapter 5** summarizes the results of two different sets of analogue experiments encompassing solute and particulate density currents.

A summary of findings and conclusions on the influence of topography for the onset of decoupling are presented in **Chapter 6,** and possible decoupling scenarios at Tarawera Volcano further investigated. Recommendations for future research regarding decoupling processes in block-and-ash flows are presented as well.

Terminology

Researchers in pyroclastic density current research come from a range of different disciplines and backgrounds such as volcanology, engineering, mathematics, fluid mechanics and general geology. Consequently, there is a wide range of terms used, further complicated by variation in the way the terms are defined and interpreted. To avoid confusion, a brief comment on the main terms and their definitions, as used throughout this thesis, is set out below.

An **ash cloud surge** is typically associated with block-and-ash flows. It is thought to be generated by fragmentation and comminution of hot pyroclasts which are elutriated from the basal avalanche to form an energetic, highly turbulent surge.

Block-and-ash flows comprise three different flow parts, (1) a ground-hugging, high-concentration **basal avalanche**, (2) a highly turbulent **ash cloud surge**, and (3) a billowing **ash plume** at the top.

The term **block-and-ash flow** describes a small-volume pyroclastic density current generated by either the gravitational or explosive collapse of either a lava dome or the front of a lava flow.

Decoupling describes the detachment of one or more ash cloud surges from a moving block-and-ash flow. The detached surge will travel topographically unconfined and often in unexpected directions.

Entrainment refers to the incorporation of substrate material into the moving pyroclastic density current. The entrained material may remain a distinctly recognizable unit, be sheared, or be crushed and mixed into the avalanche matrix or base.

"**Liquefaction**" is a state when a sediment effectively behaves as a fluid as a result of strength-loss due to the load being entirely sustained by the pore-fluid and cohesion becoming negligible (after Maltman and Bolton, 2003).

"Mobility" is the ability to move or to be moved; capacity for movement or change of place.

Nuée ardente is a term for block-and-ash flows which was coined in the late 17th century, but became more popular after the eruption of Mont Pelee in 1902 and the description by Lacroix (1904). The term "**glowing avalanche**" has been used in the same context.

Overspilling refers to the process by which parts of propagating pyroclastic density currents will not be confined to valleys or channels. It occurs mostly at abrupt channel bends due to coriolis force acting upon the currents. Typically, parts of the basal avalanche and most of the associated ash cloud surge will leave the channel confinement and spread over the surrounding landscape.

Pyroclastic density current is an "umbrella" term comprising all pyroclastic current phenomena described to date, e.g. such as pyroclastic flow, pyroclastic surge, ignimbrites, block-and-ash flows etc.

Surge-derived pyroclastic flows have been described as being rapidly sedimented from decoupled ash cloud surges, hence prolonging the run-out of the detached surge and possibly also the associated devastation.

Chapter 1

Classifications of pyroclastic density currents: 1930 - 2010

"If we knew what we were doing it wouldn't be research."

Albert Einstein

Chapter 1: Classification of pyroclastic density currents

Explosive volcanic eruptions are among the most spectacular displays of nature. They produce large amounts of pyroclastic material that is carried up in convecting columns or transported laterally in energetic pyroclastic density currents (Sigurdsson et al., 2000).

Pyroclastic density currents are generally defined as “rapidly moving mixtures of hot volcanic particles and gas that are flowing according to their density relative to the surrounding fluid, moving across the ground under the influence of gravity” (Druitt, 1998). Overall, the division of pyroclastic density currents (umbrella term) into pyroclastic flows and surges and their respective deposits (Cas and Wright, 1988) is recognized. Volcanic ash fall and the resulting deposits contribute to the concept of pyroclastic currents, they are either generated directly by the explosive eruption, e.g. falling out from an eruption column or plume, or elutriating from the moving pyroclastic flows.

Pyroclastic flows and surges are caused by to various styles of explosive eruptions, such as Plinian, Vulcanian and Pelean eruptions (Figure 1.1). **Plinian eruptions**, named for Pliny the Younger, who described the cataclysmic eruption of Mt. Vesuvius (Italy) in AD 79, are characterized by enormous explosions, generating ash columns and violent pyroclastic density currents from the collapse of the eruption column (Cas and Wright, 1988).

Vulcanian eruptions, named for Vulcano Island north of Sicily, are characterized by discrete, cannon-like explosions and the generation of series of small eruption columns with plumes that are strung downwind from the volcano (Cas and Wright, 1988). Large amounts of ejecta (andesite and rhyolite magma) can fall back around the vent, generating small-volume pyroclastic density currents.

Peléan eruptions eject large amount of gas, dust, ash, and lava fragments from a central crater. Hazardous pyroclastic density currents are generated by the fallback of

the material from a collapsing eruption column or by the collapse of a lava dome, which is generally extruded near the end of the main eruption.

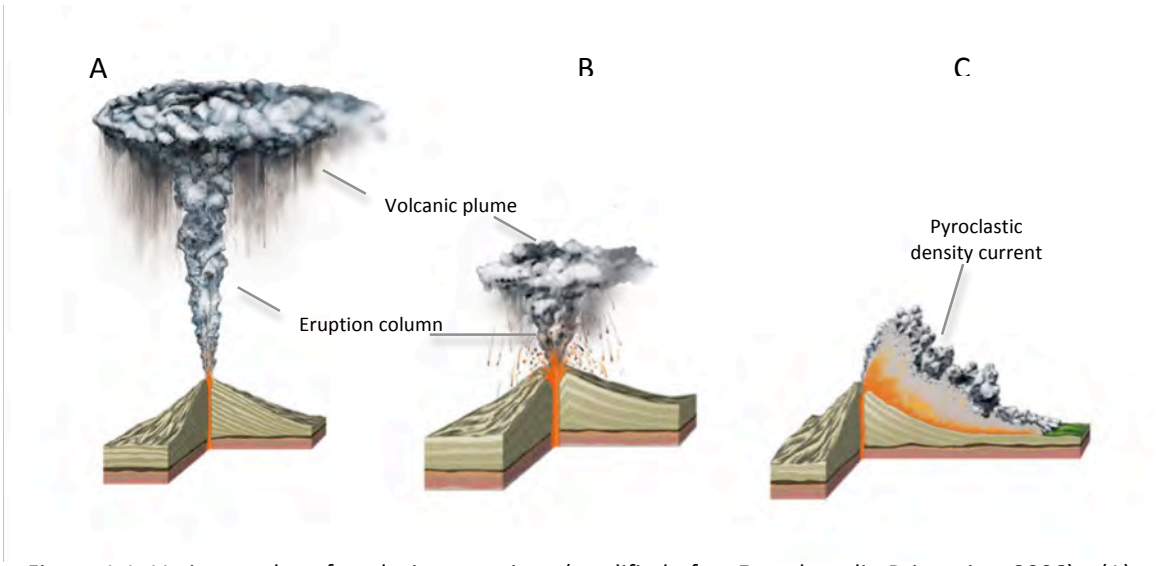

Figure 1.1: Various styles of explosive eruptions (modified after Encyclopedia Britannica, 2006) - (A) high explosive Plinian eruption, (B) Vulcanian eruption and (C) Peléan eruption style. Each of these styles is characterized by the generation of violent pyroclastic density currents. For further explanations see text (p.9).

The highly unpredictable nature of pyroclastic density currents generated by the different eruption styles creates a considerable challenge to volcanologists. Extreme temperatures (up to 800° C) and high velocities (~ 60-100 ms^{-1}) of the pyroclastic density currents pose extreme threats to the communities surrounding volcanoes, resulting too often in the loss of lives (e.g. ≈ 28 000 victims at Mt.Pelée in 1902, ≈ 3000 victims at Mount Lamington in 1951; Tanguy et al., 1998).

The first eyewitness descriptions of pyroclastic flows during the AD 79 eruption of Mount Vesuvius, given by Pliny the younger during the actual eruptive event, provided us with a first insight into these phenomena (Cioni et al., 2000).

In his second letter, Pliny the younger described a “dreadful black cloud…torn by gushing flames and great tongues of fire” (www.eyewitnesstohistory.com). Later while trying to escape, Pliny saw “a thick black cloud advancing over land behind us like a flood”. These descriptions gave possibly the earliest impression of pyroclastic density currents descending from Mount Vesuvius. Other authors such as Frank Perret, Tempest Anderson and John S. Flett gave rather graphic descriptions of the

nuée ardente phenomenon as well, comparing the billowing clouds with "charging horses or lions" (Perret, 1937).

Although the term "pyroclastic density currents" is nowadays widely recognized by volcanologists, another more old-fashioned expression can be traced through the volcanological literature until today - "nuée ardente" has been used in a broad sense to include all kinds of pyroclastic flows (e.g. Smith, 1960), for merely the pyroclastic surge (e.g. Van Bemmelen, 1949), or also for a combination of both (e.g. Abdurachman et al., 2000). Nowadays the term is applied in a more restricted sense to refer specifically to small-volume monolithologic block-and-ash flows generated by the collapse of actively growing lava domes or lava flows on steep terrains.

1.1.The origin of the concept "nuée ardente"

Most scientists credited the introduction of the term "nuée ardente" into the volcanological literature to the French volcanologist Alfred Lacroix (1863-1948, Figure 1.2) after the eruption of Mt. Pelée in 1902. Nuées ardentes swept over the town of St.Pierre, Martinique, enveloping people in gas-rich, billowing clouds of extremely hot pyroclastic fragments.

However, forty years earlier Ferdinand Fouqué (1828-1904, Figure 1.2), a French geologist with a passion for volcanology, used this expression to describe a similar volcanic occurrence during the fissure-vent eruptions of San Jorge in the Azores Archipelago in 1580 and 1808. During his travels to the Azores in 1867/68, Fouqué (1873) found a transcription of a priest from the nearby village of Santo Amaro by the name of João Inácio da Silveira (1767-1852) who witnessed the eruption in 1808. The Portuguese priest used the phrase "ardente nuvem" for the description of the formation of a "fearful and burning cloud" from "a typhoon of fire […breaking…] out of the volcano" (Hooker, 1965). This first quite accurate description corresponds well with recent observations of advancing block-and-ash flows at e.g. Merapi and Unzen volcanoes (e.g. Miyabuchi, 1999; Ui et al., 1999; Abdurachman et al., 2000).

Lacroix didn't observe either the cataclysmic eruption of Mt. Pelée in May or the eruption in August 1902. He had been sent by the French Academy of Science as a part of a scientific mission to monitor the eruptions in the Lesser Antilles after the events in May. During his early reports to the Academy in July 1902, Lacroix referred to the pyroclastic density currents as "nuages noirs" (black clouds), "nuages denses" (dense clouds) and "nuages obscurs" (dark clouds), descriptions based solely on local eyewitness accounts.

Figure 1.2: The founders of the nuée ardente concept – on the left Alfred Lacroix (1863-1948) and his mentor Ferdinand Fouqué (1828-1904) in the middle. The picture on the right shows Frank Perret, who devoted his life to the observation of nuées ardentes at Mt. Pelée (Sources: http://www.mount-pelee.com, 2001-2009).

After he had observed smaller pyroclastic density currents in December 1902, he described them as "nuages denses" and "nuages lourds" (heavy clouds). Only after the eruptions of Mount Pelée in January 1903, Lacroix starts to use the expression "nuées ardentes" with no further mentioning of "nuages denses" in later reports. The change is quite noticeable, perhaps because of his association with Ferdinand Fouqué. Not only was Fouqué his professor and mentor, but also his father-in-law. Hooker (1965) surmised that intensive discussions between Fouqué and Lacroix might have led to the former recalling the tales from San Jorge and unearthing the article he published in the *Revue Scientifique* in 1873, giving Lacroix the opportunity to change his former descriptive terms to "nuée ardente".

Lacroix tried to explain his change from "nuage dense" to "nuée ardente" in his comprehensive report for the French Academy of Science (Lacroix, 1904). He said that

he convinced himself that the volcanic phenomenon at St.Pierre resembled the description of the eruptions of San Jorge in 1580 and 1808. He acknowledged that nuées ardentes which he thought had never been mentioned before in the scientific literature, were already described by the inhabitants of San Jorge during the eruption in 1808. After his return to France, he thought it was a good idea to revive the phrase "nuée ardente" because it was fairly expressive (Hooker, 1965). His usage of the term "ardent" was meant to indicate that the cloud was burning (brûlant), not glowing as in incandescent.

Whether or not Lacroix was correct in believing that the pyroclastic density currents he observed at Mt. Pelée and the volcanic phenomenon at San Jorge were similar in their appearance, he definitely revived the term "nuée ardente" that had been overlooked for many years. Due to the rarity of these eruptions and the limited travel opportunities in the 19th century, there was probably no chance to follow up on Fouqué's description with accounts of similar events and occurrences, possibly explaining why the phrase "nuée ardente" fell into oblivion for nearly forty years.

But if Lacroix had not interpreted the pyroclastic density currents at Mt. Pelée as being completely different from an "ordinary", effusive volcanic eruption, this phenomenon would have not have received the attention and acceptance which is nowadays still manifested in the retained usage of his expression.

During his observations at Mt. Pelée, Lacroix observed various nuées ardentes from different eruptive processes, naming them as follows:

I. Nuée ardente peléenne d'explosion dirigée
II. Nuée ardente peléenne d'avalanche
III. Nuée ardente vulcanienne
IV. Nuée ardente du Massif du Katmai
V. Avalanche sèche

The first group incorporates all pyroclastic occurrences from the explosive eruption of a lava dome, generating block-and-ash flows and the associated deposits. Examples were reported from Mt. Pelée in 1902/03. Group II comprises nuée ardentes generated by the gravitational collapse of a lava dome or a lava flow front, nowadays

also known as block-and-ash flows. The third group involves pyroclastic currents from the collapse of a vertical eruption column, whereas the fourth includes currents generated from fissure eruptions, which has first been described at Katmai volcano in Alaska. Nuées ardentes emerged simultaneously from numerous fissures opened in a valley, covering the ground to a depth of more than 100 feet, resulting in the Valley of Ten Thousand Smokes (Fenner, 1937). Avalanches sèches (dry avalanches) represent volcanic rock avalanches generated by the collapse of unstable material from the volcano flanks without an explosive component, e.g. observed at Stromboli volcano (Italy) in 1906 (Glangeaud, 1907) and in 1930 (Rittmann, 1944).

1.2. Further nuée ardente descriptions

While Alfred Lacroix has been credited with the first use of the term "nuée ardente", other volcanologists contributed further knowledge at the beginning of the 20th century. In July 1902, two British researchers, Tempest Anderson and John S. Flett, observed the eruption of the Soufrière volcano on the island of St.Vincent, 50 km away from Martinique, only one day before the cataclysmic eruption at Mt. Pelée. They described a "red hot avalanche" arising from a fissure in the flank of the volcano, "pouring over the mountain slopes right down to the sea" (Anderson and Flett, 1903). The surface of the main mass of the avalanche was "billowy like a cascade in a mountain brook", "covered by innumerable minor excrescences, rounded, and filled with terrific energy" (Anderson and Flett, 1903).

More direct observations of nuées ardentes were made by Frank Perret (Figure 1.2), an American electrical engineer, during another eruptive episode of Mt. Pelée in 1929. After building himself a small observatory near the volcano, he spent 3 years studying nuées ardentes. His descriptions of the currents were as graphic as those of Anderson and Flett, including phrases such as the "cloud ceases its upward expansion, spreading out horizontally" while at the same time "developing upwards in cauliflower convolutions of dust and ash". The incandescent material took the form of "forward springing jets, suggesting tossing heads of charging horses or lions…" (Perret, 1937).

1.3. Application of the nuée ardente concept for pyroclastic deposits

Not long after the establishment of this concept, scientists in Great Britain applied Lacroix's idea to Ordovician volcanic rocks in North Wales, proposing a "probable Pelean origin" of the volcanic material (Dakyn and Greenly, 1905).

Lacroix's model was also applied to the massive, pumice-rich deposits that had been deposited during the Late Pleistocene eruption at Laacher See, Germany (Schmincke, 2003). The deposits were termed Brohltaltrass, "trass" being a descriptive term during the 19th and early 20th century for unwelded, pumice-rich and massive flow deposits. Nowadays these kinds of deposits are mostly described as ignimbrites (Fisher and Schmincke, 1984).

The pyroclastic flows from the 1783 Asama eruption in Japan were explained by the nuée ardente concept (Yamasaki, 1911), as were the "sand flows" of Fenner (1923) resulting from the 1912 eruption at the Valley of Ten Thousands Smokes and the pumiceous deposits in the Crater Lake region in Oregon (Moore, 1934).

1.4. Development of the pyroclastic density current concept

1.4.1. Minefield pyroclastic flow terminology

Following the establishment of the nuée ardente concept by Lacroix, various classifications for pyroclastic density currents have been proposed. Numerous volcanologists from different countries tried to adapt or update Lacroix's fundamental classification (e.g. Escher, 1933; Rittmann, 1944; Murai, 1961; Wright et al., 1980). Three main types were classically distinguished and resurfaced in nearly all new categorizations (Table 1.1) – these are the **Peléan/Pelée-type**, describing an explosive eruption immediately before or during the rise of the volcanic dome, the **Merapi-type**, characterized by the gravitational collapse of either a lava dome or the front of a lava flow and the **(Soufrière) St.Vincent-type**, initiated by the fallback of pyroclastic material from the outer parts of a collapsing vertical eruption column.

Revisions and changes of these main types often led to great confusion in the identification and description of the individual pyroclastic density currents and their deposits. Most authors tried to establish new and certainly better classifications; the amount of descriptive terms for pyroclastic density currents is large, but commonly inadequate to classify the certain current types. The list of terms (see section 1.8.) includes e.g. nuée ardente (Lacroix, 1904), (hot) sand flow (Fenner, 1923), pyroclastic avalanche (Nairn and Self, 1978), hot rock avalanche (Mellors et al., 1988) and glowing avalanche or glowing cloud (Macgregor, 1952). The use of the synonyms for pyroclastic density currents is unfortunately not limited to the early days of these classifications, nowadays lots of authors still struggle with the terminology and cannot seem to find common ground.

So far sixteen classifications from different countries and decades have been collected and compared. A detailed description of each individual terminology would lead to successive repetitions of at least of the main three types – the Pelean type, the Merapi and the St.Vincent type. A comprehensive list of the classifications collected is represented in Table 1.1. In the following paragraphs a few selected categorizations will be described in detail to show a progression within the last eight decades, e.g. Macgregor (1955), Williams (1957), Aramaki (1957), Murai (1961), Wright et al. (1980) and Bardintzeff (1985) as well as Branney and Kokelaar (2002).

Many authors tried to establish a suitable and thorough classification. However, early attempts were mostly translations into other languages, e.g. into Dutch by Escher (gloedwolken, 1933) or into German by Rittmann (Glut-und Aschewolken, 1944). Without major changes these authors adopted Lacroix's nomenclature, and more authors followed this approach in later decades (e.g. MacDonald, 1972 or Williams and McBirney, 1979; Table 1.1).

Lacroix 1930	Escher 1933	Neumann van Padang, 1933	Perret 1933	Rittmann 1944	Cotton 1944	Macgregor 1952	Williams 1957	Aramaki 1957	Murai 1961	MacDonald 1971	Williams & McBirney, 1979	Wright 1980	Smith & Robool 1982	Bardintzeff, 1985	Cas and Wright, 1988	Branney and Kokelaar, 2002
nuées ardente Peleenes d'explosion dirigee	Gloedwolken van het Pelee type		block and ash flows	Glutwolken (glowing clouds) - absteigender Pelee type (descendante-descending)	Pelean variant- 2nd order Nuée ardente - horizontal or oblique explosive discharge from dome flank	Pelee discharged lateral type	Peléan type	Nuée ardente	nuée ardente - Pelee type (Merapi type)	Pelean type - low angle explosion	crumbling lava dome - Merapi type	block-and-ash flow: Nuée ardente	Nuée ardente	nuées ardente sensu strictu - Pelee type	dome collapse - discrete explosions interrupted column collapse	fully dilute pyroclastic density currents
				Glutwolken (glowing clouds) - zurueckfallender St.Vincent type (falling-back)		pelee directed lateral type				Merapi type - dome collapse avalanche	crumbling lava dome - Pelean type					
						Pelee vertical type		Intermediate type	nuée ardente - Sakurajima type	soufriere type - vertical explosion				nuées ardente sensu strictu - Santiaguito type	eruption column collapse - vertical explosion from dome eruption column collapse	
nuées ardentes d'explosion vulcaniennes	Gloedwolken van het St.Vincent type	Explosivgloedwolken (glowing clouds formed by volcanic explosions)		Glutlawinen (glowing avalanches) - primaerer Merapi type (directe-primary)	Pelean variant - 1st order Nuée ardente; vertical explosive discharge from open volcanic crater	St.Vincent vertical type/ Mount Katmai tuff-flow type		pumice flow	ash flow - St.Vincent type		summit crater - St.Vincent type	pumice flow	scoria flow	nuées ardente sensu strictu - St.Vincent type	eruption column collapse - continuous eruption column collapse	
							Vertical explosion type (Krakatoan)		intermediate type			scoria flow	pumice-ash flow		eruption column collapse - continuous gas streaming interrupted column collapse	
									ash flow - Krakatoa type		summit crater - Krakatoan type	semi-vesicularandesite flow			eruption column collapse - upwelling at vent "instanteneous collapse"	
nuées ardentes avalanches	Gloedwolken van het Merapi type	Afstortingsgloedwolken				Merapi lateral disintegration type	Pelean type	Nuée ardente				block-and-ash flow: Nuée ardente	Nuée ardente	glowing avalanches - Merapi type	lava dome/flow collapse - explosive dome collapse	granular fluid based pyroclastic density currents
											summit crater - Asama type				lava dome/flow collapse - gravitational dome collapse	
Nuées ardentes peleenne d'avalanche		Glowing cloud formed by lava avalanche												glowing avalanches - Arenal type	dome collapse - landslide triggering explosive collapse of cryptodome	
nuées ardentes du Massif du Katmai					Pelean variant - 1st order Nuée ardente (Katmaian type; Fenner 1937) Vertical explosive discharge from fissures	concealed fissure-orifice type		pumice flow	ash flow - Valley of Ten Thousand Smokes type		fissures - Valley of Ten Thousand Smokes type					
						Novarupta tuff-flow type	Fissure eruption type (Valley of 10000 Smokes)				fissures - Valles type					
Avalanches sèches				Glutlawinen (glowing avalanches) - sekundaerer Stromboli type (indirecte-secondary)					hot ash avalanche - Vesuvius type							

Table 1.1: Compilation of all published classifications of pyroclastic density currents, from 1930 to the present day.

Macgregor (1955) was the first volcanologist to give a comprehensive classification of nuées ardentes, by not only organizing the individual currents according to the locality or volcano name where a specific flow style was first observed, but by identifying the flows by their source area and the mode and style of the eruption they are generated from (see Table 1.2). With the introduction of further flow types he expanded previous classifications by his Santa Maria and Novarupta types. The Santa Maria type is characterized by the mild lateral explosion of a dome on the flanks of a volcano, whereas the Novarupta type can be compared to the Katmaian or Valley of Ten Thousands Smokes flow type (see Lacroix's group IV).

Nature of eruption		Mode of eruption	Source	Specific type of eruption	Magma	Volcano or locality name to link with specific type of eruption and magma
Generalized description	Major subdivision					
Nuée ardente pyroclast eruptions: i.e. eruptions of gas and mobile, gas-generating (self-explosive) debris of new lava, accompanied by hot or glowing gas-and dust-clouds	Tholoidal gas-and-ash avalanche eruptions*	Non-explosive	Summit-crater tholoid	Lateral disintegration type	Trachytic	?
					Rhyolitic	?
					Andesitic, incl. dacite	Merapi
			tholoid on flank of volcano	Lateral disintegration type*	Andesitic, incl. dacite	? Santa Maria
		Explosive	Summit-crater tholoid	Discharged lateral type**	Andesitic, incl. dacite	Mt. Pelée
				Directed lateral type***	Andesitic, incl. dacite	Mt. Pelée
				Vertically initated type	Andesitic, incl. dacite	Mt. Pelée
			tholoid on flank of volcano	Discharged lateral type**	Andesitic, incl. dacite	Santa Maria
				Directed lateral type***	Andesitic, incl. dacite	? Santa Maria
				Vertically initated type	Andesitic, incl. dacite	?
			Summit crater	Vertically initated type	Andesitic, incl. dacite	St.Vincent
				Vertically initated type	Rhyolitic	Mount Katmai
	Non-tholoidal gas-and-ashflow eruptions **	Explosive	Low-level crater and (possibly) adjacent fissures	Vertically initated type	Rhyolitic	Novarupta
			Many distributed fissures	Vertical concealed fissure-orifice type	Rhyolitic	?

* Discharged debris comprise large or small blocks derived from the tholoid, as well as finely comminuted lava.

** Discharged debris is mainly finely comminuted lava.

* No initial explosion.

** Mild initial explosion

*** Violent initial explosion.

Table 1.2: Classification of nuées ardentes pyroclast eruptions (modified after Macgregor, 1955).

The importance of the incorporation of the deposits into the classifications was pointed out by Williams (1957). He discussed in detail the characteristics of the deposits related to his three flow types – the Peleen type (Peléan + Merapi type combined), the Krakatoan type (St.Vincent type from Escher = nuée ardente d'explosion vulcaniennes by Lacroix, Table 1.3) and the fissure eruption/ Valley of Ten

Thousands Smokes type, e.g. induration, vesicularity. His research suggested for the first time a relationship between pyroclastic flows types and textural and constituent characteristics of their deposits.

Lacroix (1930)	Escher (1933) and Fenner (1937)	MacGregor (1952)	Aramaki (1957)	Williams (1957)	Murai (1961)	MacDonald (1971)
Nuée ardente peléene d'explosion dirigée	Pelée type	Pelée discharge lateral type	Nuée ardente	Peléan type	Nuée ardente	Pelée type
		Pelée directed lateral type			Pelée type	
Nuée ardente peléene d'avalanche	Merapi type	Merapi lateral disintegration			Merapi type Sakurajima type	Merapi type
Nuée ardente d'explosion vulcanienne		Pelée vertical type	Intermediate type		Intermediate type	Soufrière type
	St.Vincent type	St.Vincent vertical type/ Mt.Katmai tuff flow type	Pumice flow	Vertical explosion type (Krakatoan)	Ash flow	St.Vincent type
Nuée ardente du Massif du Katmai	Katmaian type			Fissure eruption type (Valley of 10000 Smokes)		Krakatoan type
						Valley of 10000 Smokes type
						Ash flow type

Table 1.3: Compilation of various pyroclastic flow classifications, modified after Smith and Robool (1982).

Volcanologists from Japan attempted to set up classifications based solely on observations from Japanese volcanoes. Aramaki (1957) and Murai (1961) both adapted the three main types from Lacroix - Pelean, Merapi and (Soufrière) St.Vincent type (Table 3), but each introduced a different type as well. The Asama flow type is an intermediate flow type between the Krakatoan and Pelean type with the pyroclastic current foaming over the summit crater rim and rushing downslope. Murai distinguished between nuées ardentes, intermediate flows and ash flows, the new Sakurajima type fitting into the first category. Examples for nuées ardentes are Mt.Pelée (1902/03), Merapi (1930/31), Hibok Hibok (1948-53) and Mount Lamington (1951/52) for Murai's Pelean nuée ardente. His "ash flow" group includes the St.Vincent, the Valley of Ten Thousands Smokes and the Krakatoa type, with explosive eruptions in these individual localities in 1902, 1912 and 1883 respectively.

Glowing avalanches (synonymous for nuées ardentes) are part of the fragmental flows described by MacDonald (1972, Table 1.1), and the aforementioned three main nuée ardente groups are also distinguished, with the addition of hot ash accumulations on steep slopes during the 1906 eruption of Vesuvius, putting them in a separate group of hot-ash avalanches. These hot-ash avalanches are regenerated nuées ardentes, reactivated by e.g. the shock of an earthquake, triggering a landslide-like movement of the mixture of gas and pyroclastic fragments.

Later classifications (after 1980) tried to follow the suggestions of Williams (1957) to incorporate details of the deposits according to field criteria (e.g. relative amounts of pumice, scoria, poorly vesiculated fragments and ash) by for example emphasizing the degree of vesiculation in relation to the eruptive mechanisms (Wright et al., 1980, Table 4). This was one of the first attempts to close the gap between the classic names and descriptive parameters of the deposits.

Wright et al. (1980) proposed a general nomenclature for pyroclastic flows and their deposits as well as a separate categorization for pyroclastic surges based on the density of glass fragments and their vesicularity. The authors distinguished only two major flow types – generated by the lava/dome collapse or from the eruption column collapse. Instead of using the term nuée ardente for all pyroclastic flows, Wright suggested only applying this phrase to block-and-ash flows (term introduced by Perret, 1937) generated by collapse of a lava dome and lava flow front or even to avoid this phrase altogether because the exact meaning was (and still is) rather ambiguous. Pyroclastic currents developed from the collapse of an eruption column have been separated by their degree of vesicularity into pumice flows, scoria flows and semi-vesicular andesite flows and their respective deposits (Table 1.4). Wright was also the first author to not link the various eruption styles and modes to specific locality or volcano names as most of the other authors did (e.g. Macgregor, 1955; Murai, 1961).

:

Essential fragments	Eruptive mechanism		Pyroclastic flow	Deposit
vesiculated			Pumice flow	Ignimbrite Pumice and ash deposit
	Eruption column collapse		Scoria flow	Scoria and ash deposit
Decreasing average density of juvenile clasts			Semi-vesicular andesite flow	Semi-vesicular andesite and ash deposit
	Lava/dome collapse	explosive	Block and ash flow: nuée ardente	Block and ash deposit
Non-vesiculated		gravitational	Block and ash flow: nuée ardente	Block and ash deposit

Table 1.4: Genetic classification of pyroclastic flows by Wright et al. (1980).

Another attempt to classifiy (calc-alkaline) nuées ardentes not only by locality or volcano name, but also by glass chemistry combined with the morphology and grain-size analysis was made by Bardintzeff (1985). Five eruptive styles were distinguished (Figure 1.3):

1. Merapi type: avalanche from a solid dome.
2. Arenal type: avalanche from a partly liquid dome.
3. Santiaguito type: small nuée ardente from a dome lava flow.
4. Pelée type: directed nuée ardente associated with a dome.
5. St. Vincent type: vertical nuée ardente from an open crater

Bardintzeff distinguished avalanche-nuées from nuées ardentes. In his classification, the avalanche-nuées are subvided into the Merapi s.s. sub-type, where a collapsing dome (sometimes only a few days old) is more or less pulverized by a phreatic explosion, and the Arenal subtype which is generated from a collapsing block-lava dome with a still liquid interior. When the dome is collapsing, new magma pours out and due to oversteepening of the flow front, pyroclastic flows are generated. The nuées ardentes sensu stricto are divided into the Santiaguito type, characterized by high explosivity of the eruption, the Pelée type and St. Vincent type.

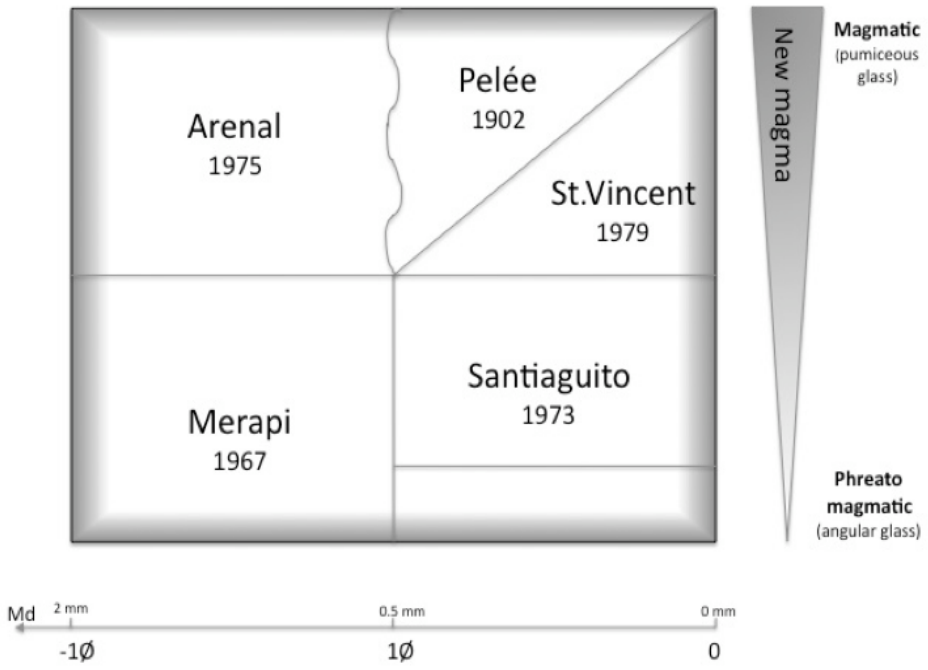

Figure 1.3: New classification of nuées ardentes, according to grain-size and glass-grain morphology by Bardintzeff (1985).

The latest in a long line of classifications is the two-fold classification by Branney and Kokelaar (2002) that totally abstains from previous classifications and from the use of terms like pyroclastic flow or surge. They managed to combine various hypotheses and observations of pyroclastic density currents to form a catalogue of flow and sedimentation processes for the various end-members. While keeping in mind that there is a continuous spectrum of pyroclastic currents, the authors define fully dilute pyroclastic density currents at one end and granular fluid based currents at the other end of the spectrum with all gradations existing in between. This classification is based on processes and conditions that dominate around the lower flow boundary between the basal part of the density current and the substrate.

In fully dilute pyroclastic density currents, the rare interactions between clasts have little effect on particle support, segregation and the current rheology, even toward the current base. Such currents have flow-boundary zones dominated by direct fallout or by traction. Particle transport and support are dominated by effects of turbulence of the fluid phase (dusty gas) at all levels in the current.

Clast transport and support are significantly influenced by clast interactions and/or fluid escape in granular fluid-based currents, in lowermost levels of the current. The two types of currents are entirely intergradational (for a detailed description refer to Branney and Kokelaar (2002) – *Pyroclastic density currents and the sedimentation of ignimbrites).*

1.4.2. Pyroclastic surge classification

Within the last 40 years pyroclastic surges have been acknowledged as a common and violent component of explosive volcanic eruptions. Pyroclastic surges are now widely recognized as "dilute suspension currents in which particles are carried in turbulent suspension" (Druitt, 1998).

Initially pyroclastic surges were defined by the analogy to the base surges that accompany large surface explosions, such as from nuclear weapons between 1940 and 1950 (Wohletz, 2001). From the 1960's onwards the base surge phenomenon was recognized to occur during volcanic eruptions. Milestones in the work of pyroclastic surges have been achieved by authors such as R.V. Fisher (1977, 1979), the first volcanologist to apply the nuclear base surge concept to the eruptions at Taal volcano in 1965 after observing the nuclear tests at Bikini Atoll, and J.G. Moore (1967) who formalized the concept of volcanic base surges at Taal volcano.

Four different kinds of pyroclastic surges have been distinguished, on the basis of their deposits and on the nature of the eruption – (1) base surges, (2) ground surges, (3) ash cloud surges, and (4) blast surges.

(1) Base surges

These surges generally develop from the collapse of overloaded vertical eruption columns, blasting out from the base of the column. Many of these base surges contain a great deal of condensed steam, so they are often wet and sticky (Francis, 1993). They are best known from small basaltic eruptions, e.g. Taal volcano, 1965 or East Ukinrek, 1977.

(2) Ground surges

The term “ground surge” was coined by Sparks and Walker (1973), but at that time was used to describe all types of pyroclastic surges. But shortly afterwards, the term was established for those surges found at the base of pyroclastic flow units or for those associated with some fall deposits (Wright et al., 1980). Ground surges are thought to be precursors to dense pyroclastic flows, preceding their flow front (Cas and Wright, 1988). They are generated by earlier, small collapses of the margins of a vertical eruption column, from directed low concentration blasts and out of the head of a moving pyroclastic flow.

(3) Ash cloud surges

Fisher (1979) distinguished ash cloud surge deposits from those of ground surges, because of their emplacement on top of the pyroclastic flow unit, indicating a possible origin in the elutriation of the ash from the top of the moving flow.

(4) Blast surge

In addition to the three main types, a fourth type of pyroclastic surge was recognized after the eruption of Mount St.Helens in 1980 and the eruption of Bezymianny in 1956 – the lateral or directed blast surge (Kieffer, 1981). Due to the rapid decompression of internal parts of a growing dome or a conduit, large-scale slope failures result in the directed blast of the pyroclastic material.

For nearly 20 years after their official introduction into the volcanological literature, pyroclastic surges were not incorporated into the concept of pyroclastic density currents (umbrella term). Smith and Robool (1982) were the first to include surges in their classification. The authors define a pyroclastic flow as comprising two flow parts – an underflow (pyroclastic flow sensu strictu) and an overriding turbulent gas and dust cloud (surge component). Differences in density and concentration within the flow parts are reflected in the related deposits. Thus Smith and Robool (1982)

deemed it appropriate to differentiate flows from surges and to classify their different types of deposits separately (Table 1.5).

Eruptive mechanism	Pyroclastic flow	Underflow deposit	Surge deposit (ground and ash cloud surge)
Lava/dome collapse	Nuée ardente	Block and ash	Dense andesite surge
Eruptive column collapse	Scoria flow	Scoria and ash	Scoraceous surge
	Pumice-ash flow (small volume)	Pumice and ash	Ash pumice surge
	Pumice-ash flow (large volume)	Ignimbrite	

Table 1.5: Classification for pyroclastic flows by Smith and Robool (1982) that includes the separate categorization of flow and surge deposits.

Bardintzeff (1985) includes surges in his classification as well, but not as a separate pyroclastic occurrence, only as part of his nuée ardente definition (see Figure 1.3). The calc-alkaline nuées ardentes he observed and described contain the flow and the surge part combined, but the possibility of the generation of a pyroclastic surge without the flow component (base surge) was not acknowledged.

1.5 Prospective thesis classification for pyroclastic density currents

With the sheer volume of information on all types of pyroclastic density currents, the confusing terminology and the inconsistent classification schemes, it is nearly impossible to commit to one specific classification. Searching through numerous papers from the last 100 years and comparing the most important classifications, the terminology used in this thesis for future references and descriptions of the block-and-ash flow deposits at Tarawera volcano is a compilation of different categorizations.

Most of the aforementioned classifications rely heavily on the fundaments of Lacroix (1904), but it is important to remember that most volcanoes show more than one

style of eruption during their eruptive history, e.g. during the last 200 years of the eruptive activity at Merapi volcano, pyroclastic density currents were not only generated by the collapse of the growing lava dome, but also by the collapse of an eruption column. Referring to “Merapi style” pyroclastic flows, a term that has nowadays mostly been used for currents generated by lava dome collapses, is then confusing for readers who are familiar with the eruptive history of the volcano. This Indonesian volcano is only one of the many examples for volcanoes showing numerous styles of eruptive activity, other examples are Soufrière Hills Volcano at Montserrat and Mt.Pelée at Martinique.

Hence a classification that is solely based on the classical distinction of the flow according to the volcano locality does seem not to be not the best approach to describe and label the various current types. The incorporation of the deposits and related pyroclastic surges is an important factor in a suitable classification. Analyzing the flows and their deposits based on grain size distribution and vesicularity is a better approach to distinguish the individual flow types.

So combining Macgregor’s (1955), Wright’s (1980) and Smith and Robool’s (1982) classification might be a more suitable approach for further research (Table 1.6), especially because Wright et al. (1980) officially included block-and-ash flows as a separate group of pyroclastic density currents.

A clear explanation of the generation of block-and-ash flows is essential for the research and the investigation of the block-and-ash flow deposits at Tarawera Volcano on the North Island of New Zealand. Therefore the incorporation of block-and-ash flows into the classification is necessary.

Nowadays the expression “block-and-ash flow” is used for small-scale pyroclastic density currents resulting from the gravitational or explosive collapse of a lava dome or lava flow front (Freundt et al., 2000). Sometimes the pyroclastic density currents resulting from the fallback of pyroclastic material during the collapse of an eruption column have been classified as block-and-ash flows as well (Fisher and Heiken, 1982; Cas and Wright, 1988).

In this thesis the term “block-and-ash flow” will be applied only for the description of small volume pyroclastic density currents generated by the collapse of a lava dome or the front of a lava flow, either gravitationally or with an explosive component. The suggested initiation of block-and-ash flows by the collapse of an eruption column (Sigurdsson et al., 2000) is not included within this scheme (Table 1.6).

Non-vesiculated ↓ vesiculated	Mode of eruption		Source	Specific type of eruption	Pyroclastic flow	Pyroclastic flow deposits	Pyroclastic surge
	Lava dome collapse	Non-explosive	Summit-crater dome	Lateral disintegration type	Block-and-ash flow	Block-and-ash flow deposit	Ash cloud surge (part of the BAF)
			Dome on flank of volcano	Lateral disintegration type*			
		Explosive	Summit-crater dome	Discharged lateral type**			
				Directed lateral type***			
	Eruption column collapse			Vertically initated type	Scoria flow	Scoria flow deposit	Base surge
			Dome on flank of volcano	Discharged lateral type**	Pumice flow/Ash flow	Ignimbrite/Ash flow deposit	
				Directed lateral type***			Blast surge
				Vertically initated type			Base surge
			Summit crater	Vertically initated type			
	Fissure eruptions	Explosive	Low-level crater and (possibly) adjacent fissures	Vertically initated type			Ground surge
			Many distributed fissures	Vertical concealed fissure-orifice type			

* No initial explosion ** Mild initial explosion *** Violent initial explosion

Table 1.6: Classification of block-and-ash flows used in this thesis, representing a compilation of the classifications of Macgregor (1955), Wright et al. (1980) and Smith and Robool (1982). The clear distinction of block-and-ash flows (BAFs) is important for the following chapters of this PhD thesis.

These days pyroclastic density currents have been recognized as comprising various flow parts due to gas content and the density differences of the pyroclastic material itself and between the currents and the ambient fluid. The flow components are a ground-hugging basal avalanche, an overriding pyroclastic surge and a billowing, dilute ash cloud on top.

While some authors use the phrase “block-and-ash flow” only for addressing the high-concentration dense basal avalanche, the overriding ash cloud surge is herein recognized as being part of the block-and-ash flow. It develops during the transport of the gas-rich pyroclastic mixture and will be more pronounced due to increased

density differences between the individual flow parts. While it is part of the block-and-ash flow, during transport the ash cloud surge can separate from the basal avalanche, resulting in ash cloud surge deposits which can be distinguished from deposits of the basal avalanche e.g. by grain-size distribution or bedding features.

Various authors use “nuée ardente” as a synonym for a block-and-ash flow (e.g. Abdurachman et al., 2000; Miyabuchi, 1999; Michol et al., 2008), often in combination with previously described classifications such as Merapi-type or Pelean type for individual lava dome collapses. There is still confusion about the exact definition of the “nuée ardente” concept, sometimes this phrase is used only for the surge component, sometimes for the complete pyroclastic density current. The present categorization scheme will completely refrain from using names of flow localities for labeling the flows, and the term “nuée ardente” was not included within the scheme because of its ambiguous definitions and usage.

1.6. Conclusions

Understanding of the concept of explosive volcanic eruptions and the generation of pyroclastic density currents has changed dramatically within the last century, due to observations of recent volcanic eruptions at e.g. Unzen Volcano (1990-95) and Merapi Volcano (1995-2008).

The existing literature on pyroclastic density currents is extensive, complex and often confusing. There are too many terms and different concepts due to difficulties in the interpretation of the deposits and the still incomplete understanding of the flow dynamics of these dense mixtures of hot volcanic particles and gas.

The development of a suitable classification for pyroclastic density currents is not an easy task. However, the confusion evident in most of the nomenclatures used in the past and even nowadays is a great hindrance in the scientific progress. Without clear and concise terminologies, the research presented may sometimes be misunderstood due to contradictory statements and descriptions of numerous deposits as well as the use of different languages.

After comparing numerous classifications and balancing their advantages and disadvantages, a collection of three classifications has been chosen to distinguish individual pyroclastic flows and surges and their deposits at Tarawera volcano in New Zealand, described in this thesis.

1.7. Nomenclature

1.7.1. Definition of pyroclastic flow types used in the collected classifications

Asama type - Flow formation intermediate between those of Peléean type and those of St. Vincent and Krakatoan types. Initial discharge of gas-rich magma produces a pumice fall followed by two pyroclastic flows of diminishing gas-content.

Arenal type - gravitational collapse of a lava dome with a still liquid interior. The eruption starts with rockslides and rockfalls during the gravitational collapse of the crater/dome wall. Due to the sudden discharge of lava from the resulting crater, pyroclastic flows formed during descent.

Krakatoan type - Pumiceous flows discharged by voluminous upwelling from summit-vents and circumferential fractures on composite cones; eruptions commonly result in the formation of a caldera.

Merapi type - Flows form by non-explosive disintegration and collapse of the flanks of domes and summit-spines or by breakup of the snouts and levees of viscous lava flows on steep slopes. These flows result gravity-collapse of the oversteepened flanks of domes and unstable summit-spines. Also known as **Nuée ardente peléene d'avalanche** and **Sakurajima flow type**.

Pelean/Pelee type - Flows form by explosive eruptions immediately before or during the rise of domes. These are produced by explosions before and during the rise of volcanic domes. Also known as Nuée ardente peléene d'explosion dirigée.

Santiaguito type - flows generated from the collapse of a lava flow front. Also known as **Santa Maria flow type.**

(Soufriere) St.Vincent type - Flows produced by backfall of ejecta from the margins of vertical eruption-columns. The pyroclastic flows originate by "fallback" of the outer, more slowly rising parts of the eruption-column, produced by gravitational collapse. Also known as Nuée ardente d'explosion vulcanienne.

Valles type - Eruptions of siliceous pumice from arcuate fissures formed by regional arching of the roofs of large bodies of rising magma; volumes of ejecta are usually so

great that the roofs of the magma chambers collapse along the arcuate fissures to produce calderas.

Valley of Ten Thousands Smokes - Eruptions from one or more short linear fissures, the location and trend of which are unrelated to a cone or crater. Also known as Katmai type or Novarupta type or Nuée ardente du Massif du Katmai.

Vesuvius type – pyroclastic ejecta is deposited on the steeper parts of the volcano flank, triggering by earthquakes or rainfall can result in the reactivation of the deposits, resulting in a dry avalanche, comparable to a landslide. Also known as Stromboli type or Avalanche sèches.

1.7.2. Definitions of modern terms (Encyclopedia of Volcanoes, 2000)

Block-and-ash flow - small volume, monolithologic pyroclastic currents generated by the collapse of a lava dome or the front of a lava flow. Generation can either be gravitational or with a slight explosive component.

Ignimbrite – welded or unwelded, pumiceous, ash-rich deposit of pyroclastic density currents, this term was formerly used for strongly welded deposits only.

Nuée ardente – French for "glowing cloud, the term is often used as a synonym for pyroclastic flows and/or surges. Due to contradictory definitions, the usage of this term is not recommended.

Pyroclastic density current – particulate gaseous volcanic flow moving along the ground. This term includes both pyroclastic flows and surges.

Pyroclastic fall – rain-out of clasts through the atmosphere from an eruption jet or plume during an explosive eruption.

Pyroclastic flow – a pyroclastic density current where most of the material and momentum is contained in a basal concentrated particulate dispersion.

Pyroclastic surge –pyroclastic density currents where the material and momentum are widely distributed through a deep, dilute and highly turbulent particulate suspension

1.8. List of alternative terms for pyroclastic density currents

Descriptive terms for pyroclastic flows (+ surges)	Authors
Afstortingsgloedwolken	Neumann van Padang, 1933
Afstortingsglowdwolken	Escher, 1933
Agglomerate flow	Gorshkov, 1959
Agglomerate stream	Gorshkov, 1959
Ash cloud surge	Miyabuchi, 1999
Ash flow	Smith, 1960
Ash hurricane	Sparks et al., 1973
Aso lava	Matumoto, 1943
Avalanches seches	Lacroix, 1930
Awan panas	Voight et al., 2000
Base surge	Wright et al., 1980
Blast surge	Mellors et al., 1988
Block-and-ash flow	Perret, 1937
Burning cloud	Anderson and Flett, 1903
Co-ignimbrite ash cloud	Cas and Wright, 1988
Explosivgloedwolken	Neumann van Padang, 1933
Explosivgloedwolken	Escher, 1933
Foam lava	Locardi & Millempergher, 1967
Froth flows	McCall, 1964
Gas and ash flow	Smith, 1960
Globule lavas	Johnson, 1968
Gloedwolken	Escher, 1933
Glowing avalanche	Bardintzeff, 1985
Glowing cloud	Bardintzeff, 1985
Glutlawinen	Rittmann, 1931
Glutwolken	Rittmann, 1931
Hot ash flow	Bridge and Demicco, 2008
Hot avalanche	Francis et al., 1974
Hot cloud	Smith, 1960
Hot rock avalanche	Mellors et al., 1988
Hot sand flow	Fenner, 1923
Ignimbrite	Marshall, 1935
Incandescent tuff flow	Fenner, 1948
Lava debris flow	Smith, 1960
Nuee ardente	Lacroix, 1930
Phoenix cloud	Cas and Wright, 1988
Pumice flow	Aramaki, 1957
Pyroclastic avalanche	Nairn and Self, 1978
Pyroclastic flow	Fisher and Schmincke, 1984
Pyroklastischer Block-und-Asche-Strom	Schmincke, 2003
Pyroklastistischer Blockstrom	Schmincke, 2003
Scoria flow	Aramaki, 1957
Welded mud lava	Smith, 1960

Descriptive term for pyroclastic surges	Authors
Ash cloud surge	Miyabuchi, 1999
Base surge	Wright et al., 1980
Blast surge	Mellors et al., 1988
Burning cloud	Anderson and Flett, 1903
Co-ignimbrite ash cloud	Cas and Wright, 1988
Glowing cloud	Bardintzeff, 1985
Glutwolken	Rittmann, 1944
Hot cloud	Smith, 1960
Nuee ardente	Lacroix, 1930
Phoenix cloud	Cas and Wright, 1988

Descriptive terms for deposits	Authors
Aso lava	Matumoto, 1943
Clastolavas	Maleyev, 1965
Eutaxite	Fritsch and Reiss, 1868
Hai ishi (ash stones)	Smith, 1960
Ignimbrite	Marshall, 1935
Ignispumites	Panto, 1962
Piperno	Sparks et al., 1978
Schmelztuff	Weyl, 1954
Shirazu	Taneda, 1954
Sillar	Jenks and Goldich, 1956
Tuff lava	Smith, 1960
tufolava	Abich, 1882
Welded tuff	Iddings, 1909

Chapter 2

Decoupling in particulate density currents – with emphasis on block-and-ash flows

"If we knew what we were doing it wouldn't be research."

Albert Einstein

Chapter 2: Decoupling in particulate density currents with emphasis on block-and-ash flows

2.1. Introduction

Particulate density currents encompass a wide range of different types, such as debris flows and avalanches, snow avalanches, turbidity currents and pyroclastic density currents. These flow types are of great importance in nature, not only acting as agents of sediment tranport and deposition, but also because of their potentially destructive capability, including devastated vegetation, destruction and burial of houses and the loss of lives. When fully developed, pyroclastic currents have a three-layered structure (e.g. Druitt, 1998; Bareschino et al., 2007) – a ground-hugging, basal avalanche comprising a high concentration of dense particles, an ash-cloud surge that is composed of fine particles supplied from the lower layer and an ash-cloud plume on top (Figure 2.1). Pyroclastic currents have been observed to experience a separation of these flow parts, termed decoupling (Fisher, 1995), and posing a major hazard to communities and infrastructure. While several authors acknowledge the possibility of decoupling processes in pyroclastic density currents (e.g. Abdurachman et al., 2000; Bourdier and Abdurachman, 2001), little is known about the initiation of these processes, when and how they can occur and their hazard potential.

2.2. Terminology

Decoupling describes the detachment of the turbulent, dilute ash layer from the underlying basal avalanche during down slope movement, resulting in independent movement, often in different directions (Fisher, 1995). These processes have been described for block-and-ash flows generated during volcanic eruptions within the last two descades (e.g. Merapi Volcano in 1995, Bourdier and Abdurachman, 2001;

Soufriére Hills Volcano in 1997, Cole et al., 2002), for subaqueous turbidity currents (termed "flow-stripping") and powder snow avalanches. Flow stripping has been described as the process by which the upper part of a subaqueous turbidity current is stripped off the main body (Piper and Normark, 1983), commonly occuring at channel bends. The part of the flow that escapes the channel is the dilute or low-density, fines-rich part of the flow. The abrupt change from confined to unconfined flow as the upper part of the flow leaves the channel results in rapid sedimentation at and near the levée crest; a similar process was documented at Merapi Volcano during the eruption in 2006 (Charbonnier and Gertisser, 2008). These overspilled block-and-ash flows posed a previously underestimated hazard during the transport and emplacement of generally channel-confined flows at Merapi Volcano.

2.3. Decoupling processes

Fisher (1995) published a hazard assessment for the phenomenon of decoupling within pyroclastic currents, providing a basis for other authors to recognize similar flow behaviour at volcanoes such as Unzen (Ui et al., 1999), Merapi (Abdurachman et al., 2000) and Soufriére Hills (Druitt et al., 2002). At least four general processes are thought to lead to decoupling – (1) gravity segregation that increases particle concentration in the basal avalanche, therefore reducing the concentration in the upper part of the current; (2) the development of lower boundary processes in the basal avalanche that can cause erosion of particles from the substrate which then

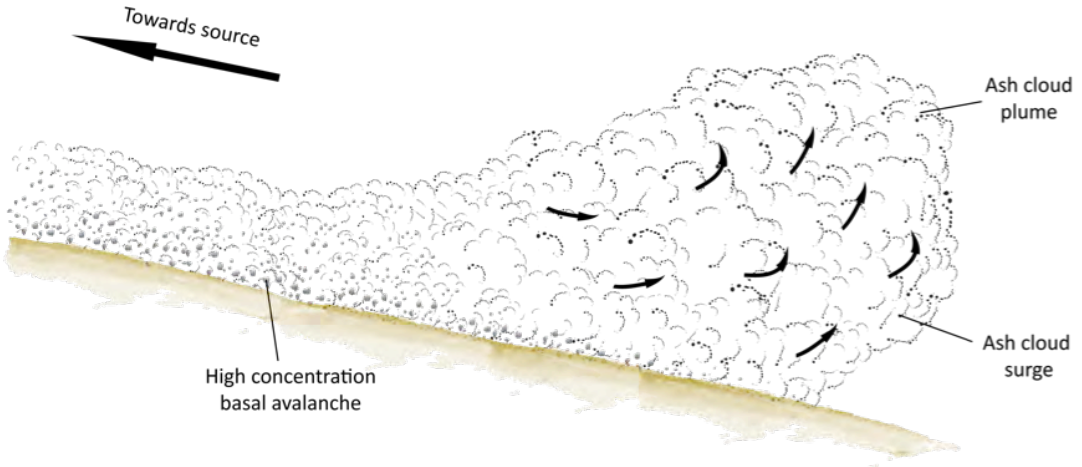

Figure 2.1: Overview of various flow parts within an advancing block-and-ash flow (modified after Fisher and Heiken, 1982).

will be incorporated into the avalanche, again increasing particle concentration at the base; (3) the increase in turbulence caused by interaction of the ambient fluid (air) with the outer surface of the moving current, and (4) elutriation of particles from the basal part of the currents due to gas release, possibly from the fragmentation of vesicular clasts; residual pressurized gas in the vesicles will be set free and move upwards through the current, emitting fine particles that form an ash cloud.

2.3.1. Gravity segregation

During their advance across the landscape, pyroclastic density currents develop complex spatial and temporal variations, resulting in non-uniformity and stratification of the flows, and in the formation of a high-concentration basal avalanche and a more dilute, overriding ash cloud surge layer. Currents may become laterally and vertically stratified in terms of grain size and sediment concentration, e.g. due to variable settling velocities of different particle sizes, variations in turbulence intensity within the flow (Kneller and Buckee, 2000; Buckee et al., 2001), entrainment of air or water at the margins of the flow (Hallworth et al., 1996) and entrainment of sediment from the underlying substrate. Gravity acts to increase the clast concentration towards the base of the current and/or segregate clasts vertically according to their sizes, shapes and densities.

The way in which particle concentration increases toward the base of the current depends on the Rouse number. The particle Rouse number, Pn_i is the ratio of the settling velocity, w_i, of a given population of clasts, *i*, to the turbulence intensity, ku^* ($k \cong 0.4$ is von Kármán's coefficient and u^* is the shear velocity), that is given by (Branney and Kokelaar, 2002):

$$Pn_i = \frac{w_i}{ku*}$$

or, for suspensions with clast populations of more than one settling velocity, the distribution Rouse number, *Pn* is given by:

$$Pn = \frac{1}{\bar{S}} \sum_i S_i \left(\frac{w_i}{ku*} \right)$$

where $\bar{S}$ is the height-averaged volume concentration of all clasts and S_i is the height-averaged concentration of clast population *i* ('population' here means all clasts of a given settling velocity, w_i; clasts of different sizes, densities and shapes may constitute a single population if their settling velocities are equal). Low Rouse numbers (*Pn* < 1) correspond to small particles and efficient suspension by turbulence, and result in gradual downward increases in concentration, whereas high Rouse numbers (*Pn* > 1) result in steep concentration gradients near the base of the current. There are some limitations to the application of the Rouse Number for pyroclastic density currents – it was developed for open channel flows, such as rivers, with negligible flow retardation whereas the upper boundaries of pyroclastic flows undergo significant shear due to mixing with the ambient fluid, significantly affecting turbulence and corresponding shear-stress and particle concentration profiles (Garcia and Parker, 1993; Kneller and Buckee, 2000). In addition, the upper flow boundaries are also modified by thermal convection, causing further shearing, mixing and thermal expansion of the suspension cloud. Further limitations are related to currents undergoing sedimentation, because the suspended load is then no longer in equilibrium with the bed (Dobbins, 1944) – probably a common field situation.

No consensus for calculations of particle concentrations within pyroclastic currents has been reached to date, hence calculations of the particle Rouse number is the best mathematical proxy for concentration profiles in these currents.

2.3.2. Lower boundary erosion

The interface between substrate and base of a pyroclastic flow represents a boundary zone that is characterized by gradients in velocity and particle concentration. Any clast undergoing deposition will experience different shear intensity and concentration when it crosses the boundary zone. Shear at the flow

boundary causes individual clasts to experience lift and/or drag by ambient fluid so that they slide, roll or saltate along the substrate surface before they are finally deposited (Branney and Kokelaar, 2002). Interactions between the flow and the substrate lead to localized non-uniformity, causing selective entrainment of the substrate and segregation within the lower boundary zone. This "bulking" (Scott, 1988) will lead to an increase of the concentration of the basal avalanche, creating a density difference with the upper parts of the flow.

Entrainment of material into a moving current involves the mobilization of the substrate, and depends on the erodibility and deformability of the material (compare Chapter 4). The rate of substrate erosion and entrainment is related to substrate properties (e.g. shear strength), avalanche velocity (v) and avalanche thickness (loading), and tends to increase with v^2 (Barbolini et al., 2005; Bursik et al., 2005; Takahashi, 2001). To quantify the entrainment process, an Entrainment Ratio (E_R) can be defined as the ratio between the volume of debris entrained from the path and the expanded volume of rock fragments produced by the initial rock failure. The entrainment ratio (E_R) is defined by $E_R = V_E / V_R(1+F_F)$, where V_E is the volume of entrained material, V_R is the volume of the initial rock mass, and F_F is the fractional increase of volume due to fragmentation (Hungr and Evans, 2004).

The incorporation of eroded material into the flow increases its volume, changing the bulk or basal composition to a degree that can affect its mechanical and dynamic behaviour. The entrained material mixes into the moving flow body as a function of distance traveled and of the availability of erodible material in the flow path. The location of the entrainment on the mountain slope is of utmost importance. Material entrained high on steep slopes not only adds to the volume of the flow, but it contains also a substantial potential energy which can be converted into kinetic energy during descent and run-out of the avalanche (Dufresne, 2009).

2.3.3. Elutriation processes

Pyroclastic currents contain particles ranging in size from metres to microns and materials ranging from pumice to dense rock fragments. The fragmentation of larger

clasts takes place at the same time as the generation of elutriable fine particles by surface abrasion. Residual, overpressurized gas trapped inside vesicular clasts can be released by fragmentation during transport. Typically, fine particles are elutriated out of a bed when the superficial fluid/gas velocity through the bed exceeds the terminal velocity of the fine particles. Elutriation tests done by Gravina et al. (2004) indicate that the fine fraction generated by attrition is partly elutriated and partly retained in the bed, promoting fluidization of the basal avalanche.

The elutriation of ash particles from the basal avalanche produces an ash cloud surge which is dilute and turbulent; this process has been described by Fisher (1983) as fluidization transformation. A boundary layer between the basal flow and the dilute ash cloud surge may resembles a traction carpet (Denlinger, 1987), which is non-turbulent and of high concentration. When the basal avalanche slows down due to decreasing slope, the traction carpet on its top, plus the overlying ash cloud surge, detach from the basal avalanche, outrunning it.

2.3.4. Interaction of the upper flow surface with ambient fluid

Finer ash particles elutriate from the main body by the drag force of the upward gas flow, leading to the separation into a lower dense main body and upper light hot ash cloud layer. The hot ash cloud entrains ambient air, and when it becomes lighter than the circumambient atmosphere, it detaches from the ash cloud as a plume. The rate of air entrainment into the ash cloud (surge) is determined by the Richardson Number (ratio of buoyancy forces to inertial forces in the current), which is expressed by

$$Ri = gD\Delta\rho / \rho v^2$$

where D is the current thickness, v is the velocity, ρ is the current density and $\Delta\rho$ is the density contrast with the atmosphere (Branney and Kokelaar, 2002). The buoyancy forces act to stabilize the relatively dense layer beneath the atmosphere, whereas the inertial forces tend to create turbulent mixing. Relatively slow and thick subcritical flows typically entrain little air ($Ri < 1$), whereas relatively fast and thin

supercritical flows entrain considerable air (Ri > 1). Subcritical currents tend to propagate with practically constant volume-flux, apart from the effects of sedimentation, whereas supercritical currents entrain air along their length and become progressively more voluminous, less dense and cooler, with more elutriation of ash into a buoyant cloud (Branney and Kokelaar, 2002). However, in a density-stratified current, values of v, ρ and $\Delta\rho$ vary with height, so that designation of a single Richardson number for the entire current is not appropriate. Furthermore, vertical mixing between different levels of the current may vary considerably with height above the base. Density stratification in turbulent currents tends to inhibit mixing with ambient fluid so that an expanded, but density-stratified current might entrain less air (and thus retain its heat more effectively) than if it were homogeneous (Druitt, 1998).

Thermal expansion of entrapped ambient air causes the ash cloud to inflate and rise by convective buoyancy. Density and temperature of the cloud are controlled by the mixture of ambient air, hot gas and ash elutriated from the basal avalanche. The greater the particulate surface area, the more efficient the thermal transfer into the cloud. At the base of the cloud, a gradational transition in density from that of the underlying avalanche (ρ ~ 1.0 g/cm^3) to that of the expanding cloud has been suggested (Huppert et al., 1986), which would generally have a density less than the surrounding ambient air (ρ ~ 0.0013 g/cm^3). If the entrapment of the ambient air is relatively efficient, the cloud will rise vertically from the basal avalanche. Meanwhile, in the lower part of the main body deposition proceeds, and when the body reaches the gently sloping area it eventually stops. The hot ash cloud surge travels independently for a while after the main body stops, but it soon stops due to the lack of material from the main body and detaches as a plume. However, it has been documented that through rapid sedimentation from the ash cloud surge, a secondary, “surge-derived pyroclastic flow” (Druitt et al., 2002) can develop, associated with a weaker ash cloud (compare section 2.6).

2.4. Interaction with topography

Density currents, such as pyroclastic flows or turbidity currents, usually do not flow onto flat, featureless surfaces, but onto terrains with pronounced topography. The interaction of the flows with this topography controls not only the general dynamics, but also the distribution and nature of the deposits (e.g. Lipman and Mullineaux, 1981; Druitt and Sparks, 1982; Druitt, 1992). The nature of the interaction is strongly dependent on the character of the advancing flow.

Homogeneous and steady currents with a free surface are expected to interact with topography or obstacles as supercritical or subcritical flows and by partial or complete blocking of the flows by the obstacle (Rottman et al., 1985). In contrast, stratified flows will exhibit multiple flow transformations, leading to partial blocking, deflecting, decoupling (Baines 1995; Woods et al. 1998) and individual travel of the separated flow parts. Gravity segregation and the entrainment of ambient fluid are types of flow transformations, respectively termed gravity and surface transformations (Fisher, 1983), all which lead to non-uniformity and stratification.

2.4.1. Non-uniformity

During their advance, particulate density currents develop spatial variations e.g. in velocity or particle concentrations, resulting in non-uniformity. Pronounced density stratification is commonly described from observations and deposits of small-volume block-and-ash flows, wherein the lowermost levels are strongly guided by topography while the upper levels spread more widely, inflate and/or rise buoyantly (e.g. Mt Pelée, Anderson and Flett, 1903; Mount St Helens, Hoblitt, 1986; Unzen, Yamamoto et al., 1993; Soufriére Hills, Cole et al., 2002; Loughlin et al., 2002). It is not clear to what extent large pyroclastic currents that deposit extensive ignimbrites may comprise a lower high-concentration level sharply overlain by an upper relatively low-concentration level of differing behaviour, in contrast to having more gradual variations of concentration with height (Branney and Kokelaar, 2002).

Non-uniformity around topography can be characterized by a dimensionless parameter, the internal Froude number, F_i, which is a function of the flow velocity and the reciprocal of the flow height and the density stratification:

$$F_i = U/(Nh)^{0.5}$$

where U is the depth-averaged velocity, h is a characteristic length scale (e.g., height of topography or thickness of the current), and N is the buoyancy frequency, given by

$$N = \left| \frac{g}{\rho} \frac{d\rho}{dz} \right|^{\frac{1}{2}}$$

where ρ is a reference density (in this case that of the ambient fluid) and dp/dz is the density as a function of height z. Low values of F_i result in the stratification of the current into a lower, denser part flowing around the topography, and an upper, more dilute part that moves over the topography (Kneller and McCaffrey, 1999).

Both parts are separated by a boundary zone or critical level (Valentine, 1987) above which all fluid has sufficient energy to climb over the obstacle, and below which the fluid will either be blocked or stopped, or will simply move around the obstacle without upward movement (Baines, 1995; Woods et al., 1998), depending on the height of the obstacle. This critical level is referred to as “dividing streamline” (Snyder et al., 1985; Figure 2.2). The height of the dividing streamline, H_s, is approximated by

$$H_s = h(1 - \theta F_i)$$

where θ is about 1 (Hunt and Snyder, 1980), and it may depend on the shape of the obstacle (Baines, 1979; Snyder et al., 1985).

The behaviour of pyroclastic density currents around obstructing topography typically varies with the forward velocity of the current, the obstacle height, the current density and, most signicantly, the density stratifcation within the current

(Valentine, 1987; Castro and Snyder, 1993; Lane-Serff et al., 1995; Muck and Underwood, 1990; Alexander and Morris, 1994). A wide range of stratification types has been envisaged (e.g. Chun and Chough, 1992; Felix, 2001) - including laminar stratified currents (Schaflinger et al., 1990), stratified turbulent currents with laminar basal levels (e.g. Fisher, 1966; Vrolijk and Southard, 1998), and turbulent stratified currents with gradational vertical changes of concentration or density (e.g. Valentine, 1987; Cole and Scarpati, 1993). In density stratification, gravity acts to increase the clast concentration towards the base of the current and/or segregate clasts vertically according to their sizes, shapes and densities (compare section 2.3.1).

Generally density stratification within these currents continues along the direction of the flow. It is highly likely that density stratification will become more pronounced with increasing distance from the vent, due to downward migration of the particles with time. Deposition of particles from the lower flow boundary can be counteracted by entrainment of substrate material from the ground.

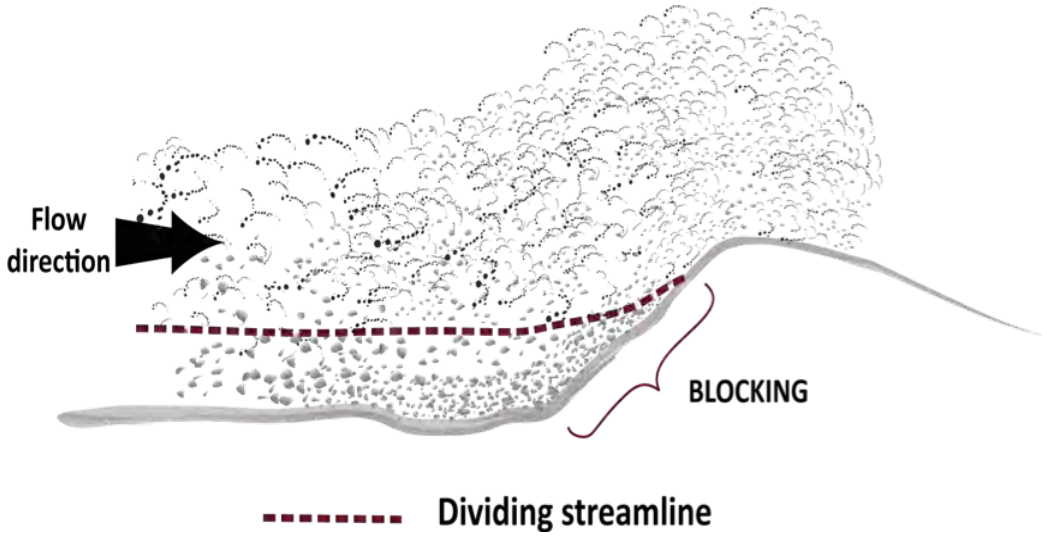

Figure 2.2: Blocking of a stratified pyroclastic density current as it encounters a barrier. The dashed line indicates the position of the dividing streamline; below it material cannot flow over an obstacle (modified after Valentine, 1987).

The dense basal layers might be blocked when encountering a ridge or barrier, but similar dense layers may form again by gravity segregation (comparable to “surge-derived pyroclastic flows” by Druitt et al., 2002) as the overriding more dilute flow

approaches the next ridge or barrier, and so forth. At some point, however, density contrasts within the flow begin to lessen and further blocking may not occur.

Pronounced density stratification has been inferred from observations and studies of the deposits at Mont Pelée (Anderson and Flett, 1903), Mount St.Helens (Hoblitt, 1986), Unzen volcano (Yamamoto et al., 1993) and Soufriére Hills Volcano (Cole et al., 2002; Loughlin et al., 2002). For example, at Mount St Helens, the orientations of trees felled by the 18 May 1980 blast-initiated pyroclastic current indicate topographically induced deflections and channelling, combined with flow separation (Kieffer, 1981; Sisson, 1995). Variations of particle fabrics in the Ata ignimbrite, Japan (Suzuki-Kamata and Ui, 1982), indicate topographic deflections during deposition. Similar features in the Campanian ignimbrite, Italy, have been interpreted "as recording backwards reflection" caused by local topography (Fisher et al., 1993).

2.4.2. Decoupling styles

There a several modes of individual advance of the separated flow parts that can classify as decoupling. The basal avalanche can either slow down or come completely to rest while the ash cloud surge travels ahead and deposits a thin ash layer below

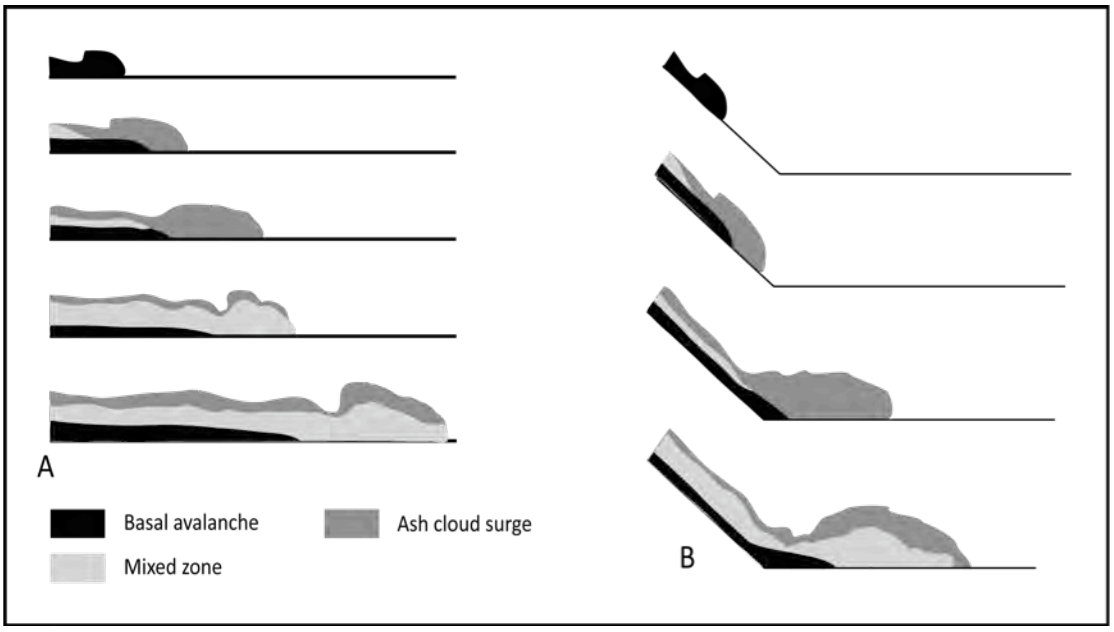

Figure 2.3: Simplified sketch of possible decoupling scenarios. (A) The basal avalanche will show a decrease in velocity when flowing over nearly flat surfaces, the ash cloud surge can rush ahead. (B) Density current encountering a break in slope will experience a thickness decrease in the basal avalanche and increased turbulence of the more dilute flow levels.

the overriding block-and-ash flow. This scenario is most likely associated with a break in slope or the runout over a nearly horizontal plain (Figure 2.3), when the basal flow show a drastic decrease in kinetic energy and momentum, as has been documented at Merapi Volcano (Abdurachman et al., 2000). Two locations were described as onsets of decoupling – a prominent, 80m high cliff high on the slope as well as the pronounced break in slope at the base of the proximal cone. There, the basal avalanche is expected to strongly, and continuously, reduce its velocity, eventually through a hydraulic jump that would lead to the transfer of more particles into suspension due to increased turbulence (Bourdier and Abdurachman, 2001).

The entrainment of substrate material further from the source can contribute to the reduction of energy, because the current has to transfer energy into the substrate to mobilize and entrain it, resulting in limited travel-distance of the basal granular flow.

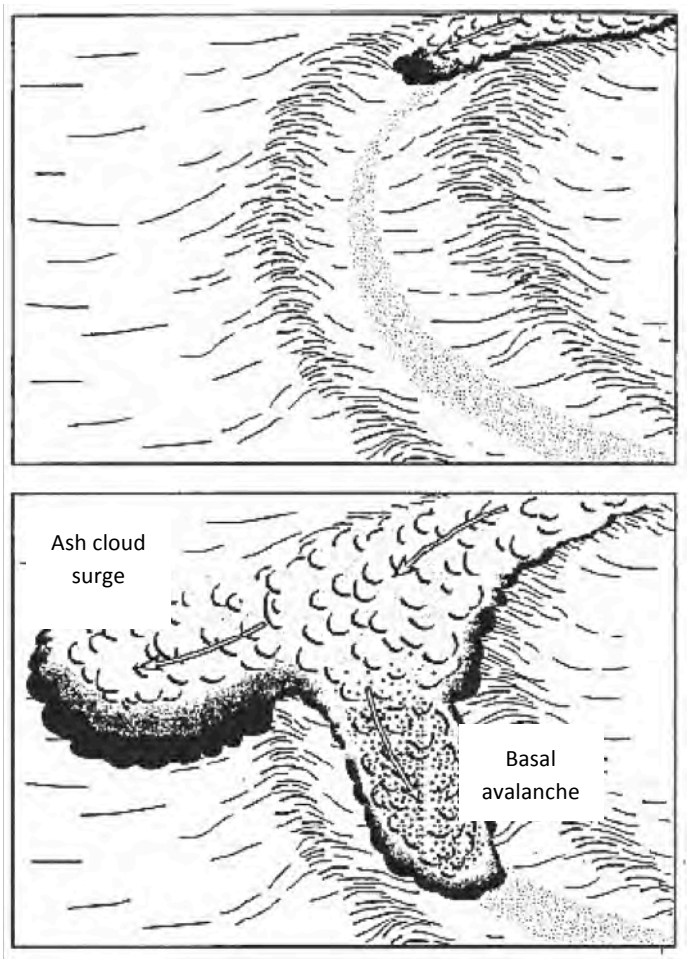

Figure 2.4: Decoupling can occur when the basal avalanche is channelled and directed away by curved valleys. The unconfined ash cloud surge will move straight ahead (modified after Piper and Normark, 1983).

Another possible decoupling scenario is the result of channelling of the basal avalanche within valleys high on the volcanic slope, either in straight or curved channels. In particular, curved and meandering channels will direct the confined basal avalanche away from the unconfined ash cloud surge that can travel straight ahead (Figure 2.4), as has been observed at Volcán Tungurahua in Ecuador (Stinton and Sheridan, 2008). During the confined advance of the basal underflow, decoupling can occur repeatedly, due to the fact that fragmentation will continue within the granular avalanche and new ash cloud surges can be formed.

When stratified flows encounter obstacles in their path, such as ridges, dams or buildings, the lower part can be blocked and diverted around the obstacle, while the ash cloud surge can mount and overtop the obstacle (Figure 2.5). This behaviour has been described mostly in powder-snow avalanche research, where the influence of deflecting dams and mounds has been studied in detail e.g. by Naaim-Bouvet et al. (2002), Hákonardóttir et al. (2003), Primus et al. (2004) and Sampl et al. (2004).

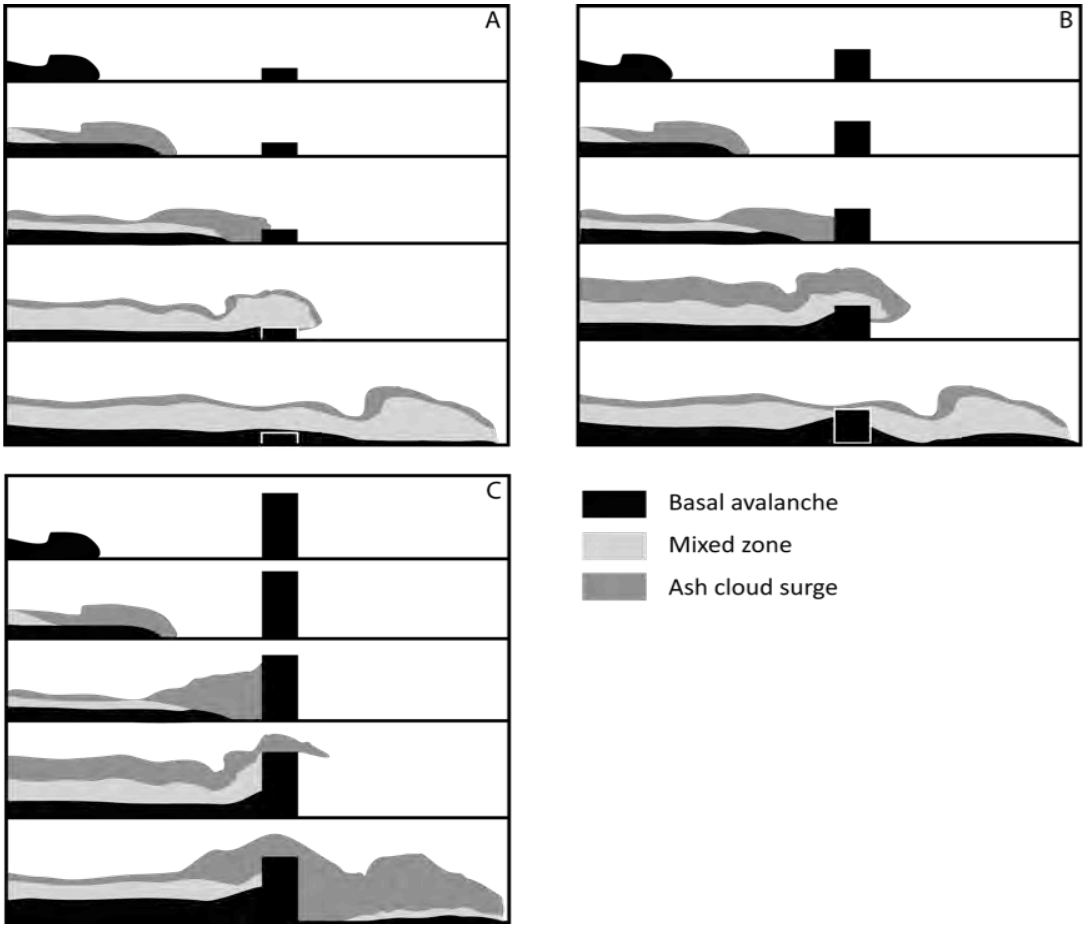

Figure 2.5: Simplified sketch of stratified currents encountering barriers of various heights, resulting in partial blocking and the generation of "secondary" currents after flow passed over barrier (modified after Amy et al., 2005).

Overspilling of parts of valley-confined basal avalanches, as has been described at Merapi Volcano (Charbonnier and Gertisser, 2008), is an underestimated hazard during these events, but cannot be termed decoupling. The same holds true for pyroclastic density currents entering a lake or the ocean, although a separation of the flow parts can be observed (Freundt, 2003). The hot flows enter the water and the dense avalanche travels as a submarine debris flow, while the less dense part of the original flow will travel over the water surface. Due to the fact that the flows enter a new and denser medium after their subaerial formation, this behaviour cannot be regarded as decoupling or flow stripping which will occur only within the same ambient fluid, air or water respectively.

2.4.3. Influential topographic features

Typically, the interactions of any pyroclastic currents with pre-existing topographies include channeling along pre-existing valleys and channels, blocking or deflection by natural and artificial barriers, velocity decrease due to changes in the slope as well as decoupling.

The effect of topographic barriers on pyroclastic density currents has been studied in detail for dilute, voluminous currents such as the Taupo Ignimbrite (Legros and Kelfoun, 2000), but not quantitatively for smaller block-and-ash flows. The question is how does the interaction of a block-and-ash flow with the topography affect its flow behaviour with regard to possible decoupling or flow stripping? Fisher (1995) recognized the possible accentuation of decoupling effects by pre-exisiting topographies and pointed out the need for a quantitative study of the influence of (topographic) barriers and restrictions of the pyroclastic flows path. He emphasized that the encounter of the pyroclastic density current with the pre-existing topography, especially with steep mountain ridges of high relief, can lead to decoupling.

Pyroclastic density currents can interact in several ways with the pre-existing topography and any man-made barriers, their flow behaviour is determined by their volume and temporal downslope development. Large pyroclastic density currents

(mass fluxes > 110 kgs^{-1}), generated by eruption column collapses, have been described as climbing topographic barriers over 1 km high more than 20 km from their source, e.g. the Ito ignimbrite travelled 70 km over topographic barriers of > 600 m (Aramaki and Ui, 1966), whereas the Taupo ignimbrite mantles mountains as high as 1.5 km up to 45 km from the volcano (Wilson, 1985). Smaller flows, e.g. block-and-ash flows, usually have shorter runouts (< 10 km) and are not able to climb such topographic highs; their flow dynamics are more heavily influenced by the pre-exisiting topography, even more than that of voluminous currents.

Larger pyroclastic density currents travel as dilute, buoyant flows (Woods et al., 1998), whereas block-and-ash flows exhibit usually flow transformation and stratification. Stratified flows are more strongly influenced by the landscape, river channels and valleys or ridges can confine and divert parts of the flows, whereas others can move unconfined.

A series of factors will control the dynamics of the block-and-ash flows and their possible decoupling, such as the profile of the volcanic slope with slope breaks, valleys and ridges as well as the heights of barriers and their distance from the source.

2.4.3.1. Breaks in slope

The flanks of volcanoes are usually steep, with proximal slope angles of > 40°. Breaks in slope typically occur at the foot of the lava dome near the summit of the volcano and at the foot of the volcano itself, e.g. at Ngauruhoe volcano in New Zealand the slope angle decreases from > 30° to 20° high on the slope and further to < 10° near the foot of the volcano (Nairn and Self, 1978). Similar slope characteristics have been documented e.g. at El Chicon volcano (Macias et al., 1998), Merapi volcano (Bourdier and Abdurachman, 2001) and Colima volcano (Saucedo et al., 2002). Pyroclastic density currents encountering a dramatic slope reduction will drastically reduce the velocity of the basal avalanche, causing the development of a turbulent, vigorously convecting ash cloud, possibly as a consequence of air entrainment within a hydraulic or granular jump (Woods and Bursik, 1994). While the basal avalanche

decelerates, the upper ash cloud continues to move at a nearly constant rate (Nairn and Self, 1978; Denlinger, 1987; Palladino and Valentine, 1995; Freundt and Bursik, 1998) and so detaches, becoming an independent dilute pyroclastic current (Fisher and Heiken, 1982; Mellors et al., 1988; Fujii and Nakada, 1999; Takahashi and Tsujimoto, 2000).

The reduction in speed can lead to a decreased transport capability for larger clasts and their deposition, as has been documented e.g. for the Neapolitan Yellow Tuff (Cole and Scarpati, 1993), at Laacher See volcano (Freundt and Schmincke, 1985), Mount St.Helens (Levine and Kieffer, 1991) and El Chichon volcano (Macías et al., 1998). However, the continued breakage of particles and release of gas within this flow can aid propagation of the current beyond the break in slope; these processes sustain an upward gas current which is capable of keeping large particles moving within a fine-grained matrix (Saucedo et al., 2004).

The decrease in the bed slope can lead to the direction of parts of the momentum flux per unit area into the substrate, increasing the normal stress at the substrate layer (Iverson and Denlinger, 2001) and resulting in greater normal bed frictional forces (Sulpizio and Dellino, 2008). Deceleration of the current due to an increase in normal bed stress and lowering of the slope increases velocity gradients and flow turbulence (Gray et al., 2005) that may in turn increase the elutriation of fines and lofting. Beyond the break in slope, flow deceleration migrates into the flow-boundary zone and reduces the granular temperature (Iverson, 1997) in the basal underflow. Both processes combined can increase frictional forces at the base of the current, forcing the basal underflow to decelerate and deposit. The ash cloud surge can rush ahead and be deposited below the block-and-ash flow deposit, as has been observed at Merapi in 1994 (Abdurachman et al., 2000) and Soufriére Hills Volcano in 1997 (Druitt et al., 2002).

2.4.3.2. Confined flow conditions

Volcanic slopes are often deeply incised by river valleys and channels, generally extending to the foot of the volcano and beyond, e.g at Merapi volcano and

Soufriere Hills Volcano. These channels are usually the most significant morphological feature of the volcanic landscape, dominating the motion of pyroclastic density currents and their depositional behaviour. The morphology of the channels is highly variable, with regard to shape (e.g. U- or V-shaped), depth and width as well as the channel character (sinuous, meandering or straight).

Channeling of pyroclastic density currents within these valleys depends on their morphology, especially depth and width; generally most of the coarse basal underflow will be confined to the valleys, whereas the billowing ash cloud surge can move unconfined, not following the direction of the basal avalanche (Abdurachman et al., 2000).

Confining block-and-ash flows to pre-exisiting channels and valleys generally prolongs their travel distance. Flows confined to the channels have longer run-outs, maintain higher velocities for longer periods of time, and usually have shorter travel times (Stinton, 2007). Unconfined flows exhibit lateral spreading with thin deposits, whereas confined flows usually deposit within the channels, reaching deposit thicknesses of several tens of metres. Successive pyroclastic currents will rapidly fill the valleys, therefore reducing the channel depth and width and smoothing the pre-exisiting rough topography.

Channel parameters, such as axial slope or cross-sectional geometry, are known to affect in-channel flow dynamics in subaerial meandering channels (Engelund, 1974; Nelson and Smith, 1989). The cross-sectional geometry of these channels can be described bythe width to (1) depth ratio, (2) channel symmetry and/or (3) sinuosity. Natural subaerial channels often display a well-developed channel asymmetry; within sinuous systems the outside levée is constantly higher and/or wider than the inner leveé (Pirmez and Imran, 2003). This asymmetry is the result of channel overspill at bend apexes.

Sinousity has been used to describe the geometry of meandering subaerial channels and submarine canyons, varying from occasional bends in the channel to highly sinuous channels with numerous cut-off bends. Channel sinuosity is measured as the ratio between the channel axis (centre line) length and the overall down-channel distance for a given reach of channel. A sinuosity of 1 therefore represents a straight

section of channel, with increasing values representing increasing sinuosity (Wynn et al., 2002), and increasing probability of decoupling.

Sinuous valleys and channels typically exhibit abrupt changes in curvature, leading to slowing of the heads of the flows, increasing flow depth and causing parts of the flow body to spill over channel margins. If the change in valley direction is more gradual, most of the basal avalanche will be diverted, whereas the ash cloud surge will move independently, not following the course of the valley.

Where pyroclastic currents pass through a constriction in the channel, their thickness increases by a factor proportional to that of the reduction in channel width (Stinton and Sheridan, 2008). For flows confined to constricted channels, run-out is longer than for comparable flows in to non-constricted channels. Flows in channels with uniform width have longer run-outs than corresponding unchannelled flows. This suggests that channelization of the flows preserves momentum by inhibiting spreading. Channel constrictions may also lead to the development of pulses as flows are impeded in an incremental fashion from front to rear. When running up the outside of channel bends, the flows slow and thicken. Flows can also move overbank at the bends, resulting in laterally unconfined flows that slow and thin rapidly.

The most common processes by which sediment is transferred from channelized currents to overbank flow are referred to as flow stripping (see section 2.2) and flow spilling (Piper and Normark, 1983; Clark and Pickering, 1996; Peakall et al., 2000; Kassem and Inram, 2005). Flow stripping usually takes place along the outer bank of a bend, with the separated upper fraction of the current moving independently out across the overbank surface (Piper and Normark, 1983). Flow spilling is not a site-specific mechanism, but describes a process in which a supra-channel fraction of a current spreads laterally out across the overbank surface (Clark and Pickering, 1996). This lateral spreading is interpreted as being a consequence of the gravitational collapse of the non-confined portion of the density current. Another recognized process producing overbanking flow is referred to as inertial overspill (Hay, 1987). This is the result of spatial changes in channel width and takes place only when the curvature of an outer bank exceeds that of the channel axis, as has been observed at

Merapi volcano for block-and-ash flows in 2006 (Charbonnier and Gertisser, 2008).

2.4.3.3. Obstacles/barriers in the flow path

Pyroclastic density currents encounter barriers during their advance - natural obstacles in form of ridges and hills as well as artifically designed dams (e.g. SABO dams; Sigurdsson et al., 2000), deflecting mounds and buildings. The behaviour of pyroclastic density currents around obstacles or obstructing topographies will vary with the velocity of the currents, the obstacle height, the current density and density stratification within the flow (e.g. Valentine, 1987; Lane-Serff et al., 1995; Alexander and Morris, 1994).

Homogeneous and steady currents (if they ever exist in reality) with a free surface are expected to interact with topography or obstacles as supercritical or subcritical flows, by partial or complete blocking with and without a lee jump or by complete blocking of the flows by the obstacle (Rottman et al., 1985). Large, dilute pyroclastic density currents (mass fluxes ≥ about 100kgs^{-1}) have been described to climb topographic barriers up to 1 km high even more than 20 km from their source, e.g. the Taupo ignimbrite mantles mountains as high as 1.5 km up to 45 km from the volcano (Wilson, 1985).

In contrast, stratified flows such as block-and-ash flows, will exhibit flow transformation; partial blocking will lead to decoupling of the upper, dilute and turbulent flow part that will move over the obstacle whereas the granular basal avalanche will either be ponded, or diverted around the barrier (Baines 1995; Woods et al., 1998).

The behaviour of the current when meeting an obstacle depends on the height of the obstacle relative to the thickness of the flow. If the obstacle is smaller than the flow, it is likely to have little effect on the flow behaviour but may influence bed-form character and sediment distribution.

If the obstacle is considerable higher than the head height, the flow splashes up the obstacle to a height about twice the flow thickness (Simpson, 1997) and a hydraulic jump is reflected from the obstacle (Edwards, 1993). For obstacles that are much

higher or larger than the current, two scenarios can be considered, based on the extent of density stratification of the current. For relatively poorly stratified currents, the maximum run-up height is probably dependent on the bulk Froude number of the current by energy conservation (Rottman et al., 1985):

$$h_{\max} = \frac{1}{2}\left(\frac{\overline{U^2}}{g'}\right)$$

For strongly stratified currents, Kneller and McCaffrey (1999) suggested an expression for maximum run-up height that takes velocity and density profiles of the current into account. This expression is based on the energy balance arguments by Allen (1985):

$$h_{\max} = y + \frac{\rho_y u_y^2 (1 - E)}{2g\Delta\rho_y}$$

where u_y is the downstream component of velocity at initial height y, g is gravity acceleration, $\Delta\rho_y$ is the density difference between the fluid at initial height y and the ambient fluid, and E is the fractional energy loss due to friction. The value of y that yields the highest run-up of any parcel of fluid in the current is given by:

$$\frac{d}{dy}\left[y + \frac{\rho_y u_y^2 (1 - E)}{2g\Delta\rho_y}\right] = 0$$

h_{max} is therefore a function of the velocity and density profiles, and cannot be generalized in systems in which density stratification is significant – as in most sediment-laden systems.

If the barrier is less than about twice the flow thickness, some of the flow is likely to pass over the obstacle and a solitary wave is reflected. In density-stratified flows the lower, denser part of the flow is likely to behave differently from the less dense cloud above, e.g. the flow may be ponded by relatively small topographic obstacles, leading to decoupling (Druitt, 1992) and part of the flow may be reflected or diverted while another part continues forward. The higher, less dense levels of the

current are less constrained by topography and may travel further, unless mixing of air is promoted and causes the current to loft.

2.4.4. Changes in topography during pyroclastic density current emplacement

The influence of topography on the flow dynamics of pyroclastic density currents is extensive and widely documented, but it is very important to consider changes in morphology during the emplacement of successive currents, e.g. resulting in mantling and smoothing of previously rugged landscapes.

The deposition from pyroclastic currents, as well as post-eruptional mass movements (lahars, debris flows) and water-induced erosion can significantly alter the topography over which subsequent pyroclastic density currents will travel. Even a slight change in the local topography could affect the behavior of the next flow.

In valleys repeatedly affected by pyroclastic density currents, it is possible for thick sequences of deposits to accumulate, gradually raising the valley floor, smoothing the landscape and decreasing the influence of channel geometries on flow dynamics. During periods of quiescence, water-induced erosion may incise wide channels with terraces, resulting in significant changes to the geomorphology of the valley (Stinton and Sheridan, 2008),

The effects of the new morphology depend on the nature and extent of the change, e.g. erosion can deepen channels, leading to confinement of pyroclastic flows and increased run-outs. Alternatively, if incised channels narrow suddenly or decrease in depth, the mobility of a flow could be severely reduced, respectively resulting in the accumulation of thick deposits in a relatively confined area or extensive lateral spreading with thinner deposits. Although meandering valleys may be partly inundated, flow spilling from earlier flows can result in overbank deposition and increased levee heights, so later currents might still be influenced by the meandering channel geometry.

Most pyroclastic eruptions are associated with generation of multiple pyroclastic density currents. At Unzen Volcano, more than 9000 block-and-ash flows, generated by multiple collapse of the lava dome, have been reported within a five-year

eruptive episode, extensively altering the pre-existing landscape, and influencing the behaviour of the flows (Miyabuchi, 1999). The generation and deposition of successive flows have to be taken into consideration for the design of evacuation plans and hazard management around volcanoes.

2.5. Case studies

The detachment of the ash cloud surge from the underlying basal avalanche has been directly observed at Mount St.Helens (Hoblitt, 1986) and at Soufriére Hills Volcano (Loughlin et al., 2002), but is typically inferred from the distribution of surge facies and surge-related destruction from well-defined pyroclastic flow events, e.g. at Santiaguito (Rose et al., 1977), Ngauruhoe (Nairn and Self, 1978), Mount St.Helens (Mellors et al., 1988), Unzen volcano (Nakada and Fujii, 1993; Yamamoto et al., 1993) and Soufriére Hills volcano (Druitt et al., 2002).

Eyewitness reports of pyroclastic density currents (e.g. Mount St.Helens in 1980; Mayon in 1984 and Ngauruhoe in 1975), especially of the billowing ash cloud, are consistent with observations of rock- and powder-snow avalanche clouds, all of which bear a striking similarities (Sheridan, 1979; Anderson and Flett, 1903). Although each turbulent (dust/snow) cloud first develops as a plume trailing the flow, the cloud often outruns the avalanche that produced it. The cloud density may increase rapidly, while its flow properties remain similar to that of the surrounding air, giving the cloud great mobility (Denlinger, 1987). The cloud then often takes a different path than the avalanche, since its movement is less influenced by the terrain.

Several case studies will be discussed in detail with special reference to decoupling initiation and possible topographic influence. Possible common similarities will be compiled and discussed to generate a catalogue of decoupling indicators.

2.5.1. Merapi Volcano, Indonesia

Merapi Volcano is one of the most active volcanoes in the world, whose eruptions are often characterized by episodic dome growth followed by repeated collapse of parts of the dome. Decoupling is a common occurrence at Merapi; Bourdier and Abdurachman (2001) collected data about block-and-ash flow activity and the impact of ash cloud surges from historic descriptions since 1930. Twenty-three of these events have been recorded, at least 16 of them were associated with destruction outside the valleys and channels on the slope, all characterized by travel

distances beyond 6.5 km. Shorter block-and-ash flows with run-outs between 5-6.5 km showed lesser destructive potential with minor damage to the vegetation. However, despite confirmation of decoupling as a recurring event at Merapi Volcano, the latest block-and-ash flows in 2006 did not show a detachment of the ash cloud surge from the basal avalanche (see section 2.5.1.2).

The volcano is characterized by a proximal slope of c. 30° within 1.5 km distance, followed by at least two breaks in slope being documented beyond 1.5 km horizontal distance from the dome. The first break in slope changes inclination from c. 30° to 20° at 1530 masl, while the second break in slope leads to the lower flank with slope angles below 20° at 1270 masl. The steep slope favours high flow velocities, supporting the transfer of particles into the ash cloud surge (Denlinger, 1987).

Kelfoun et al. (2000) suggested that the pronounced change in slope at the base of the proximal cone represents the location of detachment of the ash cloud surge from the basal avalanche due to decreased velocity, partial deposition of the avalanche and increased transfer of ash particles into the surge. Bourdier and Abdurachman (2001) suggested that for the generation of large-scale detachment of the surge, a significant velocity differential is required, allowing the surge to travel ahead of the basal avalanche.

2.5.1.1. 1994 eruption

During the eruption in 1994, block-and-ash flows were generated during the collapse of southwestern parts of the newly emplaced lava dome. The flows were mainly restricted to numerous river channels to the south and southwest (Krasak, Bedok, Boyong and Kuning rivers), showing run-outs of c. 6.5 km. The main surge associated with the block-and-ash flows detached from the basal avalanche, left the Boyong drainage and cascaded rapidly over the east lobe (Figure 2.6). Later surges were probably generated by the same block-and-ash flow as it descended along the course of the Boyong river. They were weaker than the first one possibly due to generation on gentler slopes (Abdurachman et al., 2000).

Decoupling at Merapi during the eruption in 1994 is generally influenced by the pre-existing topography. At an altitude of c. 1700 m, block-and-ash flows encountered a sudden decrease in slope, resulting in a fragmentation peak within the flows. Increase in turbulence by the break in slope enhanced mixing with the ambient air, generating voluminous ash cloud surges (Kelfoun et al., 2000). At an elevation of about 1400 m, the Boyong river channel swings to the SSE, channeling and directing the basal avalanche eastwards whereas the ash cloud surge detached and traveled straight ahead, insensitive to topopgraphic restrictions. The surge deposits were therefore emplaced before the basal avalanche arrived, and fine ash cloud surge layers can be found beneath the deposits of the avalanche.

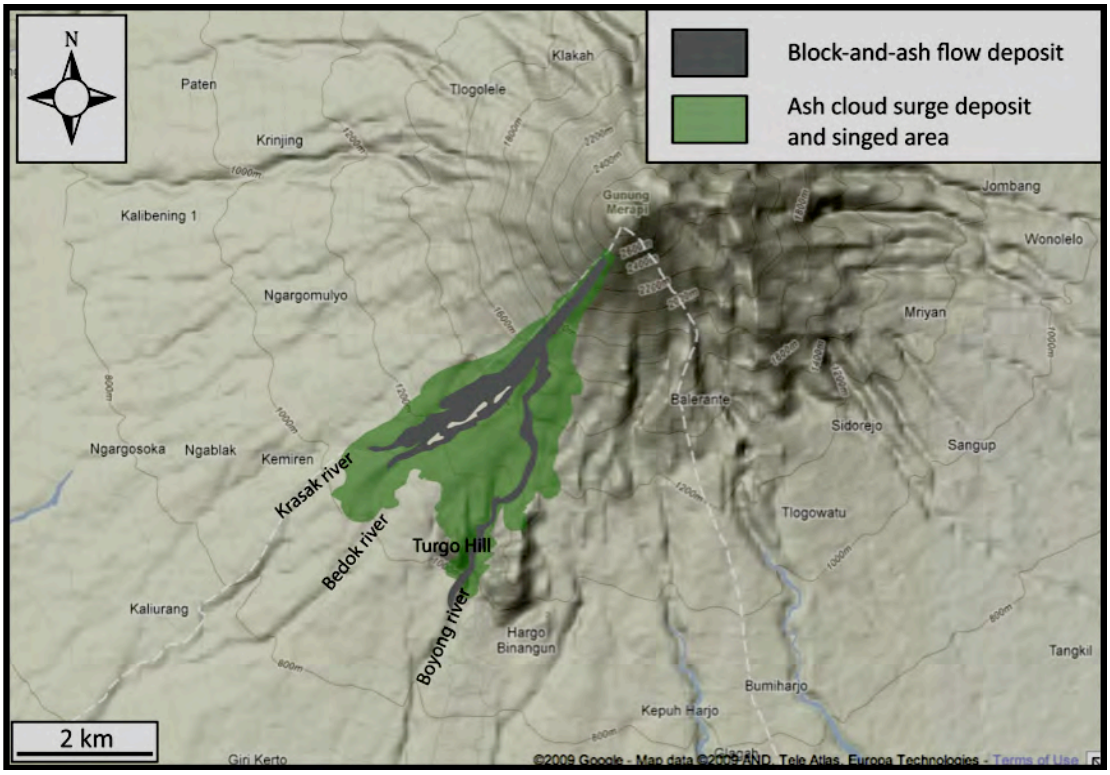

Figure 2.6: Distribution of block-and-ash flow deposits and detached ash cloud surges at Merapi Volcano during the eruption in 1994 (modified after Abdurachman et al., 2000).

Flow separation was likely aided by large-scale roughness of the flow path, particularly in the zone of wall overtopping. Thus, the surge currents were able to separate from the coarse basal flows and could pass across the interfluve. The south lobe of this surge flowed toward and around Turgo Hill to emplace its deposit even as the channeled block-and-ash flow, blocked from spreading out by the steep Boyong ravine topography (less than 20 m deep in that sector), continued its

tortuous southward movement. In this case the ash cloud surge was able to outrun the dense flow. Block-and-ash flows had volumes of 2.5-3×10^6 m^3, with H/L ratios of 0.18-0.2 (drop height 1300-1200m with c. 6.5 km run-out).

2.5.1.2. Eruption in 2006

During the eruption from May to June 2006, a series of block-and-ash flows was observed (Charbonnier and Gertisser, 2008), generated by gravitational lava dome collapse over a period of two months. Single-pulse and sustained dome collapse was described during this time, resulting in numerous flows that were emplaced in nine lobes towards the southwestern (May 2006) and southern (June 2006) flanks of the volcano. In contrast to the eruption in 1994, no separation of the basal avalanche and the ash cloud surge was detected, despite the flow encountering several pronounced breaks in slope.

However, another phenomenon of great potential risk was described – the spilling of parts of confined basal avalanches over the rims of the channels, spreading laterally onto ridges and interfluves, followed by subsequent channeling into nearby valleys. These overbank pyroclastic flows were able to sweep broader areas than the still-confined basal avalanche, partly burying the village of Kaliadem under c. 8 m of block-and-ash flow deposits. Super-elevation of up to 7 m high at bends was observed 6 km or more from the summit (Charbonnier and Gertisser, 2008). Super-elevation occurs when centrifugal forces cause the mass of debris to rise up the outside of bends.

The lack of decoupling during the eruption in 2006 was probably the result of continous infilling of the valleys and gullies on the volcanic slope during earlier block-and-ash flow events, smoothing the landscape by decreasing the valley depths and widths. The small valley depth makes it difficult to accommodate the whole influx of block-and-ash flows, meandering or branching of the channels is subdued as well, therefore the topographic influence is not pronounced enough to initiate decoupling, but can result in overspilling and more lateral spreading of the flows.

2.5.2. Unzen Volcano, Japan

During 1990-1995, Unzen volcano in Japan experienced large-scale collapse of the dacitic lava dome, generating > 9400 small-volume pyroclastic density currents during this time. This stratovolcano is situated on the central part of Shimabara Peninsula; after quiescence of nearly 200 years, the volcano erupted in November 1990, followed by continuous dome growth with associated repeated collapse of the summmit dome. On June 3rd 1991, block-and-ash flows with a volume of c. 0.5-0.7 x 10^6 m^3 were generated by the collapse of a large portion of the dome, descending the eastern slope and travelling 3.6 km towards Shimabara (Yamamoto et al., 1993). When the basal avalanche was channeled by topography, the ash cloud went straight ahead, detaching from the basal avalanche and travelling an additional 800 meters, blowing away trees and killing 43 people. The detached ash cloud surge lost its force after several hundred meters, but maintained a high temperature (Yamamoto et al., 1993). The flow direction of the ash cloud surges was indicated by downed trees, suggesting that most surges extended from steep slopes along Mizunashi River at 800 m and 570 m altitude due to topographic control (waterfalls), and from the distal end of the basal avalanche after it came to rest (Figure 2.7).

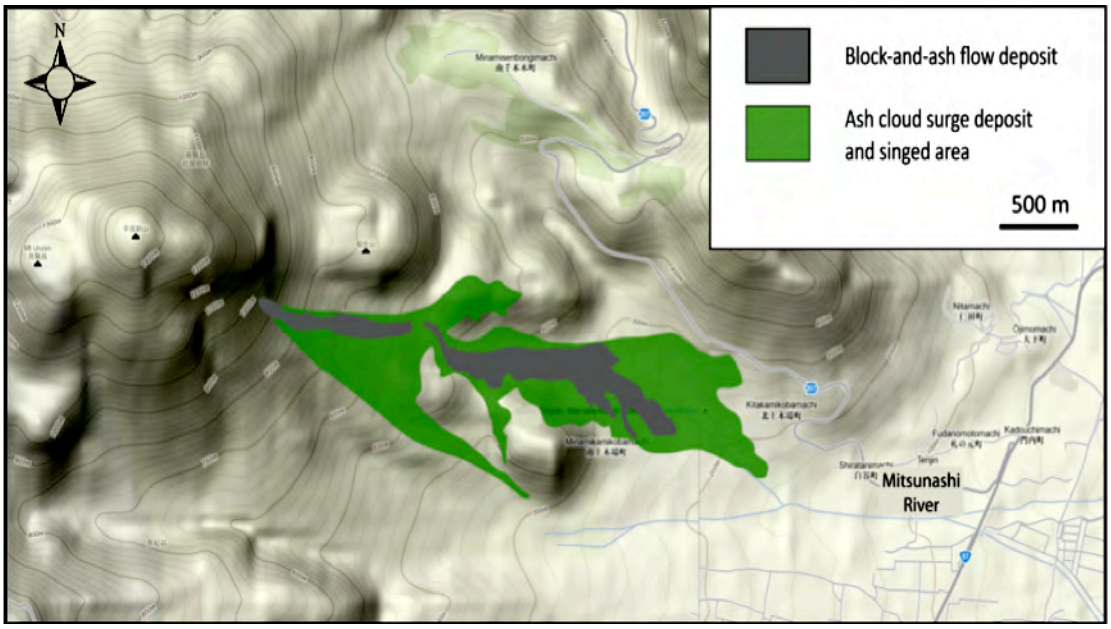

Figure 2.7: Distribution of block-and-ash flow and detached ash cloud surge deposits during the devastating eruption of Unzen Volcano on June 3rd 1991 (modified after Miyabuchi, 1999).

Mobility of the block-and-ash flows on June 3rd was determined with the energy line model of Sheridan (1979), showing a H/L ratio of 0.36. The block-and-ash flows descended over two waterfalls, marking extreme breaks in slope at 800 m and 570 m altitude, with drop heights up to 100 m (Nakada and Fujii, 1993). It was documented that the block-and-ash flows cascading over the waterfalls showed increased energy and speed, probably due to extreme fragmenation of incandescent and gas-enriched lava blocks. Similar reactivation of pyroclastic flows was described in 1929-1932 eruption at Mt. Pelée (Perret, 1937).

Later block-and-ash flows, generated on June 8th and September 15th 1991, reached travel distances of 5.5 km, detachment of ash cloud surges was described as well, but without the devastating effects of the June 3rd flows. The largest block-and-ash flow during the 5-year eruptive episode was recorded on September 15, moving down the northeastern slope along Oshigadani Valley (Miyabuchi, 1999). After the flow passed a confluence of the Oshigadani and Mizunashi River Valleys, the ash cloud surge rushed straight ahead to the SE, while the basal avalanche changed its course to the E due to topographic control (Fujii and Nakada, 1999), leaving the ash cloud surge to travel up to 900 m to the south (Figure 2.8).

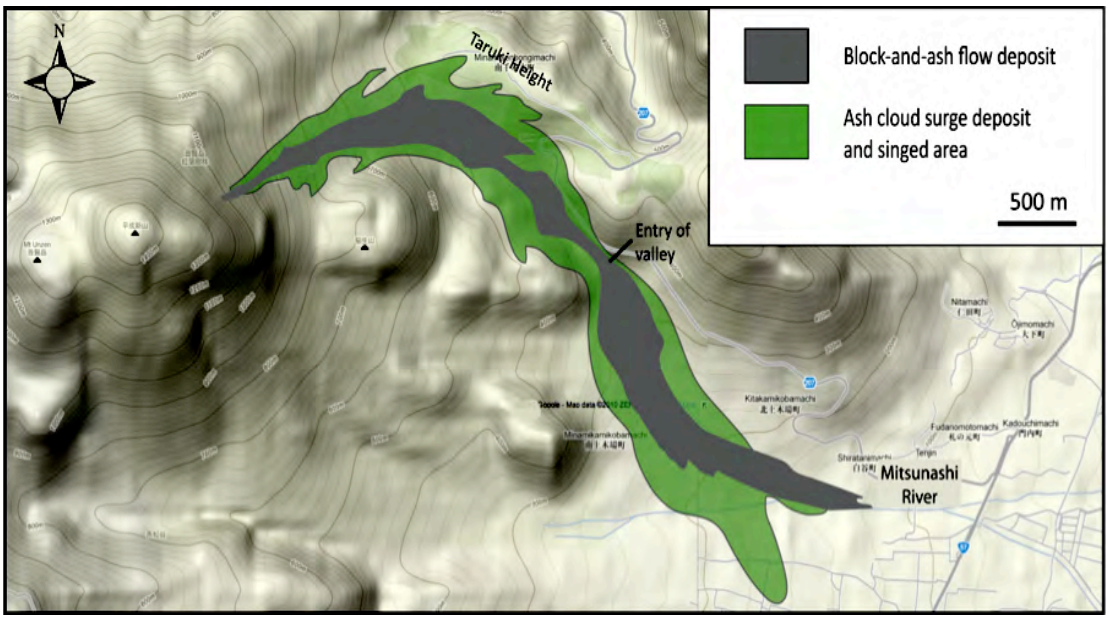

Figure 2.8: Distribution of block-and-ash flow and detached ash cloud surge deposits during the devastating eruption of Unzen Volcano on September 25th 1991 (modified after Miyabuchi, 1999).

2.5.3. Soufriére Hills Volcano, Montserrat

Soufriére Hills Volcano on Montserrat was active between 1995-1999. The collapse of eruption columns from vulcanian eruptions resulted in pumice-and-ash flows, whereas collapse of the andesitic lava dome generated numerous block-and-ash flows (Druitt et al., 2002). A new phenomenon was documented at Soufriére Hills Volcano, characterized by the transformation of the pyroclastic surge into a dense pyroclastic flow with a weaker surge component, due to rapid sedimentation from the parental surge. The new pyroclastic flow, termed "surge-derived pyroclastic flow" (Calder et al., 1999; Druitt et al., 2002) traveled substantially beyond the parent surge (compare section 2.6).

The growth of the lava dome within the English Crater began in November 1995; collapse of parts of the dome generated short block-and-ash flows (max. 2.7 km) in 1996. In 1997, the lava dome filled English Crater, directing the pyroclastic currents over the southern flank, with travel distances up to 4.1 km along White River valley. These flows were less topographically confined due to the progressive infilling of the valley by previous deposits. Similar development could be observed for the northern

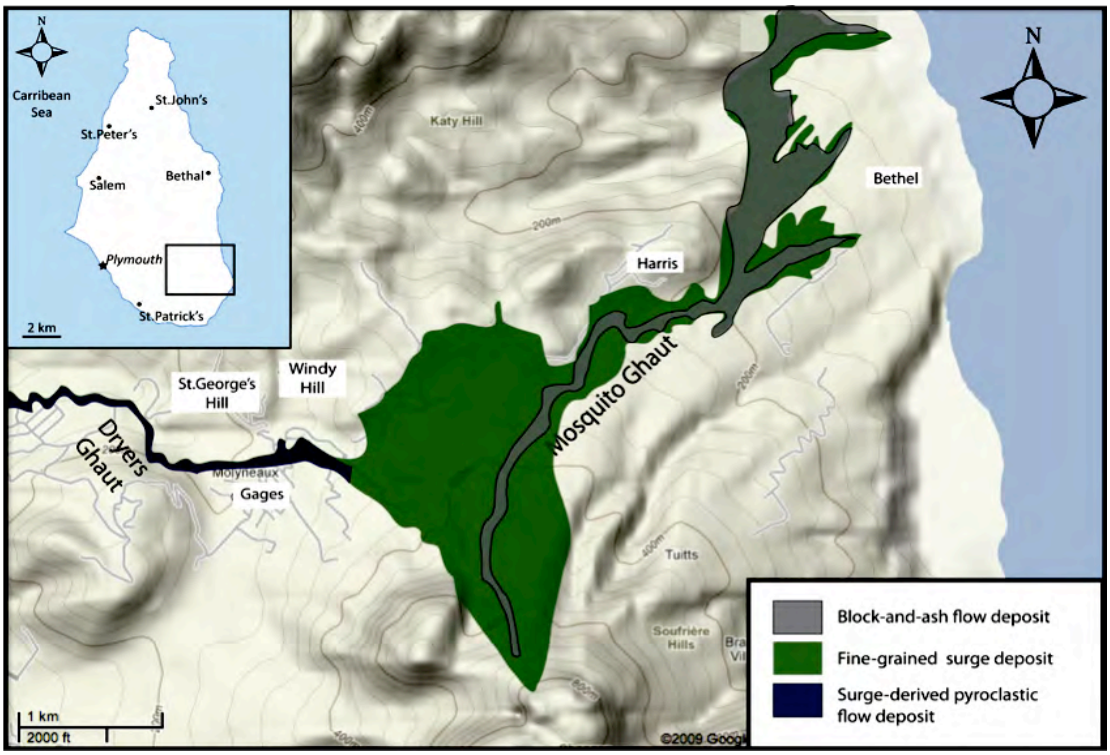

Figure 2.9: Distribution of block-and-ash flow and detached ash cloud surge deposits during the eruption of Soufriere Hills Volcano on June 25th 1991 (modified after Cole et al., 2002).

flank of the volcano, where rockfalls and small flows first moved c. 200 m down Tuitt's Ghaut, later block-and-ash flows traveled c. 3.1 km down the same ghaut.

Decoupling was observed in June and December 1997, often associated with the generation of surge-derived pyroclastic flows from the detached ash cloud surge. During the eruption on June 25, three individual flow pulses were recorded, travelling down the NE flank of the volcano (Loughlin et al., 2002). The first flow was confined to Mosquito Ghaut and Paradise River, reaching as far as the the beginning of Pea Ghaut near Bethel (Figure 2.9). The second pulse immediately followed the first, being more powerful and of longer duration. The flow was again largely constrained by river valleys, however, associated surges were able to spill out of them, especially on the outside of rightward bends in the Mosquito Ghaut. The deposits from the second flow pulse decreased the depth of the valleys and provided a relatively flat base on which the following flows could rapidly advance. As a consequence, the third flow was able to almost completely fill Mosquito Ghaut, and large surges were able to escape to the N and NW, this time extending further than the previous surges. Further, the block-and-ash flow itself was able to escape from the river bed in several places (Figure 2.10), e.g. at bends in the ghaut and where the river bed was not deep enough to restrain the flow.

Detailed studies of Mosquito Ghaut showed that detachment of surges always occurred at channel bends with a minimum angle of 30°, often in association with a constriction of the valley. Shortly after initiation, block-and-ash flows travelled down drainages to the NE, while large part of the ash cloud surge detached (Figure 5.10, location x) and moved northwards over Farrell's Plain and were then blocked by the opposing hillside (Loughlin et al., 2002).

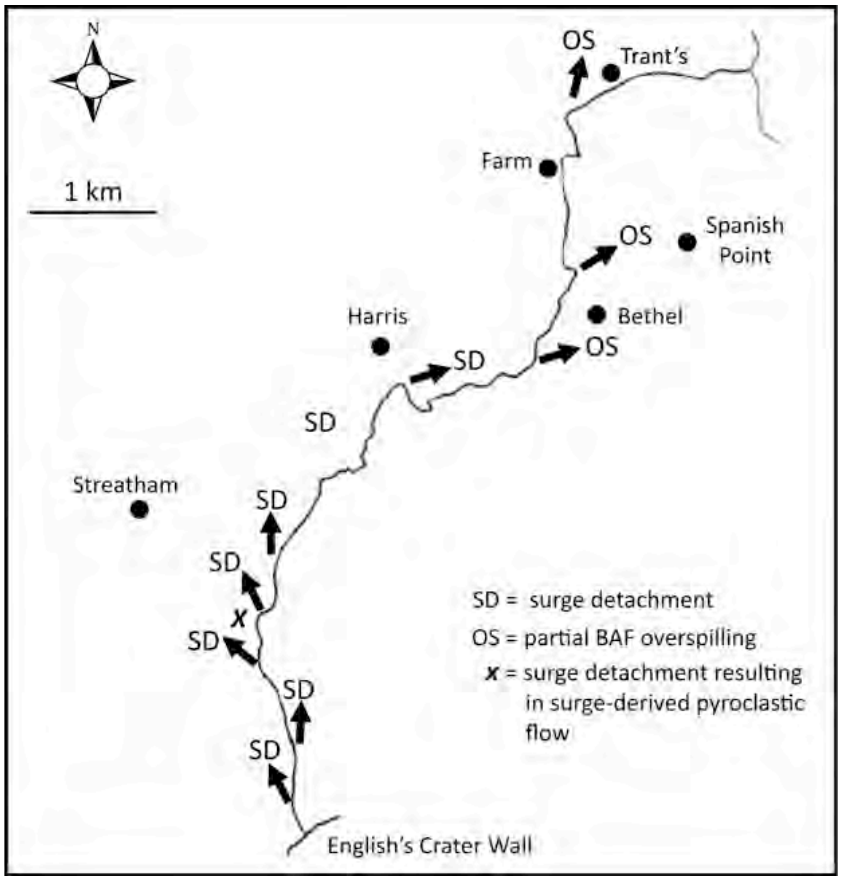

Figure 2.10: Locations of detachment of the ash cloud surge (SD) from the block-and-ash flow descending Mosquito Ghaut. At Location x, a large surge detached and further transformed into surge-derived pyroclastic flows moving towards Streatham. Three major flow pulses traveled down the Ghaut, parts of the last pulse spilled over the valley margins (OS) (modified after Loughlin et al., 2002).

A similar process occurred on 26 December 1997, where a highly energetic pyroclastic density current was generated during the collapse of the southern wall of English' Crater. Much of the basal, higher-concentration part of the current was channelled down the White River valley to the sea, while the upper, more dilute part spilled over the saddle between Galway's Mountain and the South Soufriere Hills (Figure 2.11). Surge-derived pyroclastic flows formed in all drainages inundated by the upper, more dilute part of the density current, including substantial ones down Germans and Gingoes Ghauts. Decoupling of the ash cloud surge occurred directly after generation of the pyroclastic current, the major part of the surge travelled unconfined down the southern flank of the volcano, whereas a smaller parts drained along Dry Ghaut to the northeast, transforming into surge-derived pyroclastic flows (compare section 2.6.).

In contrast to the events in June, this pyroclastic density current was more energetic due to the generation by the rapid decompression of the lava dome, creating a lateral blast. The parent surge was not confined to channels along the southern and southwestern slopes, only the largest surge-derived pyroclastic flow was drained along Dry Ghaut (Figure 2.11).

The lateral blast created a highly energetic pyroclastic surge, which spread further over the entire southwestern volcanic slope, generating several surge-derived pyroclastic flows draining along Germans and Gingoes Ghauts and smaller drainage channels (Figure 2.11). Topographic influence was not important for the decoupling of the surge to the east, merely surge-derived pyroclastic flows were channelled in pre-existing ghauts.

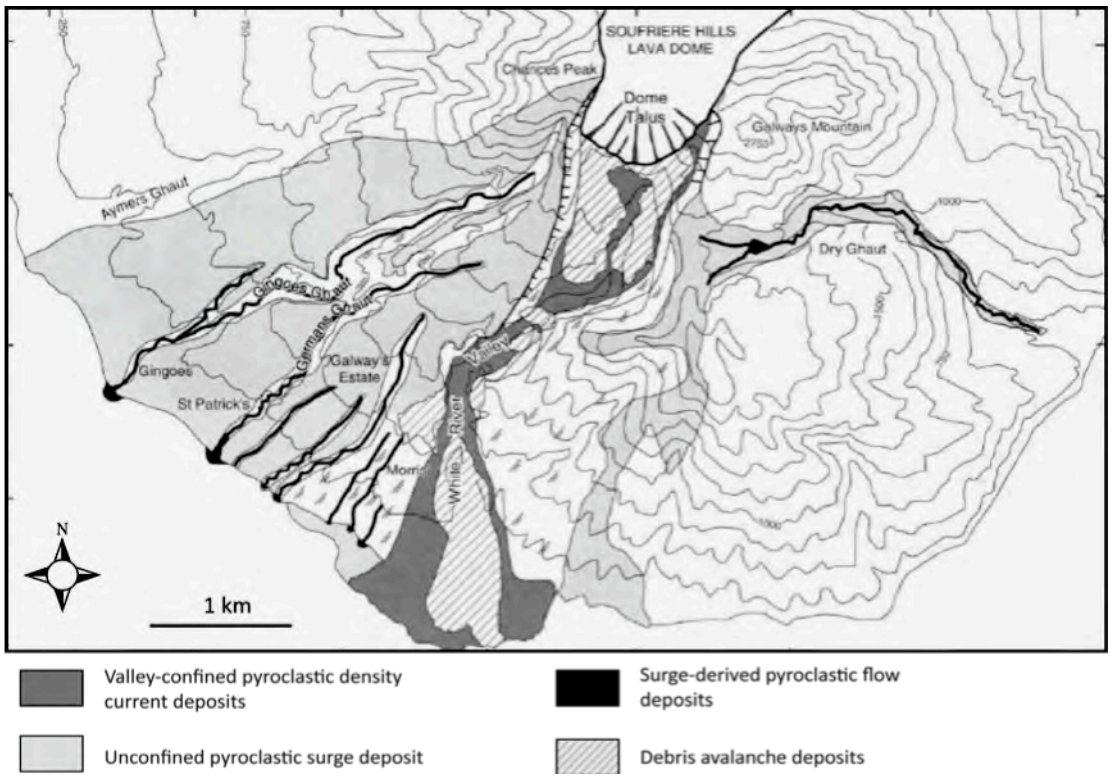

Figure 2.11: Distribution of several block-and-ash flows and associated detached surges generated during the eruption of Soufriere Hills Volcano in December 1997 (modified after Druitt et al., 2002).

2.5.4. Mont Pelée, Martinique

The eruption of Mont Pelée in 1902 is the earliest event documented using the nuée ardent concept (Lacroix, 1904). Pyroclastic density currents were generated by four different mechanisms during the eruption in 1902/03 – by the collapse of vertical eruption columns (Anderson and Flett, 1903), by directed blast (Lacroix, 1904), by the "boiling over" from the crater without the development of a vertical eruption column, and by repeated partial collapse of the growing lava dome. The pyroclastic flows destroying St. Pierre in May 1902 probably formed during the collapse of Vulcanian-type eruption columns (Fisher, 1990).

Similarly to the eruption at Soufrière Hills Volcano, Fisher and Heiken (1982) described the generation of surge-derived pyroclastic flows through gravity segregation from the detached ash cloud surge. This "secondary" block-and-ash flow developed on a gently sloping upland surface c. 100 m above the valley of Rivière Blanche. The associated ash cloud surge maintained sufficient energy to devastate the landscape to distances of c. 3 km (Figure 2.12). The surges refracted around obstacles and at one location, moved up a small valley opposite to the main flow direction (Fisher and Heiken, 1982). H/L ratios at Mont Pelée are 0.11 with vertical drop heights of c. 900m and run-out distances of c. 6 km.

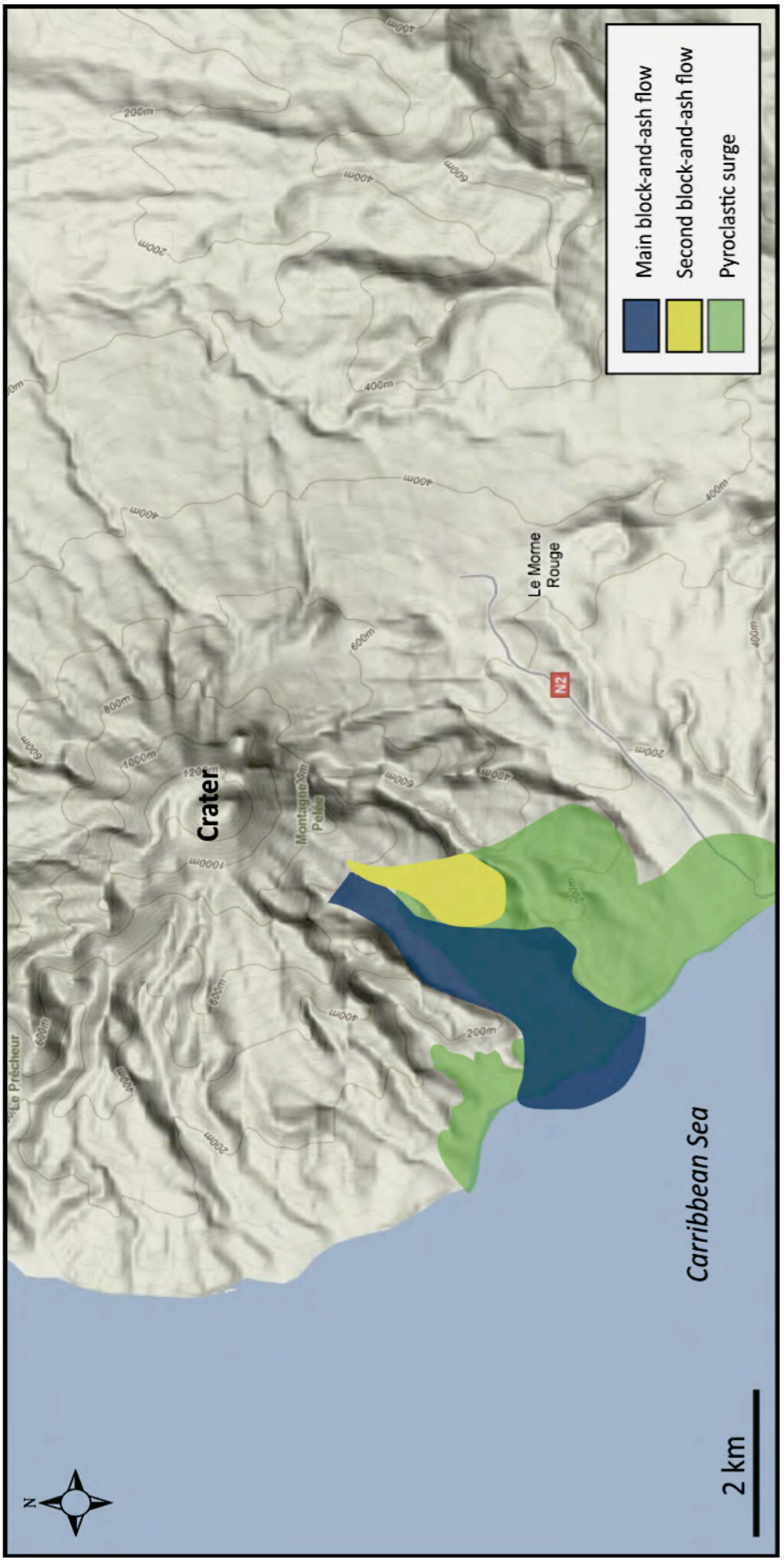

Figure 2.12: Distribution of pyroclastic density currents and associated detached surges generated during the devastating eruption of Mont Pelée in 1902 (modified after Fisher and Heiken, 1982).

2.5.5. Ngauruhoe Volcano, New Zealand

The most recent eruption of Ngauruhoe volcano in 1975 started with gas emissions followed by violently explosive eruptions, ejecting blocks up to 3 km from the vent. Pyroclastic density currents were first generated directly from the explosive eruption, followed by currents developing from the collapse of the eruption column (Nairn and Self, 1978). These currents travelled down the 900 m high volcanic cone, and large convoluted ash clouds rose 500 m above the pyroclastic flows.

The largest avalanche advanced down the steep upper slopes (30-35°) with an average velocity of 30 m/s, before encountering a break in slope (20° to 4°), then moving more slowly (c. 10 m/s) across the floor of Mangatepopo Valley. The pyroclastic density currents were channelled by low points on the summit into two main chutes, one chute below the northern fosse, the other one below the collapsed notch in the northwestern crater rim (Figure 2.13). The pyroclastic avalanches followed these shallow (< 2m) pre-existing channels on the steep upper slopes, before reaching the flatter, lower slope and valley floor and spreading out. The ash cloud surge decoupled from the slow moving basal avalanche and advanced ahead.

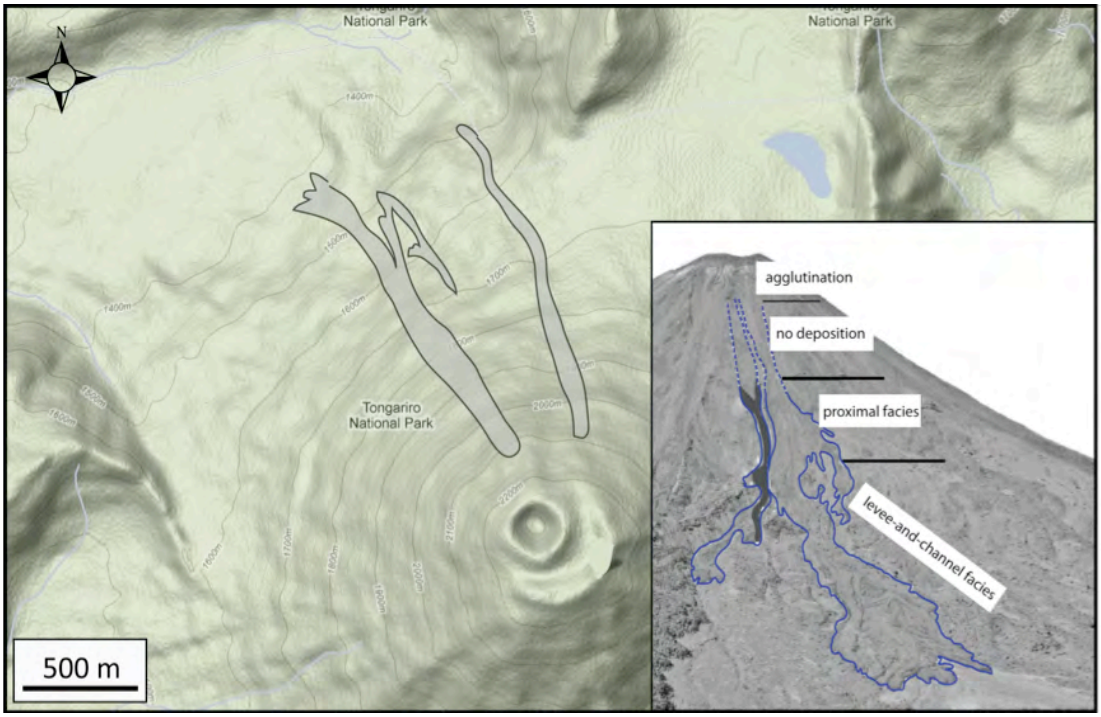

Figure 2.13: Distribution of block-and-ash flows during the eruption of Ngauruhoe volcano in 1975 (modified after Lube et al., 2007).

Travel distances for the flow range between 0.85 and 2.24 km, combined with a drop height of < 1km, resulting in H/L ratios between 0.45 and 0.8 (Lube et al., 2007).

2.5.6. Volcán de Colima, Mexico

Volcán de Colima is located in the western part of the Trans Mexican Volcanic Belt. It is the most active volcano of Mexico in historic time with more than 43 eruptions since 1576, more than 20 being explosive (Saucedo et al., 2005). In 1991, Volcán de Colima began a new episode of magmatic activity that ended with the extrusion of an exogeneous lava dome. Block-and-ash flows were generated during the extrusion of this dome in 1991, traveling down various gullies up to 4 km from the summit, giving an H/L ratio of 0.44. Their deposits are characterized by a maximum thickness of 8 m and an overall volume of 0.8×10^6 m^3.

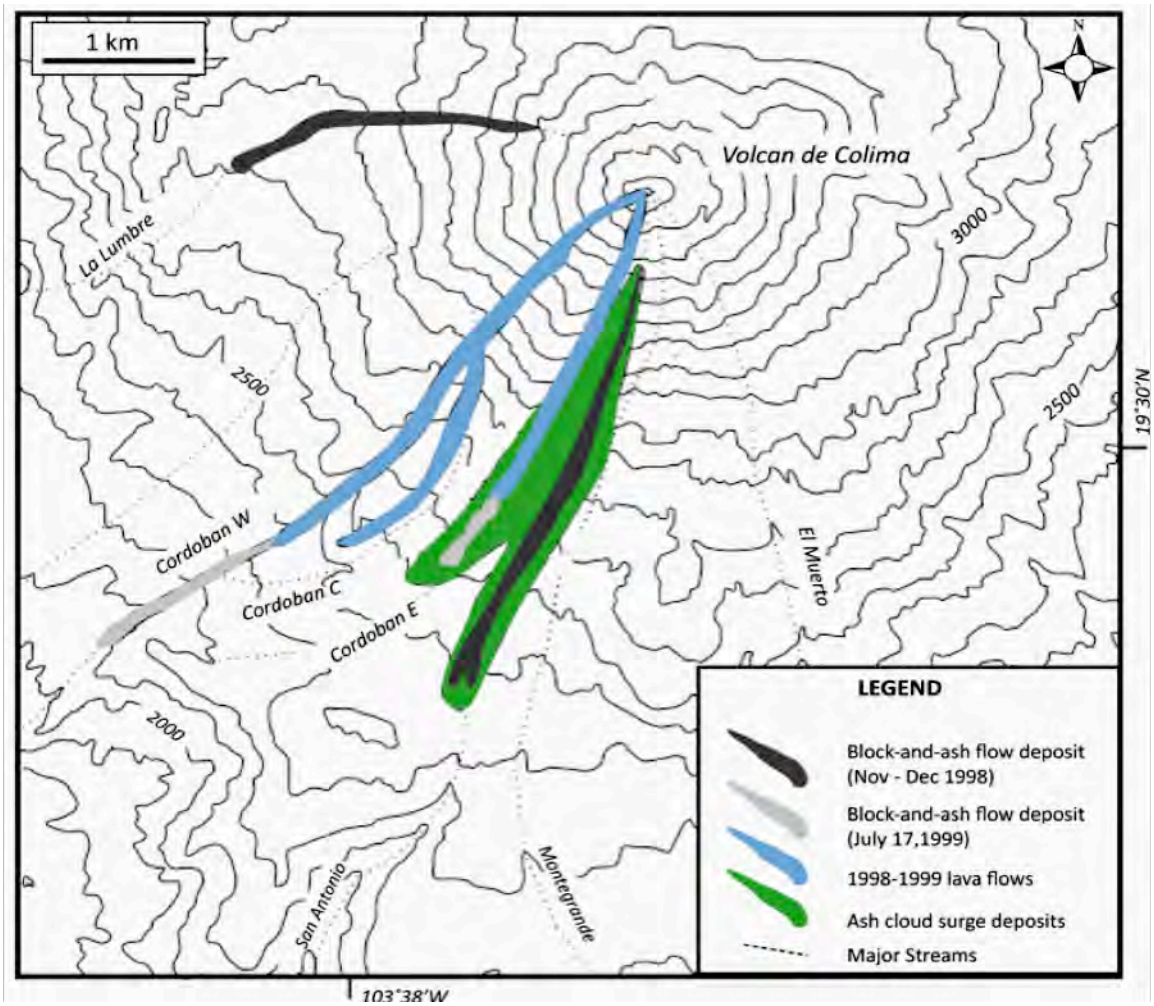

Figure 2.14: Distribution of several block-and-ash flows and the extended run-out distance of associated surges at Colima Volcano (modified after Saucedo et al., 2005).

Block-and-ash flows emplaced during the eruption in 1998-99 were generated by collapse of the fronts of new lava flows. The largest block-and-ash flows reached distances of 4.5 km from the summit (Figure 2.14), with H/L ratios of 0.42, after travelling along ravines on the western side of the volcano. In December 1999, collapse of parts of the lava dome generated block-and-ash flows moving down the eastern flanks. Only after a few seconds, gravity segregation divided the flows into a dense basal avalanche and a turbulent ash cloud. After approaching a break in slope (2 km from source at 2500 masl) which decreases the inclination from >30° to 20°, the basal avalanche decelerated, while the upper ash cloud surge continued to move at a nearly constant rate (Saucedo et al., 2002), detaching from the basal avalanche as a "dilute pyroclastic flow". This flow was able to surmount topographic barriers, emplacing a massive fine-grained block-and-ash flow deposit and a dune-bedded ash cloud surge layer. For all block-and-ash flow deposits between 1998-99, volume and runout of these currents is highly variable, ranging between 3.6-8×10^5 m^3 and 3-4.5 km, respectively. H/L ratios vary between 0.42-0.48, indicating lower mobility of the block-and-ash flows.

2.5.7. Further decoupling examples

Decoupling has also been observed for pyroclastic density currents at Mount St. Helens (Mellors et al., 1988) and Santiaguito volcano (Rose et al., 1977). Comparing the deposits at Mount St. Helens with the ones at Mont Pelée (Fisher and Heiken, 1982), Mellors et al. (1988) deduced that the pyroclastic density currents were derived from a rock avalanche in May 1986 and had undergone decoupling, due to the deceleration of the coarse basal avalanche, giving the ash cloud surge the chance to continue downslope independently.

Santiaguito Volcano erupted in 1973. Pyroclastic density currents resulted from the collapse of the distal ends of a dacitic lava flow. The basal avalanche was confined to narrow river valleys, whereas the ash cloud surge outran the avalanche (Rose et al., 1977). H/L ratios for these pyroclastic density currents are c. 0.15.

2.6. A step further – "Surge-derived pyroclastic flows"

The possibility of the detachment of the ash cloud surge from the basal avalanche, followed by the generation of a "secondary" basal avalanche from the parental surge, was first described at Mont Pelée in 1902 (Fisher and Heiken, 1982). Surge-derived pyroclastic flows were generated through gravity segregation from the detached ash cloud surge, developing on a gentle slope c. 100 m above the valley of Rivière Blanche. The associated ash cloud surge maintained sufficient energy to devastate the landscape to distances of c. 3 km. The term "secondary" pyroclastic flow has been used to describe these occurrences (Brantley and Waitt, 1988), but it is imperative to distinguish them from secondary pyroclastic flows formed by the remobilization of ignimbrite, that were described following the 1991 eruption at Mount Pinatubo (Torres et al., 1996). The term 'secondary' implies a time gap between the emplacement of the surge and its remobilization to form concentrated flows. This was generally not the case at Montserrat, Mount St. Helens or Mont Pelée, where the emplacement of the pyroclastic surge and its derivative pyroclastic flow were basically simultaneous.

The most fundamental and detailed description of this prevously neglected phenomenon was given for the eruption of Soufriére Hills Volcano, Montserrat, between 1995-1999 (Druitt et al., 2002), probably increasing the perception of this volcanic risk.

Three individual block-and-ash flow pulses were recorded on 25th June 1997 (compare section 2.5.4); dense basal avalanches travelled down drainages to the NE of the volcano (Figures 2.15 and 2.16). Surges detached from major block-and-ash flows at a prominent bend in a valley to the NE (Loughlin et al., 2002), moving then northwards over a plain and were then blocked by an opposing hillside. It was suggested that the deceleration of the detached surge generated a dense pyroclastic basal avalanche by rapid sedimentation of suspended-load fall-out, and this high-concentration avalanche then drained into a river valley, where it moved another 3 km to reach the outskirts of a still populated village.

Figure 2.15: Deposits of detached ash cloud surges which transformed into a surge-derived proclastic flow travelling down Belham River valley on June 25, 1997 (photos courtesy of P.Kokelaar).

The surge-derived pyroclastic flow deposit consisted mainly of ash and lapilli of dense, juvenile andesite, and was noticeably finer-grained than typical block-and-ash flow deposits of Soufriére Hills Volcano (Cole et al., 1998; Cole et al., 2002). Blocks up to 10 cm diameter made up a small percentage of the deposit, but these were heterolithologic with many altered and weathered rocks, suggesting that they were picked up by the flow further upstream. Eyewitnesses on 25th June described a pyroclastic surge moving down the northern flanks of the volcano as the block-and-ash flow travelled down, confined to Mosquito Ghaut (NE). The surge reached the main road near Riley's Yard where it lost momentum and stopped its lateral advance. Eyewitnesses on the road near Farrell's Yard saw an ash cloud flowing west down the main road at a high angle to the original flow direction. They commented on how the ash was confined to the road, hugging the ground, “boiling” and “moving round bends like a vehicle” (Loughlin et al., 2002).

A similar process occurred on 26 December 1997, when the upper parts of the pyroclastic density current spilled over the saddle between Galway's Mountain and the South Soufriére Hills. Here another dense surge-derived pyroclastic flow formed and travelled 2 km down Dry Ghaut. The Belham River valley flow had a broader catchment area and a larger volume than Dry Ghaut. The former consequently travelled as a wave of debris up to 6 m high, reaching a distance of 3 km from the limit of the parent surge, whereas the Dry Ghaut flow was less than 2 m thick and outran its parent surge by only 1 km (Druitt et al., 2002).

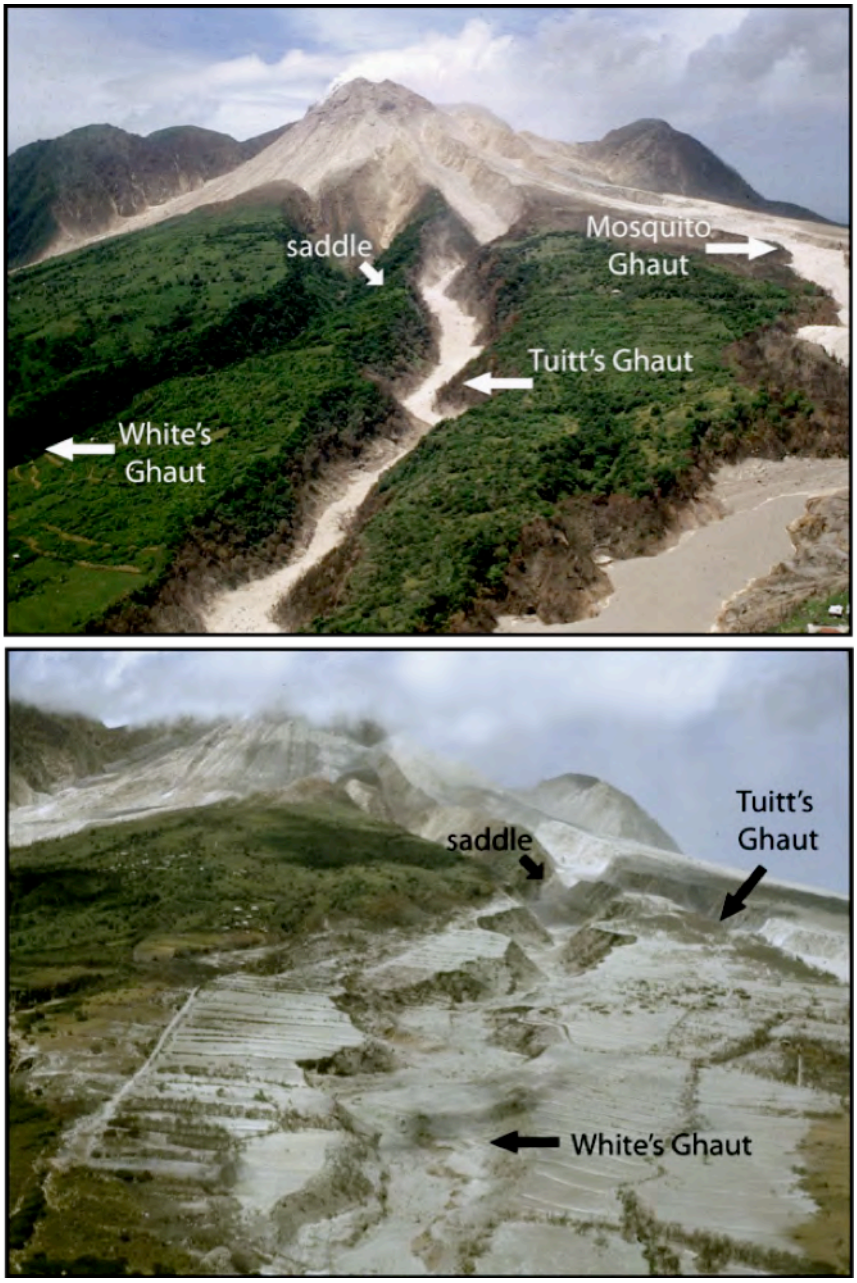

Figure 2.16: Block-and-ash flows inundated several ghauts to the N and NE of Soufriere Hills Volcano. The upper picture show the volcanic flank before the eruption in June 1997, the lower picture after ash cloud surges detached and devastated the landscape (pictures courtesy of P.Kokelaar).

The surge-derived flows were extremely mobile; given their very small volumes compared with typical Soufriére Hills block-and-ash flows, they had remarkably long runouts beyond the main pyroclastic surge impact zones (3 km and 1 km respectively for the Belham River valley and Dry Ghaut). Calder et al. (1999) compared the mobilities of the three types of Montserrat pyroclastic flows with those of cold-rock avalanches, using both L/H (the inverse of the conventional parameter H\L; e.g. Hayashi and Self, 1992) and a parameter $AV^{2/3}$ based on a recent scaling analysis of avalanche dynamics (Dade and Huppert, 1998). H is the maximum vertical height drop and L is the horizontal distance to the flow terminus, A and V are the areas and volumes respectively of the resulting deposits. Calder et al. (1999) showed that the surge-derived pyroclastic flows had mobilities significantly greater than block-and-ash flows or cold-rock avalanches, and comparable to, or greater than, those of pumice-and-ash flows formed by fountain collapse on Montserrat in August, September and October 1997. L/H and $AV^{2/3}$ for the surge-derived flows are 6-15 and 130-360 respectively, whereas for pumice-and-ash flows they are 3.3±2 and 135 ± 18 and for block-and-ash flows 4.5± 0.5 and 34±4 (Table 2.1).

Feature	June 25 (Belham Valley)	26 December (Dry Ghaut)
Similarities		
Origin of pyroclastic flow	Rapid suspended-fallout load from pyroclastic surge	
Nature of flow	Concentrated granular flow with well-defined upper surface	
Flow velocity	10 m/s, with weak associated ash cloud surge	
Nature of flow deposit	massive, poorly sorted, weak normal grading; unusually fine-grained for pyroclastic flow deposit	
Differences		
Volume of surge deposit (m^3)	800000 (not DRE)	150000 (not DRE)
Volume of surge-derived flow deposit (m^3)	90000	50000
Flow thickness in transport (m)	≤ 6	≤ 1-2
Runout beyond surge (km)	3	1
Ground slope at terminus (°)	2	7
Mobility ratio L/H	15 ± 5	6 ± 1.5
Temperature of flow deposit	310-400	120-140

Table 2.1: Comparison of the surge-derived pyroclastic flows of 25 June and 26 December 1997 at Soufriere Hills Volcano (after Druitt et al., 2002).

The high mobility of the surge-derived flows was probably not affected by temperature, since the emplacement temperatures (120-410°C) were lower than those of less 'mobile' block-and-ash flows (up to 650°C). If the flows were partially fluidized by escaping gas, two possible gas sources could be attrition of juvenile clasts and rupture of gas-filled vesicles during transport, and incorporation and combustion of vegetation. Calder et al. (1999) tentatively attributed the high mobility of the surge-derived flows to rapid sedimentation of material from turbulent suspension and the formation of a poorly sorted granular flow with low frictional resistance.

Surge-derived pyroclastic flows generated in June and December 1997 at Soufriére Hills were formed by suspended-load fallout from pyroclastic surges, which generated granular, basal flows of ash and lapilli that drained gravitationally into neighbouring valleys and topographic depressions. The flows were highly concentrated with well-defined upper surfaces, they travelled at a few metres per second and the associated overriding surge clouds near the distal limits were very weak (Druitt et al., 2002). Usually, the deposits are systematically finer-grained than typical block-and-ash flow deposits of Soufriére Hills Volcano, but have grain-size compositions within the range of those of the associated, parent surge deposits.

“Secondary” pyroclastic flows in the sense of surge-derived flows were inferred from deposits at Taapaaca Volcano, Andes (Clavero et al., 2004). Ash cloud surge deposits, usually associated with block-and-ash flows at Taapaaca Volcano, cropped out in areas where no deposits of the main body of the flow were present, indicating a detachment of the surge from the basal underflow. Surge-derived flow deposits occur only localized, consisting of massive, mainly fine-grained, thin layers, less than 1 m thick (Clavero et al., 2004).

Rapid sedimentation of granular materials can generate excess pore pressures in the accumulating sediment layer, reducing the intergranular friction and allowing the sedimented layer to flow away (Freundt, 1999). Experiments showed that rapid sedimentation of monodisperse particles from low-concentration suspensions onto a topographic slope can lead to the formation of a high-concentration flowing granular layer (Nir and Acrivos, 1990), because particles that have settled down to the surface

of the substrate can and will continue to move downslope. Another possible explanation for the development of a high-concentration layer within polydisperse currents is the tendency for larger clasts to reside as bed load in the lowermost parts of the currents. Pyroclasts settling rapidly onto a slope from a fully dilute pyroclast density current (surge) may continue to flow downslope in the form of a thin basal concentrated dispersion (e.g. modified grainflow), either before they properly come to rest, or by remobilization of a loose, momentarily deposited layer. Even where there is little or no topographic slope, a process similar to that in the experiments of Nir and Acrivos (1990) may occur, but in which the basal high-concentration dispersion is driven along the ground by shear exerted from the overriding part of the current as a traction carpet, rather than simply by draining downslope.

2.8. Discussion

Decoupling within pyroclastic density currents is widely recognized. Stratification of the parent current is a pre-requisite for the onset of decoupling, also known as flow stripping. As Fisher (1995) suggested, several mechanisms can indirectly contribute to non-uniformity of pyroclastic currents, which eventually lead to decoupling. The influence of rough topography on the dynamics of pyroclastic density currents can accentuate decoupling, but the detachment of the ash cloud surge from the basal avalanche does not necessarily depend on it.

Topography usually influences the general flow behaviour, e.g. erosion and deposition (e.g. Fisher, 1990; Thornburg et al., 1990; Ui et al., 1999), by controlling the nonuniformity of the currents and by confining them (e.g Wilson and Walker, 1985; Branney and Kokelaar, 1992). The behaviour of pyroclastic density currents around obstacles or obstructing topographies will vary with the velocity of the currents, the obstacle height, the current density and density stratification within the flow (e.g. Valentine, 1987; Lane-Serff et al., 1995; Alexander and Morris, 1994).

Turbidity currents, like pyroclastic density currents, will encounter topographic irregularities during their advance downslope; the influence of topography may be more enhanced for pyroclastic density currents due to steeper volcanic flanks (c. >

30°; submarine slopes < 10°). Typically, volcanic slopes are characterized by steep angles and rough topographies, such as drainage and river valleys, which are often meandering and usually extending beyond the base of the volcano. The probability is high that on volcanic slopes which are dissected by deep valleys, the basal avalanche will follow the course of the channel, so even slight meandering can lead to partial blocking of the basal avalanche; the ash cloud surge can then separate from the rest of the flow. When the basal avalanche follows the course of the channel, variations in the channel gradients, marked by breaks in slope, will possibly lead to generation of additional energetic ash cloud surges from the confined basal avalanche. It has been established that the detachment of the ash cloud surge from the basal avalanche can occur anywhere, but it seems to be concentrated on the steeper slopes of the volcano (> 25°). Further changes in the direction of the channels can result in detachment of more than one ash cloud surge, as has been observed at Soufriere Hills Volcano on June 25th 1997 (Loughlin et al., 2002). Decoupling occurred high on the slopes; near the foot of the mountain, overspilling of the block-and-ash flow was usually documented, but no further decoupling occurred (compare Figure 5.14). Therefore, flow transformations can occur along the whole travel distance of confined flows and should be anticipated for possible hazard assessments.

Name of volcano	min. sinuosity	max.sinuosity	ave. sinuosity
Ngauruhoe	1.05	1.15	1.1
Colima Volcano	1.1	1.51	1.24
Merapi Volcano	1.07	1.17	1.13
Unzen Volcano	1.08	1.27	1.17
Soufriere Hills Volcano	1.16	1.47	1.26
Mont Pelee	1.15	1.3	1.21

Table 2.2: Sinousity of subaerial valleys and channels for selected volcanoes.

Meandering of valleys on volcanic slopes can be quantified by a measure of sinuosity. All the case studies described showed average channel sinuosities between 1.1-1.3 (Table 2.2), with a sinuosity of 1 representing nearly straight channels. Therefore even slightly meandering and braiding channels can cause decoupling, and this should be taken into consideration for possible hazard delineation plans. What also has to be taken into account is that sinuosity will only be an influential factor when the channel depth allows accommodation of most of

the basal flow. The deposition of pyroclastic flow material and post-eruption erosion or mobilization will alter the topography over which successive flows will travel. If valley floors are raised due to progressive infilling by successive pyroclastic density currents, the previously rugged topography will be smoothened and chances for the detachment of the surge will decrease, while lateral spreading and overspilling will be enhanced. Sudden narrowing of incised channels or extreme meandering will severely impede the mobility of pyroclastic density currents, leading to superelevation and accumulation of massive deposits in these valleys. Sharp bends will most likely result in overspilling or decoupling (Stinton and Sheridan, 2008).

Typically, the depth of valleys on volcanic slopes decreases with increasing distance from the summit, sometimes associated with the widening of the valleys. Therefore, channeling of the flows and possible constrictions of the valleys will most likely occur high on volcanic slopes, so the probability of decoupling is higher there. The influence of the depth of valleys and channels is significant, specifically in relation to the height of the flow. This parameter determines the effectiveness of the valley to channel the pyroclastic density current, but typically the height of such a current can only be estimated during the eruption, but not determined in advance. Therefore determining the effect of channel geometry has to rely on studies of earlier eruptions and distribution patterns, possibly in combination with ground penetrating radar studies to identify previous channel depths and widths (Gomez et al., 2008). The paths block-and-ash flows will take down a slope will have to be examined individually, with regard to channel constrictions, changes in the slope gradient and in the channel directions, in order to determine probable decoupling locations and patterns.

It has been directly observed, and inferred from depositional patterns, that a detached ash cloud surge can travel independently, sometimes in a different direction than the rest of the flow. Travel distances of the detached surge range between several hundred meters and few kilometers; however, the run-out distance will increase drastically when, due to rapid sedimentation, surge-derived pyroclastic flows form that will behave similarly to the parent block-and-ash flows, as has been documented at Soufriére Hills Volcano (Druitt et al., 2002). Typically, run-out

distances of an ash-cloud surge are determined by the density and velocity at which the surge is detached from the avalanche. The density distribution in the surge, however, depends upon the Rouse number, which represents a ratio of particle-settling velocity to scale of turbulence, and increases as the surge deflates during flow (Valentine, 1987). The surge rapidly loses mass as particles settle out of suspension until the surge density is less than that of the ambient atmosphere. Then the surge ascends as a buoyant plume. The lofting of a large ash plume from the parent pyroclastic surge leads to deceleration and associated rapid sedimentation that generates the secondary surge-derived flows.

The factors initiating decoupling work in an intricate interplay, thus it is not always possible to determine or distinguish individual parameters or actually predict that decoupling will occur in specific environments. Comparison of several case studies revealed some similarities, such as sinuosity and curvatures of the channels. However, volcanoes known for the generation of block-and-ash flows have to be studied individually. With regard to the history of the volcano, possible distribution patterns and topographic irregularities, which will most likely be traversed, have to be identified to assess the probability of decoupling.

Chapter 3

Block-and-ash flow deposits associated with the Kaharoa eruptive episode (AD 1314 ± 12) at Tarawera Volcano, New Zealand

"Research is formalized curiosity.

It is poking and prying with a purpose."

Zora Neale Hurston

Chapter 3: Block-and-ash flow deposits associated with the Kaharoa eruptive episode (AD 1314±12) at Tarawera Volcano, New Zealand

3.1. Introduction

The North Island of New Zealand comprises several active volcanic centres, most of which are concentrated within the Taupo Volcanic Zone (TVZ). The volcanic zone is c. 350 km long and up to 50 km wide. Mount Ruapehu marks the southwestern end, the

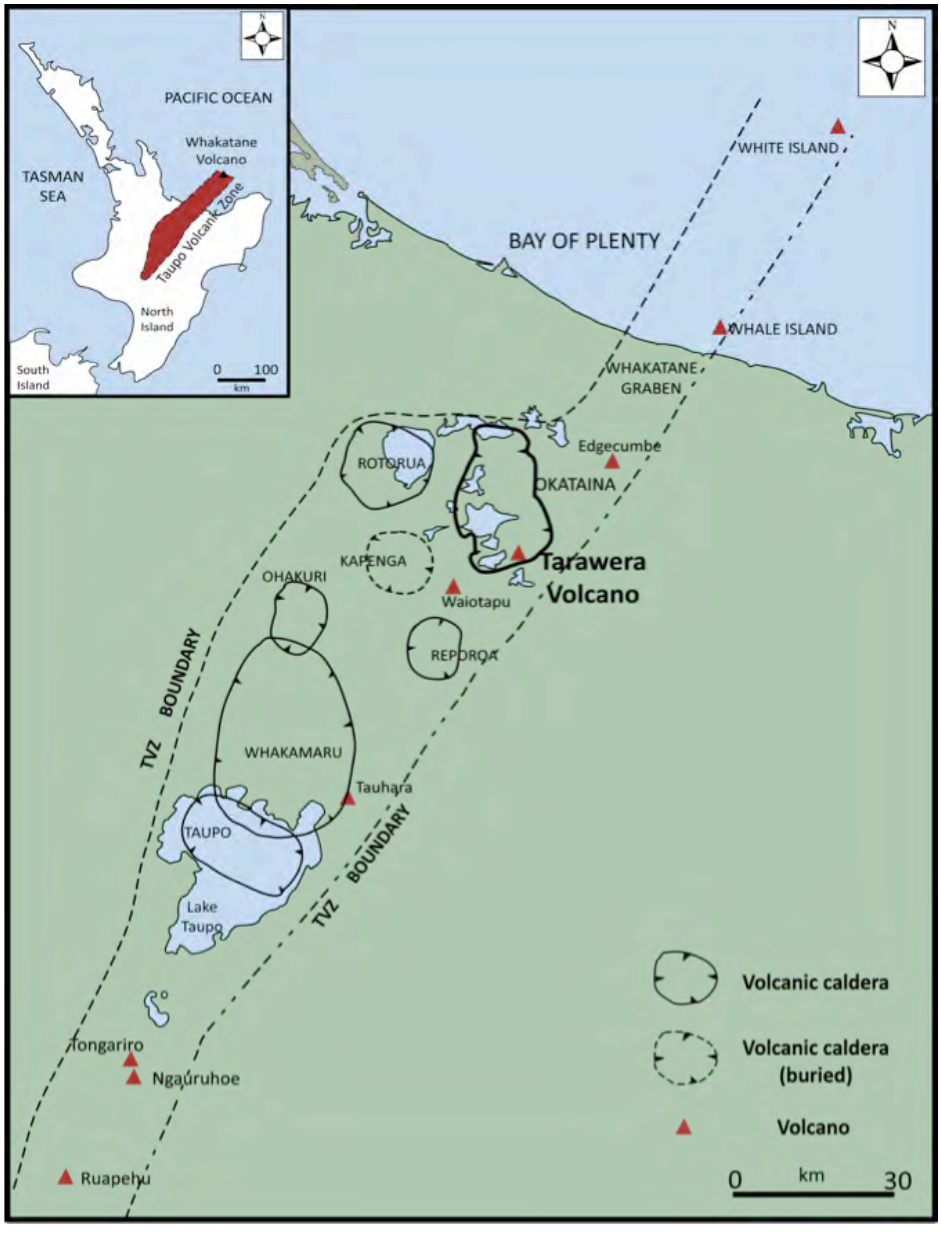

Figure 3.1: Location of Tarawera Volcano within the Taupo Volcanic Zone (TVZ). Also shown are calderas and volcanoes located in the TVZ (modified after Cole et al., 2009).

zone extends along the Okataina Volcanic Centre in the north and continues further 200 kilometres offshore, with the submarine Whakatane volcano considered to be the northeastern limit (Figure 3.1).

The Okataina Volcanic Centre (OVC) is one of seven rhyolitic calderas and caldera complexes within the Taupo Volcanic Zone (Cole et al., 2009) and one of two caldera complexes in the axial rift zone of TVZ that have been erupted in the last 2000 years. The OVC is characterized by a grouping of rhyolite domes and their remnants within the Taupo Rift (Cole et al., 2009). Two intra-caldera massifs were formed, the Haroharo and Tarawera dome complexes.

Tarawera Volcano was built over the last 22 000 years during four large eruptive episodes – Okareka, Rerewhakaaitu, Waiohau and Kaharoa (Table 3.1).

Location of eruption	Eruption type	Date/Age	Reference
Tarawera	Basaltic	1886	Walker et al. (1984) Sable et al. (2006)
Kaharoa	Rhyolitic with basaltic inclusions	c. 1314 AD	Nairn et al. (2001) Leonard et al. (2002) Nairn et al. (2004)
Waiohau	Rhyolitic	13.6 ka	Speed et al. (2002)
Rerewhakaaitu	Rhyolitic	17.6 ka	Darragh et al. (2006) Shane et al. (2007a)
Okareka	Rhyolitic, preceeded by small explosive basaltic eruption	21.8 ka	Nairn (1992) Darragh et al. (2006) Shane et al. (2007b)

Table 3.1: Stratigraphy of the eruptions at Tarawera Volcano (after Cole et al., 2009).

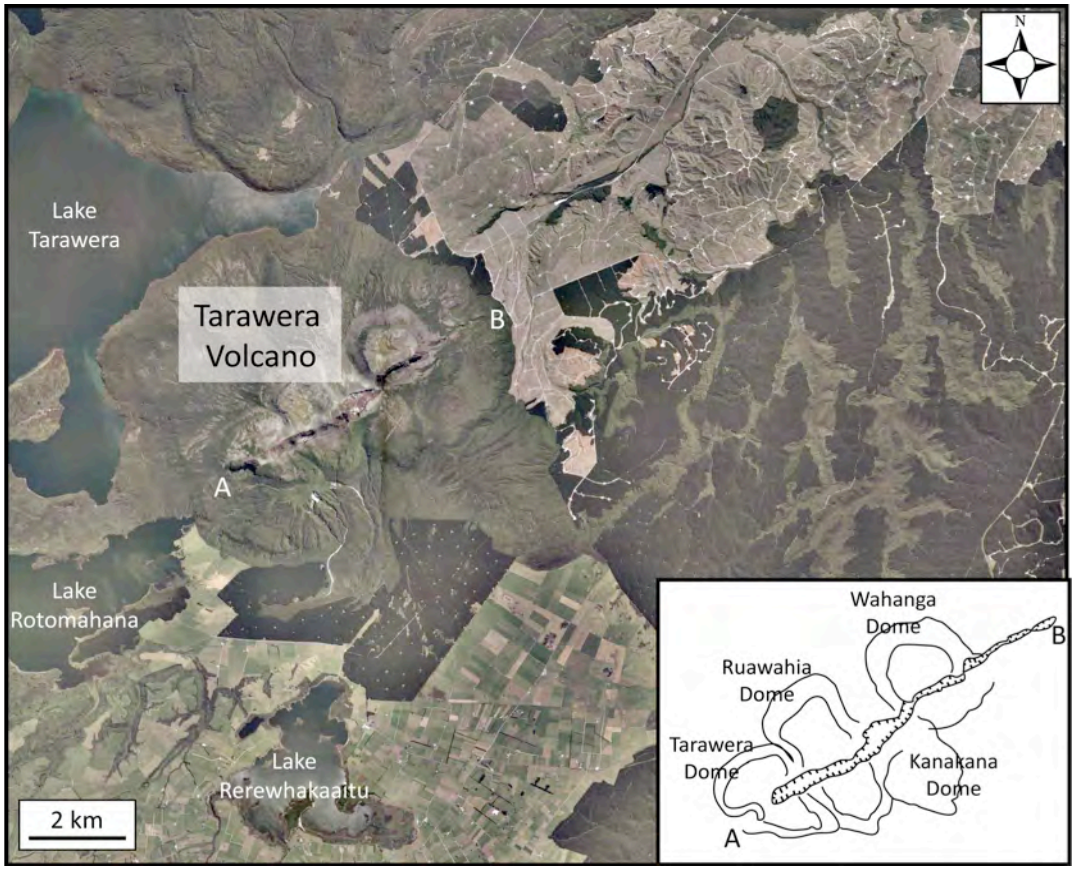

Figure 3.2: Topographic map of Tarawera Volcano and the surrounding country, featuring the alignment of domes (profile A-B, inlet sketch) and vents resulting from the destruction of the domes during the Tarawera eruption in 1886.

The latest dome-building event is the Kaharoa eruptive episode (AD 1314 ± 12; Hogg et al., 2003), characterized by rhyolite eruptions from seven vents along a linear zone across the massif. The basaltic eruption in 1886 (Table 3.1) cut through parts of several domes built during the Kaharoa eruption along a c. 8 km long fissure linear zone (Figure 3.2), possibly destroying minor vents which would have been correlated to the Kaharoa eruption (Nairn et al., 2001).

No observations of the eruptions are recorded, but from studies of stratigraphic sections, it has been deduced that the Kaharoa eruptive episode commenced with small explosive eruptions from a vent that opened probably near the summit of the massif. Larger phreatomagmatic eruptions resulted in the formation of a crater on the northeastern end of the complex. These vent-opening eruptions were followed by a series of major plinian eruptions, dispersing seven pumiceous rhyolite pyroclastic falls to the southeast (units A-H; Sahetapy-Engel et al., 2000; Figure 3.3). After the deposition of widespread pumice-rich pyroclastic density currents (unit Hpdc and RC

beds), plinian and subplinian fall eruptions were dispersed also north and northwest of the volcano (units I-M).

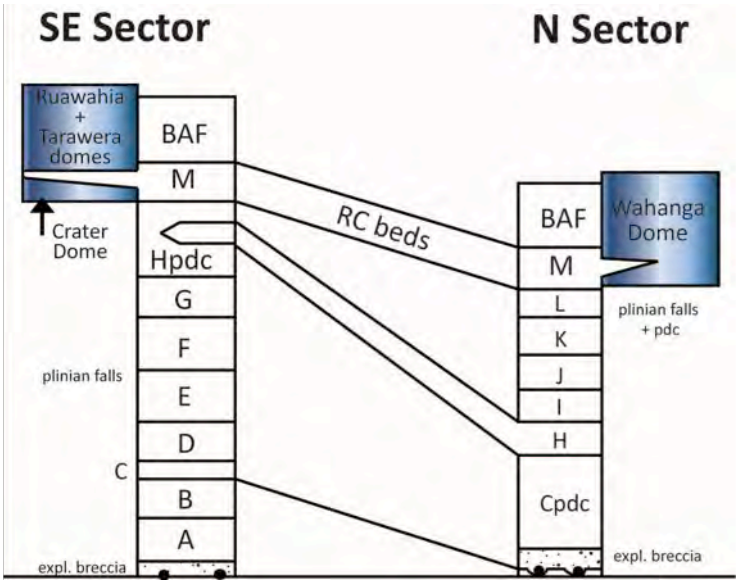

Figure 3.3: Correlation diagram for Kaharoa eruptive units in southeast and northern sectors, with pyroclastic fall units A-M (Nairn et al., 2001). The Cpdc, Hpdc, and RC beds are pyroclastic density current (pdc) deposits, interpreted as proximal correlatives of the C, H, and M distal fall units, respectively (modified after Nairn et al., 2001).

The eruption switched to a dominantly effusive phase, with additional explosions through the dome. The resulting vent locations were obscured by the extrusion of several rhyolite domes during the later stages of the eruption. Crater Dome was the first dome to be extruded, followed by Tarawera and Ruawahia domes, and Wahanga Dome was the last to be emplaced during the approx. 4-5 year long eruptive episode (Nairn et al., 2001).

Gravitational collapse of Ruawahia and Wahanga domes occurred contemporaneously with their mostly endogenous growth, producing small-scale block-and-ash flows (BAFs) directed to the south, north, and northeast, which overlie the Kaharoa pumiceous pyroclastic deposits around the volcano (Leonard et al., 2002).

The deposits emplaced during the Kaharoa eruptive episode were first described by Grange (1929) in his classification of the soils of Rotorua County. He mapped the Kaharoa series (pumiceous rhyolite and glass fragments) as being the parent material

for the soils north of Lake Rotorua and Lake Rotoiti. The Kaharoa deposits are mantled by material from the 1886 eruption (Tarawera Series).

The structure of the Tarawera Volcanic complex was initially described by Cole (1966), followed by studies of the petrology (Cole, 1970a and c) and eruptive history (Cole, 1970b), creating a comprehensive foundation for future work in this region. Cole noted that a flow breccia (now recognized as being deposited from pyroclastic flows) to the south of the mountain occurred at some time during the period of dome building, as was a lahar breccia which was later re-labelled as deposits from block-and-ash flows.

Detailed mapping by Nairn (1981) identified further lavas and pyroclastics from the Kaharoa eruptive episode, resulting in re-interpretation of early Tarawera volcanic structures. Nairn (1989) was the first to publish a geological map (V16AC) for the Tarawera Region, combined with a stratigraphic sequence for the volcanic complex.

Although previous descriptions include the pyroclastic deposits from the Kaharoa eruptive events, a re-interpretation of the deposits and their emplacement from block-and-ash flows is needed. Investigations of the block-and-ash flows were initiated by Ceinwen Scutter as part of a PhD project supervised by Dr. I.A. Nairn and Prof. S. Self. This included detailed sampling of the deposits from the domes to the distal extents, resulting in descriptions of the proximal Kaharoa deposits (not limited to the block-and-ash flows), including stratigraphic sections and granulometric studies that were published by Nairn et al. (2001). This initial PhD project was cancelled, until during the course of my research it was decided to integrate a detailed description of the block-and-ash flow deposits around Tarawera Volcano into my PhD thesis. Previously taken samples from Ceinwen Scutter could not be utilized, because they were disposed off while being in storage. Therefore, with referral to previously mapped deposit extensions, new samples were taken during several weeks of additional fieldwork at Tarawera Volcano between December 2008 and December 2009 (compare sample location map in Appendix A-2).

3.2. Description of lava domes involved in the generation of block-and-ash flows during the Kaharoa eruptive episode

3.2.1. Ruawahia Dome

Ruawahia Dome is the largest of the domes in the Kaharoa formation, with an estimated height of 120 m and a volume of 4×10^8 m^3 (Nairn et al., 2001). Dome extrusion occurred from two apparent vents – the main central vent directly northeast of Crater Dome, and a later but higher vent to the northeast, beneath the summit of Ruawahia Dome. Two main lobes flowed to the northwest and southeast of the central vent area. The southeast flow was confined to the valley between Kanakana Dome and the Rerewhakaaitu tuff dome, displaying a 300 m high flow front onto the valley floor. The northwestern lobe initially overlapped the Tarawera Dome margins to the south, and was then partly confined by a low ridge developed in the underlying Puha lava flow (15 ka). The dome surface is deeply buried under the ejecta of the 1886 basaltic eruption near the rift craters, but near the flow margins the lava is exposed with a very ribbed surface (Nairn et al., 2001). Collapse events during the growth of the two southern lobes produced the voluminous block-and-ash flows that will be described in detail in the following sections.

3.2.2. Wahanga Dome

This dome was extruded in a radial fashion within a shallow depression on the north-sloping surfaces of the Waikakareao lavas (11 ka) to form a nearly circular dome in plan view (Figure 3.2 sketch). The growth of the dome was partly confined by the Ruawahia tuff cone and a pre-existing collapse scar in the Waikakareao lavas to the west and the Waiakakareao lava slopes to the south. The north and northwest faces of the dome are unconfined, showing signs of marginal collapse. After the generation of block-and-ash flows directed to the east, the extrusion of Wahanga Dome most likely continued, because no collapse scars are visible on the eastern side of the dome. The block-and-ash flows overlie RC beds, deposits from pumice-rich pyroclastic density currents, showing the RC pyroclastic eruptions had ended before the extrusion of

Wahanga Dome started. The lava dome thickness is c. 100m, with an estimated volume of 2×10^8 m^3 (Nairn et al., 2001).

3.3. Distribution of the block-and-ash flow deposits

This PhD project included extensive field work and a survey of the extent of the block-and-ash flow deposits around Tarawera Volcano, to allow the construction of a detailed distribution map and the recognition of individual flow units related to the generation and emplacement of block-and-ash flow deposits during the latest stages of the Kaharoa eruptive episode.

Block-and-ash flows (BAFs) were generated from the gravitational collapse of the outer rims of at least two of the lava domes, Ruawahia and Wahanga Domes. Two major pyroclastic fans are distributed to the northeast and south of the volcano (Figure 3.4) respectively with volumes of c. $1x10^8$ m^3 in the northeastern and c. 5×10^7 m^3 in the southern fan. The smaller fans to the north and northwest display volumes of $1x10^7$ m^3 and 4×10^6 m^3 respectively (Table 3.2). In general, volume calculations of these deposits assume a flat base to the flow deposits. As the topography at Tarawera Volcano is complex (e.g. deeply incised valleys, river streams, lava plateaus), these volumes are likely to be minima.

LOCATION	ORIGIN	VOLUME	RUN-OUT	CHARACTERISTICS
Northeastern fan	Wahanga Dome	$1x10^8$ m^3	5.4 km, then up to 9.2 km	complex topography – collapse gully, deeply incised valleys
Southern fan	Ruawahia Dome	$5x10^7$ m^3	7.6 km	confined in proximal regions, median to distal regions unconfined
Northwestern fan	Ruawahia Dome	$1x10^7$ m^3	min. 4 km	total run-out obscured due to drainage into Lake Tarawera
Western fan	Ruawahia Dome, maybe Tarawera Dome	$4x10^6$ m^3	max. 2 km	total run-out obscured due to drainage into Lake Tarawera

Table 3.2: Volume distribution of block-and-ash flow deposits at Mount Tarawera during the AD 1314± 12 Kaharoa eruptive episode (after Nairn et al., 2001).

The block-and-ash flow fans form the uppermost deposits in most exposures around the volcano, the deposits mantling eruptives from earlier stages of the eruptive episode such as airfall and non-welded, pumice-rich pyroclastic density current deposits. Generally, the deposits of the main body of the flows are capped by an ash cloud surge deposit and/or ash fall deposits, and are often overlain by thick scoria cover from the 1886 basaltic eruption at Tarawera Volcano.

Depending on the pre-existing topography, the exposed thickness of the block-and-ash flow deposits range from < 1 m to more than 30 m, representing veneer and valley-filled deposits around the volcano.

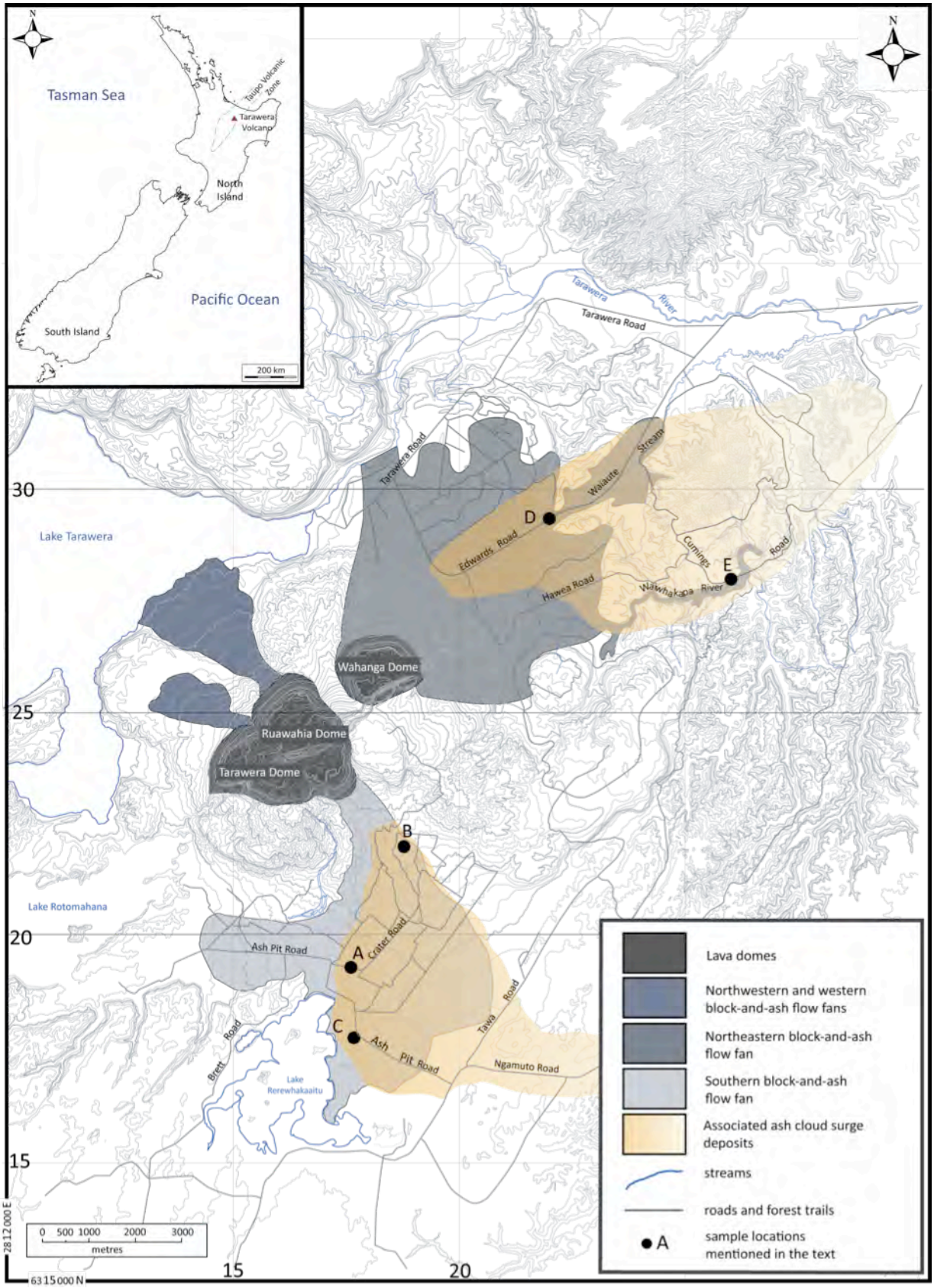

Figure 3.4: Topographic map showing the distribution of block-and-ash flow and associated ash cloud surge deposits around Tarawera Volcano (modified after Nairn et al., 2001).

3.3.1. Northeastern block-and-ash flow fan

During the collapse of the outer eastern parts of Wahanga Dome, several block-and-ash flows were generated, travel directions are mainly to the northeast and the east.

The largest block-and-ash flow fan was distributed to the northeast of the volcanic complex, reaching run-out distances up to 9.4 km. Irregular topography, such as deeply incised valleys, river streams, a collapse gully and an explosion crater (Figure 3.5) as well as widely distributed older lava plateaus influenced flow dynamics and run-out distances for the pyroclastic currents, resulting in several currents which traveled in different directions (Figure 3.5). Topographic channeling occurred between the medial and distal regions, flow dynamics were further influenced by two major breaks in slope, dissecting the run-out path in three slope segments.

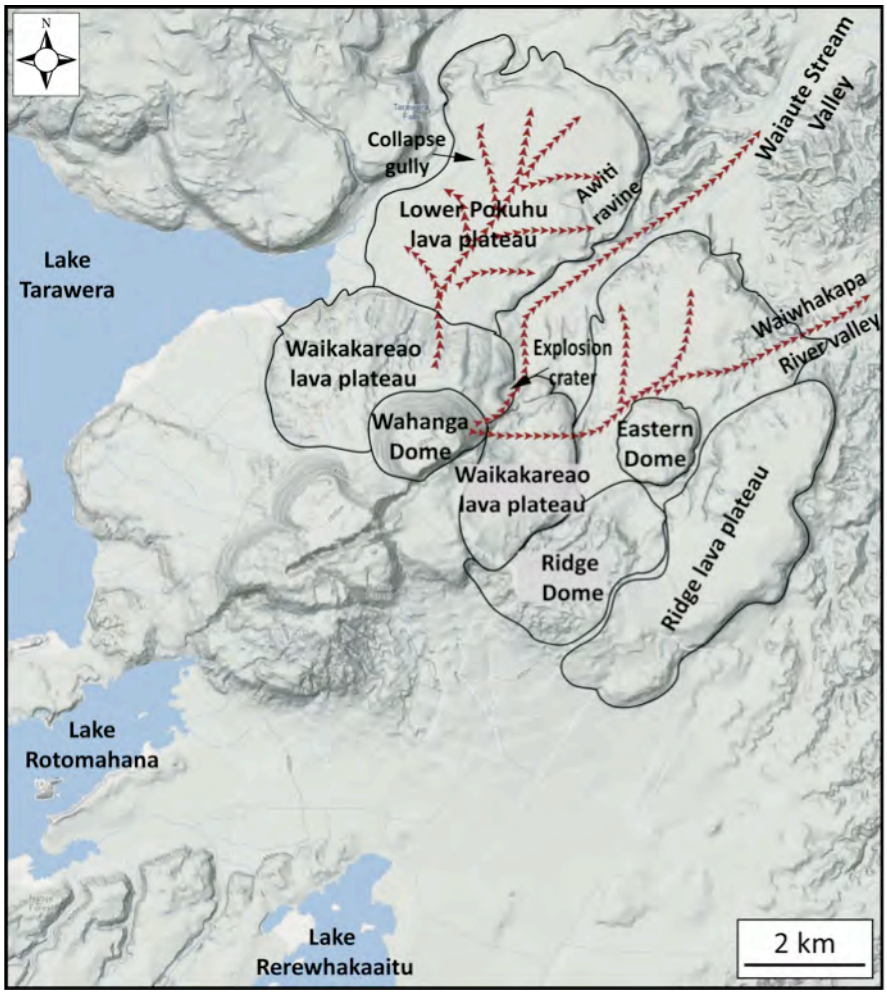

Figure 3.5: Terrain map of the northeastern and eastern slopes of Tarawera Volcano. Travel directions of block-and-ash flows (marked by red arrows) are heavily influenced by the pre-existing topography.

Breaks in slope occurred at 1 km and 1.5 km from the dome. The upper part of the volcanic flank is inclined at c. 28°, the first break in slope changes the inclination to c.7° directly where the dome margin is surrounded by an apron of Waikakareao lava (ca. 11 ka). The second break in slope in the northeastern and eastern direction is a more subtle change in topography (Figure 3.6).

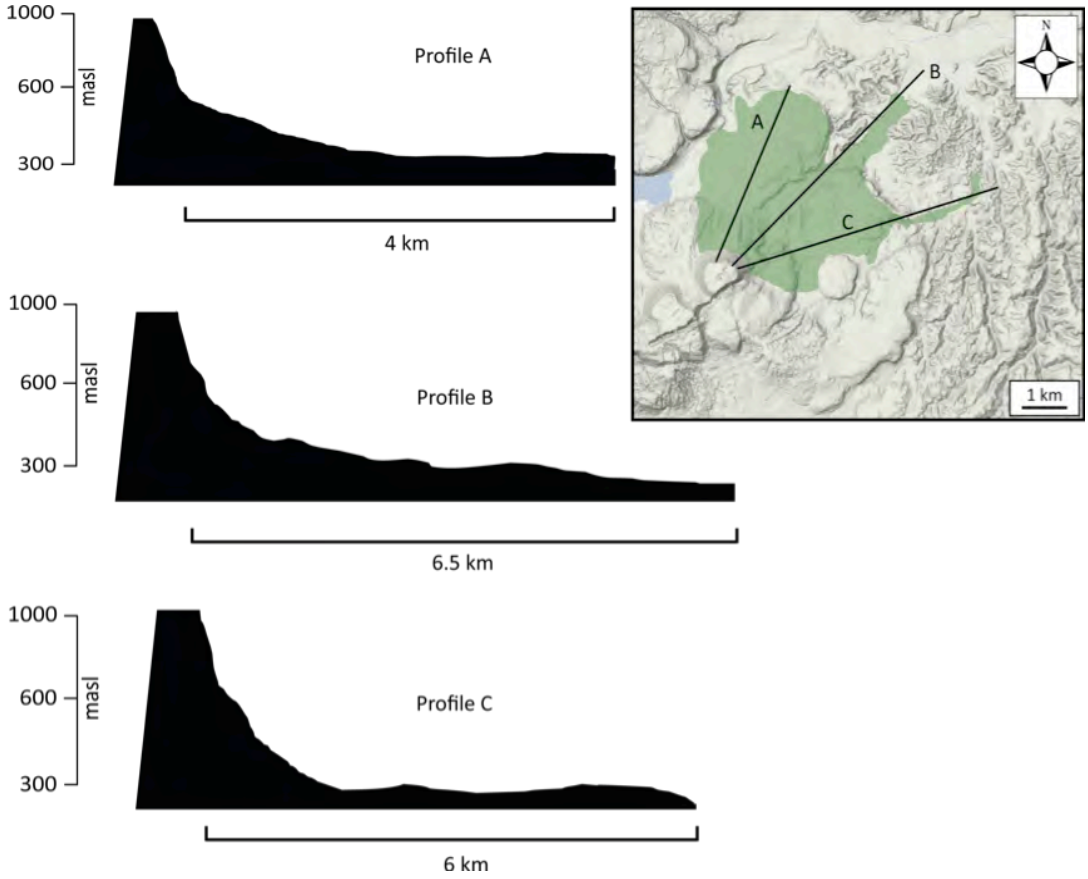

Figure 3.6: Slope reliefs for the northeasthern block-and-ash flow fans at Tarawera Volcano along three profiles (A, B and C).

Block-and-ash flows directed to the NNE spread across the near flat surface of Lower Pokohu lava, probably limited by low marginal levees ridges of the emplaced lava flows (Hodgson and Nairn, 2005). Block-and-ash flows that traveled to the northeast were strongly channeled first by crossing an explosion crater near the first break in slope ("Northeast Crater") and further by older Pokuhu and Waikakareao lava plateaus, leading the currents into the Waiaute Stream Valley (Figure 3.6) and prolonging their run-out up to 9 km. The Waiaute Stream Valley had been infilled by c. 30 m of block-and-ash flow deposits with a gently sloping surface. On the western rim of the valley,

the block-and-ash flows traversed rough topography leaving deposits high in the steep gullies tributary to the valley.

Eastward-directed block-and-ash flows traveled diagonally over the previously emplaced Waikakareao lava flows before being channeled along the Waiwhakapa River Valley, reaching distances of up to 8.5 km from the dome.

3.3.2. Southern block-and-ash flow fan

Successive collapse of Ruawahia dome generated block-and-ash flows directed to the south that were mainly confined in the most proximal parts of the mountain. First channeled between the outer parts of Kanakana Dome and Ridge Dome to the east and the Rerewhakaaitu tuff cone to the west (Figure 3.7), the flows then spread out in the distal regions up to 7.6 km from the dome. They encountered only gentle

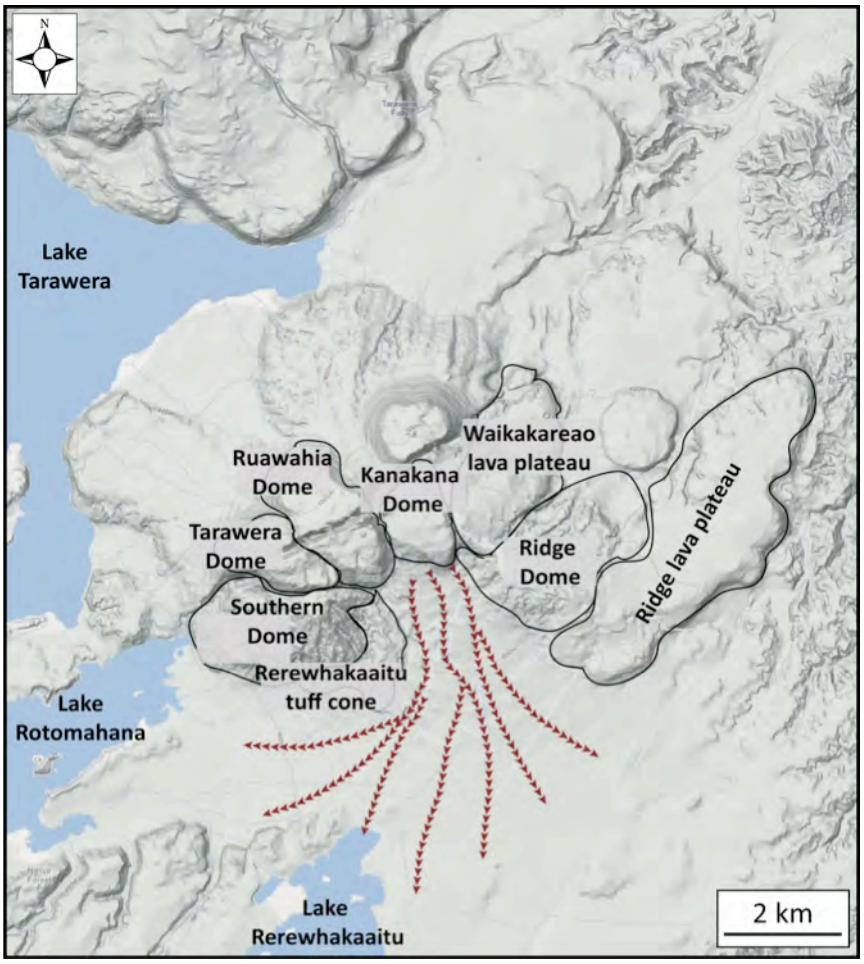

Figure 3.7: Terrain map of the southern slopes of Tarawera Volcano. Travel directions of block-and-ash flows (marked by red arrows) are only slightly influenced by the pre-existing topography.

topography from the underlying the 11 ka Waiohau pyroclastic fan.

In contrast to slopes of Wahanga dome, the margin of Ruawahia dome marks the only major break in the southern slope with a decrease in the slope inclination from 38.5˚ to < 15˚, while the lower flanks are gently sloping to a nearly horizontal run-out plain (Figure 3.8). To the west, the block-and-ash flow fan merged into a lahar plain that drained into Lake Rotomahana.

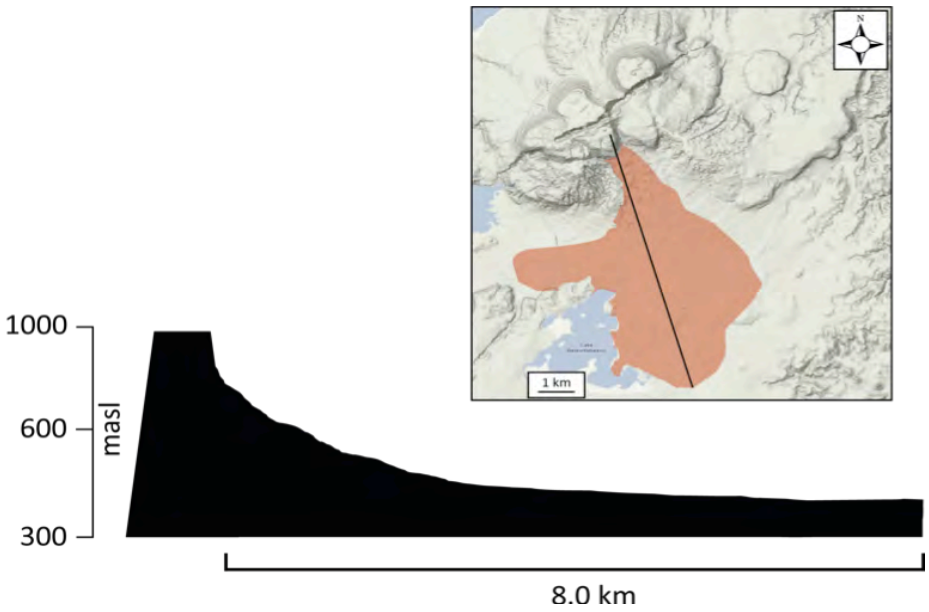

Figure 3.8: Slope relief for the southern slopes of Tarawera Volcano, representing a nearly horizontal run-out plain.

Complex channeling, like in the northern deposits, is absent in the deposits south of Ruawahia dome, but minor topographic variations such as small ridges (< 100m high) could have deflected or influenced the direction of the flows. The small chain of hills near the northern shore of Lake Rerewhakaaitu (c. 4.5 km from the dome), representing the margin of the caldera, probably resulted in parting of the flows, draining parts of the pyroclastic material into the lake, therefore concealing the complete extent of the pyroclastic fan to the south.

3.3.3. Northwestern and western block-and-ash flow fans

Two smaller block-and-ash flow fans were deposited to the northwest and west of Ruawahia Dome. The fan to the west traveled from the dome over a plateau of Te Puhua lava (600-400 masl), experiencing a break in slope from the margin of the dome at 600 masl. The lava plateau terminates with a steep drop into Lake Tarawera, from 400 masl to less than 300 m (surface of the lake). The run-out of the flow is c. 2.5 km (Figure 3.9, Profile A), flow thicknesses could not be determined due to inaccessibility of this side of the volcanic slope.

The northern flow shows a longer run-out with at least 3.4 km, but the total extent is obscured by drainage of the material into Lake Tarawera (Figure 3.9, Profile B). The flow was channeled near the break in slope at the margin of the dome by the Te Puha lava plateau to the west and the Waikakareao lava plateau to the east, therefore probably increasing the travel distance of these flows. The slope inclination decreases from c. 600 at the dome margin to less than 300 m at the edge of the lake, without the dramatic cliff, which characterizes the topography of the northwestern slope. There was no change of slope at the edge of the slope, run-out of the block-and-ash flow was not impeded and would have flowed into the lake.

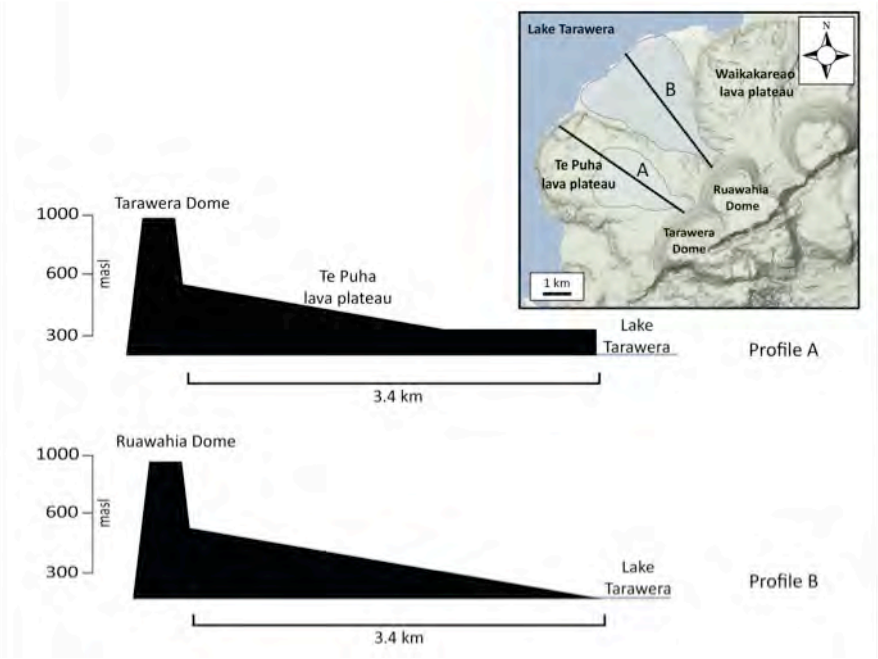

Figure 3.9: Cross-section through the northern and northwestern slopes of the Tarawera volcanic complex. Block-and-ash flows generated from the collapse of the northern rim of Ruawahia Dome were emplaced over (A) the Te Puha lava plateau and (B) channeled between the Te Pahu and the Waikakareao lava plateaus.

3.4. Influence of topography on flow distribution

The influence of pre-existing topography is mostly pronounced in the northeastern block-and-ash flow deposits. Extreme channeling along several river valleys is leading to accumulations of pyroclastic deposits up to 30 m. Various natural barriers (Figure 3.9) blocked or deflected the flows during their emplacement, resulting in ponding and the deposition of thicker flow units than in the southern deposits.

The most pronounced channeling in eastern direction occurs between the Pokuhu and Waikakareao lava plateaus (Figure 3.10), further channeling of the southeastern flows occurred along the tightly meandering channels of Waiwhakapa River, promoting the runout of the block-and-ash flows and possible decoupling of the ash cloud surge from the basal underflow (compare Chapter 6).

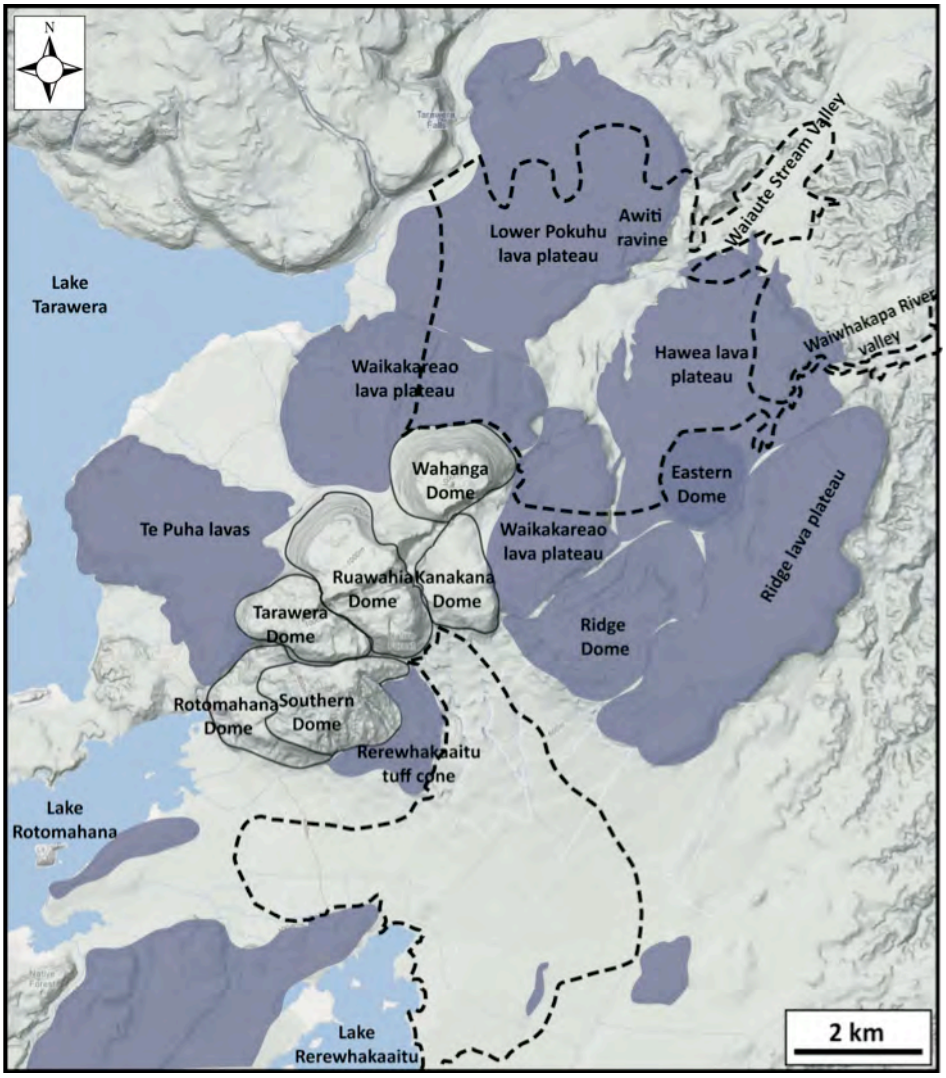

Figure 3.10: Terrain map of Tarawera Volcano and the surrounding countryside. Possible topographic channeling and deflection structures are marked in grey.

Previously emplaced Waikakareao lava plateaus governing Wahanga Dome create a first break in the volcanic slope, followed by a more gentle transition onto the lower Pokuhu and Hawea plateaus. Block-and-ash flows encountering the break will become more turbulent, sweeping over the plateau rims and then becoming channeled in the ravine between them. Some block-and-ash flows were directed over the lower Pokuhu lava plateaus, but they probably just swept over the sides into the ravine, no Kaharoa pyroclastic deposits have been found beyond the distal margins of the plateaus. Further topographic influence is represented by the round Eastern Dome, sitting within the Hawea lava plateau east of the main dome complex (elevation of c. 500 masl). Block-and-ash flows are probably deflected and even blocked, followed by channelling the along the Waikakareao lava plateau and Ridge dome into the Waiwhakapa river valley (Figure 3.10).

The southern block-and-ash flows did not encounter any major topographic irregularities, apart from slight channelling in the most proximal parts by the Kanakana dome to the east and a tuff dome to the west (Figure 3.10). Deeply incised valleys (> 20m) on the proximal slope possibly directed the flows to the south; when leaving the valleys, the flows could spread laterally without further impediment. Beyond ca. 3-3.5 km, the flows travelled towards Lake Rerewhakaaitu and drained into the lake. To the northwest of the lake, the currents were diverted to the west, towards Lake Rotomahana, by a chain of hills (c. 480 masl) representing the edge of Haroharo Caldera. To the east, no further major topographic barrier were present, supporting the lateral spreading of the flows. Shallow topographic depressions and narrow hills only resulted in the deposition of valley and veneer deposits.

3.5. General stratigraphy of the block-and-ash flow deposits

The exposure quality of outcrops in both major block-and-ash flow fans is remarkably good, quarrying for road material and significant erosion by the dam-break flood at the end of the Kaharoa eruptive episode (Hodgson and Nairn, 2005) exposed large extents

of the block-and-ash flows. Outcrops are restricted to forest roads and trails, ongoing de-and re-forestation operations sometimes impede the accessibility to the outcrops.

The stratigraphy of the block-and-ash flow deposits in both major fans is highly variable. Adjacent exposures frequently are often completely different, probably due to the rough pre-existing topography influencing the deposition of the currents.

In each of the major block-and-ash flow fans, a general stratigraphy is evident. Outcrops in both major block-and-ash flows fans are characterized by limited exposure. Commonly, only the main body and top of the deposits are exposed, with contact with the underlying substrate being obscured. Therefore determining the thickness of the flow throughout the deposits is not always possible.

The contact between the basal avalanche and the underlying substrate can only be located in three exposures in the southern deposits at Ruawahia Dome (Figure 3.4, loc. A-C, V16/179179, V16/178195 and V16/176189), and in the northeastern block-and-ash flow fan only one location (Cumings Road quarry, V16/261279) exposes tephra layers from the earlier stages of the eruptive episode.

Where the base of the block-and-ash flow unit is exposed, there is a thin red ash layer (1-3 cm), which marks the contact with the underlying Kaharoa Tephra. Locally, a fine-grained, massive layer (1-70 cm thick) is overlain by the block-and-ash flow deposit, which is usually massive without obvious signs of grading. The block-and-ash flow deposit is characterized by large rhyolitic clasts and boulders set in an ash matrix. After the deposition of the main body, there is sedimentation from the overriding ash cloud surge and the highly dilute ash cloud. Overlying the ash cloud (surge) deposit is scoria from the basaltic eruption of Tarawera Volcano in 1886.

Each block-and-ash flow unit is generally massive and poorly sorted, sorting values range between 2.1-3.8 for the main body and between 1-1.3 for ash cloud surge deposits (compare Figure 5 in Nairn et al., 2001). Abundant non- to poorly vesiculated, subangular to subrounded rhyolite blocks up to 3 m in diameter occur in a comminuted ash-sized matrix of the same material. These blocks are chemically identical to the dome lavas (Nairn et al., 2001), with rare lithics and basaltic inclusions within the deposits from the original dome material.

Fieldwork by Ceinwen Scutter in 2000 and from this study between 2007-2009 established that each of the major fans (southern and northeastern) has a maximum of three block-and-ash flow units. Accompanying finer-grained deposits probably represent either distal block-and-ash flows or associated ash cloud surge deposits.

Proximal regions of the flow show little evidence of flow units, but in most of the distal sections, up to two thin ash beds separate the clast-supported block-and-ash flows (Nairn et al., 2001). The exact identification of the flow units at Tarawera Volcano is difficult, corresponding with observations of block-and-ash flow deposits at Merapi Volcano (Indonesia) and Unzen volcano (Japan) that show that deposits from multiple flows produce massive deposits in which individual flow units are difficult to distinguish (Miyabuchi, 1999).

In the northern block-and-ash flow, massive grey flow units are commonly overlain by a thermally oxidized pinkish block-and-ash flow. These flows are separated by thin ash layers (Figure 3.11). The uppermost block-and-ash flow units are often finer-grained, but more clast-supported than the underlying thicker grey block-and-ash flow deposits, resulting in a normally-graded appearance within individual exposures of the main body in both pyroclastic fans.

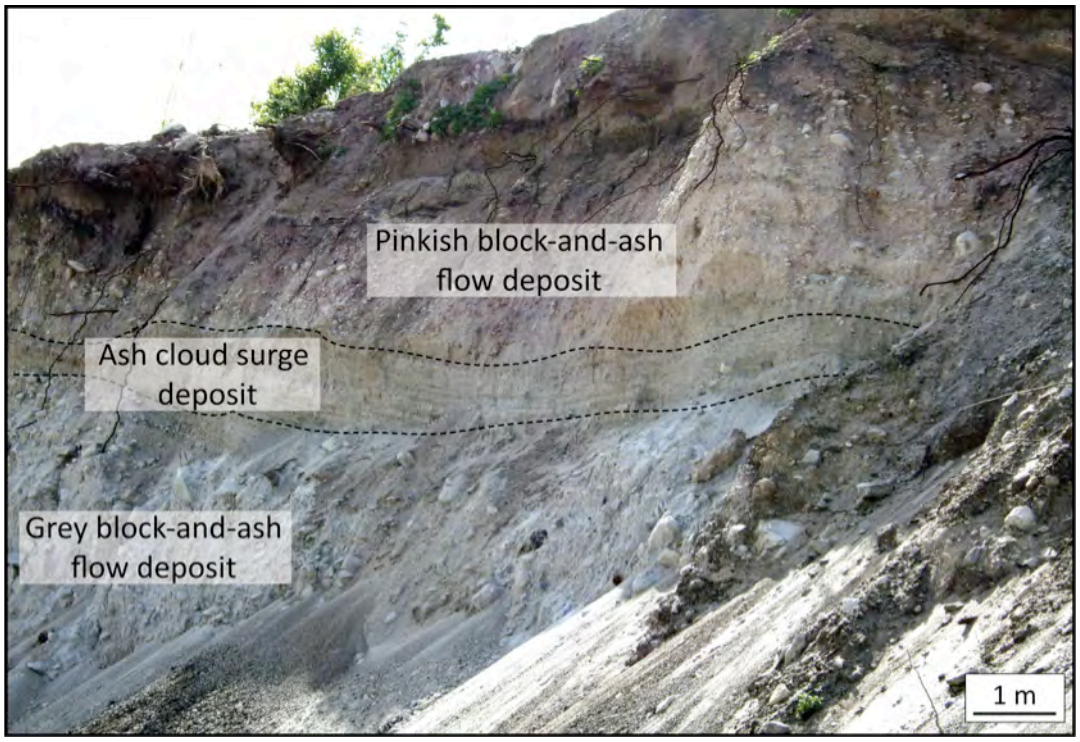

Figure 3.11: Grey block-and-ash flow deposits in the northeastern fan are overlain by pinkish, finer-grained block-and-ash flow deposits (V16/215295).

Within both major block-and-ash flow fans, the upper third of the main body is characterized by pinkish discoloration, and a red oxidation layer borders the transition to the lower, grayish part of the main body. The pinkish hue is possibly related to the leaching of iron oxide from the 1886 basaltic scoria into the underlying Kaharoa deposits (Figure 3.12).

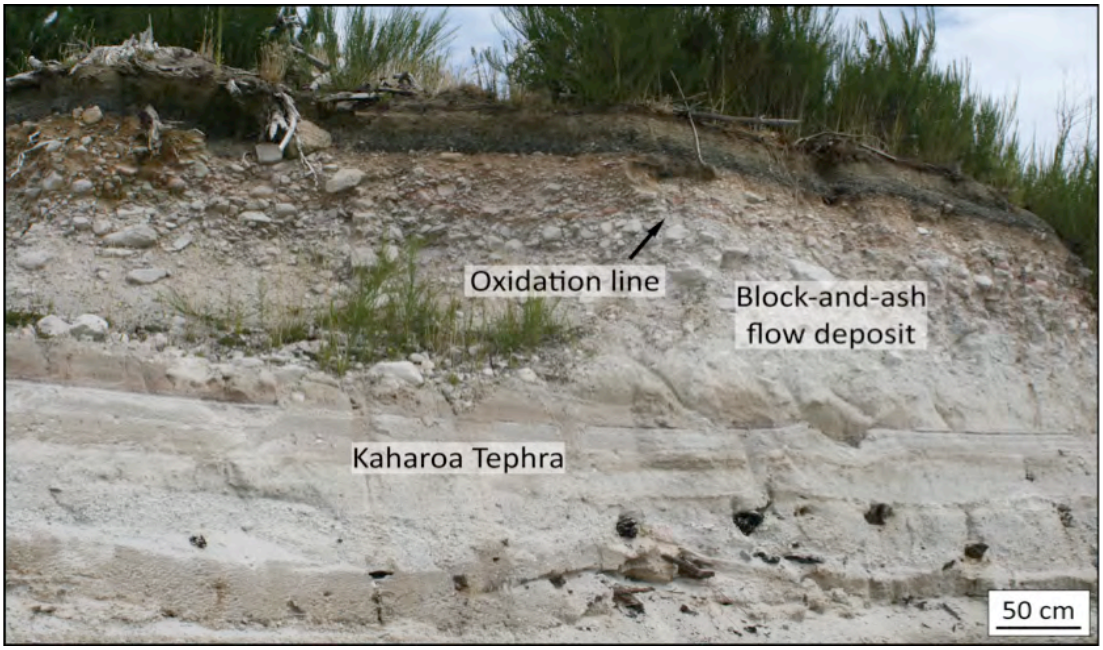

Figure 3.12: The upper third of most exposed block-and-ash flow deposits shows pinkish discoloration related to leaching of iron oxide from overlying basaltic scoria deposits from the 1886 Tarawera eruption (V16/178195).

Overall stratigraphy shows high preservation in the pre-Kaharoa valleys, with up to 30 meters in the northern, confined block-and-ash flow deposit (e.g. V16/215295; V16/261279). The southern block-and-ash flow encountered only gentle topography without major channelling, the deposits are widespread with thicknesses of max. 5 m (e.g. V16/176189).

There are two quarries in each of the major pyroclastic fans that display the most detailed section through the confined (Edward and Cumings Road) and unconfined parts of the deposits (Crater and Ash Pit Road). In the following sections, each of these quarries will be described in detail, investigating characteristic topographic and sedimentological features, beginning with the northeastern block-and-ash flow fan.

3.5.1 Edwards Road Quarry

Edwards Road Quarry (V16/215295) is located at the smallest width of the Waiaute Stream valley, at c. 3 km to the east from the dome. The quarry is located directly south of Awiti ravine and marked by a > 30 m scarp on the north face of the block-and-ash flow deposit, as a result fluvial erosion by the dam-break flood at the end of the Kaharoa eruptive episode (Hodgson and Nairn, 2005).

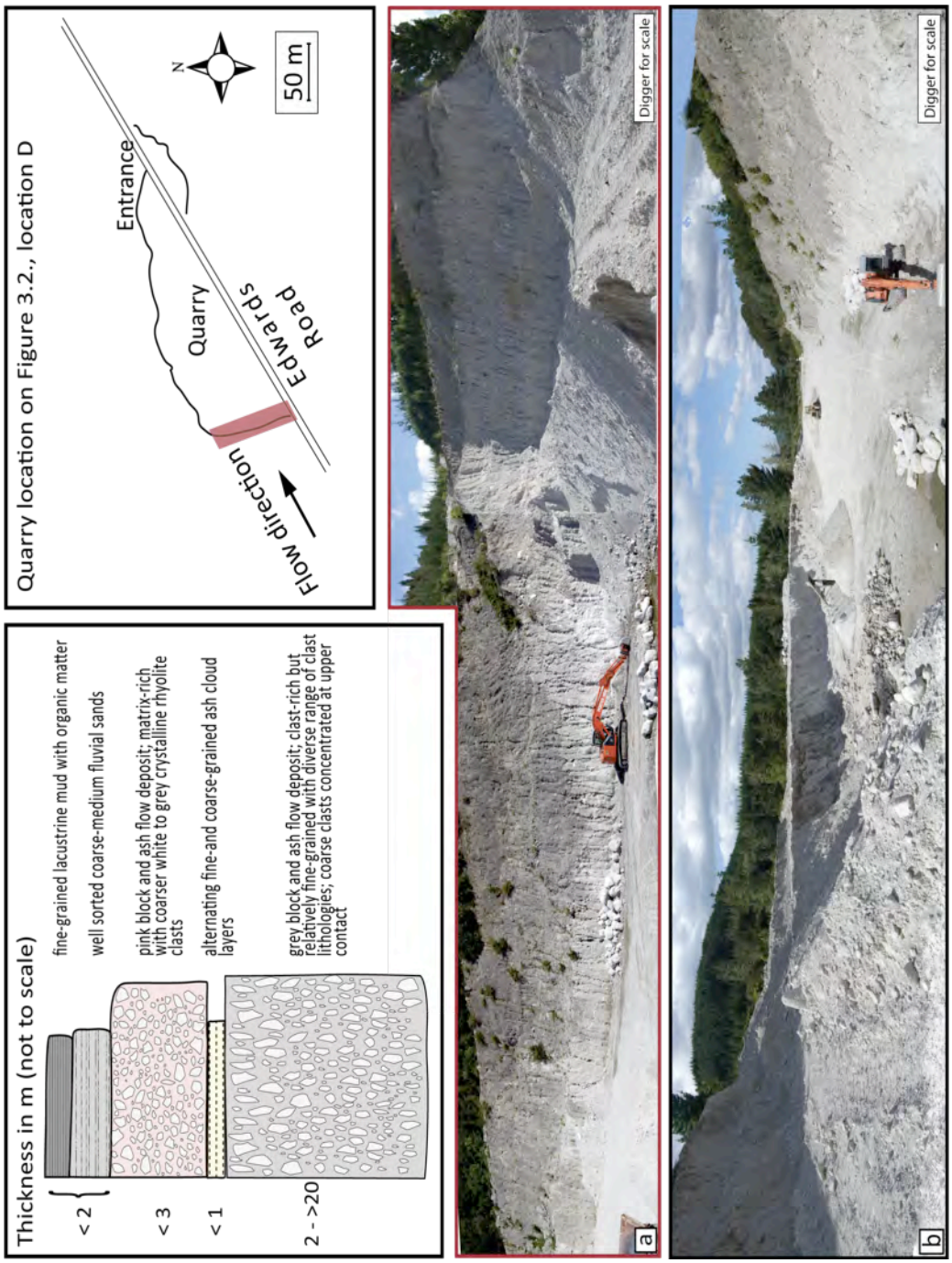

Figure 3.13: Overview of the quarry at Edwards Road (V16/215295), showing a simplified stratigraphic column (thicknesses are highly variable) for the exposure and a plan view of the quarry marking the location of (a) and (B) in red. (a) The southwestern face of the quarry shows massive grey block-and-ash flow deposits, with a thickness > 30 m. (b) View from the southwestern end of the quarry along the flow direction.

The quarry has excavated the block-and-ash flow deposits parallel to Waiaute Stream, displaying up to 30 m thick deposits in the southwestern side of the quarry (width c. 60-70 m), with decreasing deposit exposure (< 5 m) to the northeastern end (width c. 30 m).

The southwestern face exposes massive and poorly sorted grey block-and-ash flow deposits;, no bedding is visible (Figure 3.13). In the middle of the quarry face, reddish discoloration of the block-and-ash flow material by thermal oxidization indicates hot emplacement of the flows. The upper 1-2 m of this part of the quarry represents another possible flow unit. This unit seems to be finer-grained than the lower part, and

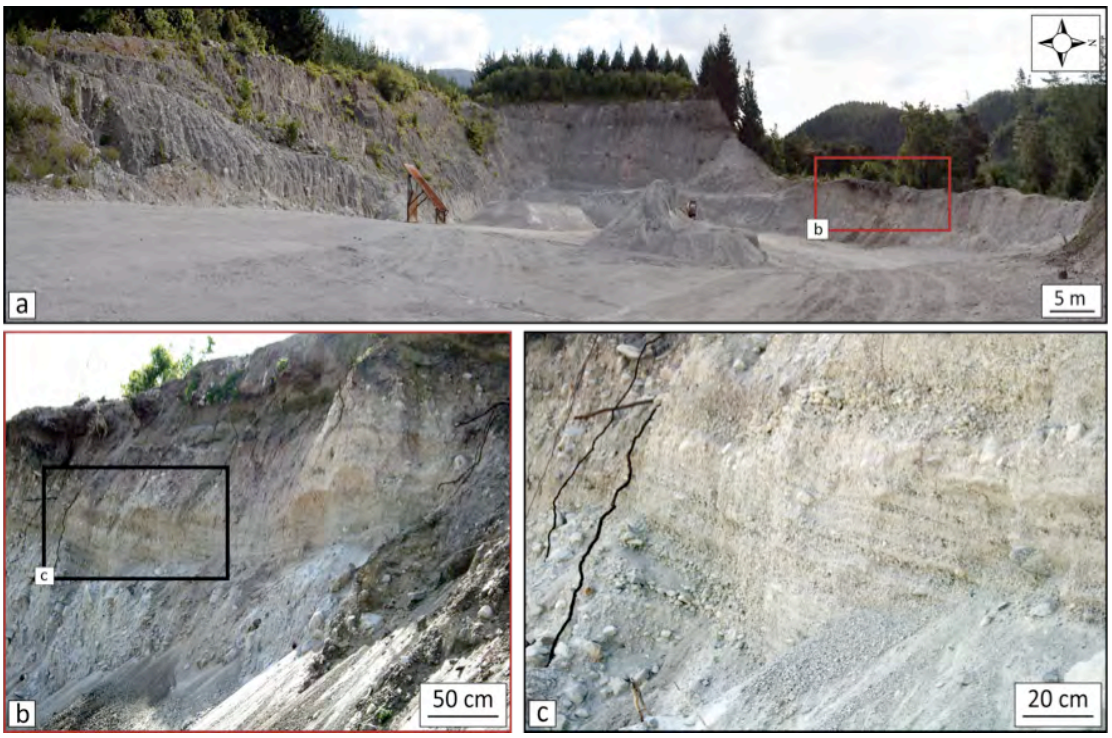

Figure 3.14: Exposure of massive block-and-ash flow deposits at Edwards Road (V16/215295). (a) Overview of the quarry to the southwest. (b) Northeast dipping ash cloud layers separate lower grey block-and-as flow deposits from upper pinkish deposits. (c) Detailed view of alternating coarse-and-fine-grained ash layers.

the clast size decreases from the lower unit to the top of the exposure.

The northern face of the quarry is characterized by massive, grey block-and-ash flows overlain by c. 1 m thick ash layers dipping to the northeast parallel to the flow direction (Figure 3.14). The top of this side of the quarry is marked by a pinkish block-and-ash flow unit, ranging in thickness between 30-120 cm. The ash layers are characterized by alternating thin fine-grained and thicker coarse-grained beds within a total thickness of 30-80 cm, dipping at c. 15° to the northeast (Figure 3.14). Further

along the flow direction, closer to the eastern entrance of the quarry, ash cloud layers again are exposed, dipping opposite to the direction of the flows, with a smaller angle (c. 10°; Figure 3.15). The material is thinly bedded with alternating fine-and coarse-grained layers. The horizontal distance between both ash layer exposures is c. 60 m, with a vertical height difference of c. 6 m. Elevation differences between the individual

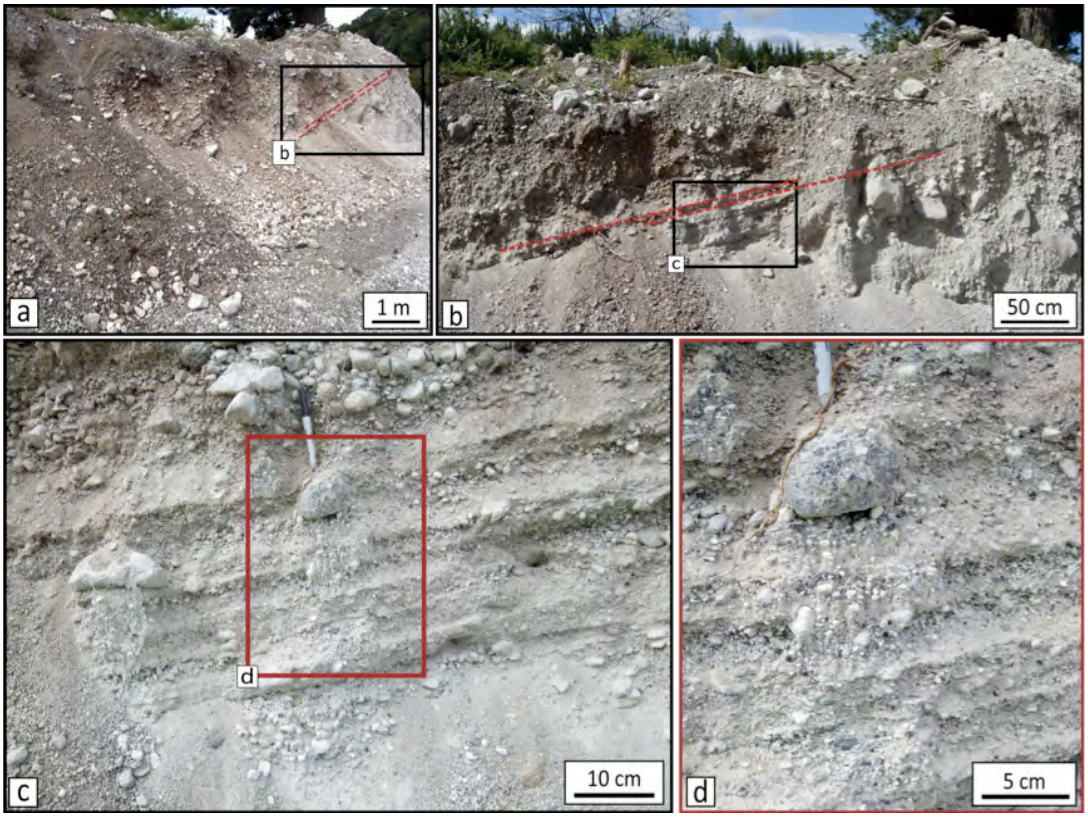

Figure 3.15: (a) Exposure of thick ash cloud layers on the northeastern face of Edwards Road quarry (V16/215295). (b) Ash cloud layers are dipping opposite the flow direction, grading into reworked section of the deposits. (c) Alternating coarse-and- fine-grained ash beds separate block-and-ash flow deposits (Pen for scale). (d) Detailed view of the ash cloud layers overlying grey block-and-ash flow deposits.

ash layers suggest possible undulating surfaces of the main body of a thick flow unit, with ash cloud surge layers mantling a surface depression.

Between both exposures of ash cloud layers along the northern quarry face, a c. 10 m long section is characterized by strong alteration and reworking, marked by dark discoloration of the complete deposit thickness. No welding was detected. Along this section, ash cloud layers are horizontal and are only found within the upper third of the deposit. These ash/lapilli layers are generally coarse-grained, but finely laminated, showing only slight undulation (Figure 3.16).

Alternating ash cloud layers were only observed on the northern side of the deposit, but this might be more due to the fact that excavation of the quarry was not pursued to the south than to the absence of these layers on the southern side of the quarry. Edwards Road runs parallel to the southern margin of the quarry, so further excavation in this direction would affect this forest track. Therefore this quarry face has not been freshly excavated; it is marked by alteration and discoloration of the surface as well as patchy vegetation cover. Depositional features such as ash cloud layers or thermal oxidation were not observed on this side.

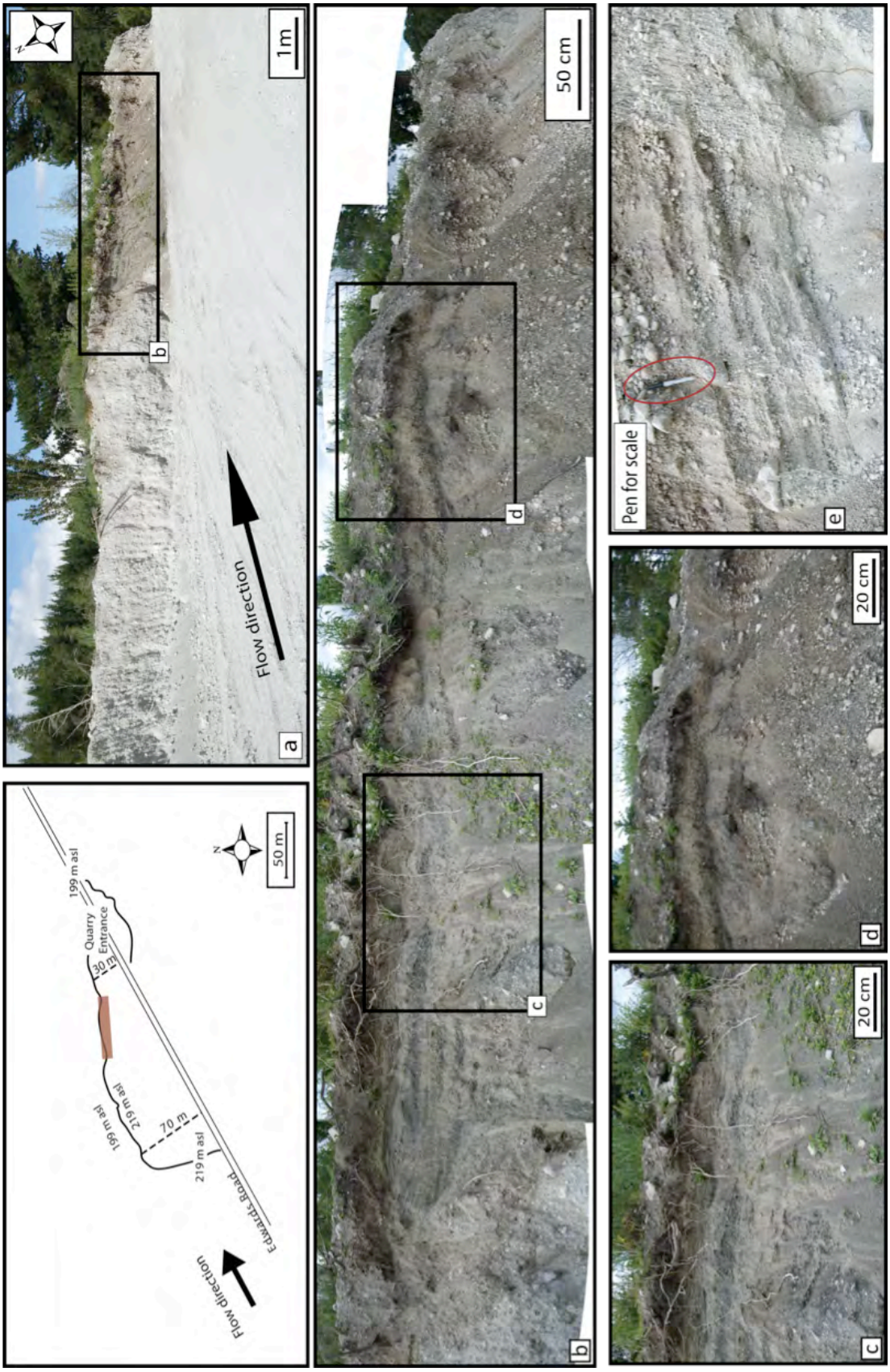

Figure 3.16: (a) Parts of the northern face of Edwards Road Quarry (V16/215295) are strongly re-worked, the location within the quarry is marked on the plan view sketch. (b) This part is c. 10 m long and characterized by strong discoloration and heavy alteration. (c) Planar ash layers dominate the upper third of this section. (d) Subdued bedding is apparent in the upper part, the lower part is massive and strongly altered. (e) Earlier described ash layers mark the transition from unaltered to reworked parts of the deposit.

3.5.2. Cumings Road Quarry

At Cumings Road (V16/261279; Figure 3.4, loc. E), c. 7.3 km from Wahanga dome, a > 10 m high quarry face exposes matrix-supported grey block-and-ash flow deposits as well as two ash-rich beds with undulating bedforms above the Kaharoa Tephra. With a length of c. 120 meters and a width of c. 40 meters, the deposits are exposed parallel to the flow direction, showing a cross-section through valley-filling block-and-ash flow deposits.

The Kaharoa Tephra underlies the two ash-rich beds with undulating bedforms that can be best observed on the northern side of the quarry (Figure 3.17). It would be reasonable to assume that the filling of the valley corresponds to the cross-section of the river valley, even though the quarry is located at least 100 meters west of the river valley. It is possible that smaller topographic depressions of various depths were responsible for the ponding of the deposits.

The fine-grained and well-sorted deposits above the tephra are interpreted as ash cloud surge deposits, being overlain by a thin ash fall deposit. Three block-and-ash flows occur above these ash-rich beds. The lower two flow units comprise a grayish ash matrix, whereas the uppermost block-and-ash flow deposit is thermally oxidized, with pink discoloration. It is not clear if the thermal oxidation marks a new flow unit or just the altered top of a massive grayish block-and-ash flow deposit. The top of the deposits is generally reworked, with gravels and cross-bedded sands. The sequence of block-and-ash flows and gravel layers is overlain by a planar laminated grey lahar deposit (Figure 3.17).

The northeastern side of the deposit is characterized by undulating and folded ash layers, with faults cutting through some of them. The extensive folding of the creamy white ash layers (thickness ranges between 30-60 cm) concentrates in the upper third of the deposit, possibly due to the emplacement of the gravel layers.

The thickness of the individual block-and-ash flow units is highly variable; the lower, matrix-rich, grey deposit is generally the thickest unit and is characterized by small obsidian chips and white-grey rhyolitic lithics. It is overlain by a pale grey, often stratified block-and-ash flow; the coarse clasts are slightly smaller than in the lowest grey block-and-ash flow deposit. The clast size of the pink deposit is smaller than that

of the lowest one, but appears to be coarser than in the second flow unit. Carbonized wood fragments can be found in all three units, but in a higher abundance in the lowest grey block-and-ash flow unit.

Figure 3.17: (a) Valley-confined block-and-ash flow deposits are exposed at Cumings Road quarry (V16/261279). (b) The northern face of the quarry shows a cross-section through a paleo-valley filled by multiple block-and-ash flow units (compare simplified stratigraphic column). (c) The underlying ash and tephra layers are slightly deformed. (d) Individual flow units show highly variable thicknesses. (e) The lowest grey block-and-ash flow deposit exhibits a sharp contact to light-colored ash layers.

3.5.3. Crater Road Quarry

The quarry at Crater Road is located c. 4 km from Ruawahia Dome (V16/178195; Figure 3.4, loc. A), with a length of c. 130 m and a width of 40 m, representing the medial parts of the deposits. The quarry is aligned approximately perpendicular to the direction of flows from Ruawahia dome. The currents seems to have traveled first > 1 km nearly horizontally after the volcanic slope graded into the run-out plain, before encountering a small ridge (< 10 m high), climbing over it and infilling a topographic depression with deposits up to 3.5 m thick that nowadays accommodates the quarry.

On the northwestern side of the quarry, the block-and-ash flow deposits (BAFD) have a thickness of < 50 cm; the contact to the substrate is exposed only within this side of the northern quarry face. Kaharoa Tephra layers underlie a greenish to orange fine-grained massive layer of c. 30 cm thickness, overlain by the block-and-ash flow deposit (Figure 3.18). In the deposits further to the east, only the main body and parts of the ash cloud deposits are displayed, showing thicknesses of > 3 m. The grey block-and-ash flow deposits are massive and clast-supported; clasts up to 2 m diameter are set in fine ash matrix.

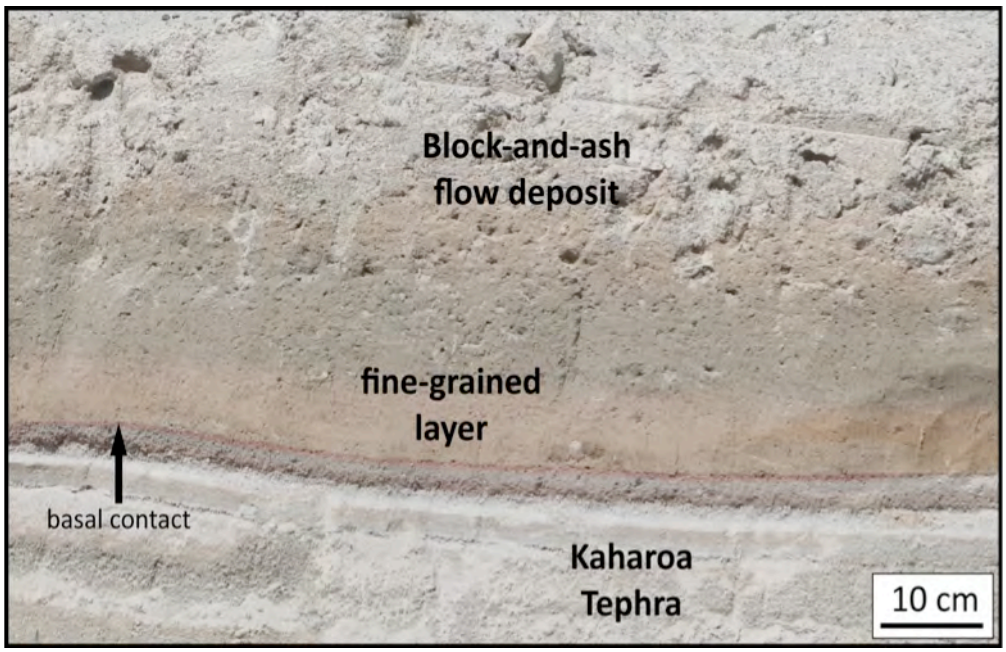

Figure 3.18: A fine-grained layer separates Kaharoa Tephra layers from block-and-ash flow deposits at Crater Road (V16/178195). The basal contact is marked by a thin reddish ash layer (arrow).

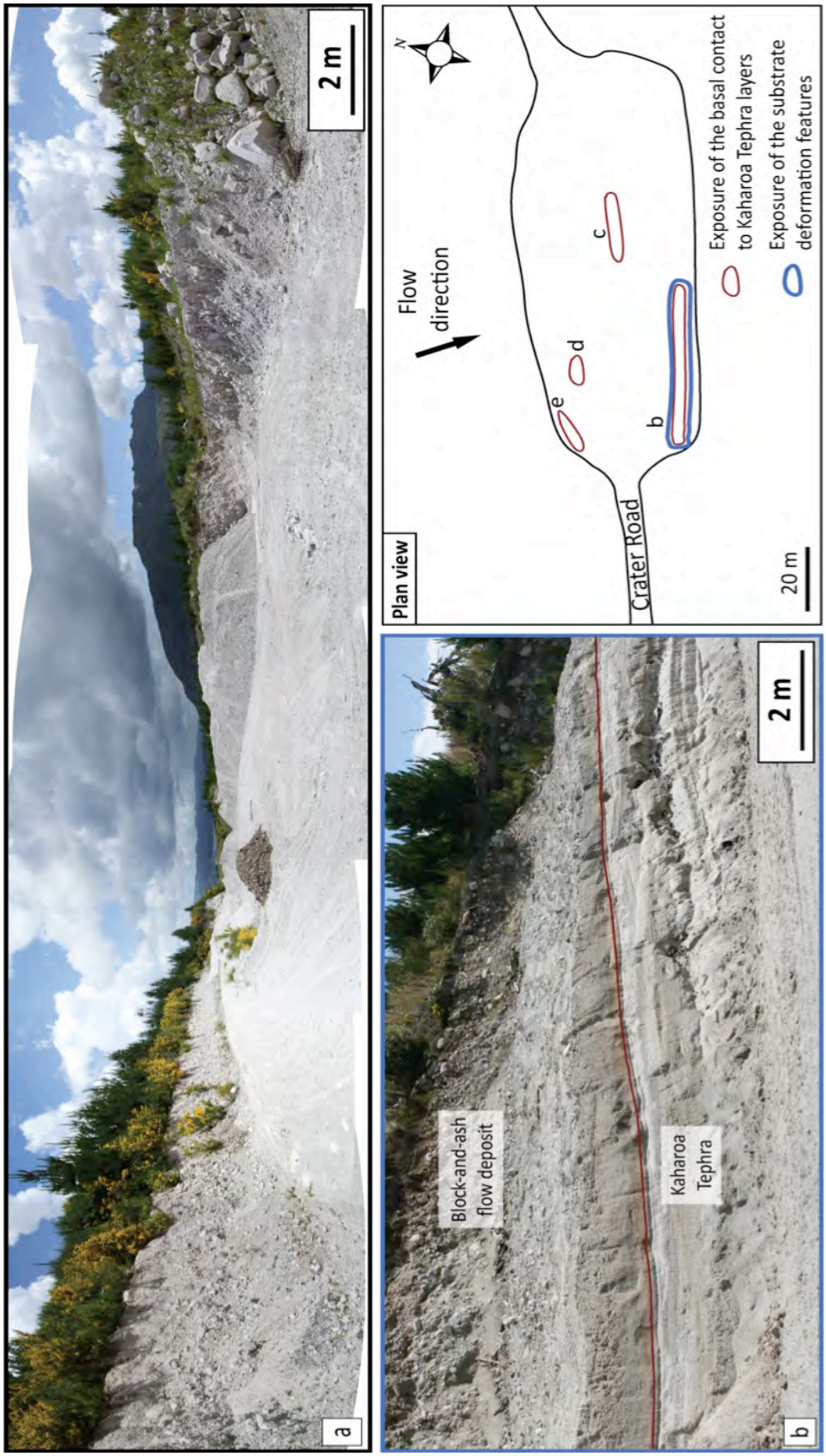

Figure 3.19: Exposure of the contact between the base of the block-and-ash flow deposit and the substrate within Crater Road quarry (V16/178195). (a) Overview of the quarry from the eastern end (see plan view sketch). (b) Exposure on the southern side of the quarry, location of the substrate deformation features.

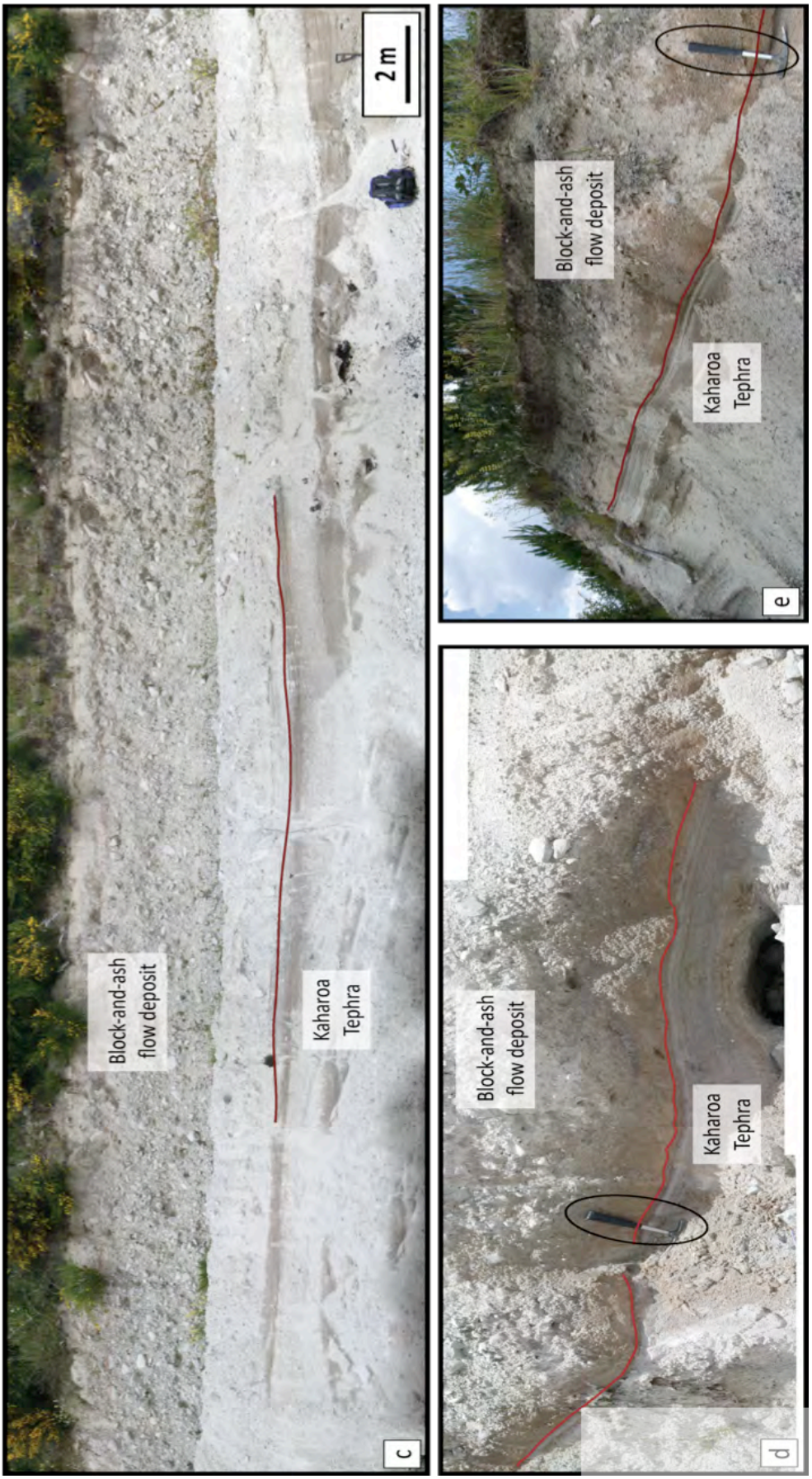

Figure 3.19 continued: c) Exposed contact (marked in red) in the middle of the quarry. (d) and (e) represent exposures on the northern side of the quarry. Hammer for scale is 30 cm long.

The southern face of the quarry shows a more continuous exposure of the contact with the Kaharoa Tephra layers, over nearly half the length of the quarry (> 60 m). The thin reddish ash layer (< 5 cm thick) that marks the contact is overlain by a greenish to orange massive, fine-grained layer, with a thickness between 3-70 cm. On top of it, up to 3 m of grayish, clast-supported block-and-ash flow material were deposited. The contact to the block-and-ash flow deposit is generally gradational, only a few locations show a sharp erosional contact (this is decribed in more detail in chapter 4).

In addition to the northern and southern side, the contact with the Kaharoa Tephra is exposed in another location in the middle of the quarry, overlain by < 40 cm of the massive, fine-grained layer; due to the extensive excavation, the block-and-ash flow deposit is missing here. At the western entrance of the quarry, the contact lies c. 4 m above the quarry floor, a few meters further on the northern side, the contact lies at 2.5 m above the quarry floor, whereas in the middle and southern regions the contact lies c. 1.70 m above the ground (Figures 3.19). The basal zone of the fine-grained layer is characterized by soft-sediment deformation structures, such as flame structures and erosion gullies, indicating a dynamic interaction between Kaharoa Tephra and this deposit during its emplacement (compare Chapter 4). These features are concentrated on the southern face of the quarry, due to the limited exposure of the contact within the quarry, but on the northern side, c. 2.5 m above the ground, the basal contact is characterized by small erosional features as well.

The exposure at Crater Road shows remarkable similarities to the ideal ignimbrite flow unit suggested by Sparks et al. (1973). This ideal sequence (Figure 3.20) comprises three parts, a fine-grained ground layer (layer 1), overlain by a graded basal ash layer (layer 2a), followed by the main body of the flow (layer 2 b), either with a sharp contact or gradational transition to the ash layer. Layer 3 generally represents the ash cloud surge deposit on top, which is not always present, generally only when the main body was deposited first and then the fine ash settled from the overriding ash cloud surge.

Comparing the deposits at Crater Road, from the fine-grained layer above the Kaharoa Tephra to the ash cloud surge deposits at the top (Figure 3.18), with the ideal

ignimbrite unit by Sparks et al. (1973), the individual parts of the deposit can be classified accordingly.

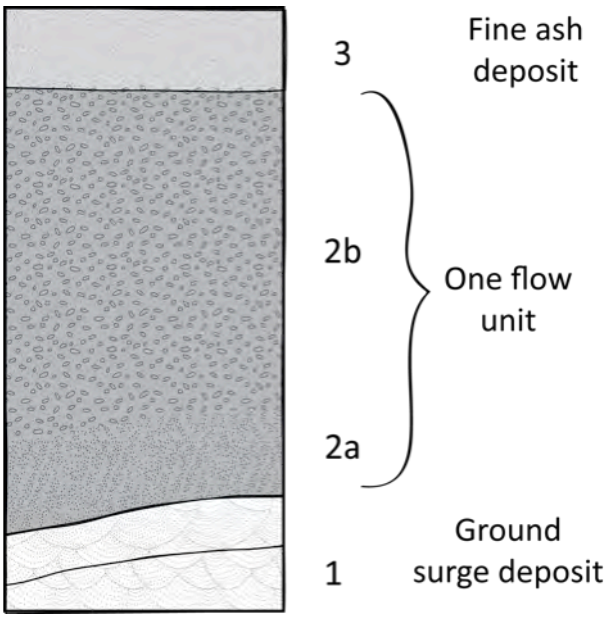

Figure 3.20: Schematic depiction of an ideal ignimbrite flow unit (modified after Sparks et al., 173). For further explanation see text.

3.5.3.1. Layer 1

A ground layer (layer 1) is not clearly distinguishable in the outcrop, the base of the block-and-ash flow deposit is generally represented by Sparks' layer 2a (1973). The contact to the underlying Kaharoa Tephra layers is characterized by a thin, reddish ash layer from the earlier stages of the eruption, reflecting the erosive nature of the basal avalanche. The red colour of the ash is possibly the result of the hot emplacement of the block-and-ash flow, so that thermal oxidization altered the topmost layers of the Kaharoa Tephra.

3.5.3.2. Layer 2a

The emplacement of block-and-ash flows can be associated with deposition of a fine-grained base, similar to ignimbrites, e.g. at Citlaltépetl volcano in Eastern Mexico (Carrasco-Núñez, 1999) or at Unzen volcano in Japan (Miyabuchi, 1999), These basal layers have been described as ranging in thickness from several centimeters to c. 1 m,

always showing a gradational contact to the clast-supported, coarse main body of the flow. The fine-grained layer beneath the block-and-ash flow deposits at Crater Road is up to 70 cm thick, very fine-grained and massive, but poorly sorted. As a result of thermal oxidation, the ash-sized material ranges in colour from orange to greenish-grey. Overlying this layer is the main body of the flow, the contact between these parts being usually gradational. The main body material is often mixed into the fine-grained parts of the basal avalanche.

3.5.3.3. Layer 2 b

The thickness of the main body ranges between 2.5 and 3 m due to variations in the underlying topography. This layer contains non- to poorly vesiculated rhyolite blocks and clasts from 1-150 cm in diameter, set in a fine-grained unconsolidated greyish ash matrix. The clasts are porphyritic and vary in vesicularity from moderately vesicular breadcrust clasts with large (0.5-1.3mm) spherical and coalesced vesicles, to almost non-vesicular, perlitic clasts with scattered domains of very small (< 20 µm) elongate vesicles (Allen and McPhie, 2003)

The blocks are mostly subangular to subrounded, some showing perlitic structures (cooling fractures). The clast-supported material of the main body is greyish-white; the deposit is massive and shows no grading. Near the base of the main body, localized accumulation zones of smaller clasts can be found.

3.5.3.4. Layer 3

The upper 50-60 cm of deposit generally comprise smaller pinkish clasts set in a matrix of the same material. A reddish thin oxidation layer that is the result of iron leaching from the overlying AD 1886 basalt into the block-and-ash flow deposit marks the contact to the ash cloud surge deposit. This layer represents deposition from either ash fall or ash cloud surge deposits. The material comprises brownish-grey ash and lapilli. The contact with the underlying main body material is usually gradational, with larger blocks often protruding from the main body into the surge deposit.

The classification of the individual parts of the deposits according to Sparks et al. (1973) is based on the assumption that the fine-grained layer represents a basal shear

layer generated during the advance of the block-and-ash flows, but further studies of the deposits revealed another relationship of these beds. Erosion gullies mark a sharp contact between the fine-grained layer and the overlying block-and-ash flow deposits, indicating a time break between their emplacements. The fine-grained layer represents an individual event, unrelated to the emplacement of the block-and-ash flow, which is exposed at Crater Road. Proposed hypotheses and detailed explanations for the origin of this layer are provided in Chapter 4.

3.5.4. Ash Pit Road Quarry

Another quarry in the southern pyroclastic fan is located at Ash Pit Road near the shore of Lake Rerewhakaaitu (V16/176189; Figure 3.4, loc. C), representing the distal regions of this fan. The quarry is c. 150 m long, and 60 m wide, and is divided by a farm track into two parts. The main part is located to the south, whereas the second part is comparatively smaller and located to the northwest (Figure 3.21 sketch). The thickness of the exposed BAF deposits range between c. 1 - 5.5 m from the south to the north. The total thickness of the BAF deposit could not be determined, as nowhere in the quarry is a complete section through the deposit exposed.

The contact with the underlying Kaharoa Tephra is exposed in the middle and the southwestern region of the quarry (see Figure 3.21). In the smaller, southwestern section, a thick sequence of various tephra and ash layers from earlier stages of the Kaharoa eruption underlies the thin exposure of the block-and-ash flow deposit. The contact between Kaharoa Tephra layers and the basal part of the block-and-ash flow is oblique and marked by a thin cross-bedded surge deposit. At this location, only c. 1.2 m of the block-and-ash flow deposit is displayed. The other section where the basal contact is exposed lies in the main quarry near the crossing of the farm track. Here the contact is c. 70 cm above the quarry floor, so the flows encountered a small topographic irregularity while traveling further towards the shores of Lake Rerewhakaaitu.

Within the rest of the Ash Pit Road quarry only the upper parts of the block-and-ash flow are exposed. From the northern to the southern end of the quarry, the deposit becomes less matrix-rich and more clast-supported respectively. Generally the more

clast-supported parts are characterized by smaller clast sizes than the matrix-rich section at the eastern margin. Large boulders found in the quarry (Figure 3.21a) are part of the block-and-ash flow deposit, however, some of the blocks were taken from other locations around and disposed off in the quarry which is used as a depository for metal, tires and wood by the owner.

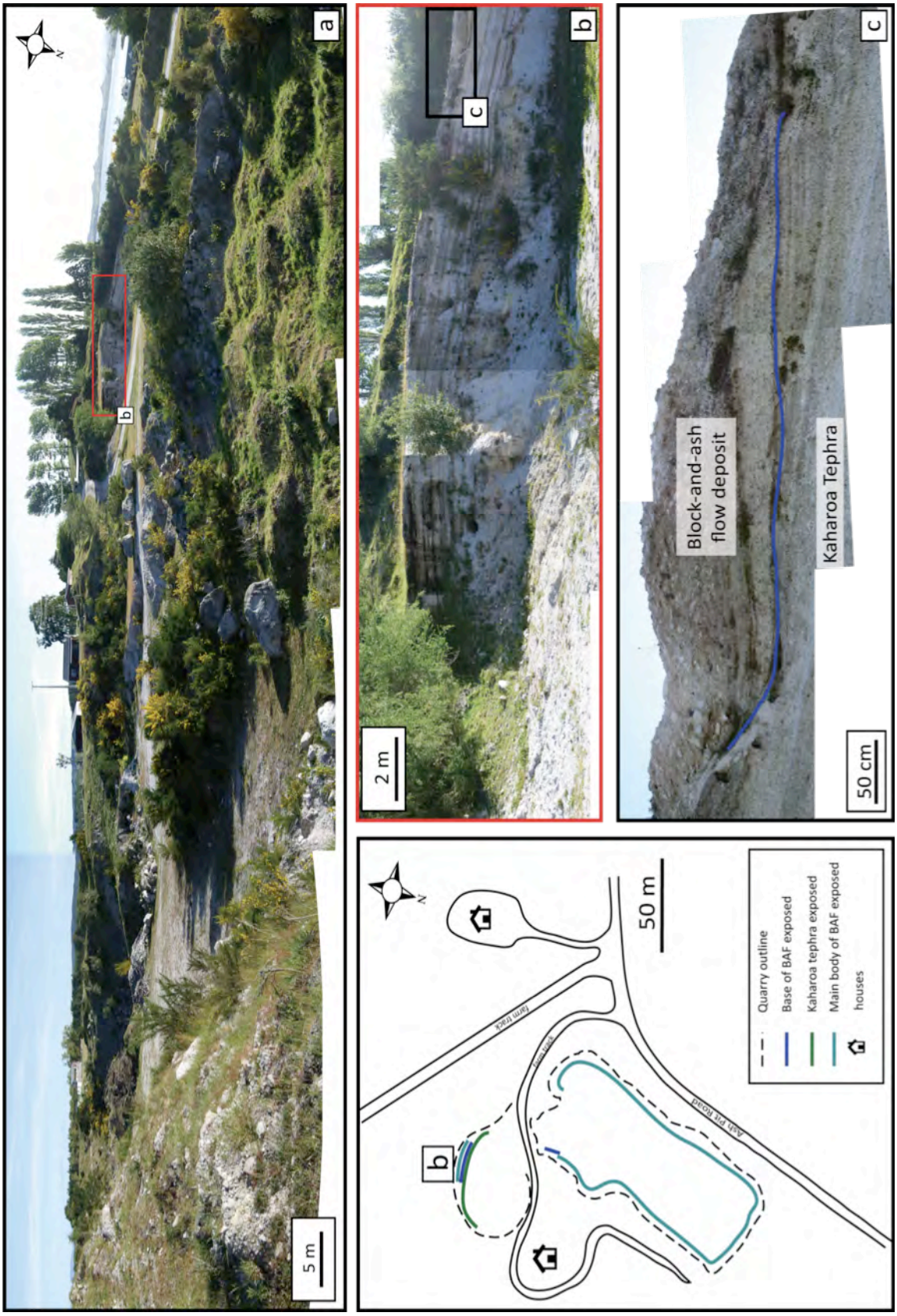

Figure 3.21: (a) Overview of the quarry at Ash Pit Road (V16/176189), representing the distal regions of the southern pyroclastic fan. The sketch shows a plan view of the outline of the quarry and exposure scenario. Exposure of the contact with the substrate is best in the smaller part of the quarry (b). But only the lowest 100 cm of the block-and-ash flow deposits are exposed (c), the total thickness of the deposit could not be determined.

3.6. General lithology of the block-and-ash flow deposits

The Kaharoa eruptive episode is characterized by four rhyolitic groups (Nairn, 1989) – dome rhyolites, pumice-rich pyroclastic flow deposits, rhyolites in block-and-ash flows and fine pyroclastic ash and lapilli, all porphyritic and hypocrystalline. The groundmass generally ranges from clear/glassy to spherulitic and from colourless to light brown, displaying highly variable vesicularity depending on the rhyolite type.

The following generalized lithological description is based on the primary block-and-ash flow deposits, making up more than 50 % of all Kaharoa pyroclastic deposits. The BAFD generally consist of rhyolitic juvenile clasts, lithics, ash and free crystals. Rhyolites are generally creamy-white or grey with dispersed biotite, ranging in size from < 1 mm (fine ash) to more than 5 m in diameter (clasts). The clasts are highly variable in size and shape, ranging from subangular to subrounded. They are chemically identical to the dome lavas (Nairn et al, 2001).

The juvenile rhyolitic component can be divided into white/clear crystalline rhyolite (poorly to highly vesicular), obsidian and grey crystalline rhyolite as well as individual crystals (quartz, biotite). Juvenile components range in density from 2.3-2.7 g/cm^3. Non-juvenile clasts within the deposits include basalt (sometimes as inclusions within the rhyolite), obsidian from the Waiohau eruptive episode and further accidental lithics. Rare plutonic lithic clasts (< 5 vol%) are mostly granitoids, plus diorite, gabbro and olivine-clinopyroxenite (Cole, 1970a; Leonard et al., 2002). These clasts were contained in the original dome lava; they were not picked up during the advance of the block-and-ash flows over the substrate.

Pumice fragments in the block-and-ash flow deposits are usually creamy-white, ranging from 2 cm to 30 cm. The fragments are set within a matrix of ash-sized material, varying from clast- to matrix-supported.

Vesicularity ranges from moderate to high (Leonard, 1999), the vesicles are often elongated, giving the clasts a fibrous texture (at least in grain size fractions smaller than 1cm). Vesicularity of the individual samples of the block-and-ash flows does not differ significantly between the southern (20-25%) and the northern (10-25%) deposits.

The phenocryst assemblage is plagioclase feldspar, quartz, biotite, orthopyroxene and opaque minerals. Phenocrysts content strongly depends on the type of rhyolite. Proximal pumiceous airfall pumice fragments show average contents of c. 25%, whereas medial airfall pumice contents are c. 11% on the average. Samples from the southern block-and-ash flow have a higher phenocryst content (33-38%) than those from the northern block-and-ash flow (c.18-27 %; Leonard, 1999).

3.7. Granulometry

Samples were taken from over 100 locations in both major block-and-ash flows (Appendix A-2) in order to establish lateral and temporal variations in sedimentology related to flow dynamics and the influence of the underlying topography. All samples collected in the field were taken from the matrix of block-and-ash flow deposits as well as from uppermost ash cloud surge deposits, in addition larger clasts were collected for further analysis. All samples were dry-sieved and weighed at the University of Canterbury, separating grain size fractions to half phi sizes between < -3 (10 mm) and > +5 phi (32 µm). Comparing the individual samples from the various flows in both pyroclastic fans was based on separating the flows into unconfined and confined flows for the northern block-and-ash flows. This is not necessary for the southern deposits, because there the lateral, unconfined spreading dominates the flow dynamics; channeling only occurred in the most proximal parts near the source.

The distribution of the individual grain size fractions ranges from unimodal to polymodal for both block-and-ash flow and ash cloud surge deposits. Polymodal particle size distributions for the block-and-ash flow deposits show main modes at 3.5 and 2.25 phi, for the ash cloud surges at 0.5 and 4 phi. The block-and-ash flow deposits are generally composed of decimeter to metre-sized blocks in a matrix of ash (sand-sized). The largest blocks are typically between 1 and 5 m in size. The matrix, resulting from the comminution of larger rhyolite clasts, is mostly coarse ash to fine lapilli-sized (max. 3 mm), with slight amounts of very fine ash-sized particles (< 20%). Ash Sorting of the deposits ranges from well sorted (σ 1.0-1.26) for ash cloud surge deposits to poorly sorted (σ 2.1-3.85) for block-and-ash flow deposits (sorting values σ for pyroclastic deposits are 0-1 = very well sorted, 1-2 = well sorted, 2-4 = poorly sorted,

and >4 = very poorly sorted; compare Cas & Wright 1988).

Block-and-ash flow deposits at Tarawera are strongly influenced by the pre-existing topography; channels and valleys were filled up to 30 m, small topographic highs are mantled by thin (< 2m) veneer deposits. The northern to northeastern flow deposits are characterized by extreme channeling of individual flows within two major river valleys between pre-existing lava plateaus. The flows generated by the collapse of the eastern rims of Wahanga Dome encountered breaks in slope which should also be reflected within the grain size distribution.

The northern block-and-ash flow fan radiates to the east and northeast (Figure 3.22). The eastern flows, channeled along the Waiwhakapa River valley, shows a progressive size decrease from the dome to the distal regions of the deposits for clasts > -3 phi (> 10 mm Ø), independent of the pre-existing topography. The flows deposited to the northeast show a decrease in clast-size from the proximal to the medial parts, but at Edwards Road quarry (Figure 3.4, loc. D), where the flows have been channeled and emplaced up to 30 m of block-and-ash flow material, the percentage of clasts > -3 phi increased, followed by a decrease to the most distal parts of the deposits. The block-and-ash flows forming the northern fan have mostly polymodal grain size distributions, apart from the most proximal samples showing unimodal grain size distributions with typical modes at -5 phi (Figure 3.22). Ash cloud surge deposits were sampled as well, however, no significant change in grain size distribution could be observed.

In the southern block-and-ash flow fan, flow channeling only occurs near the source; from the medial to distal parts the flow spread out unconfined to the east, west and south. A few deeply incised valleys on the proximal slopes probably directed the flows to the medial regions, slightly channeling the basal granular avalanche, whereas the more turbulent ash cloud surge traveled straight ahead.

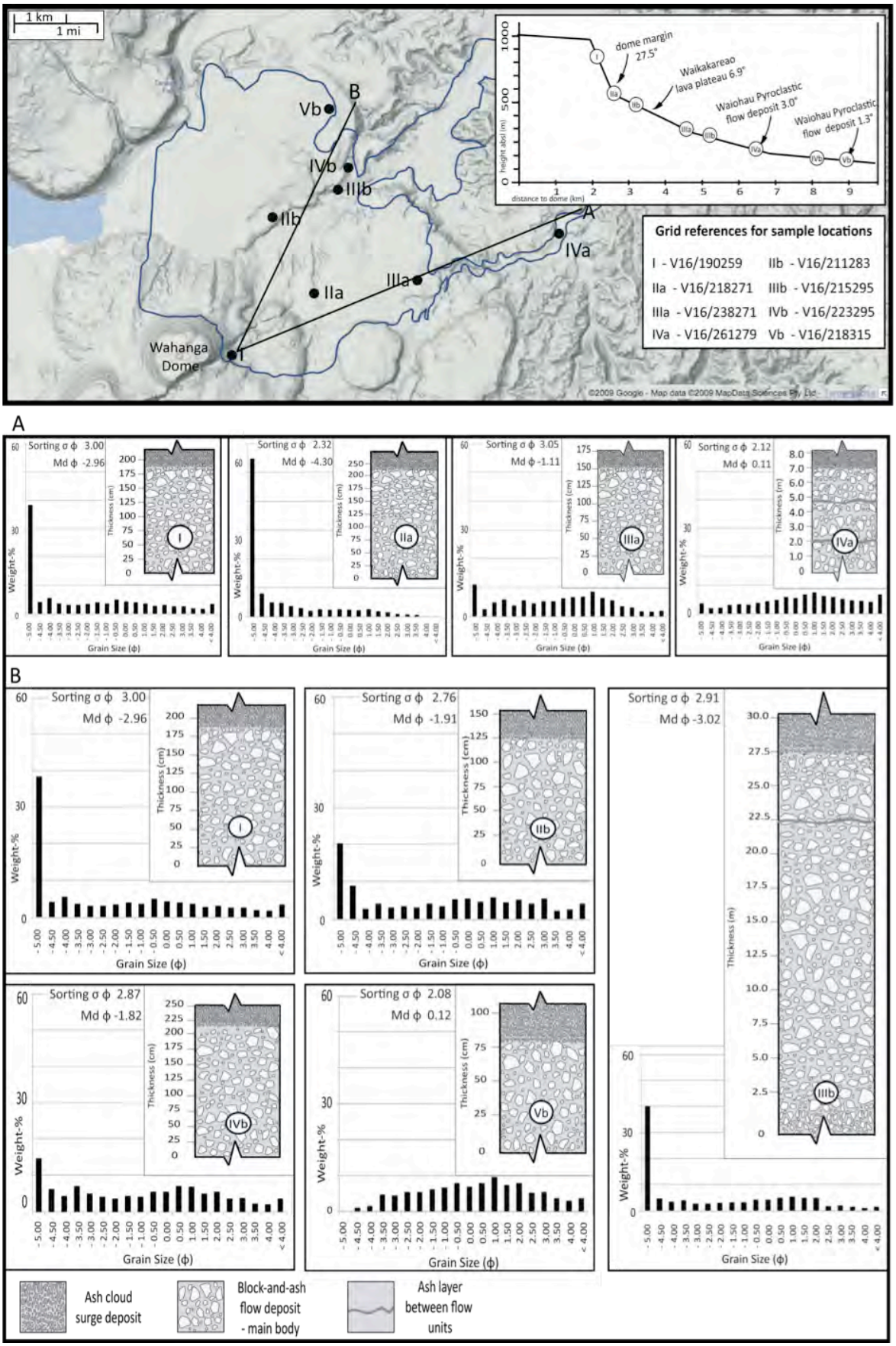

Figure 3.22: Stratigraphy and grain size distribution of the northeastern block-and-ash flow fan along two profiles (A and B) from proximal to distal regions of the deposits. Samples were taken from the main body of the deposits, representing median diameters. Sorting values for pyroclastic deposits are: 0-1, very well sorted; 1-2, well sorted; 2-4, poorly sorted; >4, very poorly sorted (see Cas & Wright 1988).

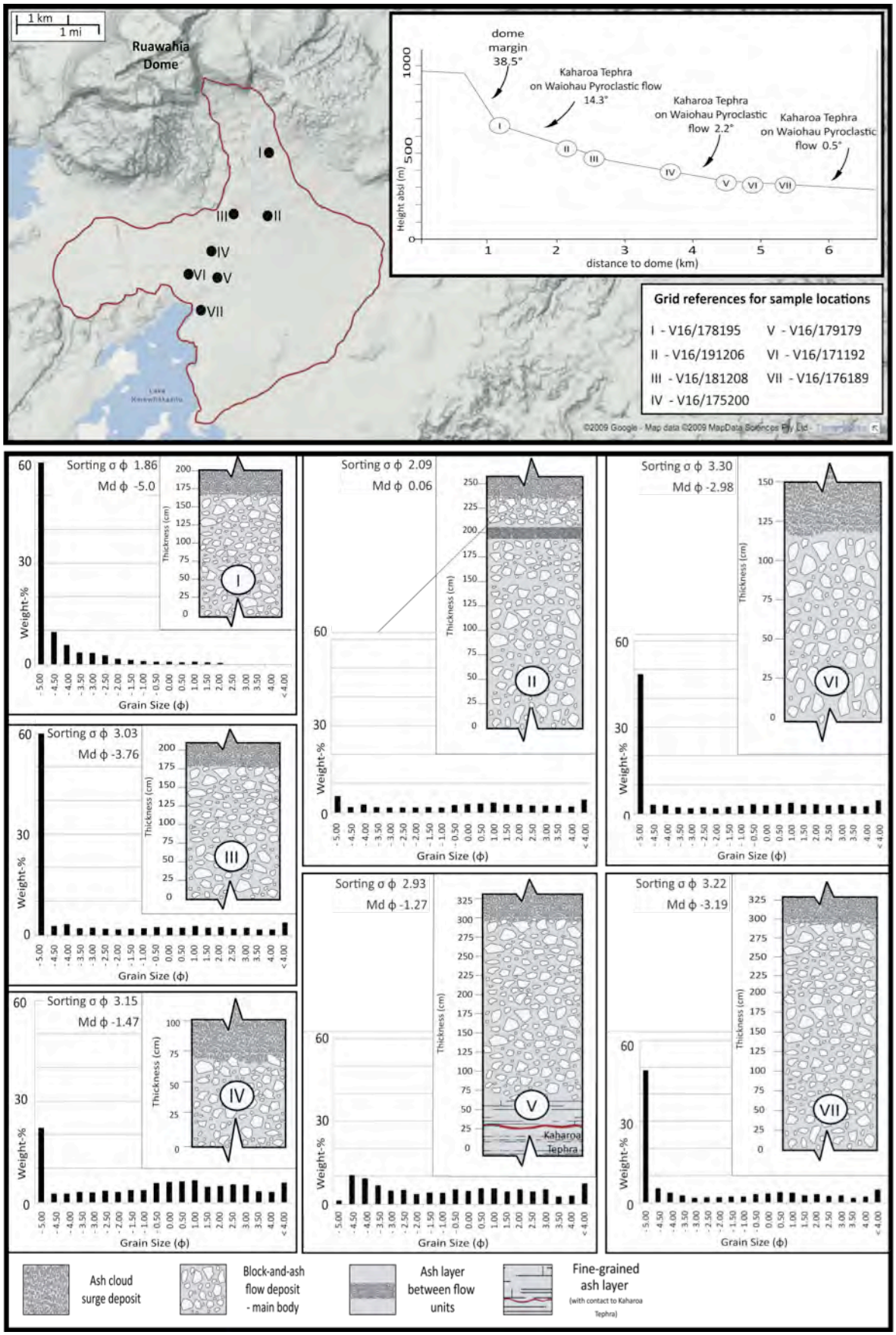

Figure 3.23: Stratigraphy and grain size distribution of the southern block-and-ash flow fan along a profile from proximal to distal regions of the deposits. Samples were taken from the main body of the deposits, representing median diameters. Sorting values for pyroclastic deposits are: 0-1, very well sorted; 1-2, well sorted; 2-4, poorly sorted; >4, very poorly sorted (see Cas & Wright 1988).

The block-and-ash flows forming the southern fan have mostly polymodal grain size distributions, apart from the most proximal samples which show unimodal grain size distributions with typical modes at -5 phi (Figure 3.23). Ash cloud surge deposits were sampled as well, however, no significant change in grain size distribution could be observed.

This fan is characterized by smooth underlying terrain, the only break in slope is the dome margin, and channeling occurs merely in the proximal regions. The grain size distribution shows a nearly steady decrease from the proximal to medial regions for clasts larger than -5 phi, from medial to distal regions an increase of this clast size is apparent, therefore no positive correlation between clast diameter and distance from the source can be made (Figure 3.24).

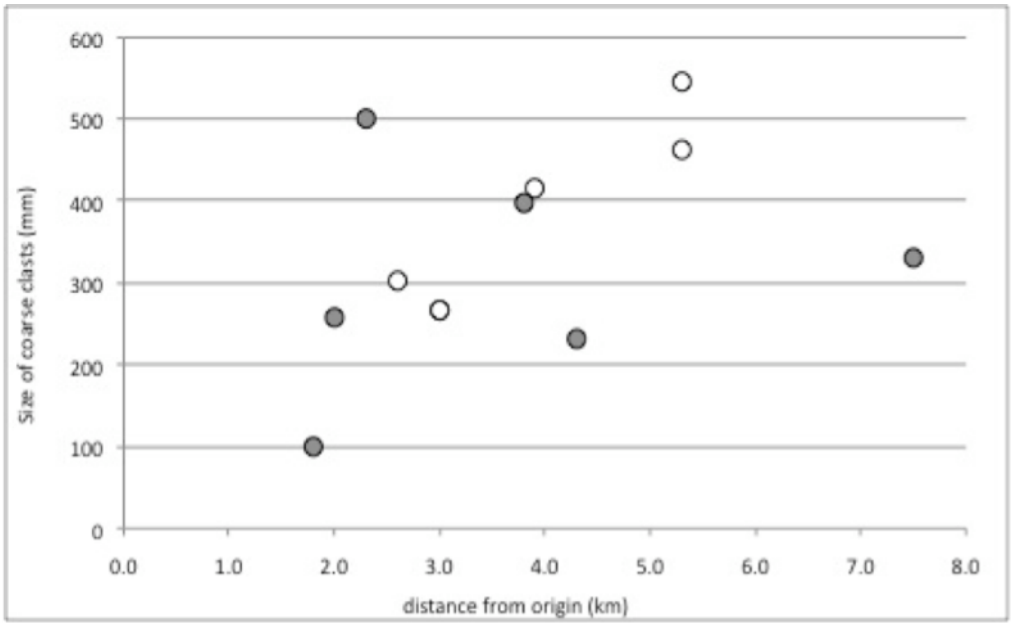

Figure 3.24: Relationship between block size and distance from the dome within both major bloc-and-ash flow fans. Open circles represent blocks from the northern deposits, samples from the southern fan are shown by closed circles.

3.7.1. Crater Road Quarry

At Crater Road, where a complete section of the block-and-ash flow is exposed, samples were taken from the fine-grained layer beneath the block-and-ash flow deposit, from different parts of the main body and the ash cloud surge deposit on top (Figure 3.25). The basal part of the deposit is fine-grained, median grain size is 2.25

phi. The lower part of the main body is characterized by a percentage increase in clasts > 10 mm, showing the transition from the matrix-supported basal part to the clast-supported main body of the deposit. The main body comprises less than 10% of fine-grained (< 3 phi) matrix ash and the percentage of clasts > -5 phi increases drastically. The ash cloud surge deposit overlying the main body is well sorted with a bimodal grain size distribution; typical modes are between 1 and 3 phi and at < 4phi.

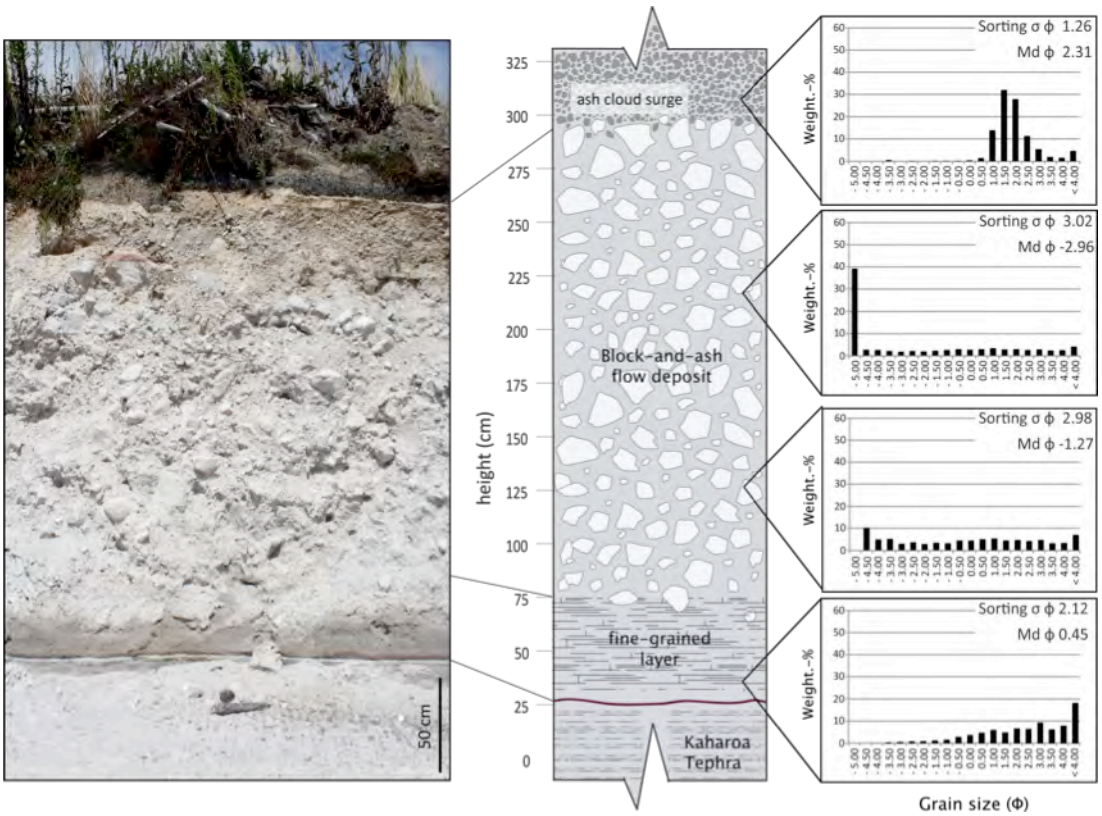

Figure 3.25: Stratigraphic profile of the distal parts of the southern block-and-ash flow deposits with a simplified grain size distribution of the different regions of the flow deposit. The profile is exposed at Crater Road (see loc. C on Figure 3.4).

3.7.2. Ash Pit Road Quarry

Samples taken from the quarry at Ash Pit Road (V16/176189) include one sample from the contact zone to the Kaharoa Tephra and two samples from the main body of the deposit, one from each side of the quarry. The basal sample is coarser grained than the exposed base at Crater Road; however, although visual observation indicate smaller clast sizes for the more clast-supported southern region of the quarry, the samples taken indicate a similar distribution for the grain size fractions (Figure 3.26).

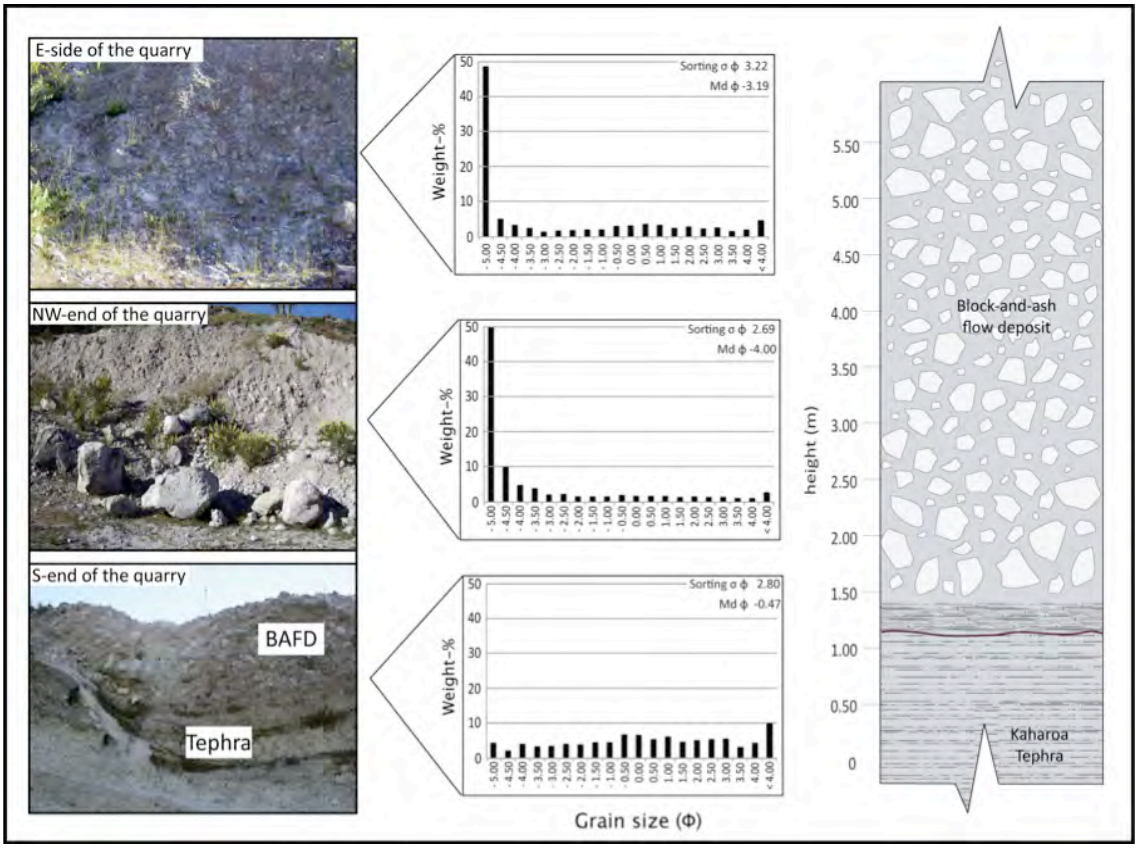

Figure 3.26: Simplified stratigraphic profile of block-and-ash flows deposits at Ash Pit Road quarry (V16/176189). Samples were taken from the contact zone with Kaharoa Tephra, and from two different locations of the main body – the sample in the middle from more matrix-supported regions, and the upper samples from clast-supported parts of the deposit. For further explanation see text.

3.7.3. Edwards Road Quarry

The northern block-and-ash flow deposits are exposed in two large quarries, both located in confined region of the deposits. Samples from the quarry at Edwards Road (V16/215295) were taken from the far end where > 20 m of a massive grey block-and-ash flow unit is exposed. Further samples were taken from the ash cloud layer on the northern side, possibly representing an ash cloud surge layer beneath a succeeding block-and-ash flow deposit (Figure 3.27).

The ash cloud layer and the underlying block-and-ash flow deposit were both sampled at the altered section on the northern side of the quarry. Comparing the samples from both main bodies showed polymodal distribution, the unaltered section being coarse-grained and poorly sorted. The ash cloud layers are slightly bedded, again the unaltered region showing poor sorting and coarser grain sizes (Figure 3.27).

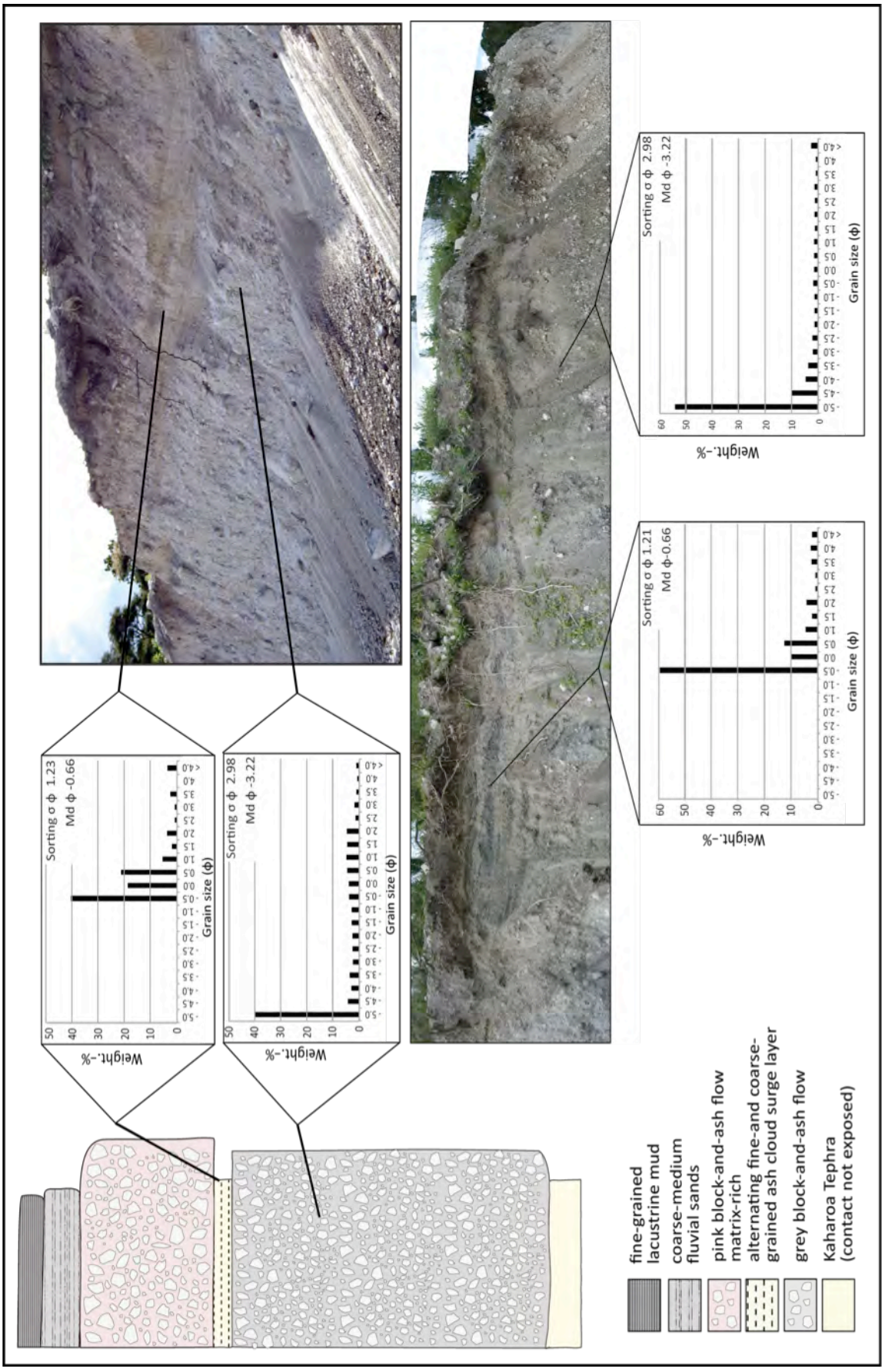

Figure 3.27: Grain size distribution in the quarry at Edwards Road (V16/215295), representing unaltered (upper picture) and altered deposits (lower picture) comprising the main body and ash cloud surge layers.

3.7.4. Cumings Road Quarry

The grain size distribution at Cumings Road (V16/261279) represents valley-fill deposits of up to 10 m. In the quarry, three individual flow units are exposed, and representative samples were taken from the matrix (Figure 3.28). The lowest grey block-and-ash flow unit is coarser-grained than the overlying pink unit, and both units are poorly sorted. The contact to the underlying light tephra layer is better sorted and finer-grained, similar to the basal parts at Crater Road. The third, diffusely stratified block-and-ash flow unit is pale grey; clasts are smaller than in the lowest grey flow unit, but larger than in the pink block-and-ash flow. In the western parts of the quarry, thin ash layers separating the individual flow units could be found, but it was not possible to trace them through the whole exposure.

Figure 3.28: Grain size distribution of the valley-filling block-and-ash flow deposits at Cumings Road quarry (V16/261279) in the northeastern pyroclastic fan, according to the different exposed flow units.

3.8. Discussion

Block-and-ash flows were generated by the collapse of the outer rims of Ruawahia and Wahanga Dome during the later stages of the Kaharoa eruptive episode. These were of larger volume than comparable flows at Unzen or Soufriere Hills Volcano (Table 3.3). Mass, volume and the vertical drop of pyroclastic density currents generally show a decrease with run-out distance, the ratio of drop height and run-out distance (H/L ratio) being an important factor for determining the mobility of the individual flows. The initiation of the block-and-ash flows due to gravitational instability of the lava dome commonly requires high slope angles. At Merapi, the flows were generated at angles of c.35° (Boudon et al., 1993), at Unzen at c.25° (Yamamoto et al., 1993) and at Soufriére Hills at c.30° (Cole et al., 1998). The Kaharoa block-and-ash flow generation at c.28-39° upper slope angles is consistent with these observations.

3.8.1. High mobility of block-and-ash flows

The relationship between vertical drop (H) of the pyroclastic mass and the eventual run-out distance of the flow (L) has been described as the apparent coefficient of friction or the Heim coefficient (Hsü, 1975). The H/L ratio is often used as a measure of mobility, with low values indicating high mobility.

The vertical drops (H) at Tarawera Volcano are slightly smaller than those at Unzen Volcano, which might suggest a smaller run-out (Table 3.3). However, the mobility of the block-and-ash flows is controlled more by the flow volume than the vertical drop (Legros, 2002). Volumes of individual block-and-ash flows at Tarawera Volcano are up to two orders of magnitude higher than at Soufriére Hills and Unzen volcano. The H/L ratio for the Kaharoa block-and-ash flows ranges between 0.15-0.17 for the southern deposit and 0.17-0.19 for the northern pyroclastic fan. Individual exposures show lower (0.09; e.g. Cumings Road quarry) or higher values (0.39; Edwards Road quarry), due to topographic influence. Comparing the H/L ratios with block-and-ash flow at Soufriére Hills (0.15 for larger flows and 0.28-0.31 for shorter flows) or Unzen Volcano (H/L ratio ≈ 0.3), pyroclastic flows at Tarawera Volcano are highly mobile with greater volumes and greater run-out.

CHARACTERISTICS	TARAWERA VOLCANO	MOUNT UNZEN	SOUFRIÉRE HILLS
Slope angle	27-39° (dome margin)	≈34° (talus slope)	≈30°
Vertical drop	610-680 m	700-1000 m	600-1200 m
H/L ratio	0.17-0.19	0.3-0.5	0.28-0.31
BAF run-out distance	ave: 5 km max.: 10 km	ave.: 1 km max.: 5.5 km	ave.: 1 km max.: 6.5 km
BAF deposit volume	max. 100 x 10^6 m^3	max.: 4 x 10^6 m^3	ave.: 5 x 10^6 m^3 max.: 9 x 10^6 m^3
Total erupted volume, including lava domes	10 x 10^8 m^3; (domes: 8.3 x 10^8 m^3)	2.1 x 10^8 m^3 DRE; (dome: ~ 1 x 10^8 m^3)	2.18 x 10^8 m^3; (dome: 1.10 x 10^8 m^3)

Table 3.3: Comparison of the characteristics of block-and-ash flows at Tarawera Volcano with similar flows at Mount Unzen, Japan, and Soufriére Hills Volcano, Montserrat.

Individual block-and-ash flows at Tarawera traveled up to five times further than the pyroclastic flows at the other two volcanoes. A number of possible explanations for prolonged run-out distances of pyroclastic density currents are presented in the literature. At Unzen it has been observed that block-and-ash flows traveled further over basement rocks than over substrate comprising recent pyroclastic material. The softer and unconsolidated pyroclastic material may have a cushioning effect and prevented further fragmentation (Nakada and Fujii, 1993). However, loose substrate material may also be incorporated into the flow, increasing the volume and the run-out. The block-and-ash flows at Unzen also show a positive correlation between velocity and run-out. Increased velocity (c. 26-28 m/s) produced BAFs that traveled up to three times further than slower flows (c. 14 m/s; Ui et al., 1999). High proportions of hot lava blocks within the block-and-ash flow can promote the generation of fine ash due to the fragmentation of the blocks during flow, either colliding with the substrate or each other. Thermal stress and the residual gas will promote breakage of the clasts, further enhancing the mobility of the flows due to possible fluidization effects initiated by fine ash production and gas release during the clast break down (Mellors et al., 1988; Nakada and Fujii, 1993; Ui et al., 1999).

While all these factors may explain increased run-out distances of the block-and-ash flows, few are applicable at Tarawera. Block-and-ash flows were emplaced over unconsolidated tephra from earlier stages of the eruption, implying an impeded run-out. The incorporation of substrate material into granular flows to prolong the run-out has been suggested for non-volcanic rock avalanches (Hungr and Evans, 2004), and this concept is also applicable to pyroclastic flows and powder snow avalanches (Barbolini et al., 2005; Ancey, 2001). The incorporation of substrate material, as observed at Crater Road quarry (compare Chapter 4), probably increased the volume of the flows and therefore the run-out of the flows.

3.8.2 Erosional capacity of the block-and-ash flows

Several erosion gullies have been cut into the Kaharoa Tephra layers, most of them probably carved by water runoff after the emplacement of the tephra layers, confirming a time break before the deposition of the block-and-ash flows proposed by Nairn et al. (2001). The tephra is overlain by a fine-grained layer, and at their interface, evidence of dynamic interaction between these deposits can be found in form of shear deformation, bulldozing and flame structures. Detailed descriptions and explanations are given in Chapter 4.

3.8.3. Time-break events within Kaharoa eruptive episode

The contact to the Kaharoa Tephra layers is locally exposed in the southern block-and-ash flow deposits. Usually the coarse block-and-ash flow deposits directly overlie the tephra, but within the large quarry at Crater Road, a fine-grained, massive layer was described, underlying the coarse block-and-ash flow deposit. It has been suggested that this layer represents the basal shear layer developing from the advancing block-and-ash flow as has been documented at Unzen Volcano (Miyabuchi, 1999). Supporting this hypothesis is the gradation between the fine-grained layer and the coarse main body of the block-and-ash flow deposit, and erosional structures found at the contact between Kaharoa Tephra and the massive basal layer (compare Chapter 4).

Erosion gullies and scour marks are common occurrences, varying in scale and shape. A

large erosion gully (c. 40 cm deep), now filled with block-and-ash flow material, reaches into the Kaharoa Tephra layers, confirming an already established time break after the emplacement of the tephra layers (Nairn et al., 2001). But at the same location, several erosion gullies (not as deep as the first one) can be found at the top of the fine-grained layer, filled by the overlying block-and-ash flow deposit, indicating a time break between their deposition. A detailed discussion about the origin of these fine-grained layers and their emplacement has been proposed in Chapter 4.

3.8.4. Evidence for hot emplacement of the block-and-ash flows

Block-and-ash flows can be generated by different eruption mechanisms, as suggested by Sparks et al. (1997) and Druitt (1998). The gravitational collapse of parts of the lava dome is the most commonly acknowledged generation process.

The outer parts of endogenous domes are cooler than the inside, therefore the emplacement of the resulting block-and-ash flows does not necessarily have to be extremely hot; typical signs of hot emplacement might be missing in the deposits. Common evidence for the hot emplacement of these flows are charred pieces of wood, including sometimes even remnants of tree trunks which have been observed at Crater Road quarry.

Another sign of hot emplacement of block-and-ash flows is welding of the sediment as has been observed at Mount Meager, British Columbia (Michol et al., 2008). But such occurrences are rare, and welding is more usually described from ignimbrites and pumiceous pyroclastic density curents. During the hot emplacement of these hot currents, plastic deformation and fusion of glass shards due to mechanical and welding compaction results in the reduction of porosity and deformation of glass shards.

At Tarawera Volcano, some indicators were observed in parts of both block-and-ash flow fans. Charred wood can generally only be found in the deposits of Kaharoa Tephra. The emplacement of the associated pumice-rich pyroclastic flows probably burned and devastated the vegetation, entraining burned trees and plants into the pyroclastic deposits.

3.8.4.1. Breadcrust bombs

Breadcrust textures can be found in volcanic bombs whose surfaces have cracked due to vesiculation and expansion of the bomb interior after chilling of its surface, indicating an explosive origin as ballistic ejecta. Generally breadcrust clasts are not common in the block-and-ash flow deposits at Tarawera, but subangular to subrounded bread-crusted rhyolite blocks were observed in the southern pyroclastic fan (e.g. V16/198217 and V16/181226), possibly being preserved by the smoother terrain underlying this fan. Along the access road to the summit of Tarawera Volcano, c. 1.6 km horizontal distance from Ruawahia Dome, a flattened breadcrust bomb was found, representing the most proximal part of the block-and-ash flow deposits from Ruawahia Dome (Figure 3.29).

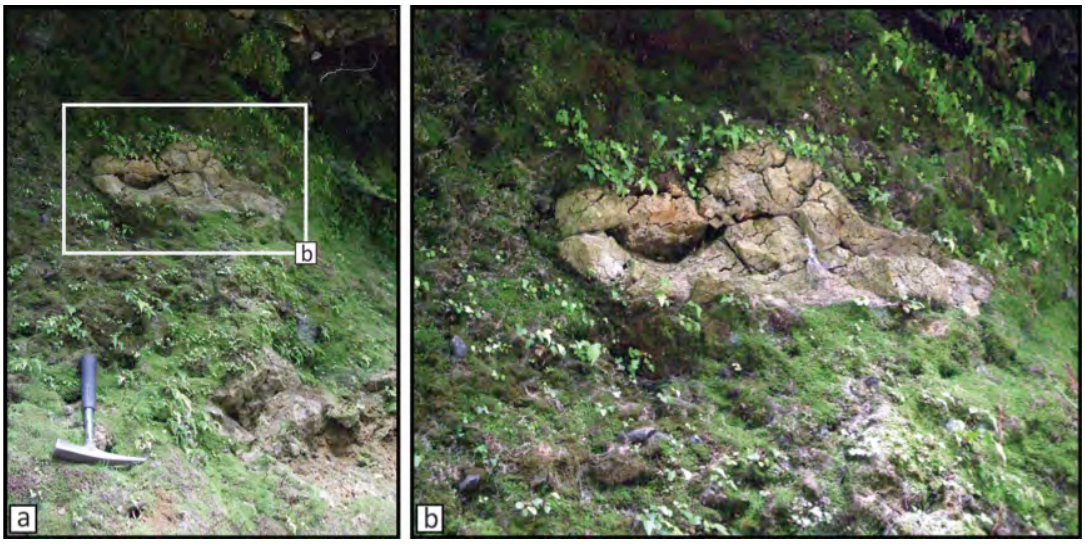

Figure 3.29: Breadcrust bomb exposed on the Access Road to the summit of Tarawera Volcano, found c. 1.6 km horizontal distance from Ruawahia Dome (V16/198217). Geological hammer has length of 30 cm.

3.8.4.2. Perlitic clasts

Perlitic clasts are abundant in both major block-and-ash flow deposits. Blocks larger than 10 cm show often cracks (Figure 3.30) caused by the hydration or heating of obsidian above softening temperatures (slightly < 900°C) and expansion of the material. At these temperatures, water trapped in the structure of the material vapourises and creates bubbles in the heat softened rock. The formation of these

bubbles allows the expansion of the material to 15–20 times its original volume and the production of a froth-like structure (Pichór and Janiec, 2009). The expanded material can be a brilliant white, due to the reflectivity of the trapped bubbles.

3.8.3.3. Gas-escape structures

Figure 3.30: Variety of perlitic clasts occurring in the block-and-ash flow deposits at Tarawera Volcano.

After the deposition of hot pyroclastic density currents, gas trapped within and between the clasts can escape from the deposits, as has been observed at the Valley of Ten Thousand Smokes, Alaska (Griggs, 1922). In ignimbrite deposits, the occurrence of gas-escape structures is often identified by fumarolic mounds on the surface. Within the deposit, smaller pipes can show that gases moved with sufficient upward velocity to transport particles. Such pipes are often enriched in crystals and lithic fragments and depleted in dust-size tephra (Walker, 1972). These fines-poor pipes usually vary from centimeters to several meters in length, and from millimeters to decimeters in width, and range from subtle to well developed.

At Tarawera Volcano, possible gas segregation pipes occur in the northern block-and-ash flow fans along Edward Road (V16/215295). Excavation of the block-and-ash flow material revealed holes in the newly exposed quarry floor (Figure 3.31). These holes could indicate a cross-section of gas-escape pipes from lower parts of the deposit, similar to the plan view of degassing pipes at Merapi Volcano (Charbonnier and Gertisser, 2008).

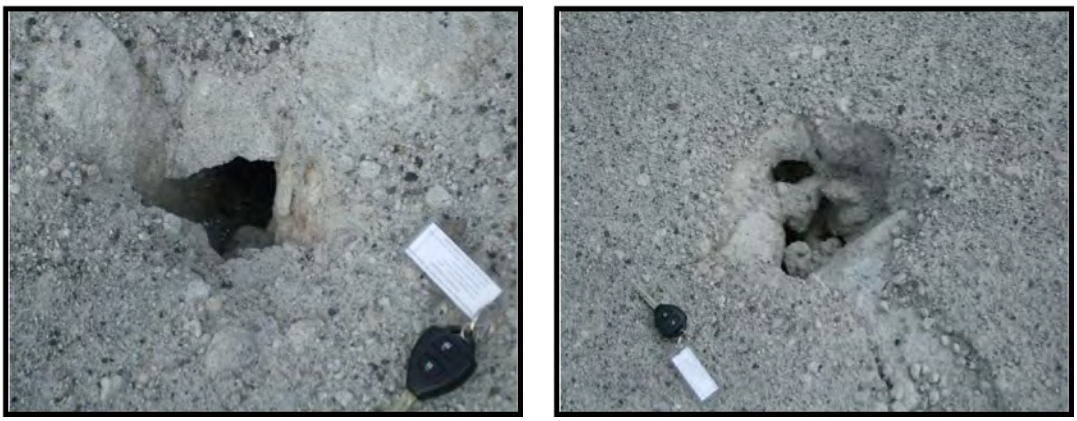

Figure 3.31: Possible gas escape structures evident at Edwards Road quarry (V16/215295). After further excavation of the quarry, these pipe-like structures were discovered, exposed on the floor of the quarry. The pictures show a plan view of the gas escape structures.

Pipe-like structures extending vertically from the surface of the deposit are prominent in most of the exposures of both block-and-and flow fans. These features vary in length and width (Figure 3.32), and seem to be fines-depleted. As these pipes have

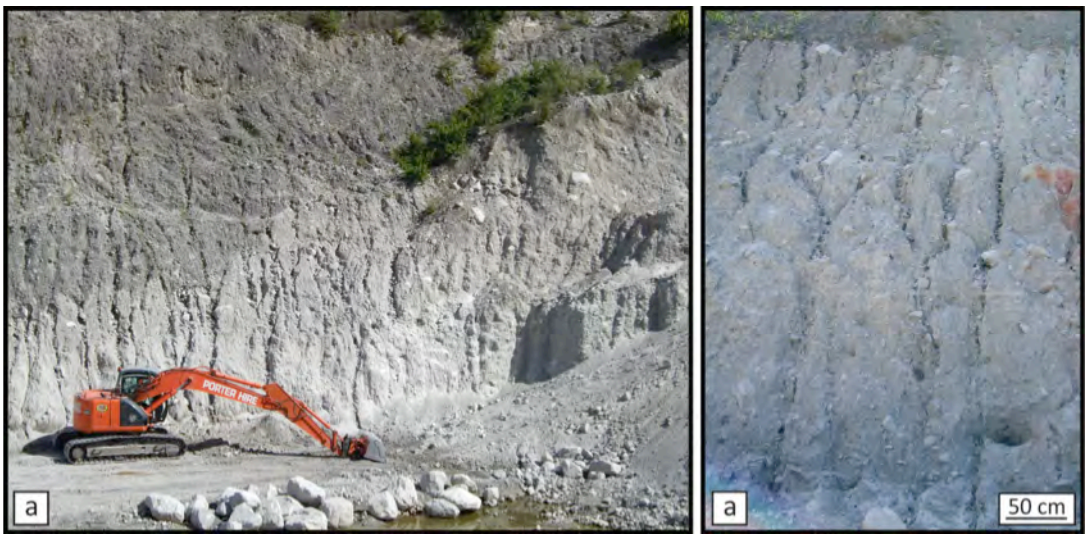

Figure 3.32: Drainage pipes caused by surface erosion from rainwater runoff on the side face of the exposed block-and-ash flow deposits at Edwards Road quarry (V16/215295). Digger for scale.

only been observed on the exposed surface of the block-and-ash flow deposits, it is more likely that they are related to drainage from rainwater and not to gas escape within the deposit.

Chapter 4

Substrate deformation structures at Tarawera Volcano, New Zealand

"Scientific research consists in seeing what everyone else has seen,

but thinking what no one else has thought."

Chapter 4: Substrate deformation at Tarawera Volcano

4.1. Introduction

The interaction of a moving avalanche with the substrate over which it flows is inevitable. Mobilization and erosion of the substrate has been described from rock and snow avalanches (e.g. Yarnold and Lombard, 1989; Barbolini et al., 2005), debris flows and avalanches (e.g. Vallance et al., 1995; Schneider and Fisher, 1998; Capra and Macías, 2000; Capra et al., 2002), turbidity currents (e.g. Hall et al., 2008; Meiburg and Kneller, 2010) and pyroclastic density currents (e.g. Sparks et al., 1997a; Miyabuchi, 1999; Abdurachman et al., 2000), often demonstrating remarkable similarities in the style and extent of interaction, independent of the avalanche type and environment.

Typically, pyroclastic density currents not only deposit material along their flow path, but also erode and incorporate sediment or vegetation into the basal part of the advancing flow. For example, Kieffer and Sturtevant (1988) described erosion furrows at Mount St.Helens, and Sparks et al. (1997b) recognized the stripping of scree and talus from the steep volcanic flanks of Lascar Volcano, resulting in striations, percussion marks and erosional furrows. Volcanologists at Soufriére Hills Volcano also documented substrate erosion and the incorporation of this material into block-and-ash flows (Cole et al., 2002).

Given the highly destructive nature of pyroclastic currents, it is remarkable that syn- or post-depositional features have only rarely been described for these deposits. The lack of descriptions may, however, be due to lack of observations rather than the absence of these features.

4.2. Substrate deformation by pyroclastic density currents

The processes acting during the emplacement of pyroclastic density currents are extremely difficult to observe directly in the field. However, evidence preserved in outcrops combined with observations made during laboratory granular flow experiments and theoretical considerations, provides a good picture of how substrates are mobilized, eroded, transported and incorporated by the moving avalanche.

For the estimation of the erosive potential of pyroclastic currents, it is important to understand when and how a sediment mass can fail, and how it can be mobilized, eroded and deformed by internal or external causes. Generally any material will fail when the applied stress exceeds the strength of the material. A pyroclastic density current can modify the substrate in several ways, e.g. by exerting shear stress, loading the substrate, transmitting shock waves through the substrate, heating it, causing expansion of pore water, liquefying it, and also fluidizing the substrate by loading or by steam generation (Branney and Kokelaar, 2002). Any combination of these effects can lower the strength of the substrate and can be important in promoting erosion by pyroclastic density currents.

These currents have been described as diverse in nature, however they seem to have some basic unifying characteristics, such as an upper low-density turbulent ash cloud and a ground-hugging, dense and less turbulent basal avalanche (Sparks, 1976). The basal part of a moving current overrides the substrate and is responsible for any depositional and erosional behaviour, containing the highest concentration of particles and possibly suppressing turbulence altogether. At the bottom of the basal avalanche, the existence of a “lower flow boundary” (Branney and Kokelaar, 2002), a “boundary layer” (Valentine, 1987; Buesch, 1992) or a “hindered settling zone” (Druitt, 1992) has been proposed, representing the interface between the current and its substrate that is characterized by an increased particle concentration and decreased turbulence. During deposition, the flow boundary lies at the top of the aggrading deposit, and each clast undergoing deposition must cross it. It has been taken that the lower boundary zone

comprises not only the base of the advancing current, but also the uppermost part of the substrate. Any interaction between substrate and current (e.g. shearing, ploughing, etc.) will therefore take place within this boundary zone. Its nature and the rate of progressive aggradation will vary according to the current velocity, concentration and rate of supply of particles to the flow boundary zone (Branney and Kokelaar, 2002).

An advancing avalanche will probably erode the uppermost layers of the substrate, while compressing lower layers. With increased travel distance, the avalanche will start to plough into the substrate, mobilizing it ahead of and underneath the avalanche front (Barbolini et al., 2005), which is typically the main area of interaction between avalanche and substrate. Shear surfaces develop; failure along them pushes the mobilized substrate into or onto the still stationary sediment ahead. Failure of the substrate under shear can also result in small parts of it being sheared into the avalanche body, and most likely incorporated into it as rip-up clasts or be crushed into the avalanche matrix.

The avalanche front can also generate a pore pressure gradient in the saturated substrate that counteracts the material's cohesive forces and frictional strength (Gauer and Issler, 2004), resulting in the fluidization of the substrate. Pore fluid pressures temporarily reach the point where the incompressible interstitial fluids carry all the applied stresses, leading to loss of shear resistance and the mobilization of the substrate which then can be incorporated into the advancing avalanche. Soft substrate can be mobilized after deposition of the currents has occurred. The increased load of the current deposit will lead to a mechanical reduction of the substrate volume (dynamic loading). Where any load on sediment is wholly sustained by interstitial fluids and cohesion is negligible, the substrate can temporarily lose its strength and can effectively behave as a fluid (liquefaction). The upward transport of particles by fluidization can drive deformation through the sediment. Separation of grains results in bed expansion, reducing pore water pressure, lowering the sediment bulk density and further contributing to the sediment deformation.

Substrate deformation features are rarely described in the deposits of pyroclastic density currents, but they can be expected for all types of pyroclastic mass movements due to the high velocity and erosive capacity of these currents. The erosive capabilities of pyroclastic flows are mainly controlled by the following factors: (1) topography, as erosional features are more commonly produced when currents flow down steep slopes or through constrictions; (2) flow energy; (3) flow thickness, which affects shearing rates; (4) flow composition, especially with regard to the proportions of lithic clasts; and (5) hardness of the substrate and availability of loose detritus (i.e. erodibility of the substrate) (Sparks et al., 1997b; Calder et al., 2000). Bulk density and volume increase as flows entrain more lithic clasts. The incorporation of substrate material therefore has significant implications for the scouring capacity of pyroclastic flows, coarse clasts are concentrated in basal carpets, which in turn, increase the basal scouring capacity of the flows. Clast durability is also important because clasts that can sustain angularity during transport will serve as more effective erosional tools (Calder et al., 2000).

4.2.1. Hard substrate

Bedrock material or previously lithified deposits will commonly show furrowed and striated surfaces with grooves and flute marks, as has been observed for the transport of block-and-ash flows at Soufriére Hills Volcano in 1996 (Cole et al., 2002). Similar structures have been described in pyroclastic surge deposits at Mount St.Helens (Kieffer and Sturtevant, 1988).

Grooves and flute markings are common in turbidites, but have also been observed in ignimbrite deposits, e.g. Abrigo Ignimbrite on Tenerife (Pittari and Cas, 2004). Similar erosional features have been documented at Lascar Volcano Chile, during the movement of pyroclastic flows in 1993 (Sparks et al., 1997a), and at Soufriére Hills Volcano, Montserrat, in 1997 (Cole et al., 2002; Ritchie et al., 2002, Sparks et al., 2002).

4.2.2. Soft substrate

Soft-sediment deformation structures form due to the disturbance of softer substrate during or shortly after the passage of the advancing current. These structures may form rapidly, probably within a few days, although laboratory experiments suggest that these features may even develop within a few minutes (Van Loon and Brodzikowksi, 1987). Loading and flame structures can develop when Rayleigh-Taylor instabilities, which perturb the surface between an upper dense layer of the deposit and an underlying less dense layer (Owen, 2003; Figure 4.1), may form during or shortly after the deposition of an avalanche. These structures have been recorded at the base of the Cerro Galan ignimbrite (Sparks et al., 1985) and at the base of ignimbrite breccias, e.g. the Poris Formation ignimbrite, Tenerife.

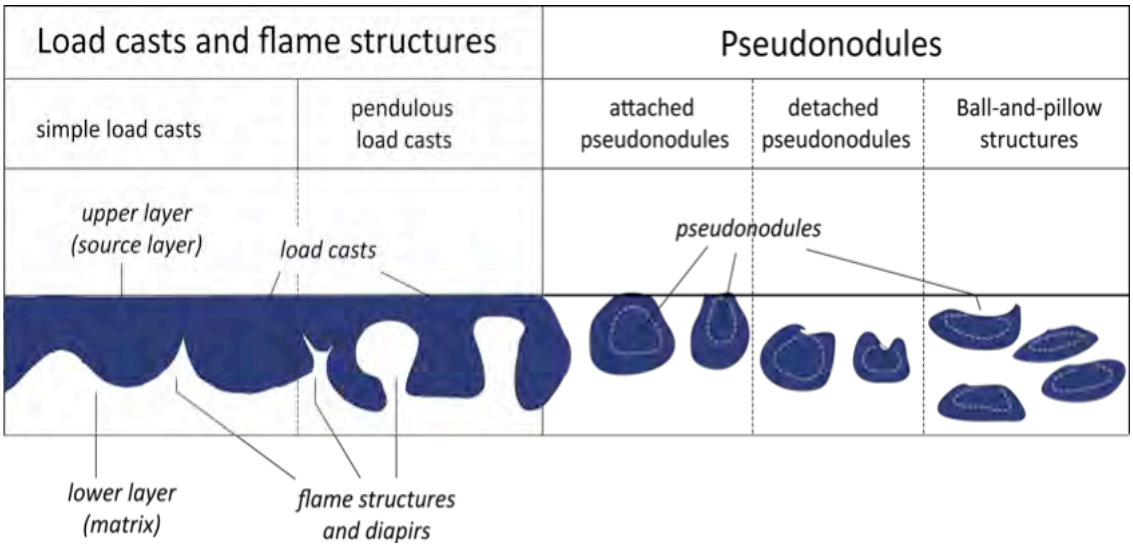

Figure 4.1: Definition diagram for load casts, flame structures and pseudonodules (modified after Owen, 2003).

Overturned strata beneath the Upper Merihuaca ignimbrite, Argentina (Sparks et al., 1985) and beneath the Taupo ignimbrite, New Zealand (Houghton and Wilson, 1986) have been ascribed to shear deformation during the emplacement of the pyroclastic density currents. Subhorizontal tongues of ignimbrite intercalated with substrate

pumice fall deposit were observed in the Cape Riva Member of Santorini, indicating that the substrate was sheared and lifted into the pyroclastic current as semi-coherent slabs (Druitt and Sparks, 1982). Soil schlieren and finger-like tephra dyklets have been described at the base of deposits at Mount St Helens and Bezymianny (Belousov, 1996). Laminar shear in just-deposited ignimbrite beneath a pyroclastic current is inferred from deformed load structures and elutriation pipes at Roccamonfina volcano (Cole et al., 1993).

4.3. Substrate deformation at Tarawera Volcano

During the early stages of the Kaharoa eruptive episode, rapidly accumulated vitric-crystal ash fall layers from the initial plinian eruptions were deposited around the volcano, described as Kaharoa Tephra (Nairn et al., 2001). Growth of Tarawera, Ruawahia and Wahanga Domes probably started shortly afterwards. These domes grew over the following 3-5 years. Multiple collapses of oversteepened margins of Ruawahia and Wahanga domes generated block-and-ash flows (BAFs) travelling to the south and northeast of the volcano in the later stages of the eruptive episode.

Three depositional units have been described at Tarawera Volcano, but generally the identification of individual units in the block-and-ash flow deposits (BAFD) can be difficult due to the limited exposure of identifying markers, such as the contact to previously emplaced deposits or surge deposits overlying the body of the flow. Therefore the number of actual block-and-ash flow deposits is probably much higher.

The majority of the exposures in the both major block-and-ash flow fans shows little evidence for significant erosion or deformation. The best outcrop representing a variety of substrate deformation features is Crater Road quarry in the southern block-and-ash flow fan (V16/195215), c. 4 km horizontal distance from Ruawahia Dome. At Crater Road, Kaharoa Tephra underlies a massive, fine-grained layer, the contact being marked by a reddish ash bed. A poorly sorted, clast-supported block-and-ash flow deposit directly overlies the fine-grained layer, showing generally a gradational contact, but locally it is sharp and erosional. For more detailed descriptions see Chapter 3, section 3.5.3.

Substrate deformation features are concentrated in the southern end of the quarry, over a length of c. 40 m (Figure 4.2); the substrate has been bulldozed, sheared and incorporated into the overlying layer. Flame structures and erosion gullies are the most common features found in this quarry.

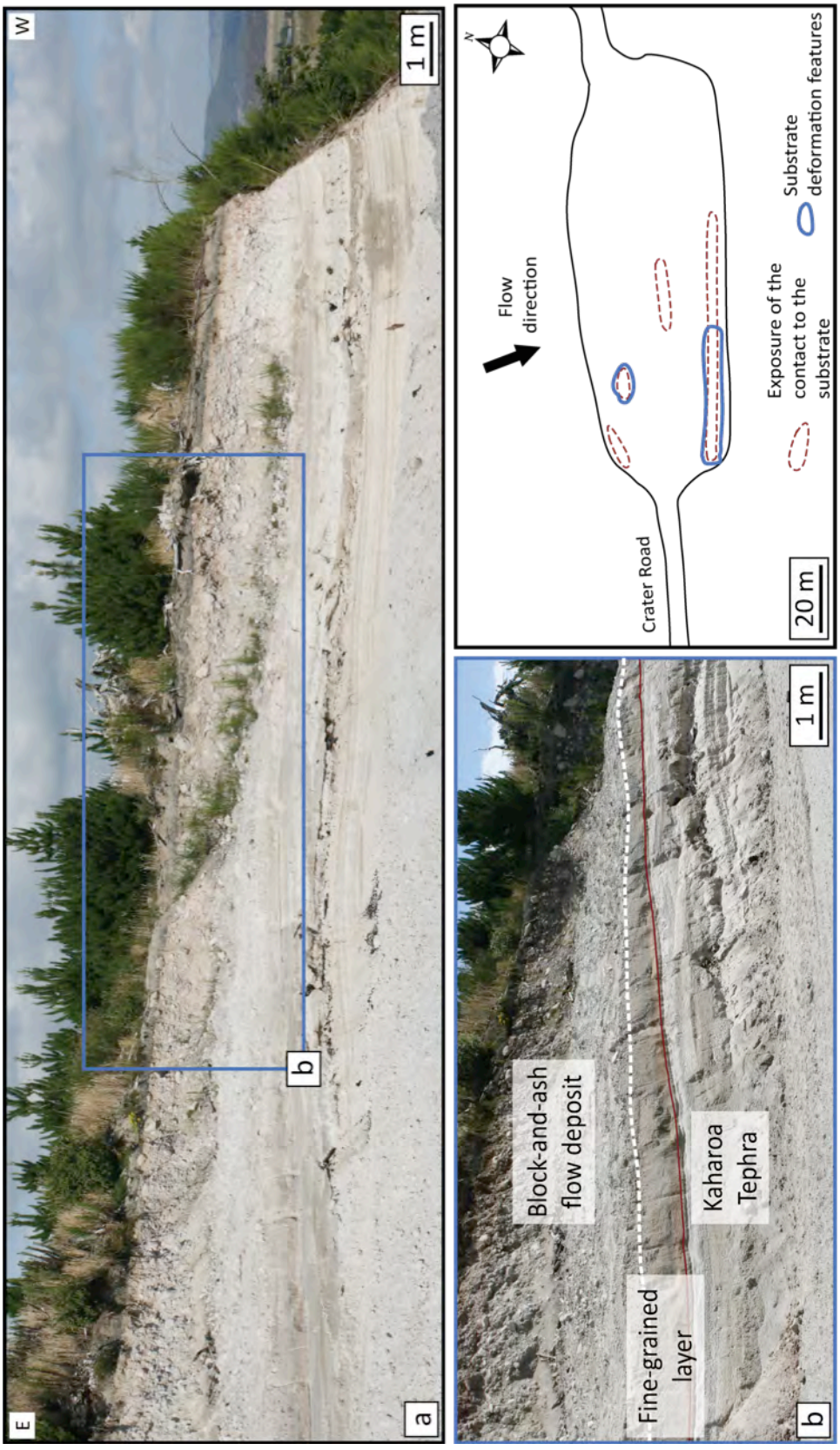

Figure 4.2: (a) Overview of the southern end of Crater Road quarry, located in the southern block-and-ash flow fan from Ruawahia Dome. The contact with earlier deposited Kaharoa Tephra is exposed only locally (sketch), and all substrate deformation features have been found in (b) the southeastern side of the quarry.

4.3.1. Deformation structures at Crater Road quarry

When exposed, the contact between Kaharoa tephra layers and the overlying massive layer is typically sharp and planar (Figure 4.3a). But locally, it can be irregular and distorted (Figure 4.3b); erosion gullies and shear deformation structures demonstrate dynamic interaction at the interface of these layers.

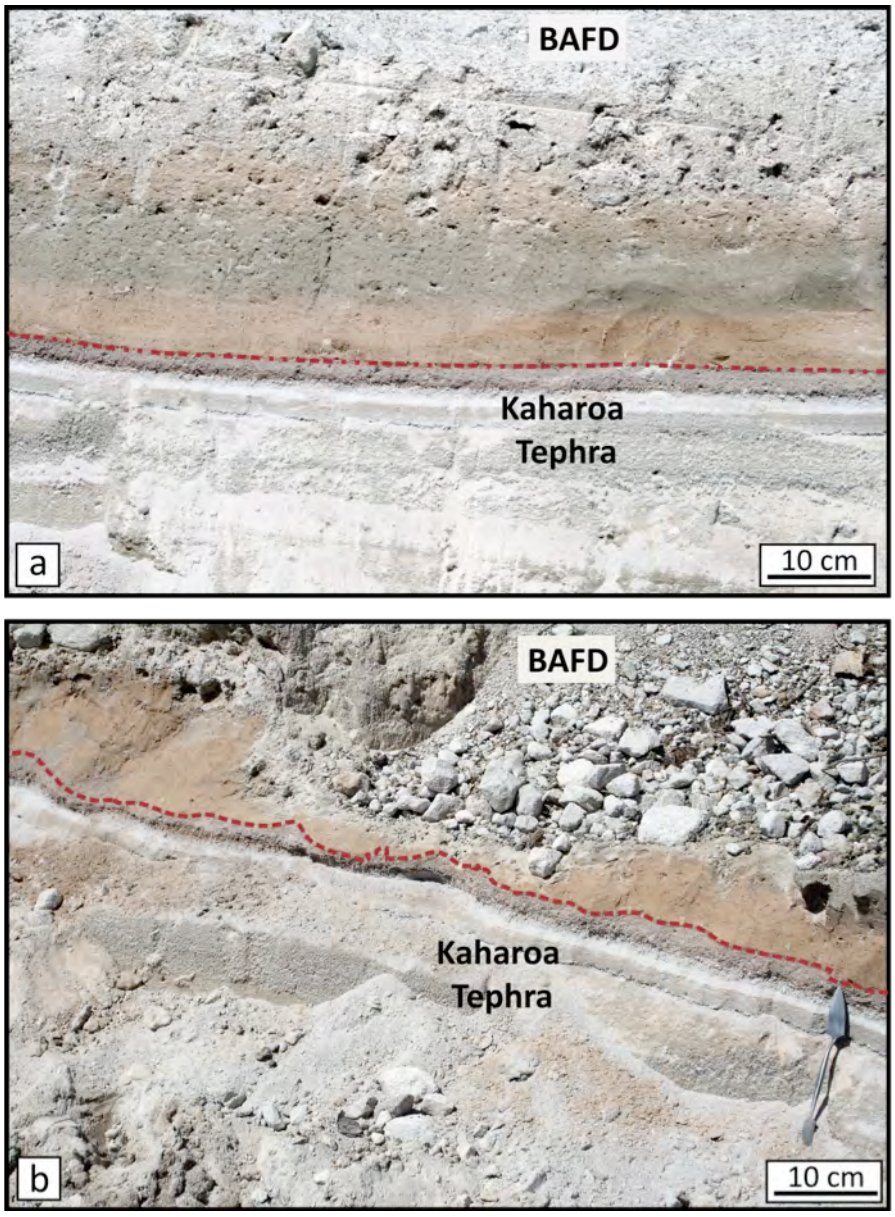

Figure 4.3: A thin red ash layer (stippled line) marks the contact with the Kaharoa Tephra beneath a fine-grained ash layer and the block-and-ash flow deposit (BAFD). (a) Typically the contact is planar, (b) but can show irregularities.

4.3.1.1. Flame-like structures

Parts of the Kaharoa Tephra have been ripped up and incorporated into the overlying fine-grained layer, probably by shear exerted on the substrate. Flame-like structures at Crater Road are generally between 5-10 cm high and max. 20 cm wide, commonly irregular in shape and occurrence, compared to similar, but more periodical and symmetrical structures found in marine or lacustrine sediments (Figure 4.4).

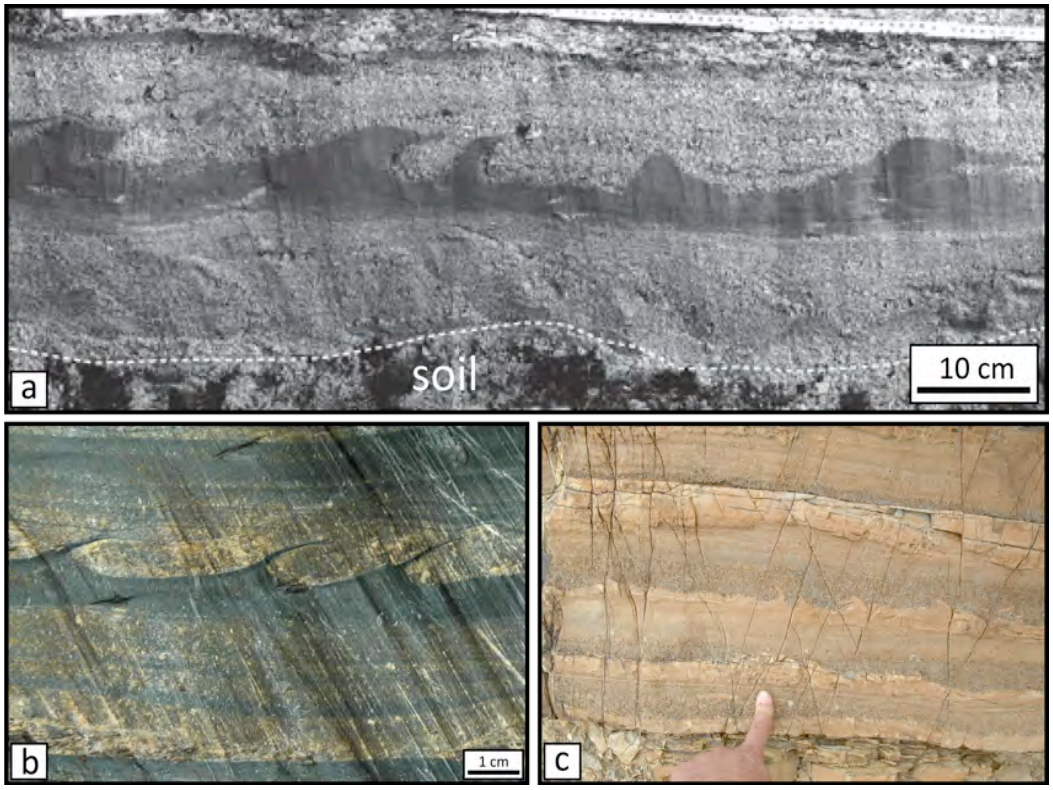

Figure 4.4: Examples of flame structures in volcanic and non-volcanic sediments. (a) Truncated flame structures in a terrestrial tsunami deposit in southern Thailand (Matsumoto et al., 2008). (b) Flame structures found in the turbiditic Precambrian Windermere Group in the Canadian Cariboo mountains. (c) Small flame-like structures were discovered in Permian sediment, Inyo County in California.

Flame structures are exposed either perpendicular (Figure 4.5) or parallel to the to the direction of the block-and-ash flows (Figure 4.6), representing cross-sections through more extensive soft sediment deformation structures.

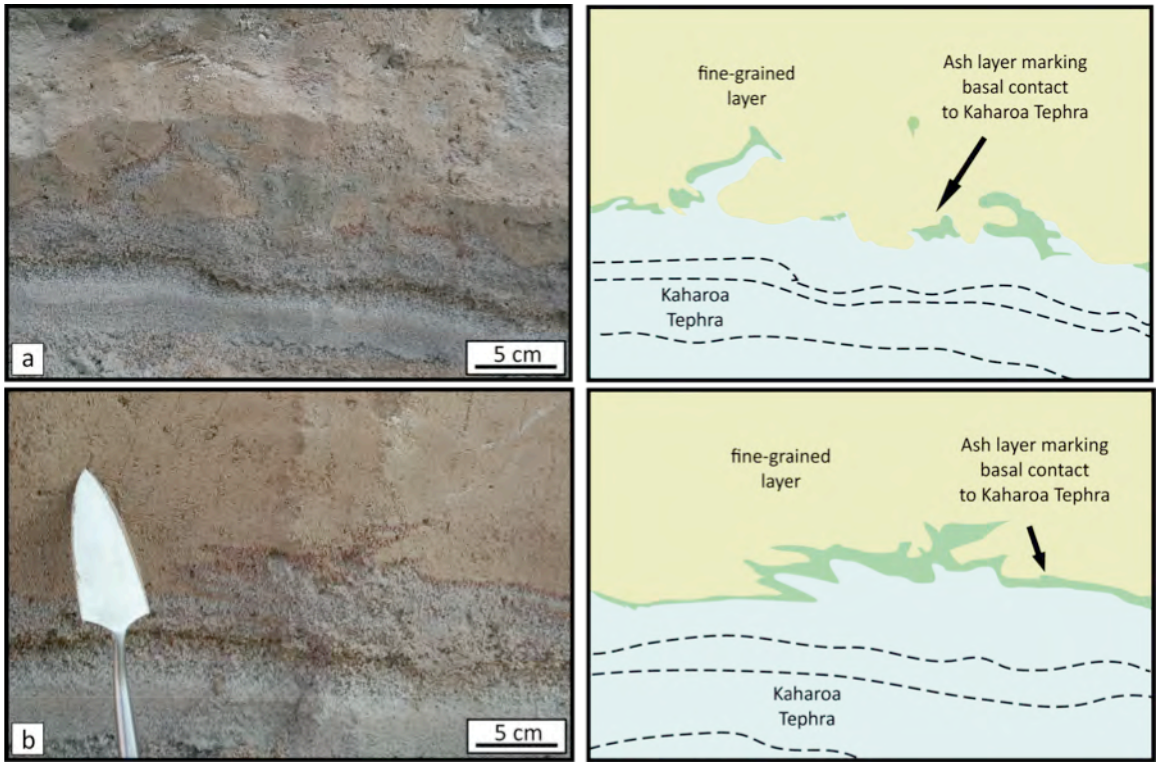

Figure 4.5: Shear exerted on the substrate mobilized the uppermost tephra layer and entrained it into the overlying fine-grained bed beneath the Kaharoa block-and-ash flow. Flame structures are exposed perpendicular to the flow direction.

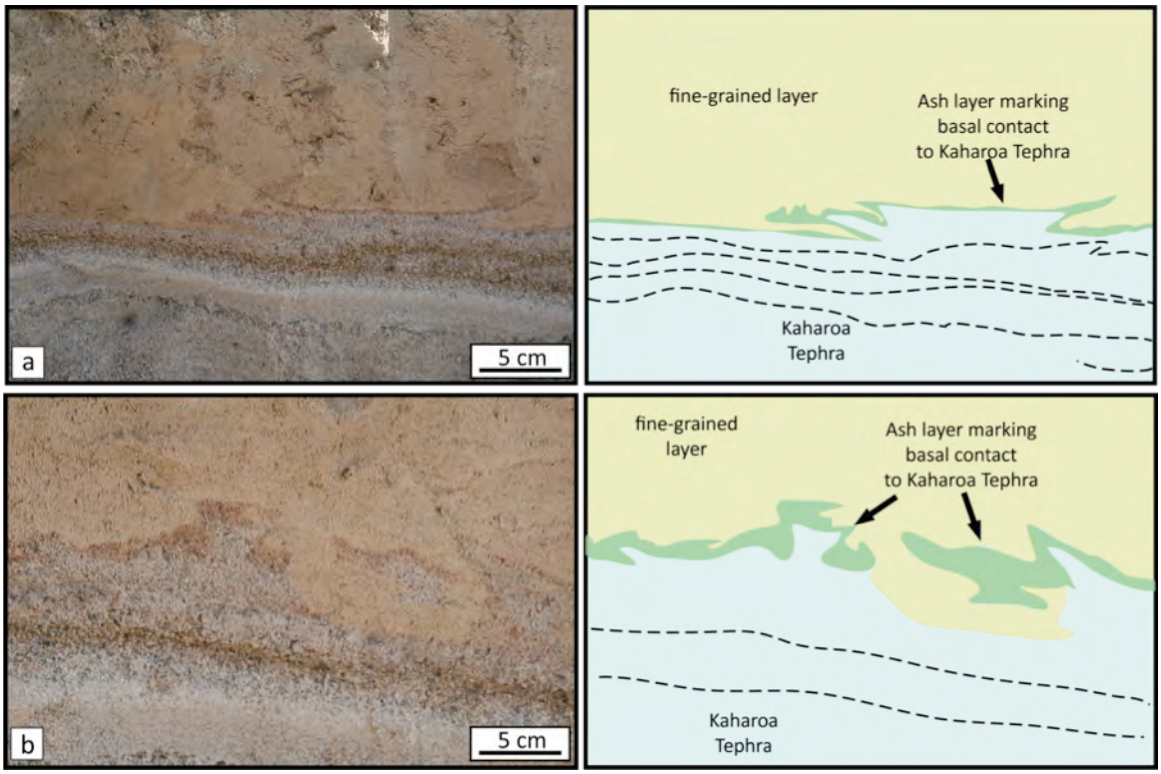

Figure 4.6: Shear exerted on the substrate mobilized the uppermost tephra layer and entrained it into the overlying fine-grained bed beneath the Kaharoa block-and-ash flow. Flame structures are exposed parallel to the flow direction (right to left).

Comparable structures have been documented in deposits from pyroclastic density currents at Monte Cimino by shear exerted during the emplacement of ignimbrites (Laberge et al., 2006). Flames of clayey sediment protruded into an overlying ignimbrite deposit as injection features, with the ignimbrite flow then ripping up and entraining clasts of the generally clayey material.

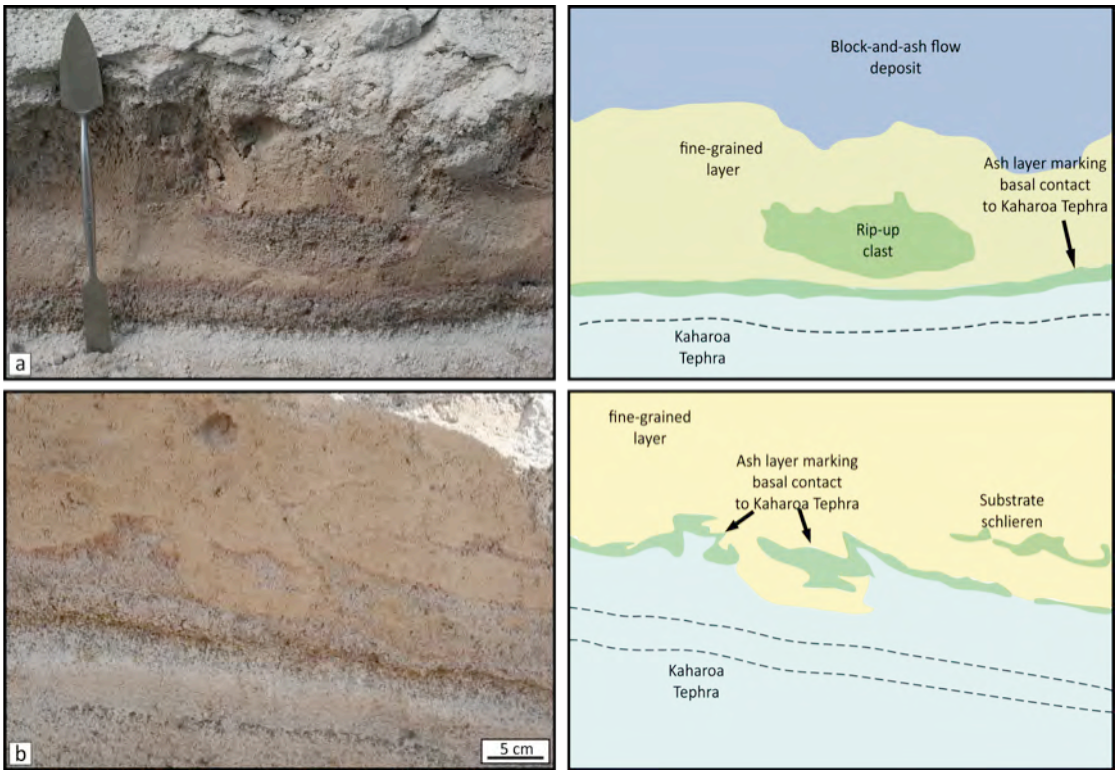

Figure 4.7: Shear deformation mobilized Kaharoa Tephra layers, flame structures and tephra rip-up clasts are preserved in the fine-grained overlying sediment layer. (a) Flow direction is perpendicular to the exposure, (b) flow direction is from right to left (spatula for scale is 40 cm long).

Remnants of Kaharoa Tephra are preserved as rip-up clasts (Figure 4.7.a) and substrate schlieren (Figure 4.7b); the uppermost few 5-10 mm were mobilized, eroded and incorporated into the base of the deposit, also demonstrating shear deformation at the top of the tephra deposits.

Flame-like structures at the interface between the unconsolidated tephra layers and the massive, fine-grained layer could also be explained as a response to unstable bulk density contrasts between these two layers (dynamic loading) or as lateral variations in

loading (uneven loading; Owen, 2003). Flame structures then represent antiforms, associated synforms are expressed by load casts and pseudonodules (compare Figure 4.1).

Load-and-flame structures have been described e.g. at the base of the Cerro Galan Ignimbrite as the result of loading coupled with loss of substrate (Sparks et al., 1985). Spectacular load structures that penetrate down more than 10 m into the substrate and in some cases have become detached 'load balls' occur at the base of welded ignimbrites in Wales (e.g. Kokelaar, 1982; Howells et al., 1985).

4.3.1.2. Ploughing

Ploughing of the substrate has been only observed in a few locations within the quarry; most of the deformation structures are more likely the result of shear exerted onto the substrate, schlieren of the substrate being dragged along and mixed with the overlying layer. One small deformation feature was documented, resembling a narrow dome with a maximum height of 10 cm and a width of c. 15-20 cm (Figure 4.8a and b). The force of the advancing detached surge probably mobilized and pushed the uppermost few centimetres of Kaharoa Tephra ahead; the avalanche front then dropped into the substrate, pushing it further ahead (bulldozing). Further excavation of this structure in c. 5 cm steps parallel to the structure revealed various shapes along the lateral extent of the deformation. A single, small flame, pointing first opposing and, after further excavation (Figure 4.8e and f), along the flow direction confirms the suggestion that ploughing, not bulldozing, with a slight shear component was responsible for the deformation and entrainment of the substrate.

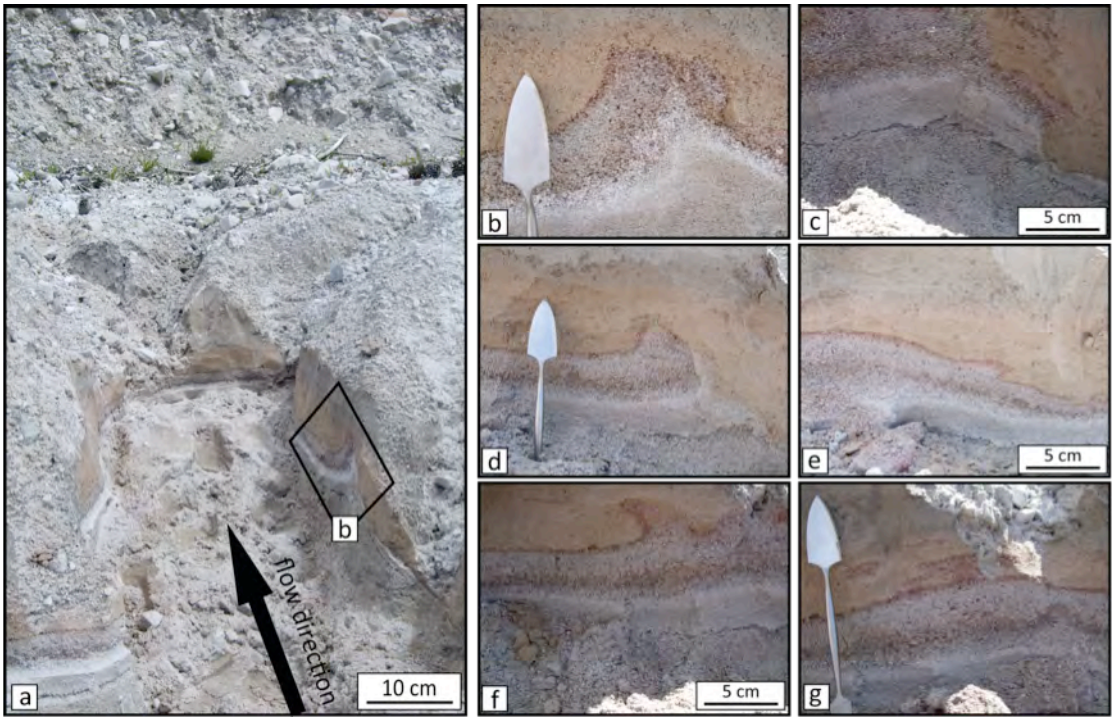

Figure 4.8: Bulldozing of the substrate was documented at Crater Road. (a) The deformation structures occur at the interface between Kaharoa Tephra and the overlying fine-grained deposit. Excavation (c-g) of the structure parallel to the flow direction revealed various flame and shear structures (flow direction from right to left).

4.3.1.3 BAF clasts mixed into fine-grained layer

Individual rhyolite block-and-ash flow clasts are sometimes mixed into the underlying fine-grained layer and surrounded by it (Figure 4.9), typically the contact between the BAF deposits and the underlying layer is sharp and planar. A possible explanation is the mobilization of the fine layer by the weight of the block-and-ash flow after deposition. Pressure exerted by uneven loading and possibly dewatering fluidized the fine-grained layer, either letting block-and-ash flow clasts sink down into the fine-grained layer or the less dense, fine material was injected upwards into the block-and-ash flow deposit. The mixed clasts were found near an erosion gully at the base of the block-and-ash flow deposit, so another explanation could be the slumping of the gully that was filled by block-and-ash flow material, pushing the clasts into the fine-grained layer.

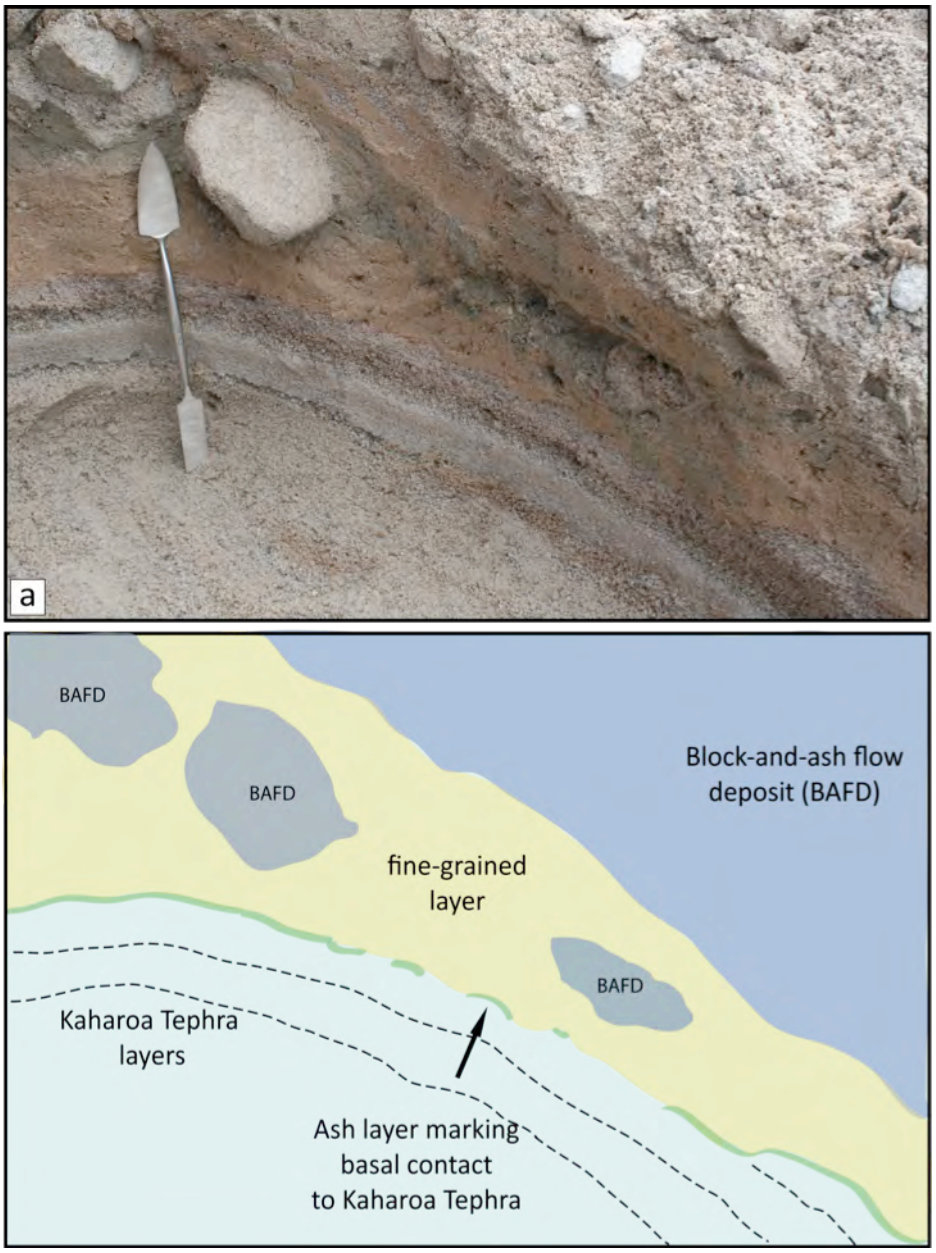

Figure 4.9: Clasts from the block-and-ash flow deposit are mixed into the fine-grained layer and completely surrounded by it, either the result of loading or of slumping of erosion gullies. Spatula for scale is 40 cm long.

4.3.1.4. Erosion gullies

Erosion is widely recorded by scour surfaces at the base of, and within, deposits of pyroclastic density currents, generally characterized by the presence of substrate-derived lithics, intraclasts, or vegetation fragments. With progressive aggradation, the substrate at first comprises the pre-existing substrate, and then consists of the loose, hot and degassing, aggrading deposit, which is readily remobilized and re-entrained. At Tarawera Volcano, erosion gullies of different scales have been recorded at Crater Road, either between the Kaharoa Tephra layers and the ash surge layer or between the ash surge layer and the block-and-ash flow deposit. In both scenarios, rills and furrows are most likely the result of water-induced gully erosion, and were extended by the overriding avalanche.

4.3.1.4.1. Erosion gully 1

This erosion gully was documented in the contact zone between Kaharoa Tephra and the fine ash layer – a depression (10 cm wide and 5 cm deep) in the usually planar contact represents a small cross-section of a larger erosion gully, which was preserved within the fine-grained ash layer (Figure 4.10a). Excavation of this depression along a trench parallel to the flow direction revealed a steeply dipping furrow of c. 50 cm length and 20 cm depth (Figure 4.10 sketch), showing erosion and entrainment of parts of the Kaharoa Tephra into fine-grained bed. The reddish ash layer is mostly eroded along the gully, only remnants of the tephra layers are preserved as rip-up clasts in the fine-grained layer. Erosion of this gully was possibly related to the movement of the advancing current that deposited the ash layer, or it may have existed before the ash layer was emplaced.

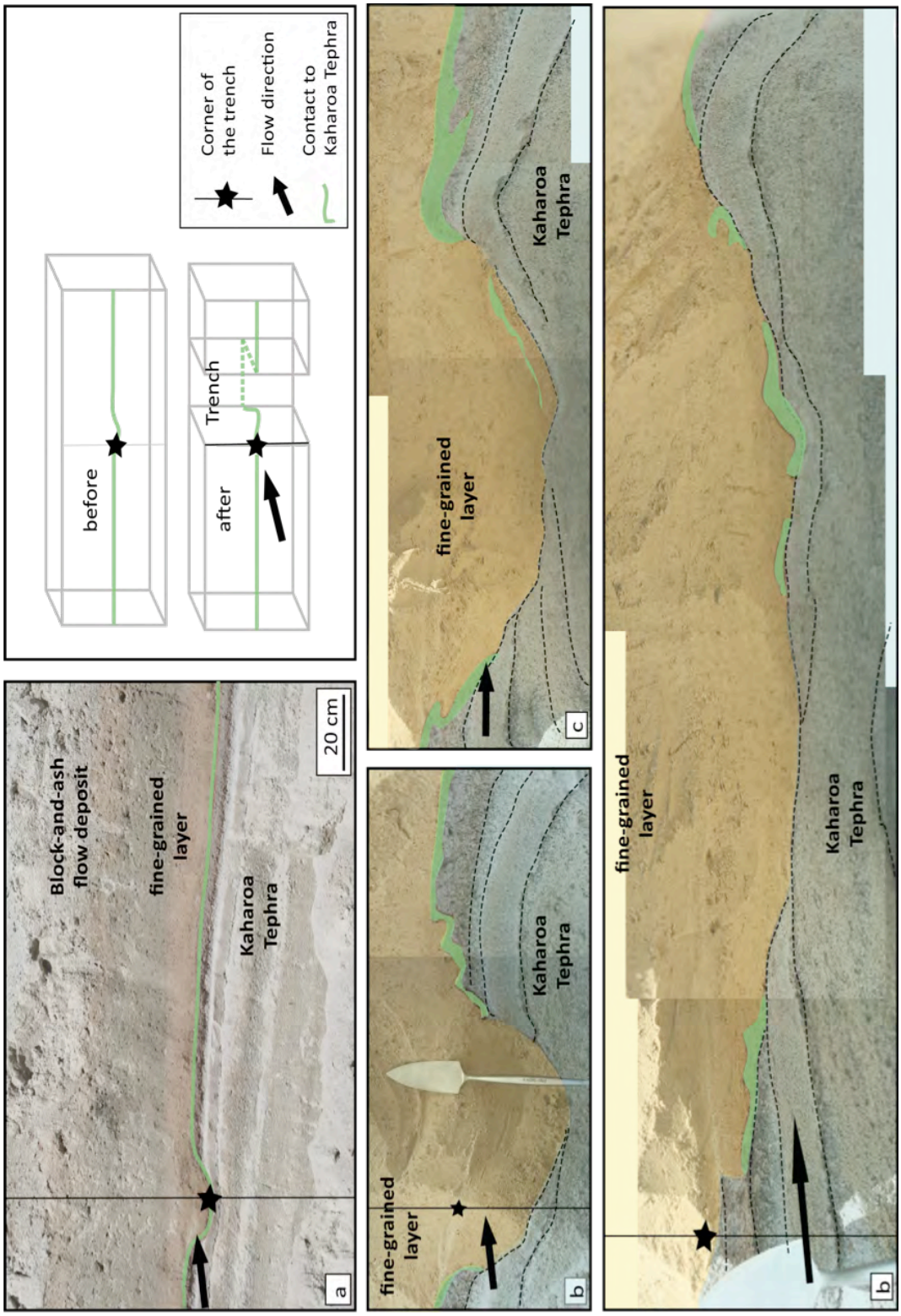

Figure 4.10: Overview of an elongated, shallow erosion gully at the top of Kaharoa Tephra layers. (a) A small depression indicates an irregularity in the bedding, (b) after excavation of a trench along the flow direction, an erosion gully was revealed. (c) Only a few tens of cm, after further lateral trench expansion, the erosion gully seems to extend and shallow (d).

4.3.1.4.2. Erosion gully 2

A deformation structure resembling a volcanic bomb sag was documented in the fine-grained layer below the block-and-ash flow deposit (Figure 4.11a). A rhyolite clast, apparently from the block-and-ash flow, seemed to have impacted the fine-grained deposit, distorting it and the underlying Kaharoa Tephra layers. After removal of the clast, a trench was excavated along the side of the deformation, parallel to the direction of the flow. Pictures were taken every 10 cm to document the extent of the deformation (Figure 4.11b). Studies of these pictures led to discarding the idea that this block represented ballistic ejecta from Ruawahia vent, because for a travel distance of c. 4km from the vent, the generation of this block-and-ash flow had to be more explosive than previously described. It is more likely that the clast traveled in the block-and-ash flow, possibly tumbling or rolling, before it was deposited in its present location. But the simple deposition of this clast could not have responsible for this deep deformation structure. It is more likely that a large, rain-induced erosion gully formed after the emplacement of Kaharoa Tephra layers. The uppermost tephra layers mantle the gully, confirmed by slumping of the bedding (Figure 4.11a). The emplacement of the fine–grained layer filling the gully seems to have been erosive as well, as the reddish ash layer marking its base has been ripped up and entrained into the lower 10 cm of the fine ash layer (Figure 4.11c). Shear exerted during its emplacement probably mobilized the substrate and mixed it into its base. After deposition of the sediment layer, the block-and-ash flow traveled over it, single clasts might have jetted ahead, or tumbling or saltating blocks within the lower boundary zone of the advancing avalanche could have fallen into the small topographic depression. The force behind the impact into the soft, fine-grained bed was large enough to send a shock wave through ash deposit, possibly deforming part of Kaharoa Tephra as well (Figure 4.11d-e). Matrix from the block-and-ash flow deposit as well as a few smaller clasts were found beneath the impacted clast, confirming its origin from the advancing block-and-ash flow.

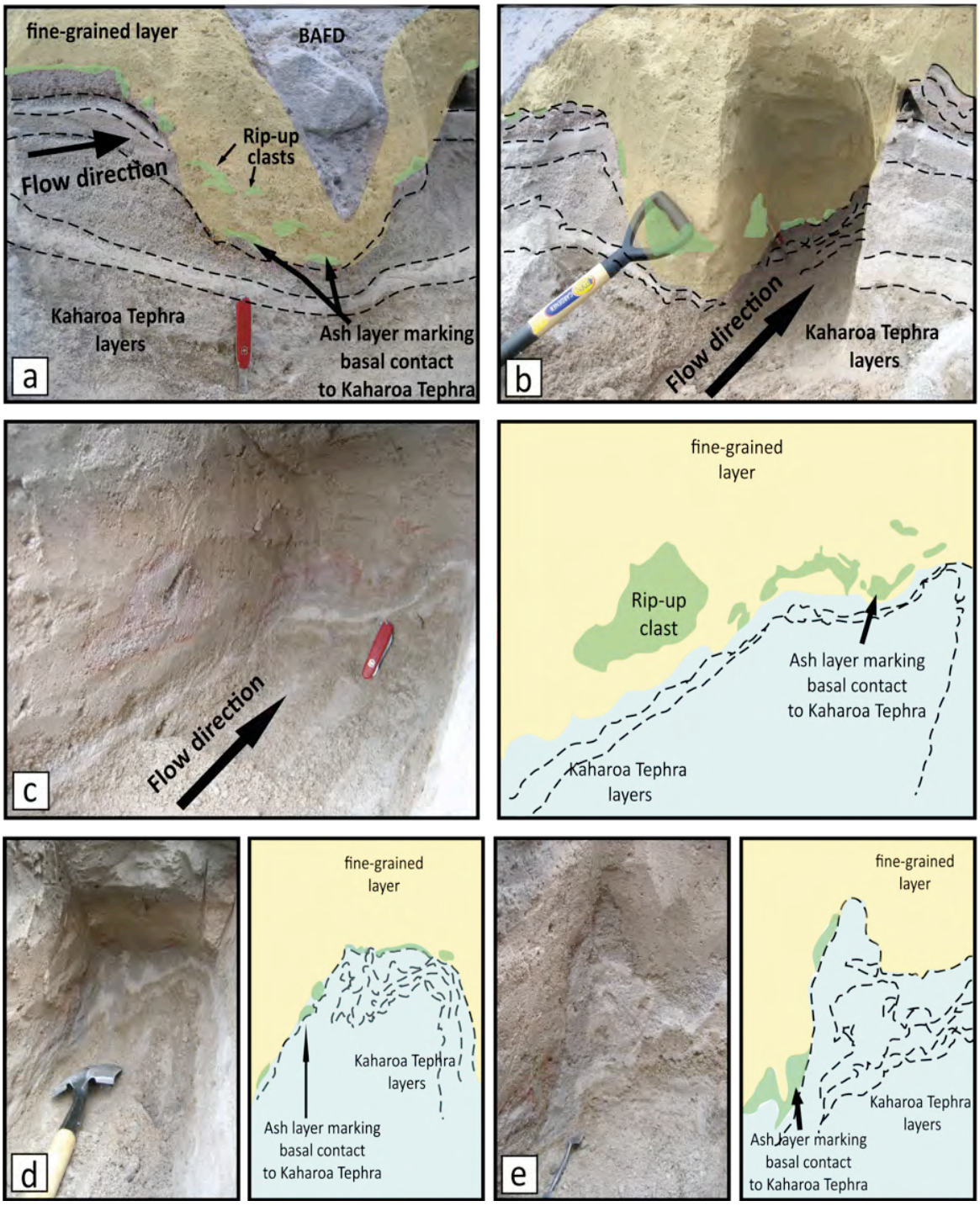

Figure 4.11: (a) Rhyolite clast in block-and-ash flow deposit (BAFD) dropped into erosion gully; (b) trench cut parallel to the flow direction to determine extent of deformation (indicated by pale green shading); (c) substrate was sheared and preserved as rip-up clasts; (d) and (e) substrate bulldozed and folded. Flow direction in pictures (d) and (e) is perpendicular to the exposure.

4.3.1.5. Correlation between erosion gullies

So far all the deformation structures described occur at the interface between the Kaharoa Tephra and the fine-grained layer overlying it. But one location near the western end of the quarry revealed deformation of the "upper interface" between the fine-grained layer and the block-and-ash flow deposit, questioning their relationship (Figure 4.12). The extent of the deformation measures c. 1.5 m in width and c. 80 cm in height, comprising several erosion gullies of different scales and shapes (Figure 4.12).

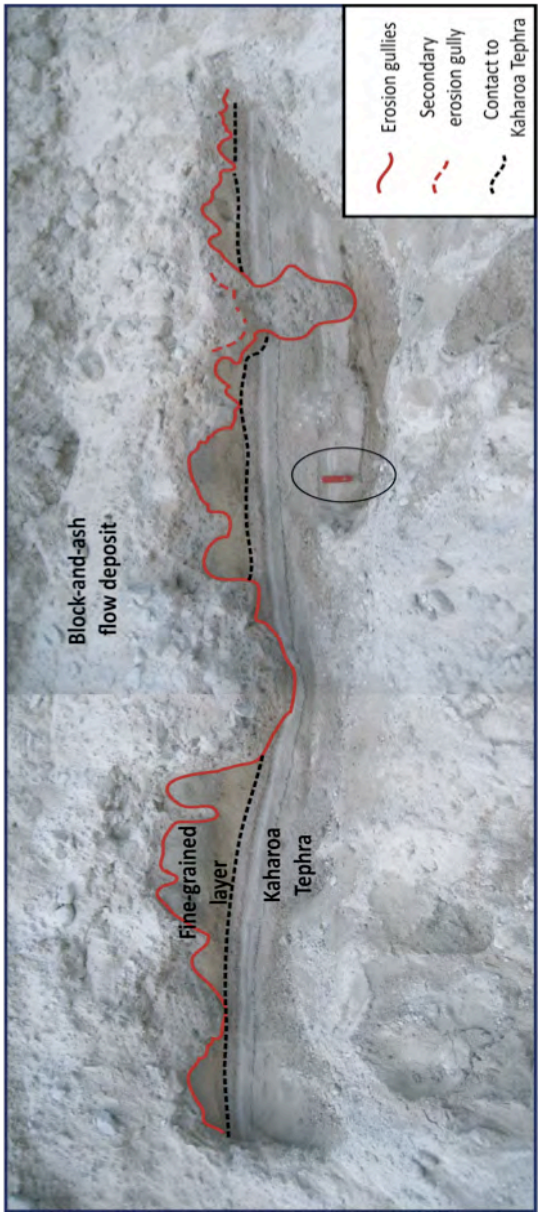

Figure 4.12: Overview of erosion gullies extending not only into Kaharoa Tephra layers, but mark also the contact between fine-grained layer and block-and-ash flow deposit. Swiss Army knife for scale.

The biggest erosion gully extends from the lower interface c. 40 cm into Kaharoa Tephra layers, being filled with BAF material (Figure 4.13a).

The exposure of Kaharoa Tephra at Crater Road comprises five individual ash beds, with thicknesses ranging between 2-15 cm for each bed. The first erosion gully penetrates all exposed layers, and the lowest two beds show slight slumping towards the gully. The overlying tephra layers, in which erosion widened the gully from c. 10 cm to 20 cm width, show no signs of slumping. The contact between Kaharoa Tephra and the fine-grained layer on top is sharp on both sides of the erosion gully, but shows slumping into the large gully, the thin reddish ash layer marking the contact tracing the small depression (5 cm deep, 10 cm wide) resulting from the slumping. Fine-grained material then filled the depression.

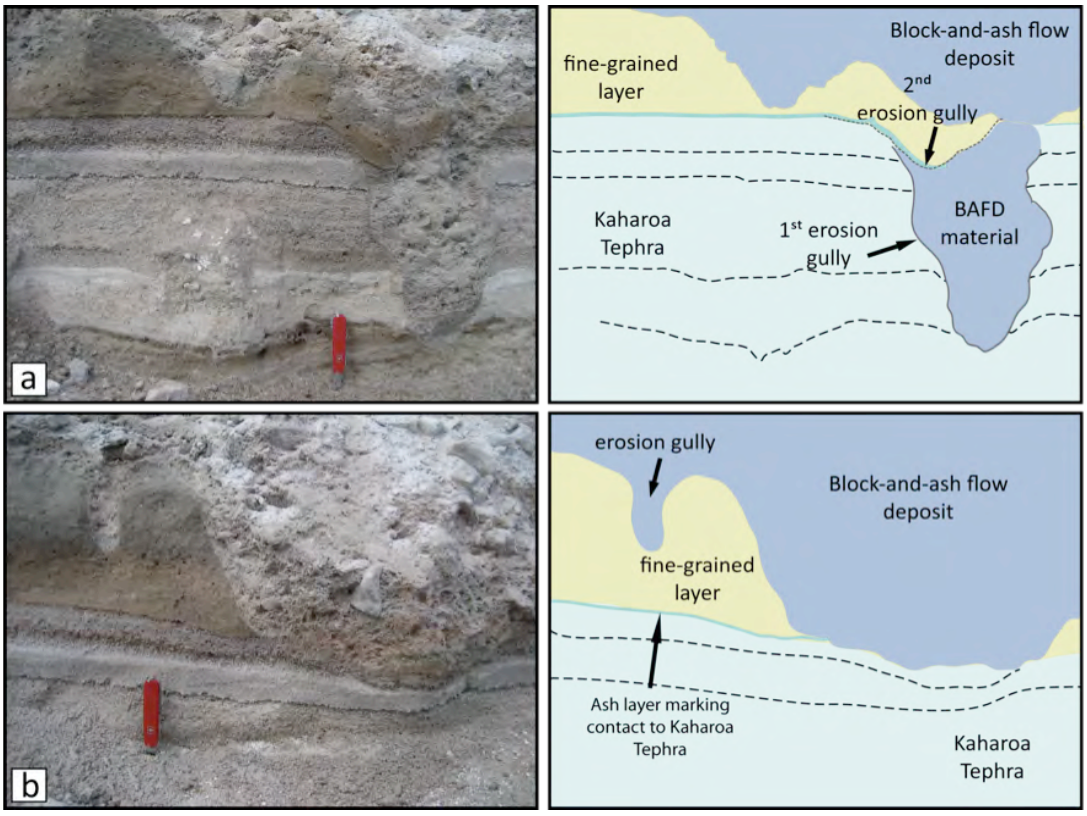

Figure 4.13: Detailed overview of a large erosion gully extending into the Kaharoa Tephra layers, which is filled with block-and-ash flow material. At the same location, erosion gullies mark the contact between a fine-grained layer and the block-and-ash flow deposit, indicating a time gap between their emplacement. Shape and size of these gullies is highly variable (compare Figure 4.12).

The large gully is filled by block-and-ash flow material, hence the complete original gully must have been "cleaned out" and infilled by block-and-ash flow material after the emplacement of the fine-grained layer. The small "secondary" depression could either result from erosion during the emplacement of the fine ash layer or from slumping of the fine-grained material after its emplacement and the evolution of the large erosion gully.

Two possible scenarios could explain the evolution of this large erosion gully cutting through Kaharoa Tephra layers and the overlying fine-grained deposit and the infilling by BAF material, considering a possible time break before the deposition of the latter.

Scenario 1 - The slumping of the lowermost exposed tephra layers indicates that erosion possibly already started during their emplacement, with fallout ash mantling the gully, resulting in the slumping of the beds towards the gully. The next two ash layers (c. 15-20 cm) were emplaced over the small gully, no slumping of these layers towards the now existent gully is apparent. The uppermost tephra layers again dip towards the gully, so erosion was effective during their emplacement. Shortly afterwards, with tephra material still filling the gully, a "secondary" erosion furrow formed, but only on one side of the first gully. A thin reddish ash layer, marking the contact to the fine-grained bed, mantles the small erosion furrow, either representing an individual ash layer emplaced during the erosion of the secondary gully or the oxidized top of a tephra layer heated during the emplacement of the overlying fine ash layer.

Scenario 2 – The large channel could have been eroded after the deposition of Kaharoa Tephra, cutting through all of the five exposed beds. The slumping visible in some of the beds would be the result of the force of water-induced erosion, mobilizing parts of them and washing them out. The erosion gully would be infilled by ash from the fine-grained layer. Between its emplacement and the deposition of the block-and-ash flow there was most likely a time break, represented by various erosion furrows of different scales marking the contact to the block-and-ash flow deposit. The smaller ones are vent-like, only 3-5 cm wide and 10-15 deep, the larger ones are wider and more deeply eroded

(Figure 4.12). An extended time gap between these layers could have promoted the cleaning out of the largest gully, which is now filled by block-and-ash flow deposit material. The second smaller depression could have resulted from slumping of the fine-grained layer, parts of which were mixed into the advancing and gully-filling block-and-ash flow.

4.4. Discussion

The dynamic interaction between an advancing avalanche and the substrate is a common occurrence for any kind of particulate density current. Shear deformation and loading are the most important mechanisms for the mobilization and erosion of any stationary sediment body, which has been overridden by a granular flow. Erosive behaviour of block-and-ash flows has been documented at Tarawera Volcano, confirming the highly energetic nature of these flows.

Block-and-ash flow deposits at Tarawera Volcano generally overlie rapidly accumulated tephra layers (Kaharoa Tephra), but the contact between these beds is only localized exposed, e.g. at Crater Road, at c. 4 km south from Ruawahia Dome. Here the typically planar contact to the tephra layers is locally distorted, and tephra is sheared into the overlying fine-grained layer, preserving tephra as flame structures and substrate schlieren. Numerous erosion gullies of different size extend into the tephra layers, confirming the time break after the emplacement of the Kaharoa Tephra as has been established by studies of the individual pyroclastic deposits by Nairn et al. (2001).

At Crater Road, a massive, 3-70 cm thick, fine-grained layer separates the Kaharoa Tephra and the coarse block-and-ash flow deposit. The contact to the block-and-ash flow deposit is mostly gradational, which previously was thought to indicate the simultaneous deposition of both layers. A similar, but coarser-grained ash layer has been observed in 1975 by Dr. I.A. Nairn (pers. communication) at Edwards Road (Figure 4.14), near the break in slope from the Waikakareao lava plateau onto the Lower Pokuhu lava plateau. Fieldwork between 2007-2009 could not retrace this basal layer,

because this part of Edwards Road (V16/196281) was by then heavily covered by vegetation.

At Crater Road, further studies of the contact zone between this fine-grained layer and the block-and-ash flow deposit showed locally exposed, small erosion furrows and gullies at the top of the fine-grained layer, implying a time break between the emplacements of those layers.

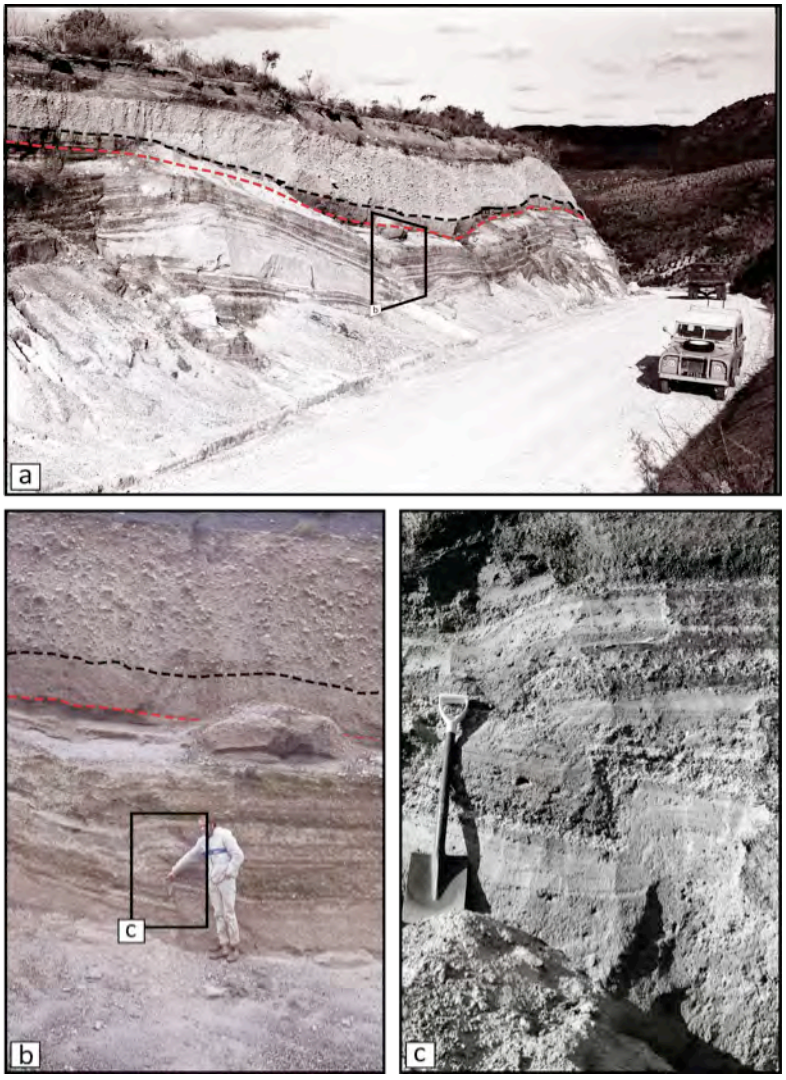

Figure 4.14: Overview of an exposure at Edwards Road (V16/196281) where a finer grained ash layer underlies block-and-ash flow deposits (BAFDs) (contact marked by black stippled line). (b) Detailed view of the contact between the block-and-ash flow deposit and Kaharoa Tephra (marked by red stippled line), exposing a fault dissecting the tephra layers. (c) Close-up view of the fault exposed in Kaharoa Tephra (pictures courtesy of Dr. I.A. Nairn).

Therefore, the most important questions are how the fine-grained layer was emplaced and where in the stratigraphy of the Kaharoa eruptive episode does this layer fit in. Some hypotheses for different scenarios are proposed, taking also a possible time break into consideration.

4.4.1. Hypothesis 1 – Simultaneous deposition of basal layer and BAFD

Nairn et al. (2001) proposed a timeline for the events during the Kaharoa eruptive episode, putting the generation of the block-and-ash flows at the end of the growth of Ruawahia and Wahanga Domes, years after the emplacement of Kaharoa Tephra. Therefore, erosion gullies cutting into the tephra layers can be explained by rain-induced erosion, starting either during or shortly after their emplacement.

The deposition of the block-and-ash flow material has been associated with the generation of a fine-grained, basal shear layer during their advance, as has been described at Unzen Volcano (Miyabuchi, 1999) and Citlatlépetl Volcano in Mexico (Carrasco-Núñez, 1999). The emplacement of block-and-ash flows can mobilize and erode the tephra layers, incorporating them into the bottom of the flows and possibly increasing the BAF travel distances. A dynamic interaction between the shear layer and the underlying substrate in form of erosion gullies or shear deformation can be expected, therefore any substrate deformation found at the contact to the Kaharoa Tephra can be explained by shear exerted from the developing shear layer.

The appearance of the fine layer at Tarawera Volcano is congruent with the description of a graded basal ash layer (layer 2a) in an idealized ignimbrite profile by Sparks et al. (1973), comprising three parts - a fine-grained ground layer (layer 1), overlain by a graded basal ash layer (layer 2a), followed by the main body of the flow (layer 2 b), either with a sharp contact or gradational transition to the ash layer. Layer 3 generally represents the ash cloud surge deposit on top. The basal layer at Crater Road is massive, lacking any stratification. Granulometry confirms the fine-grained character with up to 40 weight-% of particles < 63 µm. The percentage of particles < 63 µm decreases from 40 to 20 weight-% at the transition into the main body.

During previous studies of the block-and-ash flow deposits south of Ruawahia Dome in 2000, Dr. I.A. Nairn and Prof. S. Self (pers. communication) discovered that parts of the deposits (c. 500 m horizontal distance north of Crater Road) were reworked and deposited as lahars. This suggests that after the emplacement of the block-and-ash flows, water-induced erosion could have mobilized parts of the deposits at Crater Road as well, reworking and depositing them as lahar deposits, cutting through the block-and-ash flow deposit and into the tephra layers beneath. This could have led to the formation of the large erosion gully, extending into the underlying Kaharoa Tephra and being filled with lahar material. Smaller erosion gullies marking a sharp contact between the shear layer and the main body of the flow could be the result of the reworking.

Considering the water-induced reworking of parts of the block-and-ash flow deposits and the emplacement of the fine-grained shear layer as part of the primary block-and-ash flow, all deformation structures and erosion gullies could possibly be explained without proposing a different relationship and a time break between the fine-grained layer and the overlying block-and-ash flow deposit.

But the amount of water needed to rework the whole thickness of more than 3 m of block-and-ash flow material as well as up to 50 cm of Kaharoa Tephra beneath to cut the observed erosional gully would have to be fairly large, so the extent of reworking would probably not limited to the small section in Crater Road. No signs of further alteration in the rest of the quarry were found. Lahar deposits are commonly described as indurated and containing a vesicular matrix due to air bubbles trapped during transport (Vallance, 2000). The block-and-ash flow deposits are not indurated, bulk samples were easily taken from the exposure, and the in-situ matrix does not show any signs of air trapped inside.

4.4.2. Hypothesis 2 – Time break before BAFD emplacement

The occurrence of erosion gullies with a sharp contact between the fine-grained layer and the block-and-ash flow deposit (BAFD) suggests a time break between emplacement of both deposits.

The time break after the deposition of the Kaharoa Tephra suggested by Nairn et al. (2001) has been confirmed by erosion gullies cutting at varying depths and widths into the tephra layers, resulting from water-induced erosion. These furrows are filled with ash from the overling fine-grained layer. Further erosion gullies have been found at the upper interface to the block-and-ash flow deposit, marking a sharp contact. Rain-induced erosion possibly cut these gullies into the surface of the fine ash layer over days, weeks or even months, indicating a hiatus before the deposition of the block-and-ash flow deposit exposed at Crater Road quarry.

4.4.3. Hypotheses for the emplacement of the fine ash layer

The origin of the fine-grained layer is undetermined in this scenario, but a few suggestions can be made to explain the relation between this deposit and the rest of beds exposed at Crater Road. The following hypotheses were taken into consideration to explain the origin of this bed:

1. The generation of pyroclastic density currents directly from the vent during the growth of Ruawahia Dome occurred before the collapse of parts of the dome that generated block-and-ash flows to the south. The fine-grained layer could represent co-ignimbrite fall-out from the currents.
2. The generation of pyroclastic surges by sustained fountaining directly from the vent could result in the deposition of the massive, fine-grained layer.
3. The fine-grained layer is possibly of phreatomagmatic origin, due to an eruption from one of the surrounding lakes, similar to Green Lake plug.
4. The generation of block-and-ash flows was not limited to the end of Ruawahia Dome growth, multiple collapses of the margins occurred during growth by

oversteepening of the dome margins. Several block-and-ash flows were generated with varying volumes and travel distances, accompanied by ash cloud surges. The fine-grained layer represents either the deposits of a detached surge from a smaller block-and-ash flow or the fallout from lofted ash clouds from a block-and-ash flows with a run-out of < 4 km (distance of Crater Road quarry from the dome).

The first hypothesis suggests the generation of pyroclastic density currents directly from the vent, similar to the ones generated earlier at different stages of the eruptive episode. These have been described to underlie Kaharoa Tephra deposits south of Ruawahia Dome (Unit Hpdc; Nairn et al., 2001), reaching travel distances up to 10 km, with increased deposit thicknesses in the vicinity of Crater Road. A similar current could have been generated before the development of block-and-ash flows from Ruawahia Dome, the fine-grained layer representing co-ignimbrite ash carried downwind and deposited above the Kaharoa Tephra.

Interpretation: The base of the fine-grained layer is characterized by shear deformation structures and incorporated tephra clasts, casting doubt on the emplacement of this bed as co-ignimbrite ash fall due to the lack of shear force necessary to mobilize the substrate. Ash fall influenced by wind drift would not be able to exert enough shear stress on the substrate to deform it. In addition, the basal layer is very fine-grained, massive and poorly sorted, lacking signs of stratification; in contrast ash fall layers are generally characterized by good sorting and often clustering of ash particles or accretionary lapilli. No accretionary lapilli or other ash aggregates were observed.

The second hypothesis proposes the generation of pyroclastic surges directly from the vent of the growing Ruawahia Dome. These surges are usually associated with collapse of an eruption column or the “boiling over” of highly gas-charged ash flows directly from the crater, as has been described for Mont Pelée (Anderson and Flett, 1903) and Mayon volcano (Moore and Nelson, 1969). Similar events have been documented at Lamington volcano in Papua New Guinea (Taylor, 1958), termed “shallow-pocket explosions”.

These surges are generally characterized by massive to vaguely laminated, well-sorted deposits, enriched in pumice fragments.

Interpretation: Surges generated by boiling-over typically move radially from the vent, the occurrence of this fine layer was only observed at Crater Road south of Ruawahia Dome. The fine-grained layer is poorly sorted, showing large percentages of particles < 63 µm (up to 40%), max. grain size near the base is c. 2 mm, whereas surge deposits are often described to be fines-depleted and stratified. In addition, the fine-grained layer shows no enrichment in pumice particles.

The third hypothesis suggests a phreatomagmatic eruption from one of the surrounding lakes, similar to the proposed origin of Green Lake Plug at the margins of Lake Rotomahana. Phreatomagmatic eruptions occur when rising magma violently fragments after intersecting and mixing with shallow surface water or groundwater (Sheridan and Wohletz, 1983), resulting in the generation of wet surges as documented at La Fossa di Vulcano (Dellino et al., 1990) and El Chichón Volcano (Scolamacchia et al., 2005). Widespread occurrence of accretionary lapilli beds, deformation of the bedding (e.g. flame structures) and vesiculated horizons have been described to characterize wet surge deposits (Crow and Fisher, 1973; Lorenz, 1985; Wohletz, 1998; Nemeth et al., 2001). The deposits are usually hydrothermally altered and enriched in glassy fragments due to rapid quenching of the magma (Morrissey et al., 2000).

Interpretation: The ash layer at Crater Road is characterized by dynamic interaction with the underlying tephra, comparable to observed flame structures from wet surge deposits. But this is the only common parameter. The bed displays orange and greenish discoloration by thermal oxidation, but no indication of hydrothermal alteration can be found. Accretionary lapilli are absent, and no enrichment of glassy fragments was observed at Crater Road.

The last hypothesis suggests the deposition of this layer from a detached ash cloud surge from an earlier block-and-ash flow with shorter travel distance than Crater Road (< 4km from the dome). Nairn et al. (2001) suggested that block-and-ash flows were

generated at the end of the growth of Ruawahia Dome, but comparison with Unzen or Soufriére Hills Volcano (Cole et al., 2002) confirms that these flows may develop during the dome growth due to oversteepening of the dome margins. At Unzen Volcano, over 9000 block-and-ash flows have been recorded over a 5-year eruptive episode (Miyabuchi, 1999).

Interpretation: The growth of Ruawahia, Wahanga and Tarawera domes were suggested to occur over 3-5 years, therefore the possibility that several tens of block-and-ash flows were generated during this time is very high due to probably multiple collapses of the individual domes, as has been observed at Unzen Volcano (Miyabuchi, 1999). Oversteepening of the just developing dome could have resulted in small-volume currents with short run-out distances. The flows to the south encountered a pronounced break in the volcanic slope, so a rapid decrease in flow velocity combined with increased clast fragmentation could have lead to violently billowing ash cloud surges that rushed ahead, detaching and leading to deposition beyond the margins of the block-and-ash flow deposit. The energetic emplacement of the detached surge could explain the shear deformation of the Kaharoa Tephra layers. Two depositional units have been described in the proximal regions, a pink block-and-ash flow bed overlying a thicker grey deposit. The assumption that the fine-grained layer correlates with one of the proximal depositional units is incorrect, because this layer underlies the grey block-and-ash flow deposit found at Crater Road. It is more likely that the current from which the surge detached was deposited on the proximal slopes and became mixed with successive flows by progressive aggradation (Branney and Kokelaar, 2002), hence becoming indistinguishable in the field. This corresponds with observations at Unzen volcano, where individual flow units were hard to distinguish (Miyabuchi, 1999).

Detachment of the ash cloud surge from the underlying basal avalanche has been described at Soufriére Hills Volcano (Druitt et al., 2002). Comparison of the Crater Road deposits with pictures and descriptions of the detached surge layer described by Druitt et al. (2002) reveals some visual similarities (Figure 4.15).

Detached ash cloud surge deposits at Soufriére Hills Volcano are typically two-layered - a lower, fines-poor layer of friable medium to coarse ash and lapilli, and an upper, fines-rich layer of brownish-orange ash. Fines-poor samples had a median diameter (Md) of -0.5 to 3 phi, whereas fines-rich surge deposits had Md of 2.5 to 4 phi (Loughlin et al., 2002). At Soufriére Hills Volcano, the lower layer of the ash cloud surge deposit is not always exposed, depending on topographic influence.

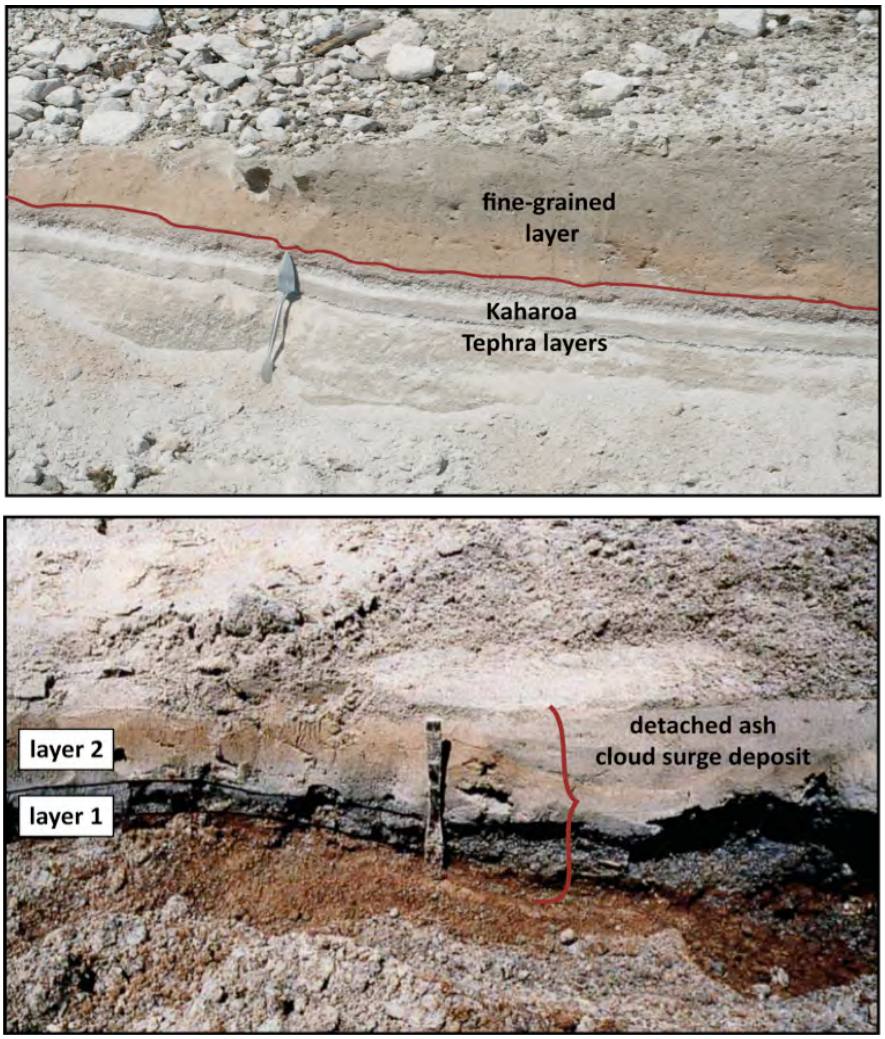

Figure 4.15: Comparison between the fine-grained layer at Crater Road, Tarawera Volcano (upper picture), with detached ash cloud surge deposits at Soufriére Hills Volcano (picture taken from Druitt et al., 2002).

A bipartite layering was not observed at Crater Road; samples were taken along a vertical profile through the fines enriched ash layer, from the contact to the Kaharoa

Tephra to the gradational contact to the BAFD. Grain-size distribution (from -1 phi to + 4.5 phi) showed a decrease in the 4.5 phi-fraction from c. 40 weight-% near the base to < 20 weight-% near the transition into the block-and-ash flow deposit. Median grain sizes ranged from 3 to 4.5 phi (see Appendix A-1), comparable to Soufriére Hills Volcano.

Ash cloud surges at Soufriére Hills Volcano detached from the basal avalanche and traveled several km beyond the extent of the block-and-ash flows, sometimes even in completely different direction due to channeling and redirecting of the basal avalanche. The southern block-and-ash flows at Tarawera Volcano did not experience channeling of the basal avalanche, but a break in slope, which was also observed at Soufriére Hills Volcano (Druitt et al., 2002), probably resulted in the detachment of an ash cloud surge and its deposition below successive block-and-ash flows.

4.4.4. Summary

No definite explanation for the generation and emplacement of the fine-grained layer can be given without further evaluation. Theories and hypotheses have been proposed and discussed according to their feasibility. The most reasonable explanation is a short time break before the emplacement of the block-and-ash flow deposit that is exposed at Crater Road. The surprisingly small number of recognized depositional block-and-ash flow deposit units could indicate that the actual number is much higher, but most likely successive currents have been mixed by progressive aggradation, as has been recorded at comparable volcanoes such as Unzen or Soufriére Hills volcano. Considering a time break before the deposition of the block-and-ash flow deposit exposed at Crater Road, the most feasible explanation is the detachment of an ash cloud surge from an earlier, smaller block-and-ash flow, because the shear deformation found at the contact to the tephra layers could only be the result of an energetic current, either a flow or a surge, not mere ash fall (Table 4.1).

Considering all evidence, it is not necessary to change the timeline for the Kaharoa eruptive episode proposed by Nairn et al. (2001), but to acknowledge the generation of

multiple block-and-ash flows and associated ash cloud surges at Tarawera Volcano with the possibility of decoupling of these flow parts, hence exhibiting different travel distances and depositional relations.

	No time break		Time break					
			Hypothesis 1	Hypothesis 2	Hypothesis 3	Hypothesis 4		
	lahar	basal shear layer	Co-ignimbrite ash fall from pdcs	boiling over from surge dome	"wet surge" by phreato-magmatic eruption	detached surge from earlier BAF		Exposed fine-grained layer
EXPECTED							OBSERVED AT CRATER ROAD	
bedding/stratification	✗	✗	✓	✓	✗	✓		✗
poor sorting	✓	✓	✗	✓	✗	✓		✓
good sorting	✗	✗	✓	✗	✓	✗		✗
enriched in pumice	✗	✗	✓	✓	✗	✗		✗
enriched in glassy fragments	✗	✗	✗	✗	✓	✗		✗
accretionary lapilli	✗	✗	✓	✓	✓	✗		✗
ash clusters	✗	✗	✓	✓	✓	✗		✗
interaction with substrate	✓	✓	✗	✓	✓	✓		✓

Table 4.1: Compilation of the proposed hypotheses for deposit emplacement and the expected deposit characteristics in comparison with the observed characteristics of the fine-grained layer at Crater Road quarry.

Chapter 5

Analogue models – Influence of topography on the flow dynamics of pyroclastic density currents

"There is no such thing as a failed experiment, only experiments with unexpected outcomes"

Richard Buckminster Fuller

Chapter 5: Analogue models - Influence of topography on flow dynamics of pyroclastic density currents

5.1. Objectives

In the preceding chapters, the influence of topography and topographic barriers on the flow dynamics of block-and-ash flows has been described for examples worldwide, suggesting that detachment of the dilute, turbulent flow phase from the granular avalanche beneath, and their independent travel, increases hazards to the surrounding communities during an volcanic eruption.

Very few direct observations exist of pyroclastic current interactions with irregular topographies, because of the highly dangerous nature of these currents. High velocities and extreme temperatures in combination with impressive billowing ash clouds make measurements difficult to obtain. To overcome this problem, reduced scale laboratory experiments developed for subaqueous turbidity currents are utilized as semi-quantitative guides for studying flow dynamics of pyroclastic density currents.

The aim of these experiments is to observe and analyse how a pyroclastic current interacts with various obstacles and topographies, how these influence decoupling and what the step-by-step processes of the encounter with an barrier are, e.g. blocking, deflecting or mounting the obstacle. First a brief summary of different modelling approaches is presented, giving a short overview of numerical and analogue modelling methods. Then the results of an analogue modelling progress report for aqueous glycerol currents and glass particulate currents are given, followed by implications for natural pyroclastic density currents.

5.2. Modelling pyroclastic density currents

Pyroclastic density currents are rapidly-moving mixtures of hot volcanic particles and gas that flow across the ground under the influence of gravity. These multiphase flows consist of particles of various sizes and densities, and a strongly buoyant hot gas phase. The complex interplay between sedimentation and entrainment, the difficulty of direct observations, and the absence of a direct record of the internal flow structure, makes the study of pyroclastic density currents challenging. During the last two decades, understanding of the dynamics of these currents has developed rapidly. Our knowledge, however, is mostly based on field observations, theoretical considerations and laboratory simulations, trying to extrapolate the results for natural pyroclastic currents.

5.2.1. Numerical modeling

Numerical simulations to study dynamics of pyroclastic density currents typically focus on the generation of the currents from eruption column or fountain collapse and the propagation of the resulting ash flows. Early theoretical models conducted by Sparks and Wilson (1976) and Sparks et al. (1978) were followed by modeling of pyroclastic flow behaviour and their run-outs based on the energy line concept (Sheridan, 1979; Malin and Sheridan, 1982), assuming the linear dissipation of flow energy along the volcanic slope with distance. This model defines a relationship between the drop in height of a pyroclastic flow (H) and the length of its travel distance (L). The ratio of H/L equals the tangent of α (slope), the straight line connecting the starting and ending points of the flow, enclosing the area that can be potentially reached by the flow, and giving indications of the topographic barriers that can be overcome by the flows (Figure 5.1). However, this model does not take into account the multiphase nature and highly varying composition of the currents, therefore probably causing misleading estimations of the distances reached by the flows and the height and nature of obstacles that can be overcome, resulting in false estimates of possible hazard zones.

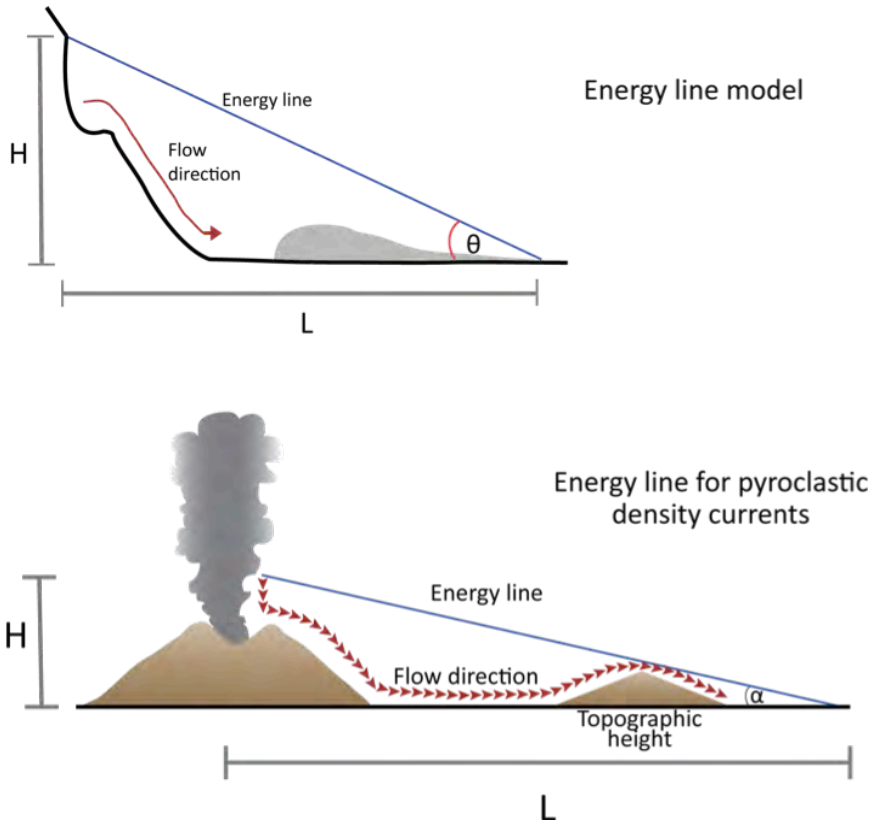

Figure 5.1: Energy line concept after Sheridan, 1979.

The limitations of early experiments gave rise to the necessity for more advanced models. In the last 20 years, two-dimensional, transient and two-phase flow models have allowed the description of the main physical features of pyroclastic density currents and their generation from eruption column collapse. These features include e.g. the propagation of the flows, generation of the ash cloud and sedimentation of particles (Valentine et al., 1991; Dobran et al., 1993; Giordano and Dobran, 1994, Takahashi and Tsujimoto, 2000). However, extent of numerical modeling used for the simulation of flow processes in pyroclastic density currents is typically limited to either dilute turbulent ash suspensions (e.g. Sparks et al., 1978; Bursik and Woods, 1996; Dade and Huppert, 1996; Freundt, 1999) or dense pyroclastic flows (e.g. Denlinger and Iverson, 2004; Kelfoun et al., 2009). Since flow stratification is widely recognized, it is important to couple the dense and dilute regions of the current and incorporate any interaction between them within theoretical simulations. Takahashi and Tsujimoto (2000) developed a model for the formation of upper surge clouds

from dome collapse block-and-ash flows. Naaim and Gurer (1998) have developed a similar model in the context of snow avalanches. Further multiphase models have been employed to consider the whole spectrum of possible granular concentrations and related rheologies within a pyroclastic current (e.g. Dobran et al., 1993; Neri et al., 2003; Dartevelle et al., 2004; Dufek and Bergantz, 2007). Doyle et al. (2010) presented a conceptual model of column collapse, where the initial current is dilute and thus the dense basal pyroclastic flow component must develop by mass transfer from the dilute current (Druitt and Sparks, 1982). This new approach captures both the mass transfer processes occurring during the column collapse and the independent propagation of the dense basal avalanche, and hence can possibly model the two-layer structure of pyroclastic density currents better than previous models.

Numerical simulations are valid tools for the simulation of stratified pyroclastic density currents, but to date focus lies on currents generated from eruption column collapses. Future theoretical models should try to take gravitationally generated block-and-ash flows further into account, similar to modeling by Doyle et al. (2010) with coupling of individual flow parts, to study their interaction and their dynamics under the influence of irregular topographies.

5.2.2. Analogue experiments

Analogue experiments are used in varied research fields to study the dynamics of density currents, e.g. in studies of snow avalanche hazards, physical volcanology or submarine reservoir research. Studies of density current dynamics typically include general propagation (e.g. Rottmann and Simpson, 1983), (sediment) entrainment (e.g. Middleton, 1966; Parker et al., 1987; Garcia and Parker, 1993), stratification of the currents (Ellison and Turner, 1959; Buckee et al., 2001), erosional or depositional behaviour (Keevil et al., 2007; Peakall et al., 2007) and even the interaction with topography or artifical barriers (e.g. Hákonardóttir et al., 2003; Morris and Alexander, 2003; Primus et al., 2004; Sampl et al., 2004; Keevil et al., 2007; Straub, 2007).

The most commonly used method used for analogue flume experiments is the lock-exchange method, where a volume of relatively dense fluid is suddenly released into a larger volume of ambient fluid of a lower density (Simpson, 1997). Studies have shown that laboratory flows generated by this method may undergo similar transformation to those described in nature, like the deceleration of the basal avalanche and the detachment of the overlying dilute cloud (e.g. Luthi, 1981; Hallworth and Huppert, 1998). Most researchers do not utilize natural bulk sediment in water, but use an appropriate substitute, due to the requirement of implementing controllable and reproducible experiments. The utilized material has to allow the reproduction of adequate density currents in water, with regard to the purpose of the simulation. Substitutes are usually salt water (plus kaolin) in fresh water (e.g. Simpson and Britter, 1979; Naaim-Bouvet et al., 2002), glycerol mixed with (sugar) water (Amy et al., 2005), methanol mixed with ethanol glycol (Woods and Bursik, 1994), silicon carbide in water (e.g. Hallworth and Huppert, 1998; Woods et al., 1998; Choux and Druitt, 2002), polysterene particles (Hermann and Hutter, 1991) and silica flour suspended in water (Baas et al., 2005).

One of the earliest attempts to simulate pyroclastic flows was made by Huppert et al. (1986) to study the generation of buoyant clouds from the flows. It was observed that extensive mixing with the ambient fluid occurred at the head of the flow and behind it to form a suspension cloud, which then rose buoyantly and eventually lofted completely. Although successful in modelling the convective cloud associated with pyroclastic density currents, segregation and sedimentation were neglected in these experiments.

The generation of pyroclastic surges from advancing block-and-ash flows was then studied by Takahashi and Tsujimoto (2000), using theoretical and experimental models. For the analogue experiments, heated sand was mixed with sodium hydrogen carbonate, and during the propagation of the flow in air H_2O and CO_2 gases were emitted violently. The propagation of the mixture generated dust clouds, resembling ash plumes associated with pyroclastic flows. These results were compared with similar tests of hot silica sand without additional sodium hydrogen carbonate, in which the sand did not flow and was deposited near the source point.

Studies of the individual propagation of block-and-ash flow parts were made by Saucedo et al. (2004), comparing the results to block-and-ash flows at Colima Volcano. Sand and silt were separately injected into a water tank; continuous feeding of sand from a hopper simulated continuous basal underflow motion during a sustained collapse event, while the silt was injected in a single event to simulate generation of fine particles during transport, with the potential formation of a dilute gravity current. Depending on the angle of the slope, either no basal avalanche formed (below angle of repose) or the basal avalanche accelerated ahead and pulled the fine cloud along (angle > 42°). According to the experimental results, Saucedo et al. (2004) suggested that the spread of block-and-ash flows is controlled by the basal underflow at steep flows, and by the dilute ash cloud surge at shallow slope angles. Near the angle of repose, the dynamics of the basal avalanche and the surge are linked by the shear exerted between them, and by transfer of particles from the basal flow into the surge by erosion.

5.3. Modeling decoupling in density currents

Decoupling in density currents is still incompletely understood. Few attempts have been made to utilize analogue experiments for simulation of the detachment of a suspension current from the underlying high-concentration basal avalanche. Flow stratification is an important pre-requisite for the onset of decoupling (compare Chapter 2). Some attempts have been made to study density-stratified gravity currents with respect to overall flow dynamics (Hallworth and Huppert, 1998; Gladstone et al., 2004) or specifically with implications for possible submarine reservoir deposits (Amy et al., 2005). These experiments often utilized solutions of aqueous glycerol to control initial stratification and enhance long duration, in contrast to particle-water slurries in which these parameters cannot be controlled properly (Amy et al., 2005). For glycerol solutions, viscosity increases with increasing glycerol concentrations, comparable to sediment currents whose viscosity strongly increases with increasing particle concentrations, hence these solutions can be used as an adequate alternate for particulate density currents, even though not all

aspects of particulate currents can be represented accordingly, e.g. normal or shear stresses, particle interaction or particle settling.

Gladstone et al. (2004) investigated density stratified currents and their propagation in the context of natural turbidity currents and pyroclastic flows which are thought to show stratification from the point of initiation. The interaction of individual layers was closely observed with respect to travel time and distance of each layer. The experimental results showed that the layer containing the greatest buoyancy propagates to the nose of the flow and drives the current. The extent of the interaction between the individual layers was a function of the stratification, and therefore grain sizes and concentrations within the currents.

Hallworth and Huppert (1998) carried out a set of lock-exchange experiments with stratified particle-laden flows moving along straight slopes, studying "abrupt transitions" from turbulent to laminar flow regimes in high concentration density currents. Silicon carbide particle solutions were released into two flumes of different length, and run-out distance and particle distribution measured. The results showed that particulate currents above certain initial volume fractions undergo abrupt arrest and separation of flow parts, with final run-out length decreasing with increasing volume concentrations. Similar results have been documented by Amy et al. (2005) for aqueous glycerol solutions with varying densities and viscosities.

The influence of topography or artificial barriers has not been specifically studied for pyroclastic density currents; most research is concentrated on snow avalanche hazards and the possible effect of breaking or deflecting dams and mounds on the propagation of the avalanches in populated mountainous regions (e.g. Primus et al., 2004; Sampl et al., 2004). The influence of topography on subaqueous turbidity currents is often studied with regard to sedimentation patterns and possible submarine reservoir capacities due to deposit thickness around obstacles (e.g. Alexander and Morris, 1994; Morris and Alexander, 2003). A first attempt to model the interaction between an avalanche and topography was made by Hopfinger and Tochon-Danguy (1977), followed by a series of experiments studying unsteady gravity current flow over deflecting and catching dams that was conducted by Beghin and Closet (1990) and Augé et al. (1995) for two- and three-dimensional

configurations. Similar experiments as those done by Beghin and Closet (1990) were carried out by Keller and Issler (1996), and later experiments were conducted by Naaim-Bouvet et al. (2002) and Primus et al. (2004). Most of these experiments deal with velocity measurements and pressure changes before and after contact with the barrier to attain information about the effectiveness of deflecting or blocking dams and mounds in regions prone to snow avalanche hazards.

5.4. Analogue experiments: scaling considerations

The presented laboratory currents were scaled as closely as possible to turbulent pyroclastic density currents. The most important dimensionless numbers used to characterize the dynamics of inertial experimental flows are the Reynolds and Froude numbers.

The Reynolds Number (*Re*) represents the ratio of inertial to viscous forces within a current, which is evaluated here using

$$\mathrm{Re} = \frac{u h_0 \rho}{\mu}$$

where u is the velocity of the front of the flow, h_0 the initial thickness of the current, and ρ and μ are the density and viscosity of the fluid driving the flow respectively. Calculated Reynolds numbers for the initial flow motion vary from > 3000 for aqueous flows with low viscosities to <10 for those with the highest viscosities, indicating a range of flow conditions from turbulent (*Re* > 2000), to laminar (*Re* < 500). The particulate density currents used in the second set of experiments are fully turbulent, Reynolds numbers range between 4000-12500 (see Appendix A-3). In comparison, natural pyroclastic density currents typically show *Re* > 10^8 to 10^{11} (Druitt, 1998); so experiments with *Re* > 2000 adequately represent field conditions.
The Froude number, *Fr*, is the ratio of inertial to gravitational forces within the flow; calculated values for the less dense glycerol currents are c. 0.7-1.2, compared to c. 0.6-1.2 for particulate currents. Consideration of these numbers indicates that the experimental models of the density currents are dynamically similar to their natural counterparts as (1) the Reynolds number, *Re*, of both the experimental and natural flows is sufficiently large to be turbulent, and (2) the Froude number at the head of

the current, Fr, is nearly of the order of unity for the experimental currents, a value that is thought to apply to the natural counterparts (Simpson, 1997).

Valentine (1987) has shown that flow stratification is strongly dependent on an equilibrium between the settling of particles and the turbulence scale of the flow that keeps the particles in suspension. This equilibrium, therefore, controls the sedimentation rate and the development of density stratification in the flow, and the nature of flow transformation as the overall density of the flow evolves during movement of the gravity current. This equilibrium between settling forces and turbulent forces can be expressed by the particle Rouse number Pn_i:

$$Pn_i = w_i / \kappa u_*$$

where w_i is the settling velocity of particles, κ is the Von Karman constant (0.4), and u_* is the shear velocity. The settling velocity can be approximated by the Stokes relationship:

$$w_i = (0.2222)\left(\frac{d}{2}\right)^2 \left(\frac{\rho_s - \rho_{H_2 0}}{\mu_{H_2 0}}\right) g$$

$$R_{particle} = \frac{w_i d \rho_{H_2 O}}{\mu_{H_2 O}}$$

where d is the particle diameter and $R_{particle}$ is the particle Reynolds number. Shear velocity u_* (Valentine, 1987) can be calculated as follows:

$$u_* = \frac{u\kappa}{\ln(30y/k_s)}$$

where u is the mean velocity of the flow and κ is the Von Karman constant (0.4). The thickness of the boundary layer of the flow, y, is unknown for the experiments, therefore two values were used (0.02m, 0.04 m), representing 20 and 40 % of the average flow head thickness of 10 cm (compare Stix, 2001). Surface irregularities on the flume floor were of the order of 2 mm (0.002 m), so this value was used for k_s.

Particle Rouse numbers range between 3.0-3.4 for the coarser glass particles, and between 1.3-1.4 for the finer glass fragments (see Appendix A-3). Typically, particles with $Pn_i < 2.5$ are supported by turbulence, those with $Pn << 2.5$ being well mixed vertically throughout the current and those with $Pn \approx 1$ being concentrated towards the base. Particles with $Pn > 2.5$ are not supported by turbulence (Valentine, 1987), and will settle out quickly.

In summary, the experimental currents capture some of the essential features of turbulent pyroclastic density currents, in that (1) they have high flow Reynolds numbers; (2) they contain particles with a wide range of Rouse numbers, from <<2.5 to >>2.5. Calculated Rouse numbers for natural particulate currents range between $10^{-3} – 10^{2}$ (values used for calculations taken from Druitt, 1998).

5.5. Experimental set-up

In the presented experiments, the flume was constructed of two 6 mm thick glass sheets (1 m x 1.50 m) set inside a rectangular wooden frame, with a width of c. 2.5 cm. Two sets of experiments of lock-exchange type were run, where the initial glycerol solutions and sediment suspension were rapidly introduced into the flume from a Perspex box with a sliding door at the end (“source”), with a volume of c. 500 ml. A false bottom was inserted into the flume, with dimensions 1 m length × 0.3 m height × 0.02 m width, with the Perspex box fixed at one end (Figure 5.2).

Each solution of varying initial viscosity was mixed before feeding into the Perspex box, and was dyed blue for better visualization and tracking the subsequent gravity current. To initiate the aqueous glycerol currents, the flume was first filled with water within a few centimeters to the top, the Perspex box was then filled with the solution and additional water was added to the flume to equalize the upper water level. The sliding door on the box was removed rapidly, the collapsing solution formed a density current that moved along the flume.

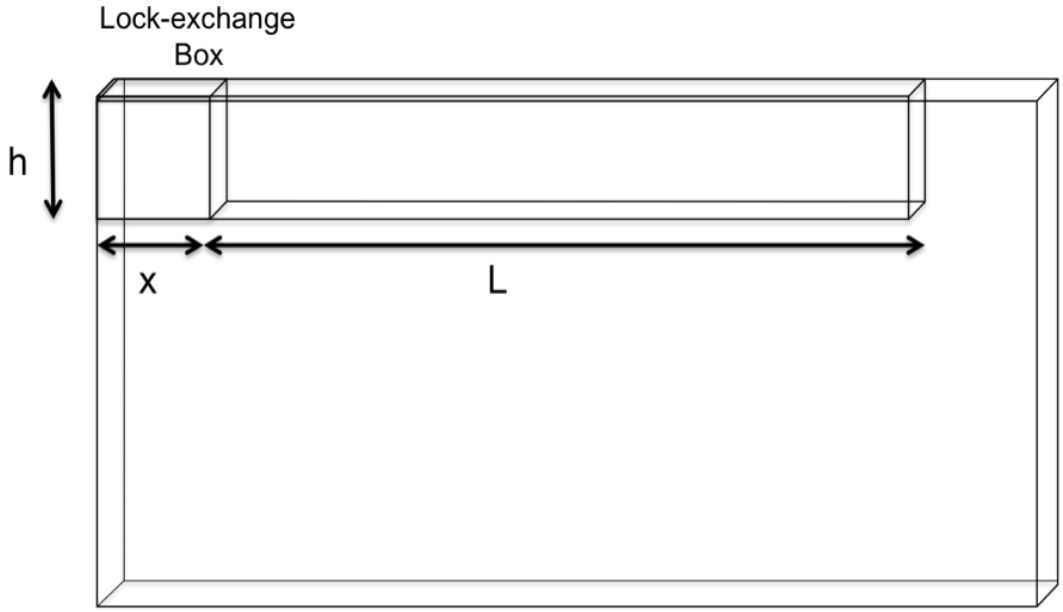

Figure 5.2: Simplified sketch of experimental set-up. L is the run-out length of the slope, h is the initial flow height, and x is the length of the lock-exchange box ("source").

The turbidity current experiments were carried out in a similar fashion. A predetermined mass of glass particles mixed with water was added to a feeder box that was placed above the flume. To initiate the particulate current, the suspension in the box was stirred vigorously. After the rapid release of the particle-water slurry into the flume, a particulate current formed that moved along the false bottom.

Simple obstacles (cube, rectangular or wedge-shaped) were placed perpendicular to the direction of the flows, spanning the whole width of the slope. The distance from the source was chosen with regard to the total slope length; 30 and 60 cm for the horizontal and inclined set-up (15°; with a length of 100 cm) for the aqueous glycerol currents, and 25 and 45 cm for the glass particle currents moving along an inclined slope (30°) with a total run-out length of 80 cm.

Each run was documented using a high-speed colour video camera, IDT High V4 (courtesy of the Department of Geological Sciences, University of Canterbury) and a regular digital camera. The high-speed video camera was set at 150 frames per second, resulting in 5000 frames recorded over 33.33 sec. The digital camera, Fuji Finepix S9500, captures movies with 30 frames per second, giving the chance to film the complete run-out of the current whereas the high-speed camera only focuses on a c. 30 cm long section of the slope, concentrating on the flow development around

an obstacle or change in topography. Using the accompanying IDT Highvision software, each run was analysed frame-by-frame.

5.6. Solution properties

For the first set of tests, a series of aqueous glycerol solutions with varying initial densities were mixed. Glycerol ($C_3H_8O_3$) has a density of 1260 kgm^{-3} and viscosity of c.1.5 $kgm^{-1}m^{-1}$ at 20° C. Densities for the solutions ranged from 1047 to 1260 kgm^{-3} (Lide et al., 2004). The solutions were mixed with different glycerol to water ratios (1:4, 2:3, 3:2, 4:1 and 5:0) for a total volume of 50 ml for each current. For aqueous glycerol solutions the viscosity increases with increasing glycerol concentrations. Although these solutions are appropriate analogues for particle-laden currents, not all aspects important for particulate currents can be reproduced, such as the influence of the Non-Newtonian rheology on flow behaviour, occurrence of yield strength and shear behaviour (Major and Pierson, 1992).

For the turbidity currents, angular glass particles of different grain size fractions, but uniform density were used. The density of crushed bottle glass has been determined to be an average of 2.4 g/cm^3 for the most popular beverage bottles (Lide et al., 2004*).* The glass particles were sieved to minimize the variations in grain size. Two different grain size fractions were then mixed with water, 2.25 phi or 3.25 phi for the basal avalanche and 4.75 phi for the suspension cloud. Each current has a total volume of 100 ml, 20 ml of glass particles mixed with 80 ml of water. Initial suspensions had a density of c. 1278 kgm^{-3} and a viscosity of c. 0.004 Pa s (see Appendix A-3).

5.7. Aqueous glycerol solutions

More than 100 experiments were run, varying the initial density of the solution, the slope of the false bottom, the size and shape of the obstacle and its distance from the source. Different types of obstacles (shape and height) were placed perpendicular to the flow direction along the slope, at 30 cm and 60 cm from the lock-exchange gate, independent of the inclination of the slope (see Appendix A-5).

Calculated Reynolds numbers for the initial flow motion vary from > 10000 for flows with low viscosities to < 10 for those with the highest viscosities (Appendix A-3), indicating a range of flow conditions from turbulent, Re > 2000, to laminar with Re < 500. Depending on the viscosity of the currents, the height of the flow and the velocity of the flows changed remarkably during and after passing of the obstacle.

A distinct gravity flow formed rapidly after the release of the sliding door of the lock-exchange box, with a characteristic head, body and tail structure. A flow head formed, with Kelvin-Helmholtz waves at the top of the head and immediately behind. These waves indicate turbulent mixing between the glycerol solution and the ambient fluid, water, in the flume (Simpson, 1997). Additionally, longitudinal waves parallel to the flow formed behind the head. As the flows became progressively more dilute with distance from the source, heterogeneities were observed; the head developed lobes and clefts, with parts surging ahead of adjacent regions.

5.7.1. Experimental results

Not all runs of the various viscosities will be described, because for each configuration up to 5 different current viscosities were tested. The amount of data is too large to be included in the main part of this thesis, therefore representative test runs will be described herein, using mostly only one specific mixture concentration of 20 ml glycerol mixed with 30 ml water. Full data are presented in Appendix A-3.

Test run 1

Avalanche: 50 ml glycerol

Slope angle: 0°

Slope length (L): 100 cm

Substrate: none

Name	time (s)	Froude number	Reynolds Number
run 1	8.68	0.14	2
run 1	9.13	0.14	2
run 1	10.12	0.14	2
run 1	13.00	0.14	1
run 1	16.50	0.14	1
run 1	20.87	0.14	1
run 1	22.65	0.14	1
run 1	31.35	0.14	1

For the first run pure glycerol was used without water. After the sudden release and the collapse of the fluid from the lock-exchange box, a slow moving laminar high-density current of c. 1-1.5 cm height formed. Flow height showed a decrease from tail to the flow front from c. 1.5 cm to < 0.5 cm. No stratification was observed during movement, but due to mixing of the upper surface of the current with the ambient fluid, a weak, dilute suspension cloud developed on the upper surface. The basal current slowly crept along the flume, with an average velocity of c. 1 cm/s, while the developing suspension cloud moved faster and detached from the current (Figure 5.3). The separated suspension current forms a distinct head, body and tail structure, as soon as it outruns the basal current. While the basal current comes to rest after c. 50 cm distance, the suspension cloud entrains further ambient fluid, getting more dilute and showing a final travel distance of c. 80 cm before it became too dilute to be distinguished from the ambient fluid.

Similar flow behaviour has been inferred to represent decoupling in pyroclastic density currents, where either due to a break in slope or the propagation over a flat run-out plain, the basal avalanche show a steady decrease in velocity, given the ash cloud surge to possibility to move ahead and detach from the basal avalanche.

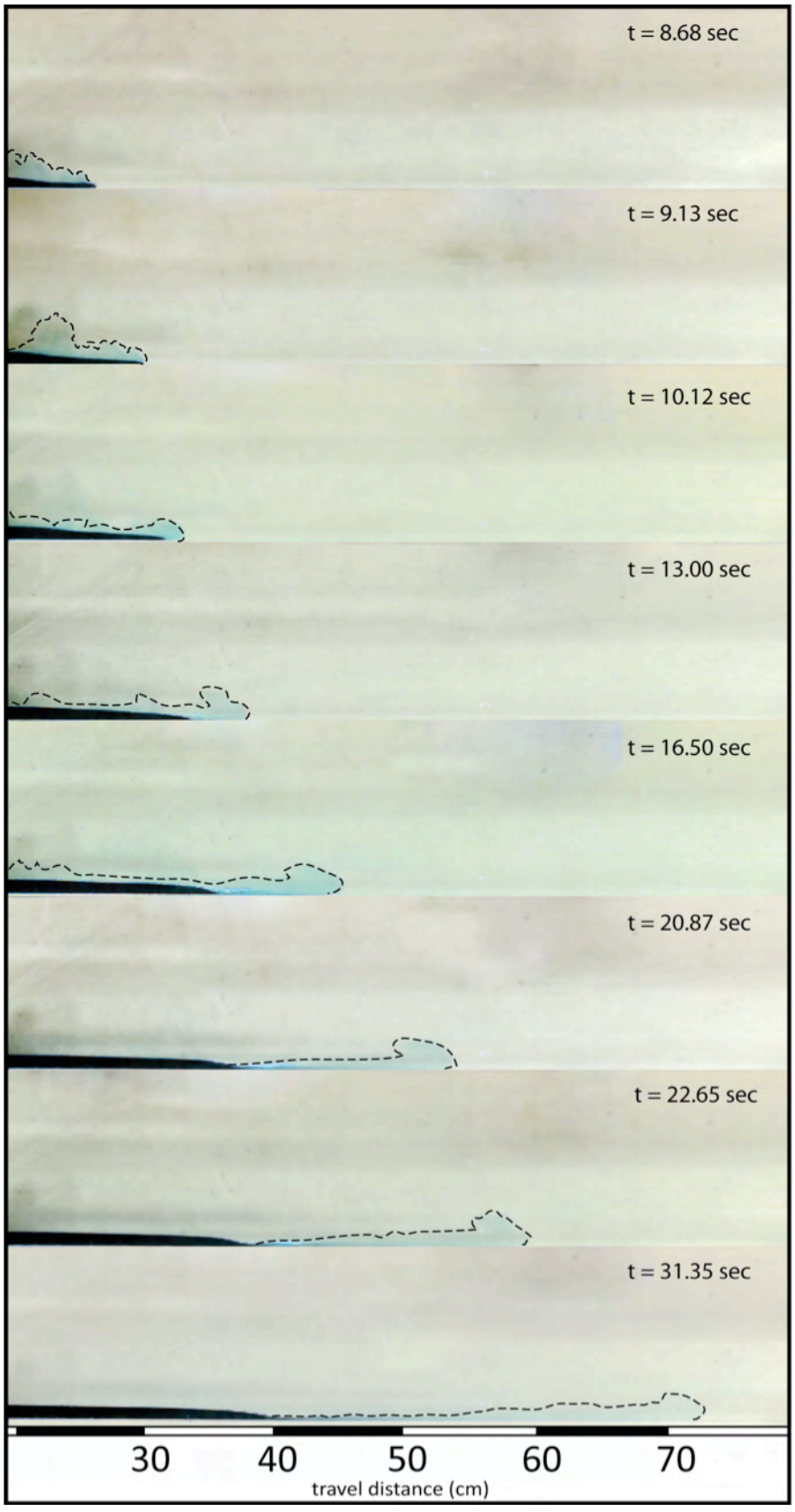

Figure 5.3: Video snapshots of test run 1. 50 ml of pure glycerol formed a laminar current from which a weak suspension cloud (stippled outline) developed due to mixing with the ambient fluid at the flow surface.

Test Run 2

Avalanche: 20 ml glycerol, 30 ml water

Slope angle: 0°

Slope length (L): 100 cm

Substrate: none

Name	time (s)	Froude number	Reynolds Number
run 2	6.35	1.10	2080
run 2	6.90	1.03	2377
run 2	7.46	1.05	2258
run 2	7.88	1.04	2317
run 2	8.72	1.13	1961
run 2	10.12	1.20	1723

Directly after release from the lock-exchange, the solution formed a distinct density current with distinguishable vertical flow levels - a dense basal avalanche, a mixing zone and suspension cloud at the top. The stratification became more distinct with travel distance (Figure 5.4). A core of dense fluid was apparent at the base of the just formed current, this core spread along the base of the propagating current, forming the high-density underflow. This underflow showed increasing depth from the head towards the tail within the first 40 cm travel distance. With increasing run-out, mixing at the flow front resulted in a turbulent flow head, stratification was less pronounced than in the rest of the flow. Stratification therefore seemed to be concentrated on the body and tail of a density current.

These first two runs replicate experiments made by Amy et al. (2005), using glycerol solutions to study “abrupt transitions” in flow behaviour in non-particulate density currents, signifying a change in dynamic regime from inertial slumping to a viscous-buoyancy phase during flow propagation. In addition to tests concerning general flow propagation along a horizontal slope, the influence of obstacles in the flow path was studied with obstacles of simple shapes, such as square, rectangular or wedge-shaped, which were placed at two different distances from the source, at 30 and 60 cm along the horizontal slope.

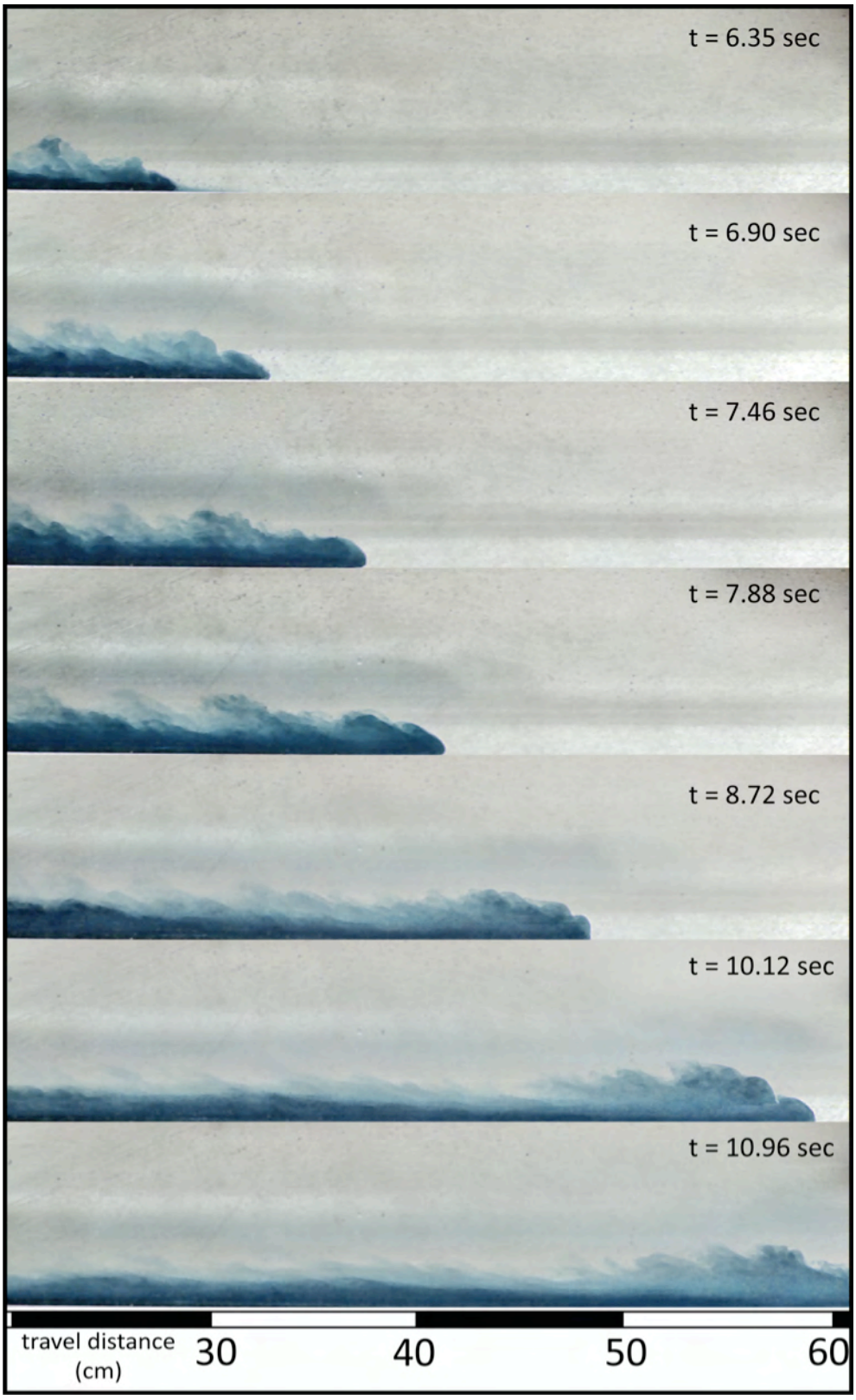

Figure 5.4: Video snapshots of test run 2. An aqueous glycerol solution of 20 ml glycerol mixed with 30 ml water moved along a horizontal slope, experiencing increasing stratification with increasing travel distance.

Test Run 3

Avalanche: 20 ml glycerol, 30 ml water

Slope angle: 0°

Slope length (L): 100 cm

Substrate: none

Obstacle: cubic, 30 cm from source

Name	time (s)	Froude number	Reynolds Number
run 3	4.06	0.80	2834
run 3	4.30	0.73	3465
run 3	4.53	0.77	3102
run 3	4.76	0.72	3476
run 3	5.46	0.66	4171
run 3	6.16	0.84	2567
run 3	6.63	0.84	2610

This run encompasses a cube-shaped obstacle placed at 30 cm distance from the source. The height of the obstacle is about half the depth of the initial current. The initial flow did not show distinct stratification (Figure 5.5), the body directly behind the head and the tail seemed to comprise a slightly diffuse dense basal avalanche. No distinct suspension cloud developed from the body, the instabilities from the head of the current resembled a lower density layer at the top of the current. When the flow encountered the obstacle, it was more than double the height of the barrier, hence most of the current climbed over it. During the jump over the barrier, the flow front became more dilute due to mixing with ambient fluid. This dilute suspension traveled ahead of the slightly denser body of the flow, but no noticeable flow stratification was observed.

The current was not fully developed before it encountered the obstacle near the source; it displayed a more uniform flow structure, hence most of the still uniform current was able to surpass the obstacle as a single current, no blocking of parts of the current could be observed.

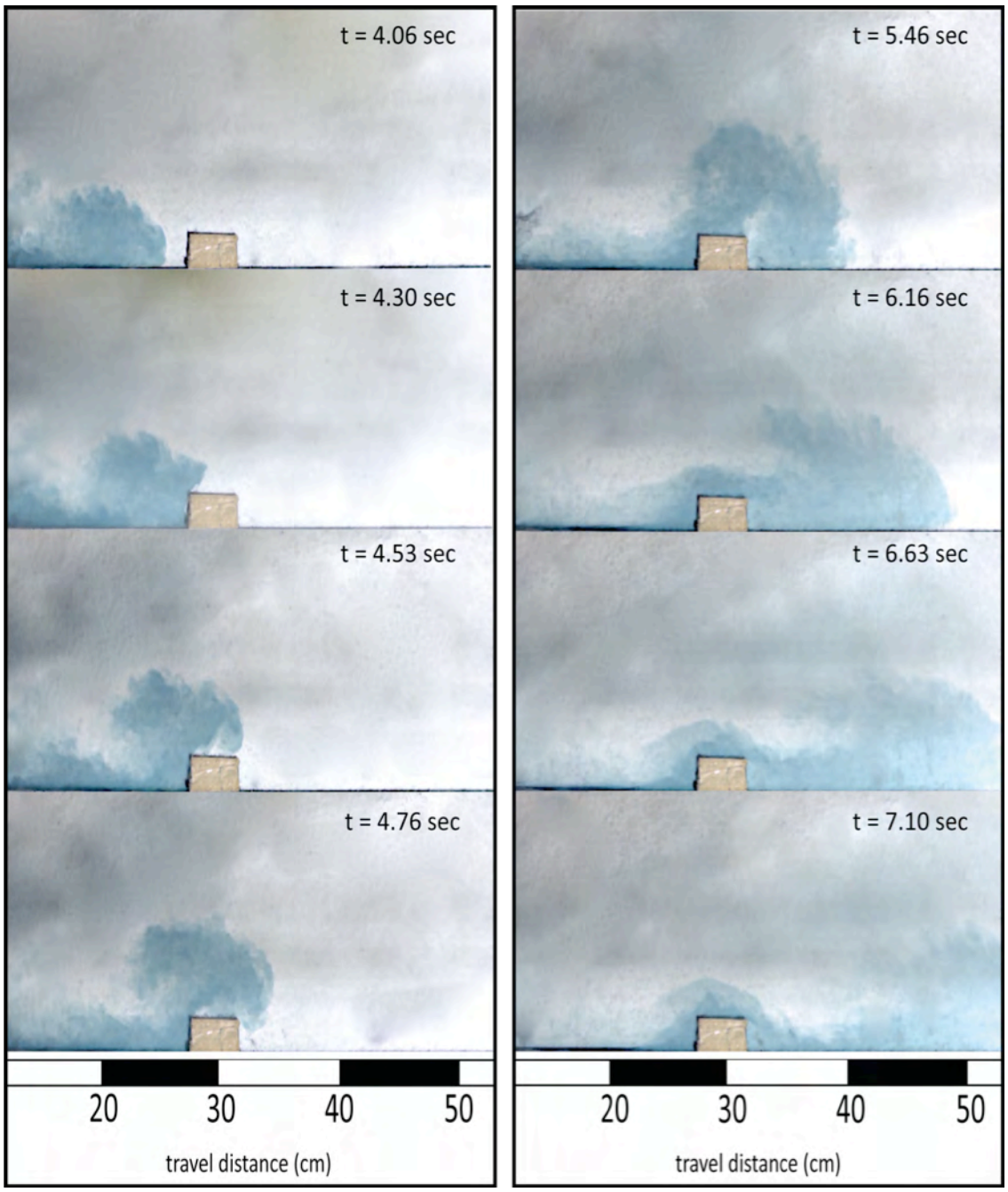

Figure 5.5: Video snapshots of test run 3. A solute density current is encountering a cube-shaped obstacle placed at 30 cm from the source.

Test run 4

Avalanche: 20 ml glycerol, 30 ml water

Slope angle: 0°

Slope length (L): 100 cm

Substrate: 2 mm quartz sand

Obstacle: cubic, 60 cm from source

Name	time (s)	Froude number	Reynolds Number
run 7	7.76	0.88	1664
run 7	8.00	0.85	1759
run 7	8.23	0.88	1664
run 7	8.46	0.88	1664
run 7	8.93	0.79	2044
run 7	9.40	0.84	1806
run 7	9.86	0.87	1711
run 7	11.03	1.00	1284
run 7	11.96	0.98	1331

When a large obstacle (relative to the height of the flow) was placed at 60 cm from the source, the current was already fully developed with a distinct flow structure and even stratified before the encounter with the barrier. Stratification of the current developed after the first 40 cm and became slightly more pronounced before encountering the obstacle. When the current reached the obstacle, the non-stratified flow head climbed and dragged some dense fluid over it. Most of the dense basal avalanche was blocked by the obstacle which was slightly lower than the depth of the flow. While the suspension cloud sheared across the basal avalanche, the latter backed up from the obstacle, equalizing its depth upstream of the barrier (Figure 5.6). The suspension cloud easily overtopped the barrier, then collapsed after its jump and again formed a dilute density current, representing decoupling due to topographic influence.

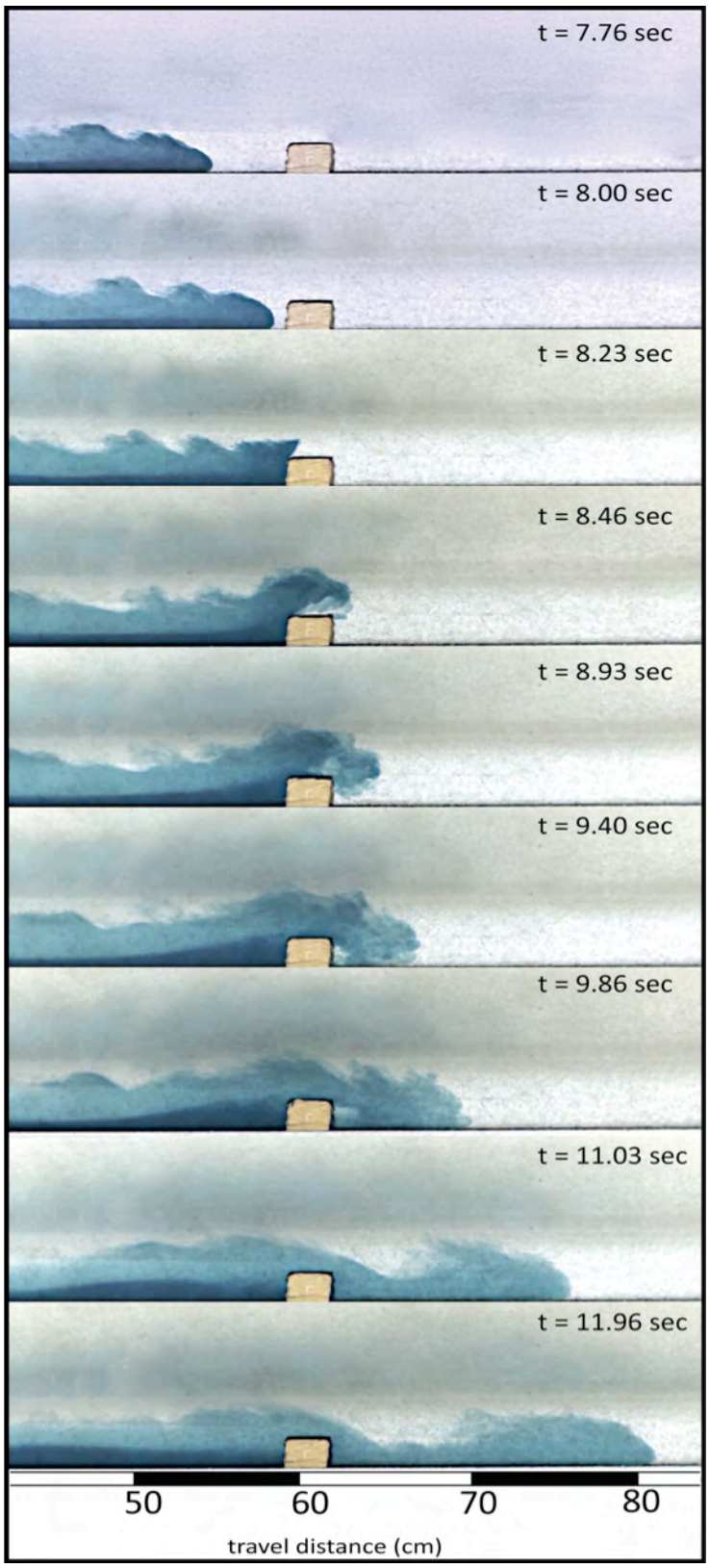

Figure 5.6: Video snapshots of test run 4. A solute density current is encoutering an obstacle at 60 cm from the source. Obstacle height is high relative to the flow depth, resulting in blocking of parts of the stratified flow.

Test run 5

Avalanche: 20 ml glycerol, 30 ml water

Slope angle: 0°

Slope length (L): 100 cm

Substrate: 2 mm quartz sand

Obstacle: rectangular, 30 cm from source

Name	time (s)	Froude number	Reynolds Number
run 5	5.50	1.01	1025
run 5	5.80	1.01	1025
run 5	6.03	1.09	891
run 5	6.26	1.06	936
run 5	6.50	0.94	1185
run 5	6.96	1.09	891
run 5	7.43	1.09	891
run 5	7.90	1.06	936
run 5	8.60	1.09	891

A rectangular obstacle was placed at 30 cm distance from the source. The aqueous glycerol solution left the lock-exchange box, and formed a density current with a distinct flow head and body, but no stratification was experienced. The current seemed to be more or less homogeneous, small parcels of denser fluid were concentrated first at the base and middle of the flow structure, shifting to the flow front when the currents encountered the obstacle (Figure 5.7). The core of denser fluid experienced mixing with the ambient fluid, resulting in less denser upper flow surfaces.

When the flow encountered the obstacle, it was nearly three times the height of the barrier, hence most of the current climbed over it. The core of dense fluid within the flow head moved completely over the barrier, dragging less denser parts of the current with it. During the jump over the barrier, the base of the flow head became more dilute due to mixing with ambient fluid. After the head fully overtopped the obstacle, mixing with the ambient fluid increased, forming a dilute suspension cloud at the flow front. The dense core sunk to the base of the current, whereas the dilute suspension moved ahead and upwards, the current hence being not uniform anymore. The change from the parcel of fluid to a dense basal underflow implied that the upper surface mixing became more significant with distance from the source, while the basal mixing zone was reduced in importance as a result of stable stratification. Non-uniformity developed only after the encounter with the barrier,

not before due to the short travel distance from source, giving the current not have enough time to fully develop.

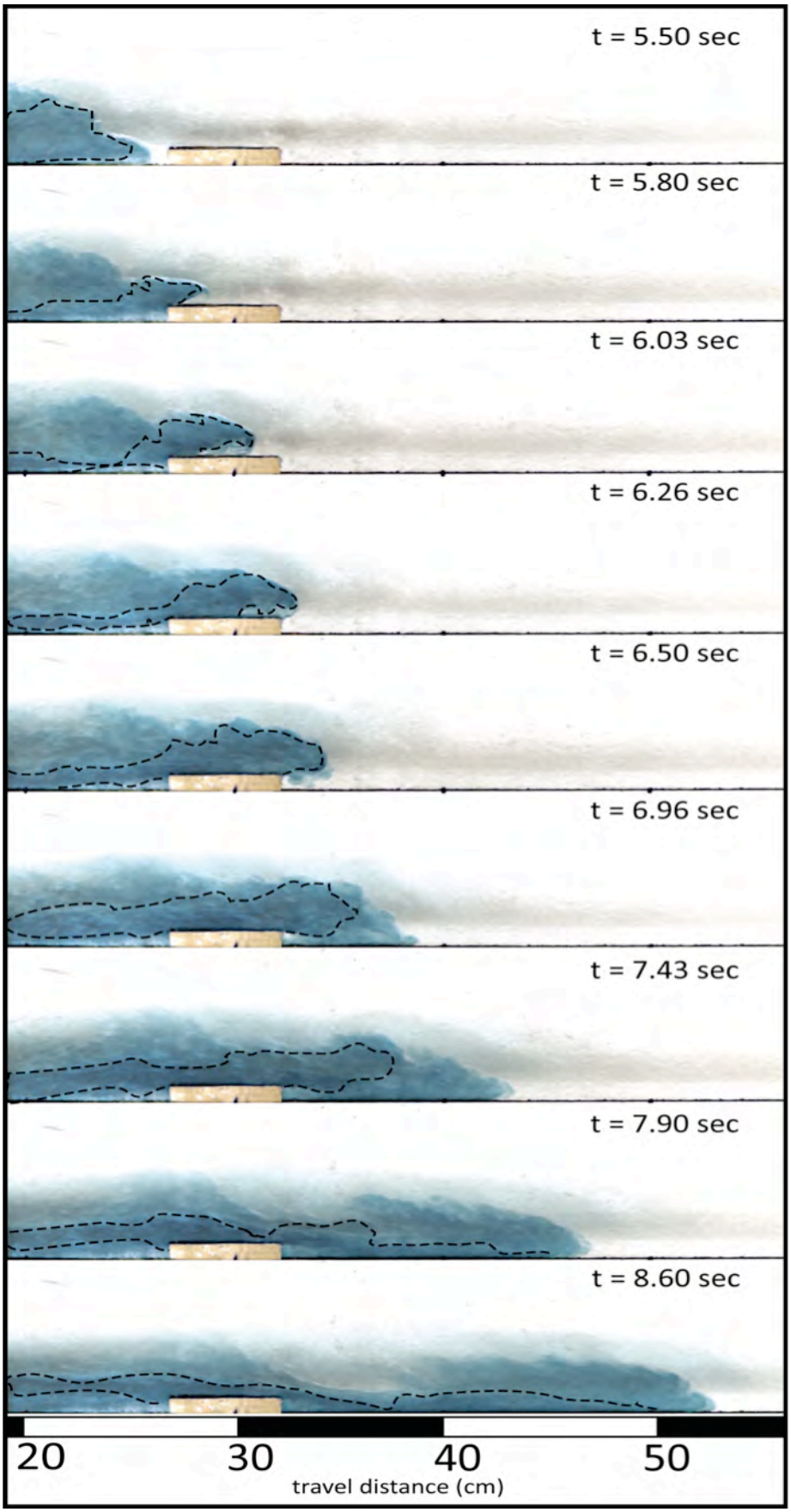

Figure 5.7: Video snapshots of test run 5. A solute current is encountering a rectangular obstacle, resulting in slight stratification of the flow.

Test run 6

Avalanche: 20 ml glycerol, 30 ml water

Slope angle: 0°

Slope length (L): 100 cm

Substrate: none

Obstacle: rectangular, 60 cm from source

Name	time (s)	Froude number	Reynolds Number
run 6	8.40	0.93	1768
run 6	8.63	0.89	1919
run 6	9.10	0.78	2525
run 6	9.33	0.80	2374
run 6	9.80	0.77	2576
run 6	10.26	0.87	2020
run 6	10.73	0.87	2020

The same obstacle as in the previous run was placed at 60 cm from the source. Similar to run 4, the current was fully developed, but more stratified before it reached the obstacle. When this happened, the flow was significantly deeper than the barrier, hence most of the basal avalanche and all of the suspension cloud moved over it and the current head collapsed downstream of the obstacle. Due to entrainment of ambient fluid at the flow front, the whole flow head and parts of the body became more dilute, the remains of denser fluid parcels dissipated due to increased turbulence in the flow head. The turbulent and dilute flow front evolved into a dilute turbulent current without a distinct denser basal avalanche (Figure 5.8), moving further along the slope and showing increasing flow thickness due to continuous entrainment and mixing of ambient fluid. Further downstream, the suspension current eventually lofted and dissipated completely.

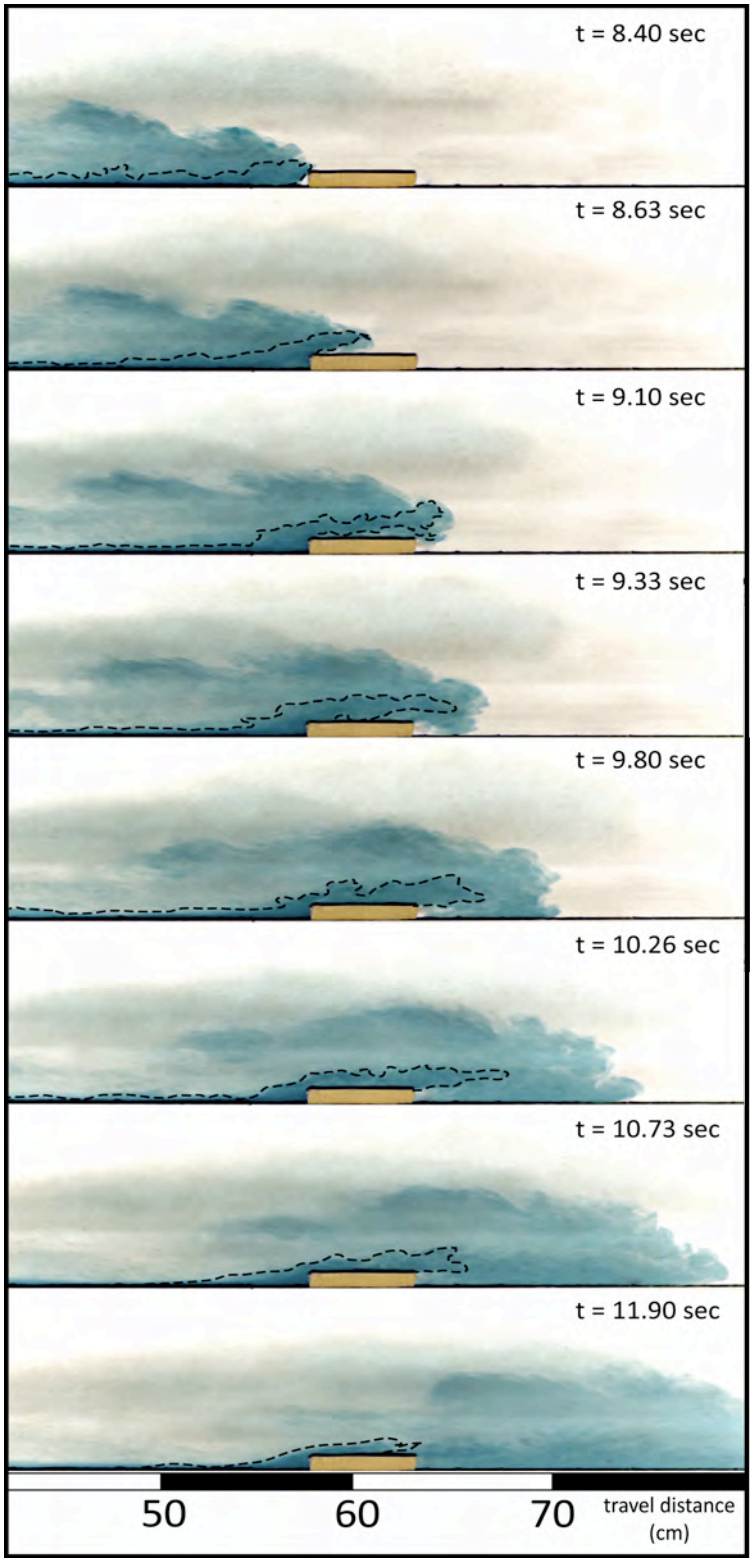

Figure 5.8: Video snapshots of test run 6. A solute density current is encountering a rectangular obstacle at 60 cm from the source. Stippled line marks a core of denser fluid in the flow structure.

5.8. Glass particle currents

Several turbidity current tests were run (see Appendix A-5), using green or brown coarse glass particles mixed with bright white glass powder and water; initial suspension density was 1278 kgm^{-3}. These slurries were rapidly introduced into the flume, the collapsing mass immediately generating gravity flows with a distinct head and body structure. Shortly after their initiation, these very turbulent currents divided into an upper less dense part overlying a dense basal region; their energetic behaviour driven by differences in grain settling velocities. Breaking waves were observed at the interface between the upper layer and the ambient fluid, indicating Kelvin-Helmholtz instabilities due to mixing with the ambient fluid. Lobes developed at the flow front, the interface between the two layers became more distinct, especially within the body and tail of the current, and the white suspension layer could be clearly distinguished from the rest of the basal avalanche.

The interaction of the particulate current with obstacles in the flow path is strongly dependent on the shape and height of the obstacle and its distance from the source. Obstacles were placed at 25 and 45 cm from the source; depending on the rate of stratification, the currents showed distinct flow behaviour when encountering the barrier.

5.8.1. Experimental results

Each obstacle configuration was tested for two different particulate currents, the first used a grain size fraction of 2.25 phi for the basal avalanche and 4.75 phi for the suspension cloud, whereas the second set used a smaller grain size fraction for the basal avalanche (3.25 phi). Only tests utilizing the coarser grain size fraction are described here due to the fact that segregation of the flow parts could be better visualized during these tests.

Test run A

Avalanche: 20 ml glass fragments, 80 ml water

Slope angle: 30°

Slope length (L): 80 cm

Substrate: 2 mm quartz sand

Obstacle: none

Name	time (s)	Froude number	Reynolds Number
run A	5.06	0.71	6384
run A	5.26	0.67	7016
run A	5.46	0.63	7980
run A	5.63	0.63	8051
run A	5.73	0.60	8780
run A	6.00	0.58	9585

Similar to the aqueous glycerol experiments, flow propagation of a confined particulate current was studied during the first test run, utilizing a slope angle of 30° and a run-out length of 80 cm. A glass-water mixture of 100 ml was rapidly introduced into the water tank, after collapse of the mixture, a distinct density current formed with an extensive head compared to the body and tail of the current (Figure 5.9). The flow head was non-uniform and highly turbulent due to mixing with the ambient fluid. Further propagation along the slope just resulted in sedimentation from the base of the flow head, while the upper parts were still fully turbulent without signs of stratification.

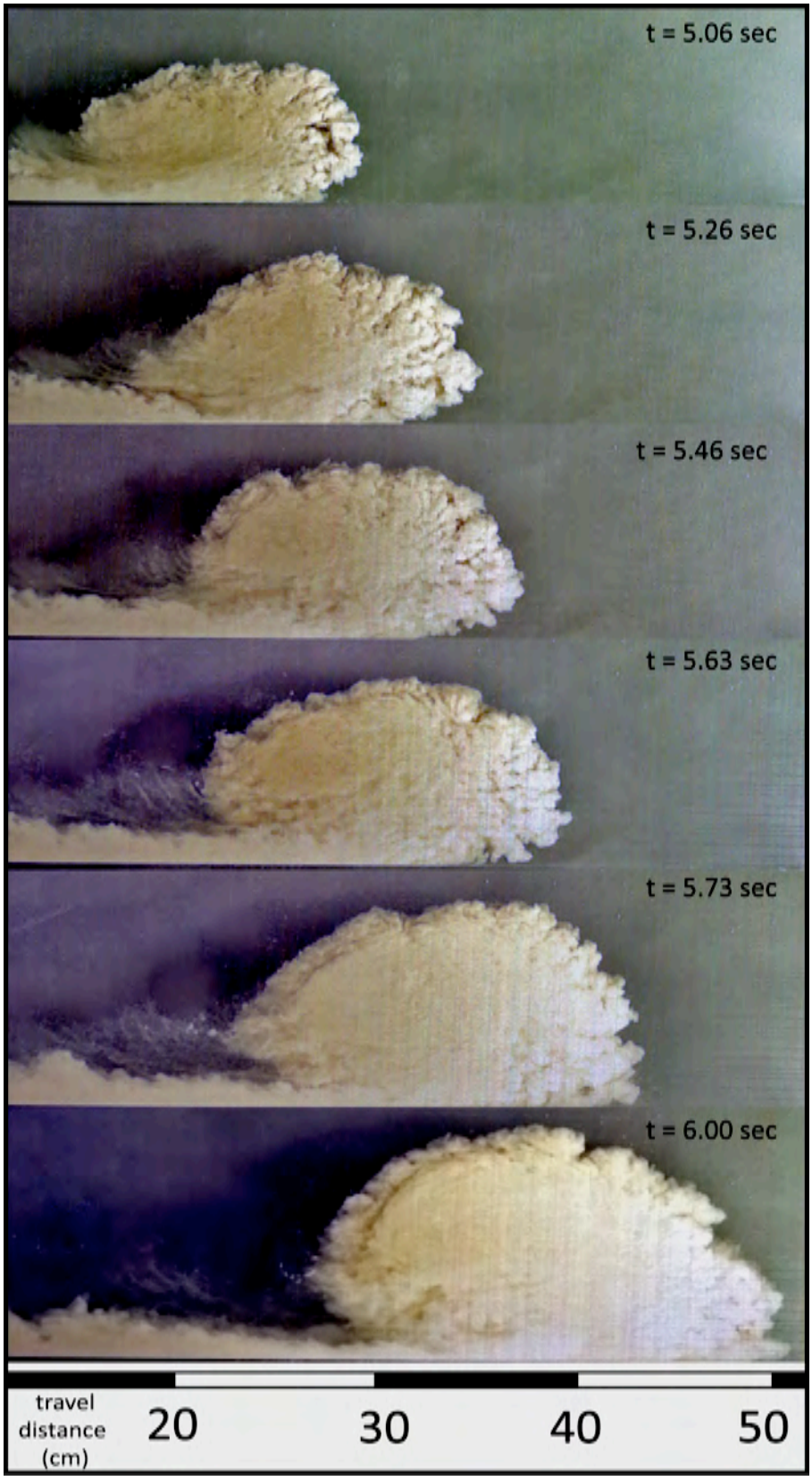

Figure 5.9: Video snapshots of test run A. A particulate density currents is developing rapidly after opening of the lock-exchange box.

Test run B

Avalanche: 20 ml glass fragments, 80 ml water

Slope angle: 30°

Slope length (L): 80 cm

Substrate: 2 mm quartz sand

Obstacle: cubic, 25 cm from source

Name	time (s)	Froude number	Reynolds Number
run B	6.83	1.10	4601
run B	7.00	0.89	6901
run B	7.10	0.80	8627
run B	7.16	0.80	8627
run B	7.26	0.69	11502
run B	7.33	0.70	11272
run B	7.40	0.65	13227
run B	7.63	0.65	13227
run B	7.73	0.65	13227
run B	8.23	0.60	15528

The same glass-water mixture was rapidly introduced into the water tank, encountering a cube-shaped obstacle at 25 cm from the source (Figure 5.10). Before the particulate current came in contact with the barrier, the flow depth was more than twice the height of the obstacle. Sedimentation of the coarse glass fragments (brown colour) could be observed to be concentrated at the bottom of the flow head, increasing directly upstream of the obstacle. Due to the extensive flow height relative to the obstacle, the upper 2/3 of the flow moved over the barrier, with the flow head being still fully turbulent. Stratification occured within the flow after the flow head passed the barrier, the body and tail of the flow were already stratified due to sedimentation of coarser particles at the bottom of the flow. After the head passed the obstacle, rapid sedimentation of glass particles started directly downstream of the obstacle, hence propagating flow exhibited flow stratification as well.

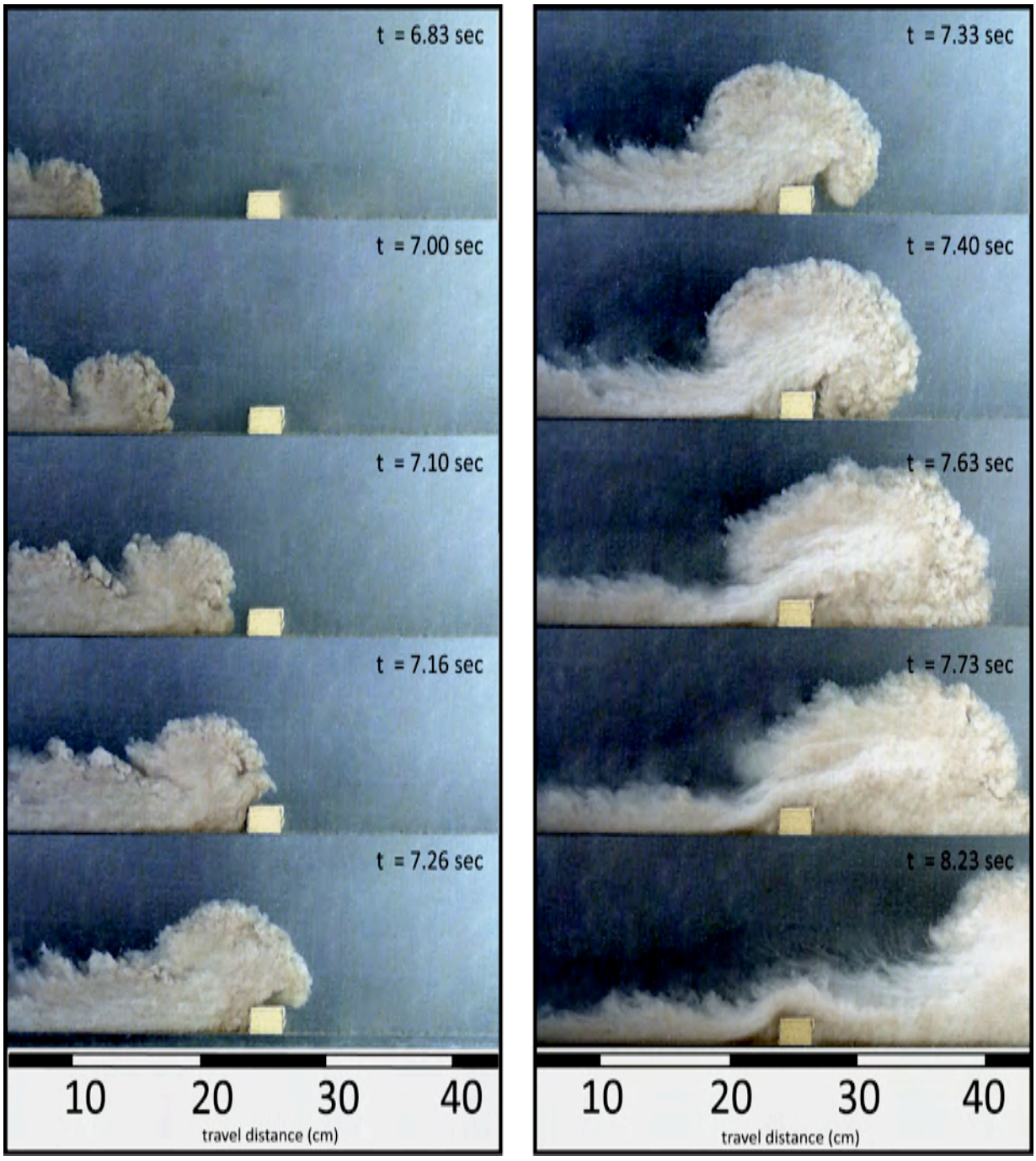

Figure 5.10: Video snapshots of test run B. A particulate density current is encountering an obstacle at 25 cm from the source.

Test run C

Avalanche: 20 ml glass fragments, 80 ml water

Slope angle: 30°

Slope length (L): 80 cm

Substrate: 2 mm quartz sand

Obstacle: cubic, 50 cm from source

Name	time (s)	Froude number	Reynolds Number
run C	7.83	1.12	8013
run C	7.93	1.02	9630
run C	8.06	1.03	9559
run C	8.13	1.00	10051
run C	8.26	0.92	11949
run C	8.36	0.91	12230
run C	8.53	0.90	12512
run C	8.66	0.83	14480

When the same obstacle as in test run B was placed at 50 cm from the source (Figure 5.11), gravitational segregation was more pronounced within the propagating current, but in contrast to glycerol solutions, individual flow levels could not properly be distinguished. At the bottom of the flow head, a basal layer started to form before the current encounters the obstacle, and sedimentation from the base of the current occurred during flow propagation. Flow stratification was significantly enhanced due to the contact with the barrier, stratification seemed to develop from the contact zone between head and body backwards, while the flow head was still turbulent. Wedge-shaped glass deposits developed up-and downstream of the obstacle: despite significant sedimentation upstream of the obstacle, a large percentage of coarse glass fragments was transported over the obstacle and sedimented further down the slope.

Figure 5.11: Video snapshots of test run C. A particulate density current is exhibiting flow stratification which will become more pronounced after encountering a topographic barrier.

Test run D

Avalanche: 20 ml glass fragments, 80 ml water

Slope angle: 30°

Slope length (L): 80 cm

Substrate: 2 mm quartz sand

Obstacle: rectangular, 25 cm from source

Name	time (s)	Froude number	Reynolds Number
run D	6.56	1.02	7860
run D	6.70	0.91	9825
run D	6.76	0.81	12445
run D	6.86	0.79	13100
run D	6.93	0.79	13100
run D	7.00	0.75	14409
run D	7.13	0.75	14409
run D	7.23	0.74	15064

A rectangular obstacle was placed at 25 cm from the source (Figure 5.12). Similar flow behaviour to test run B with the cube-shaped obstacle could be observed, with flow stratification being strongly influenced and usually initiated by the encounter of the flow with the obstacle.

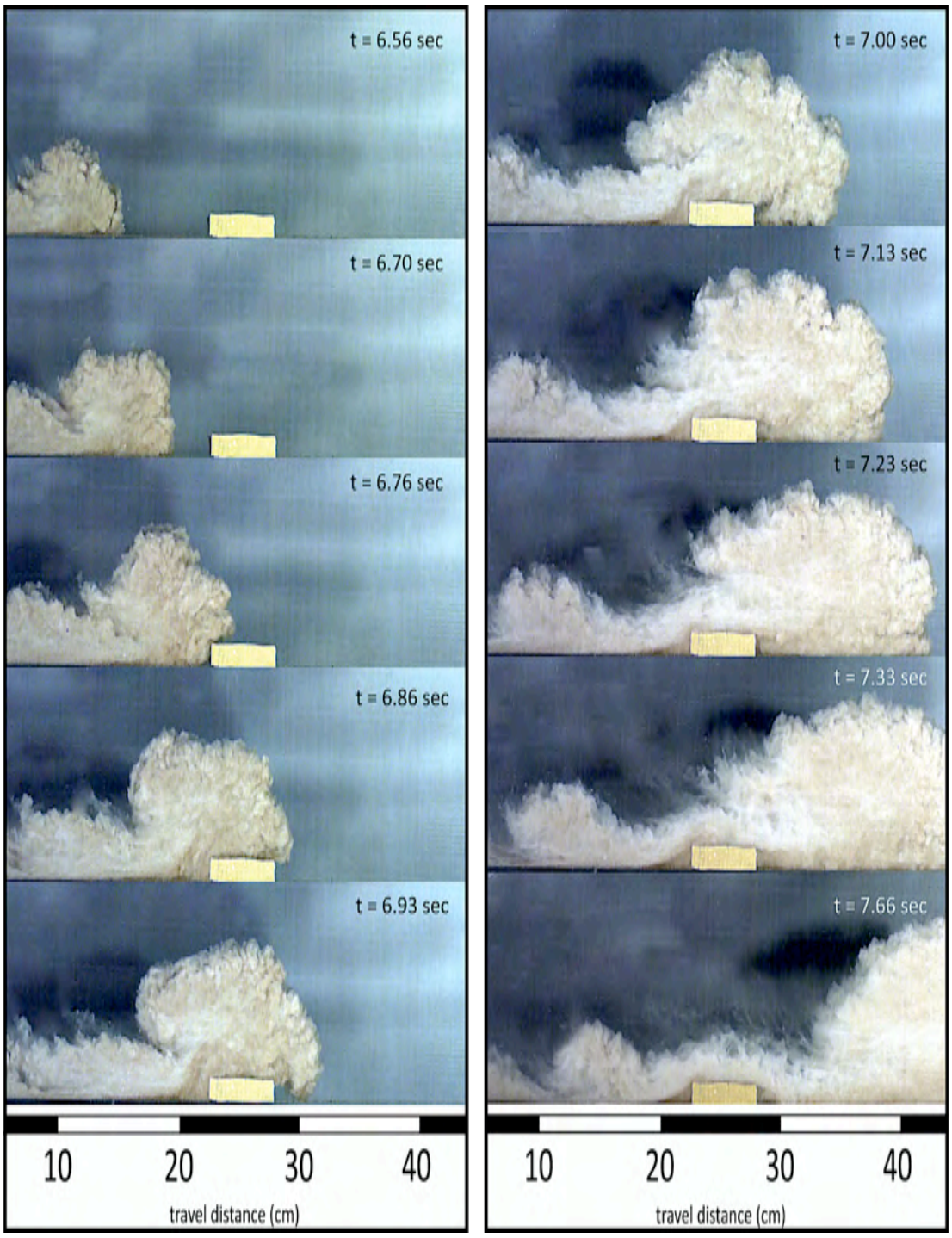

Figure 5.12: Video snapshots of test run D. A particulate current is encountering a rectangular obstacle at 25 cm from source.

Test run E

Avalanche: 20 ml glass fragments, 80 ml water

Slope angle: 30°

Slope length (L): 80 cm

Substrate: 2 mm quartz sand

Obstacle: rectangular, 45 cm from source

Name	time (s)	Froude number	Reynolds Number
run E	8.43	0.81	7061
run E	8.60	0.88	5975
run E	8.73	0.76	8147
run E	8.83	0.76	8147
run E	8.93	0.71	9234
run E	9.03	0.69	9777
run E	9.20	0.65	10863
run E	9.33	0.65	10863

A rectangular obstacle was placed at 45 cm from the source, with a greater height relative to the depth of the initial flow. The current started to show signs of sedimentation below the flow head, even before the encounter with the obstacle. Sedimentation increased significantly directly upstream of the obstacle when the flow jumped over it. Stratification increased during the propagation of the current, the flow collapsed directly downstream of the obstacle, reducing its velocity which resulted in rapid sedimentation of coarse glass fragments (Figure 5.13). Most of the sedimented particles seemed to be eroded and entrained into the moving flow. Downstream of the obstacle, sedimentation continued at the base of the body and head of the flow.

Figure 5.13: Video snapshots of test run E. A particulate current is encountering a large rectangular obstacle at 45 cm from source.

Test run F

Avalanche: 20 ml glass fragments, 80 ml water

Slope angle: 30°

Slope length (L): 80 cm

Substrate: 2 mm quartz sand

Obstacle: wedge-shaped, 25 cm from source

Name	time (s)	Froude number	Reynolds Number
run F	8.33	1.12	6978
run F	8.46	1.04	8051
run F	8.56	1.17	6441
run F	8.76	1.04	8051
run F	8.86	0.95	9662
run F	9.00	0.98	9125

A wedge-shaped obstacle was placed at 25 cm from the source, with a small height relative to the depth of the initial flow (figure 5.14). The current started to show signs of sedimentation below the flow head during its propagation over the obstacle, not before. Sedimentation increased significantly directly upstream of the obstacle when the flow jumped over it. In contrast to the other obstacles used, the jump of the flow over this ramp was longer, but resulted nonetheless in collapse and deceleration of the flow head and sedimentation of coarse particles from it. Stratification increased during the downstream propagation of the current, sedimentation continued at the base of the body and head of the flow.

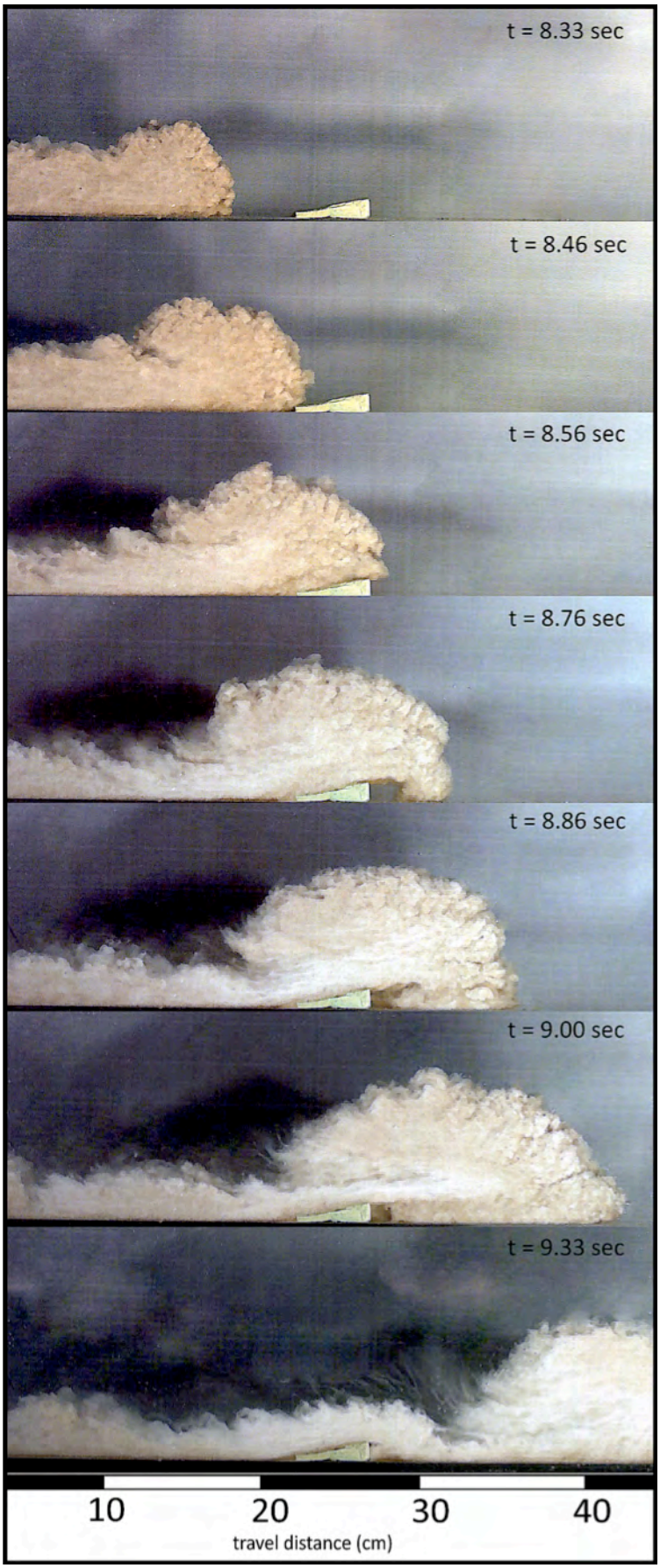

Figure 5.14: Video snapshots of test run F. A particulate density current is encountering a ramp-shaped obstacle.

Test run G

Avalanche: 20 ml glass fragments, 80 ml water

Slope angle: 30°

Slope length (L): 80 cm

Substrate: 2 mm quartz sand

Obstacle: rectangular, 45 cm from source

Name	time (s)	Froude number	Reynolds Number
run G	8.13	0.95	5591
run G	8.26	0.87	6710
run G	8.46	0.78	8387
run G	8.56	0.81	7828
run G	8.70	0.75	8946
run G	8.83	0.67	11183
run G	9.16	0.55	16774
run G	9.30	0.57	15656
run G	9.46	0.57	15656

A rectangular obstacle was placed at 45 cm from the source, with a nearly the same height as the depth of the initial flow (Figure 5.15). Stratification did not seem to develop directly after initiation of the current; only shortly upstream of the obstacle, the base of the flow head as well as the flow body directly behind the head exhibited stratification. When the flow reached the obstacles, it is only slightly higher than the barrier; most of the dense basal part was blocked, leading to a large ramp-shaped deposit upstream of the obstacle. Stratification increased during the propagation of the current, the flow collapsed directly downstream of the obstacle, reducing its velocity and resulting in rapid sedimentation of coarse glass fragments. However, due to extreme inflation of the flow front when it climbed the obstacle, a large portion of the suspension cloud moved further downstream and rapid sedimentation from the collapsing flow head led to a small wedge-shaped deposit downstream of the obstacle.

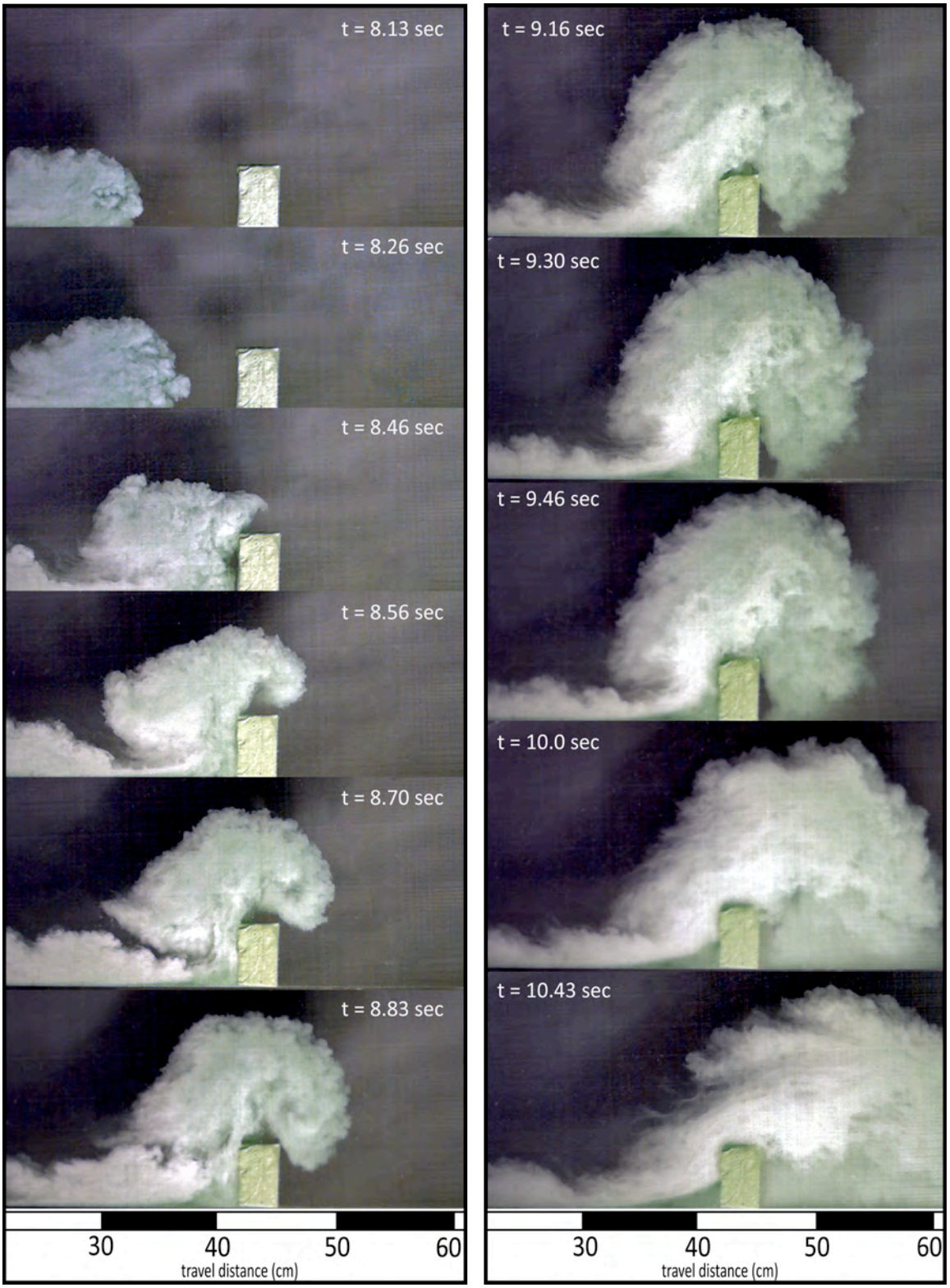

Figure 5.15: Video snapshots of test run G. A particulate density current is encountering an obstacle nearly the same height as the flow head before contact.

5.9. Comments

Vertical stratification of density and/or viscosity is a common if not ubiquitous feature of (particulate) density currents, and a prerequisite for the initiation of decoupling in these currents (see Chapter 2). Accordingly, analogue stratified density currents were used to investigate the effects of stratification on flow behaviour and possible decoupling, especially with regard to topographic influence. All currents were initiated by rapid vertical withdrawal of the lock-exchange gate, allowing the initial relatively well-mixed suspension or solution to collapse and flow across the slope. Each experimental run was recorded, and measurements of the position of the flow front and the flow height as a function of time were extracted from slow-motion replays (Appendix A-4).

The highly variable nature of the material used for the experiments led to several observations, which are contrasting in their implications for natural pyroclastic density currents.

Aqueous glycerol currents start as nearly homogeneous solutions; stratification occurs only as the result of local dilution due to increased mixing with the ambient fluid at the upper surfaces as the upper surface area increases with flow. No increase of concentration is possible in these flows, because deposition cannot occur in a solution. Thus the density of part of a solution current can never increase, a fundamental contrast with a particulate current such as a pyroclastic density current. Soon after flow initiation, these solution currents develop a distinct head and tail structure. Stratification starts shortly after flow initiation and increases with increasing travel distance; segregation of different flow layers occurs along the whole length of the flow, independently of topographic influence. Different types of flow stratification can occur, depending on the concentration of the current. Relatively low-concentration and fully turbulent gravity currents display broadly continuous concentration profiles, with a gradual upward decrease, and gradual deceleration due to increased mixing with the ambient fluid. Visual observations of higher-concentration currents confirm a two-layer structure – a high-concentration layer overlain by a more dilute, turbulent layer (e.g. Hampton, 1972; Middleton, 1993; Mohrig et al., 1998; Hallworth and Huppert, 1998; Marr et al., 2001). Flow

dynamics change with increasing concentrations; currents with slightly higher concentrations travel faster, due to their higher excess density, but deceleration occurs also gradually. However with significantly increased flow concentration, the high-density (and, with glycerol, higher-viscosity) layer will undergo an abrupt deceleration; the slow-moving front is overtaken by the less dense upper flow layer. Similar flow behaviour has been suggested for decoupling in pyroclastic density currents without any major topographic influence (Fisher, 1995).

During the encounter with an obstacle, aqueous glycerol currents will experience a hydraulic jump, typically leading to increased mixing and entrainment of ambient fluid, and a decrease in velocity. After the collapse of the flow head downstream of the obstacle, a distinct flow structure with head and tail develops again. However, the newly formed current is mostly uniform and lower in density than that before the obstacle. If density stratification does occur downstream of the obstacle it does so more slowly than upstream, presumably because the overall concentration is less. Solute density currents show maximum density during flow initiation, and dilution of the currents is a function of the distance travelled. During or after the encounter with an obstruction in the flow path, no secondary layer of higher density can segregate from the dilute mixture, a flow behaviour which has been described from pyroclastic density currents at Soufriere Hills Volcano (Druitt et al., 2002).

The glass particulate currents used in the experiments show different flow behaviour. They start as highly turbulent, relatively uniform concentration surges (because they are artificially mixed in the chamber immediately prior to release) from which secondary basal flows develop. Sedimentation from these experimental currents is the main mechanism acting on flow dynamics, and development of stratification is strongly dependent on settling velocities of the particles and the slope angle. Reynolds numbers (> 4000) show that the flow head of the currents is highly turbulent, and visual observations indicate a fairly uniform distribution of particles in the flow head. Distinct stratification of the currents, as has been observed in aqueous glycerol currents, was not observed, although rapid sedimentation of coarser particles (Rouse numbers > 2.5) led to the formation of a relatively thin basal underflow below the body of the current (see Test run E). Much

of the mass of the flow is typically concentrated in the flow head, its highly turbulent nature keeping most particles suspended during flow propagation.

Encounter with an obstacle leads to blocking of the lowermost flow layer and rapid deposition of coarse particles directly upstream of the obstacle; however, a large fraction of coarse particles is still suspended in the highly turbulent flow head. After passing the obstacle, the flow head collapses, leading to rapid sedimentation of coarser particles from the flow front and the formation again of a thin basal underflow. Similar flow behaviour has been described from pyroclastic density currents at Soufriere Hills Volcano (Druitt et al., 2002).

Caution is clearly warranted in comparing these experimental results with natural flows, since not all aspects of natural flows can be represented in laboratory experiments. However, proper scaling in terms of size and density as well as the fact that both the experimental flows and natural flows are suspensions of solid materials supported by an interstitial fluid (water, air, or gas) and will segregate into a dense basal zone and a dilute upper region, is often used to justify a cautious comparison of the experimental data with natural pyroclastic density currents. Further consideration, however, suggests that the degree of caution justified may be very high.

Aqueous glycerol currents experienced flow stratification and decoupling during the experimental tests; results show that flow dynamics are significantly influenced by irregular topography, depending on the height of the obstacle relative to the flow depth and the distance from the source. However, these solute density currents cannot simulate important processes acting in natural pyroclastic density currents, such as rapid sedimentation or elutriation of fine particles. One very obvious difference between the two types of flow seen in the present experiments is the very energetic mixing in the head of the particulate flows; presumably this is the result of the particulate nature of the flow, that allows water to easily enter the suspension between the particles. By contrast, with the solute flow, mixing between the two fluids occurs by diffusion and small-scale turbulence, quite different processes, and at a quite different rate in spite of the relatively similar flow velocities.

Glass particulate currents resemble natural pyroclastic density currents due to the use of material varying in grain size and settling velocities. However, flow stratification or decoupling could not be clearly observed during the experiments. This may be due to the sensitivity of the particulate flow apparent shade to local lighting; for example, Fig. 5.10 suggests that the apparent colour of the flow depends on whether the flow area observed is adjacent to the flume wall or slightly separated from it. Again, the reflectivity of the particulate flow appears to be a weaker function of density than that of the solute flow; stratification may well have been present, but not easily detectable optically.

In summary, these experiments illustrate the inherent difficulties of small-scale analogue modeling. Even with reasonable matching of the scaling parameters, the nature of the materials means that some aspects inferred in field-scale flows (and which should therefore be apparent in the experiments) may indeed be present but not easily detected. For example, detecting stratification in a glass particulate flow in water at small scale requires small and sensitive real-time densitometers – a challenging prospect. The use of solute currents to represent particulate flows is evidently questionable, because the independent motion of water and solids is fundamental to the dynamics of the latter, and by definition absent from the former.

Chapter 6

Conclusions and recommendations

"If we knew what we were doing it wouldn't be research."

Albert Einstein

Chapter 6: Conclusions and Recommendations

6.1. Introduction

Volcanic eruptions are accompanied by a wide range of hazards, such as pyroclastic density currents, lava flows and ash fall, which are generally only locally destructive, compared with floods or earthquakes. Nonetheless, volcanic hazards can be powerful enough to change human history, as has been observed from Vesuvius in AD 79 or the eruption of Mount Pelée in 1902, where nearly 30000 people died, after pyroclastic density currents hit the township of St.Pierre and devastated it completely (Scarth, 2002). Typically, different volcanic hazards can affect distinct sectors around a volcano at varying distances (Marti and Ernst, 2005). In addition, these hazards are typically characterized by different frequencies of occurrence and varying severity for the surrounding communities.

History (e.g. Unzen Volcano, Merapi Volcano) shows that any eruption at a specific volcano may be similar to previous eruptions (Marti and Ernst, 2005). Therefore, gathering information about types, duration, recurrence, affected areas and other characteristics that have dominated the volcano's eruptive history is important hazard assessments and associated hazards zonation maps, as well as for long-term forecasts of potential future activity.

Pyroclastic density currents, such as block-and-ash flows, are among the most lethal hazards associated with volcanic eruptions, due to their extreme temperatures (up to 1000°C) and rapid travel velocities (> 300km/h). They generally affect vast areas around a volcano and cause extensive devastation. Block-and-ash flows, generated by the collapse of a lava dome, have been described at many volcanoes during the last century, e.g. at Unzen, Colima, Soufrière Hills Volcano and Lascar. Eruptive history of the individual volcanoes, may indicate the most likely travel routes for future block-and-ash flows, as they are highly influenced by topography. However, continuous pyroclastic eruptions and the emplacement of successive block-and-ash flows will dramatically alter the pre-existing landscape, hence drastically changing flow behaviour. These changes can often lead to the separation of ash cloud surges

from the block-and-ash flows, resulting in unexpected travel directions, extended run-out distances and greater hazard potential.

Decoupling in particulate density currents is a common occurrence, as described from turbidity currents, powder snow avalanches and pyroclastic density currents, but still not enough is known about the processes involved and their complex interactions. Processes that are possibly responsible for decoupling have been described by Fisher (1995), but these are only indirectly responsible by creating or enhancing vertical density differences within the advancing flows which will lead to stratification of the currents. Stratified density currents can exhibit separation of the individual flow parts, even without the influence of rough topography, as has been described at Ngauruhoe (Nairn and Self, 1978) and deduced from field observations at Tarawera. However, comprehensive review of several documented decoupling examples worldwide (e.g. Merapi, Unzen and Soufriére Hills Volcano; compare Chapter 2) confirms the importance of topographic control on flow dynamics, which can range from small breaks in slope to channeling, blocking and diverting of the basal avalanche, while the ash cloud surge moves unconstrained by topography. Comprehensive studies of the topography for an individual volcano where previously decoupling has been described are therefore necessary to identify possible future decoupling locations around the volcano.

6.2. Decoupling at Tarawera Volcano

Detailed field studies at Tarawera Volcano, New Zealand, have led to comprehensive descriptions of block-and-ash flow deposits emplaced near the end of the Kaharoa eruptive episode in AD 1314±12. Block-and-ash flows were distributed to the south, north and east of the volcano; mapping of the widespread deposits showed extensive influence of the topography (compare Chapter 3) and inferred possible decoupling of the block-and-ash flows.

Distribution of block-and-ash flow and associated ash cloud surge deposits to the east of Wahanga Dome and to the south of Ruawahia Dome have revealed possible detachment of several ash cloud surges as well as the generation of surge-derived pyroclastic flows to the northeast of the volcano (compare sample descriptions and locations in Appendix A-2).

To the south of Ruawahia Dome, apart from slight proximal channelling (between Ridge Dome and Rerewhakaaitu tuff cone) and a break in slope at the margin of the

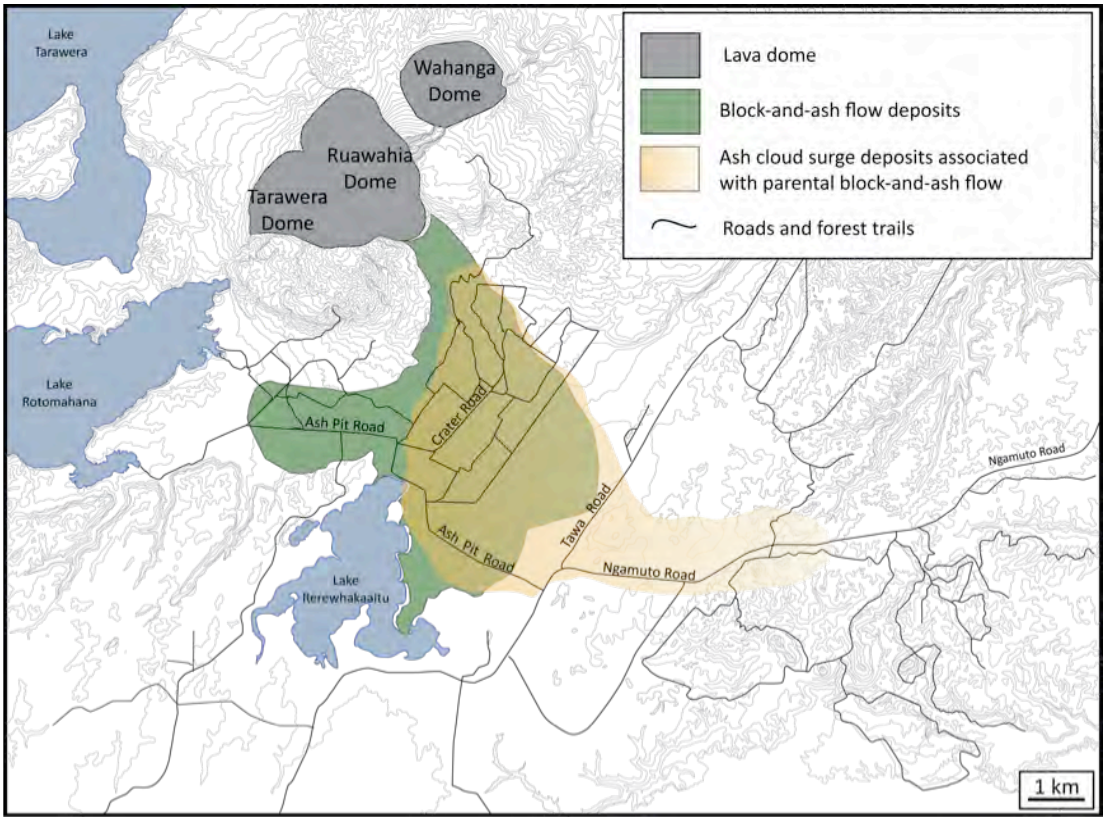

Figure 6.1: Distribution of block-and-ash flow deposits from Ruawahia Dome and the extent of detached ash cloud surges travelling beyond the limit of the block-and-ash flows (modified after Nairn et al., 2001).

dome (Figure 6.1), the block-and-ash flows did not encounter major topographic restrictions or barriers in their path. Lateral spreading from medial to distal parts controlled the travel distance of the flows. The extents of the block-and-ash flow fan range between 4 to > 7 km for the coarse-grained main body and c. 2 km beyond that for ash cloud surge deposits. Gently sloping flanks to the south of the volcano most likely led to the rapid deceleration of the ground-hugging, granular avalanche due to lateral spreading, while the more dilute upper parts maintained their velocities and overcame the basal avalanche, resulting in decoupling and the

emplacement of ash cloud surge deposits beyond the limits of block-and-ash flow deposits.

At Crater Road, c. 4 km from Ruawahia Dome, a fine-grained ash layer underlies block-and-ash flow deposits, possibly representing detached ash cloud surge deposits from earlier block-and-ash flows with shorter run-outs (compare Chapter 4). It was assumed that during the growth of Ruawahia Dome multiple block-and-ash flows were generated, so progressive aggradation probably led to amalgamation of individual flow units, making it difficult to distinguish them in the field. Remnants of possible detached ash cloud surges have been found at Crater Road as well as Ash Pit Road, directly underlying massive block-and-ash flow deposits. It was also suggested that, similar to Soufriére Hills Volcano, rapid sedimentation of pyroclasts from the decoupled surge formed a surge-derived pyroclastic flow, prolonging the run-out by up to 2 km.

In contrast to the southern flows, the northeastern and eastern block-and-ash flows from Wahanga Dome were influenced by highly irregular topography and several breaks in slope. The northeastern and eastern flanks of the volcano are governed by nearly radial Waikakareao lava plateaus, which create a first pronounced break in the slope. Block-and-ash flows to the east were then travelling nearly unconfined over the Hawea lava plateau, before they were channelled into the Waiwhakapa River valley, reaching travel distances of > 9 km. Ash cloud surge deposits were found further to the east, up to 4 km beyond the limits of the block-and-ash flow deposits (Figure 6.2).

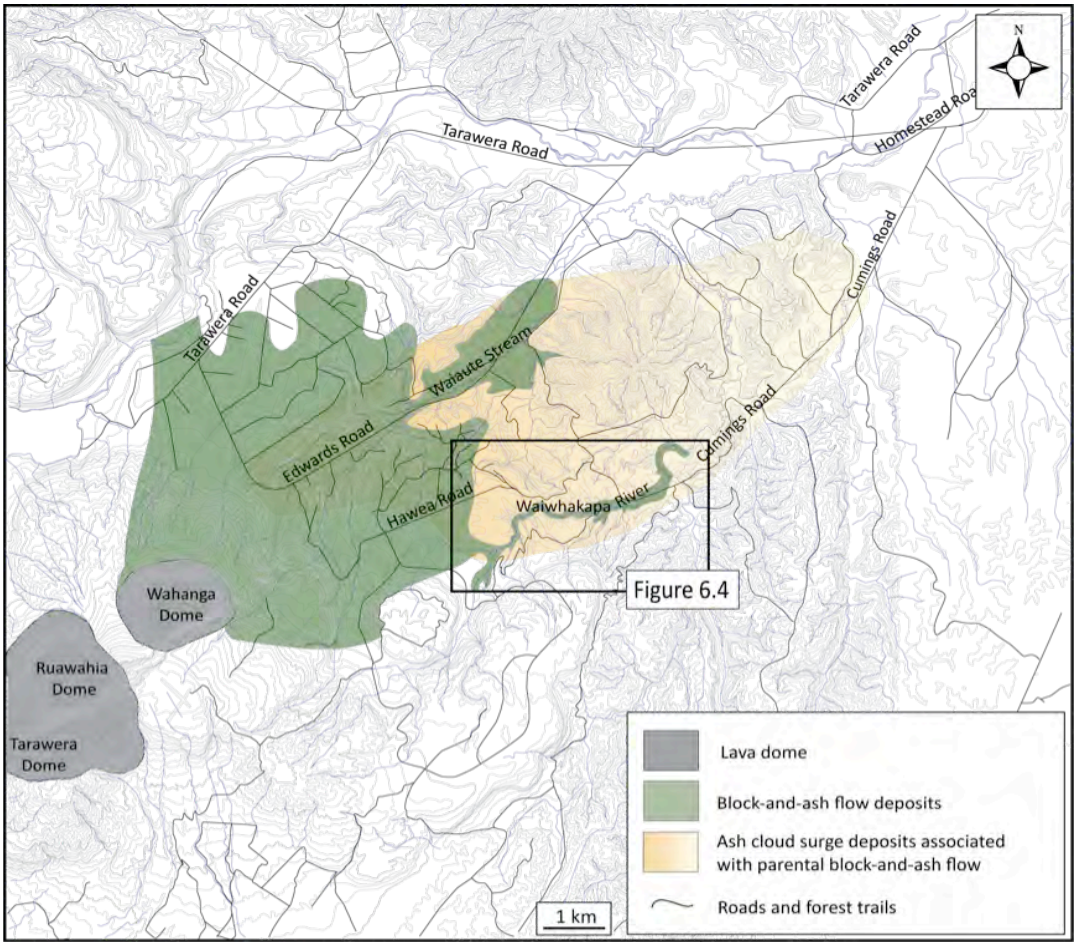

Figure 6.2: Distribution of block-and-ash flows and detached ash cloud surges generated from collapse of Wahanga Dome (modified after Nairn et al., 2001).

The valley of Waiwhakapa River along Cumings Road is characterized by small cross-sections and tight meandering of the channel, comparable to Volcán Tungurahua in Equador (Stinton and Sheridan, 2008), where the narrowing of deeply incised channels led to overspilling and decoupling. Field observations have indicated not only that the ash cloud surge detached from the channelled block-and-ash flow along Waiwhakapa River valley, but that from the detached cloud a second basal underflow ("surge-derived pyroclastoc flow") developed, prolonging the runout of the ash cloud surge by c. 1-2 km.

Finer-grained, thin deposits, resembling block-and-ash flow deposits, along Cumings Road suggest the rapid sedimentation of lapilli-sized material from the surge (Figure 6.3), similar to Soufriére Hills Volcano (Cole et al., 2002). Along this river valley, several locations for possible decoupling can be identified, based on sharp bends in the channel course, where damming of the basal avalanche can be inferred, leading

to overspilling and detachment of parts of the surge. Constriction of the river channel often corresponds with changes in the channel gradient; several drops of the riverbed are documented, ranging between 15-40 m in height (Figure 6.4).

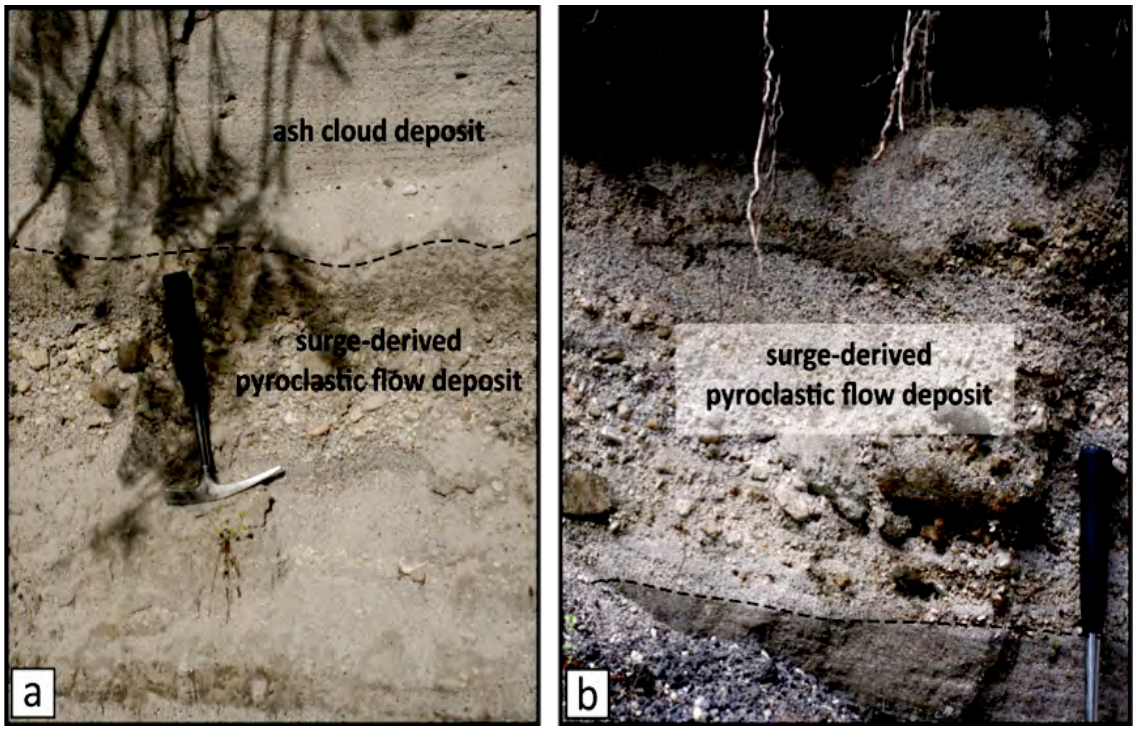

Figure 6.3: Possible surge-derived pyroclastic flow deposits along Cumings Road (V16/288305), found beyond the extent of the main block-and-ash flow fan.

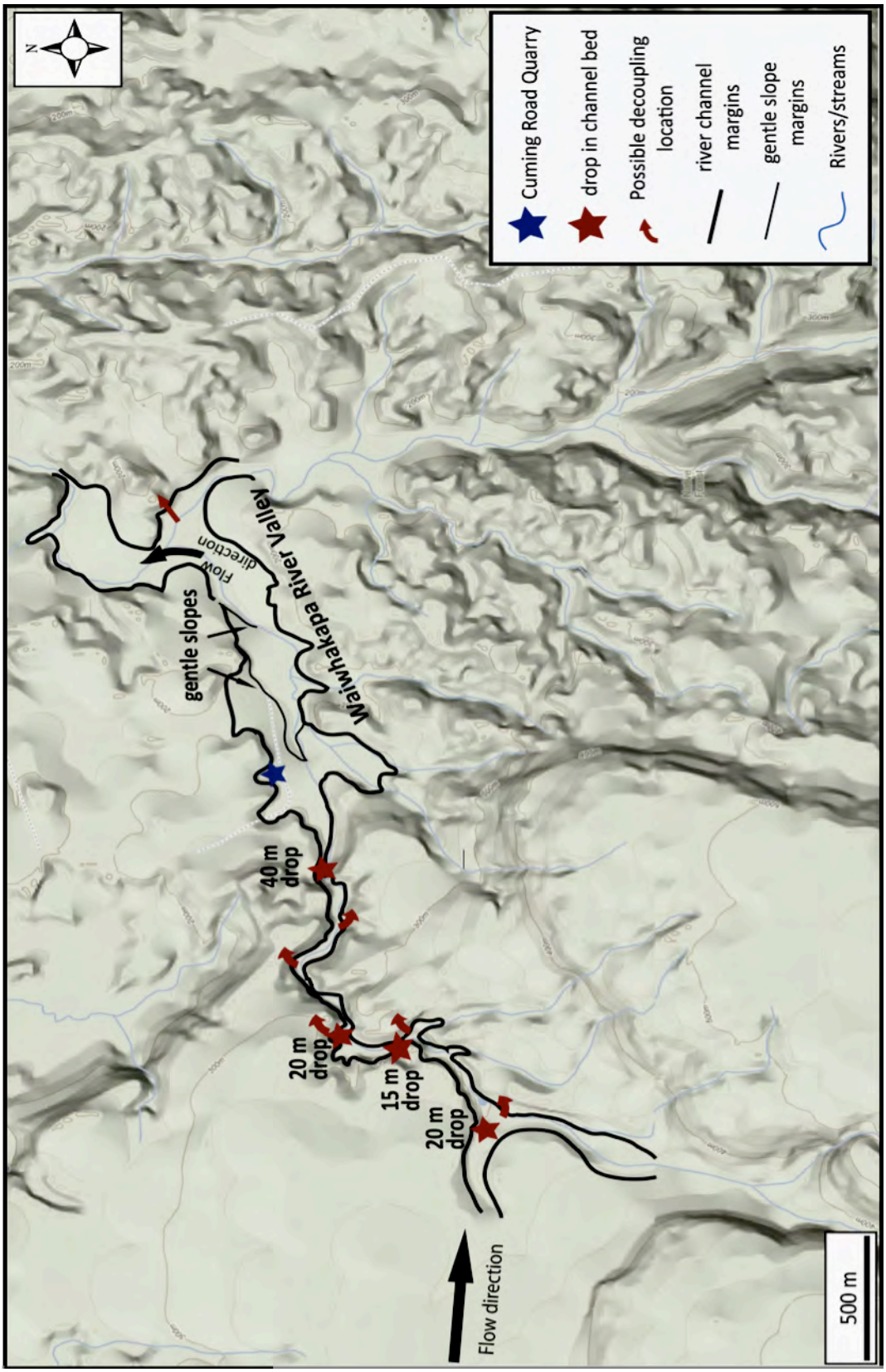

Figure 6.4: Detailed map of Waiwhakapa River Valley in the eastern block-and-ash flow fan with possible location where ash cloud surges could have detached from channelled basal avalanches.

Block-and-ash flows from Wahanga Dome encountered several steep breaks in slope, the increase in turbulence caused by the steeper slope enhanced mixing with ambient air, generating voluminous particle-rich ash-cloud surges, as has been suggested at Merapi Volcano (Kelfoun et al., 2000). The ash cloud surge detached from the basal avalanche and rushed unconfined ahead, whereas the basal avalanche followed topographic irregularities. To the northeast, the Waikakareao lava plateau governing Wahanga Dome, gradually grades into Lower Pokuhu lava plateau, and to the east into Hawea lava plateau. The Waiaute Stream Valley, located between these two plateaus (Figure 6.5), represents further topographic influence on the dynamics and distribution of the eastwards directed block-and-ash flows. The flows were channelled within the stream valley, leaving deposits up to 30 m thick, especially where the valley narrowed quickly from c. 600 m to < 150 m width, before widening again. Channelling of the basal avalanche and the decrease in channel width led to prolonged run-out distances (> 8 km) and probably to the detachment of the ash cloud surge from the rest of the flow.

Similar to Waiwhakapa River valley, the Waiaute Stream valley shows several pronounced gradient changes, ranging between 20-30 m in height. However, these gradient changes are possibly the result of fluvial erosion during the dam-break flood at the end of the Kaharoa eruptive episode (Hodgson and Nairn, 2005), after the emplacement of the block-and-ash flow deposits. A powerful and highly erosive flood occurred along the Tarawera and the Waiaute tributary valley, leading to erosional landforms and flood deposits on the Pokuhu lava plateau and along Edwards Road.

Therefore, decoupling within the northeastern flows is probably the result of major breaks in slope early in flow development and decreasing river channel width than meandering of channels and changes in channel gradient which has been observed along Cumings Road. Decoupling probably also occurred at the distal limits of the block-and-ash flow deposits along Edwards Road, where the basal avalanche came to rest and the ash cloud surge travelled ahead. Due to limited exposure beyond the margins of the block-and-ash flows along Edwards Road, decoupling can only be assumed along this valley, but not confirmed.

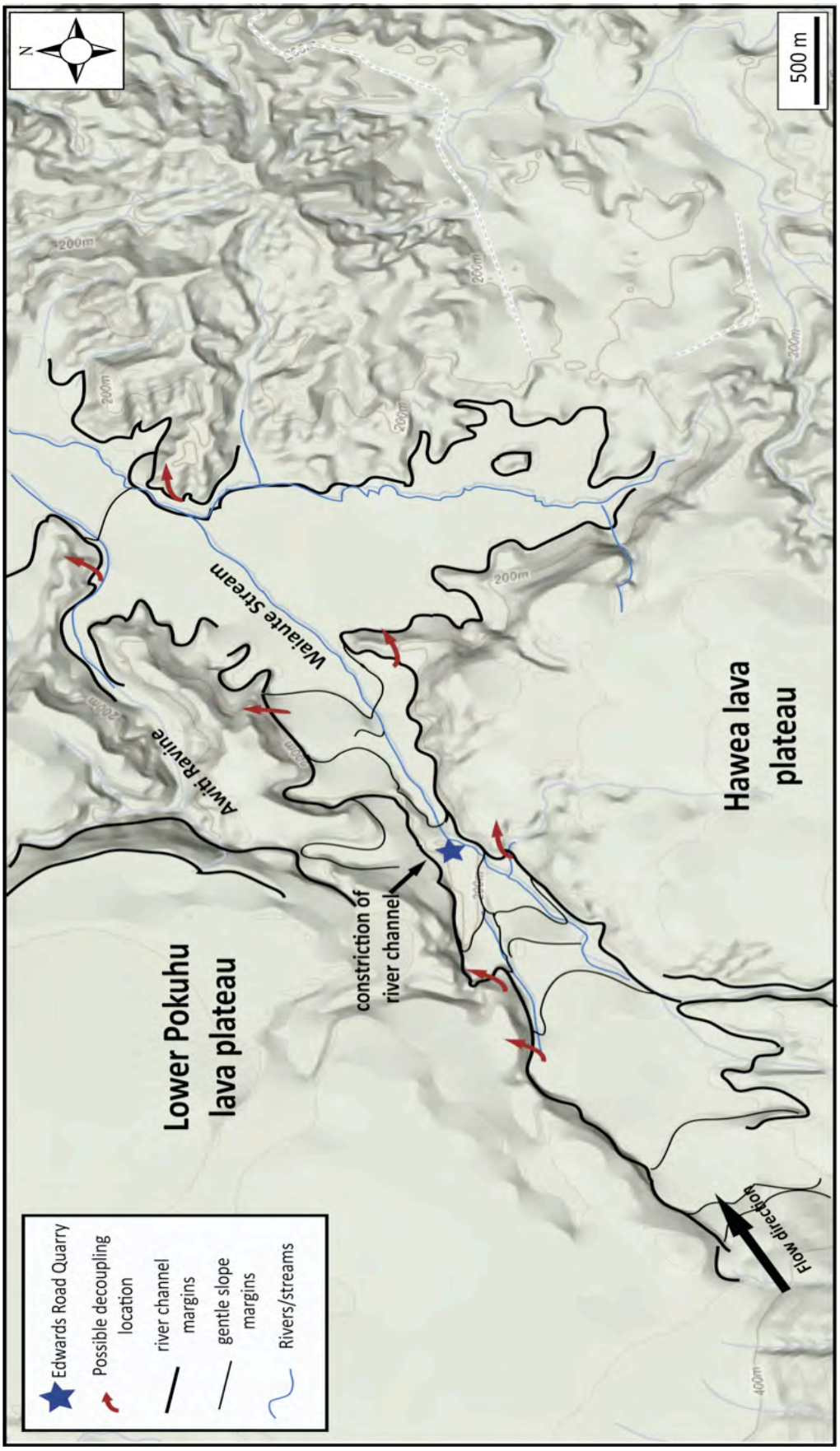

Figure 6.5: Detailed map of Awiti Ravine along Waiaute Stream in the eastern block-and-ash flow fan with possible location where ash cloud surges could have detached from channelled basal avalanches.

6.3. Conclusions

Topographic control on decoupling processes in particulate density currents is widely recognized. It is important to study documentations of previous eruptions to establish possible travel directions of future pyroclastic density currents. Topographic irregularities have to be identified and their effect on flow dynamics carefully considered for each volcano individually, as has been documented for several case studies, e.g. Unzen Volcano, Merapi and Soufriére Hills Volcano.

The influence of topography on flow dynamics and stratification of (particulate) density currents has also been confirmed by small-scale laboratory experiments with aqeous glycerol and glass particle currents, however their results have to be regarded with caution, because of the limitations of small-scale analogue simulations. Blocking and deflecting of initially stratified currents can lead to separation of the flow parts and even to the formation of newly stratified currents after the encounter with the barrier. The shape and height of an obstacle seem not to be as relevant as its distance from the source and the depth of the flow during the encounter with the obstacle. Flow stratification can start shortly after the initiation of the currents even without topographic influence, so obstructions early in the flow path will possibly lead to spilling of most of the current over the barrier, but not to decoupling. However, a review of topographic influences shows that early channeling of the currents, followed by abrupt channel bends, usually separate the ground-hugging basal avalanche from the more dilute ash cloud surge in top; the basal avalanche will follow the course of the channel, whereas the surge can move uncontrolled over the landscape.

The identification of influential topographic features needs to be continually reassessed, because their relevance for the onset of decoupling will change during the duration of the eruptive episode. Dome eruptions commonly last a few years or longer, so block-and-ash flow hazards often become modified over time. As a lava dome increases in volume and height with time, the risk of larger-scale dome collapse increases, resulting in pyroclastic currents, which tend to travel larger distances. Successive block-and-ash flows will also change the pre-existing

topography drastically, altering the travel path and dynamics of new flows. In addition, block-and-ash flows have been observed showing detachment of the ash cloud surge from the underlying basal avalanche, resulting in unexpected travel directions, run-out distances and larger areas of devastation, e.g. Unzen Volcano (Ui et al., 1999). Risk assessment and evacuation plans have to be adjusted accordingly during an eruption, to ensure the safety of the surrounding communities.

Field observations around Tarawera volcano confirm the influence of pre-existing topography on flow dynamics of multiple block-and-ash flows generated near the end of the Kaharoa eruptive episode. Ash cloud surge deposits were found up to several km beyond the margins of the block-and-ash flow deposits, indicating not only decoupling, but also the generation of further, "secondary" weaker block-and-ash flows. Decoupling of pyroclastic currents from Tarawera Volcano has not been included in hazard scenarios for future eruptions from this volcano. And the recognition of surge-derived pyroclastic flows has important implications for volcanic hazards assessments at Tarawera Volcano. The ability of pyroclastic surges to generate highly mobile, high-concentration pyroclastic flows poses an important, but so far probably underestimated, threat around lava domes. A particularly important feature of these flows is their ability to develop in drainages different from those affected by the main block-and-ash flows and associated pyroclastic surges. They therefore have the potential to impact upon areas not previously anticipated in hazard analyses.

6.4. Recommendations (for future work)

After careful consideration of the findings from this project, some tentative recommendations are made for further research:

- The results obtained from analogue experiments should be verified for larger volume experiment; possibly under unconfined conditions to model sinuous channels of varying shape, width and depth and their influence on flow dynamics.
- Further analogue experiments could comprise modeling in air to include fragmentation and elutriation processes within the advancing flows. A

possible cooperation with Massey University to use a newly developed large-scale flume should be contemplated.

* Numerical modeling of decoupling processes could verify findings in the field and establish better hazard delineation maps. Two-layer models that incorporate individual flow parts and any interaction between them could lead to a better understanding of the rheologies of block-and-ash flows.
* Additional fieldwork at Tarawera Volcano should include excavation of further parts of the block-and-ash flow deposits to expose, if possible, the contact between individual flow units or to previously emplaced Kaharoa Tephra layers. Ground penetrating radar would be useful to show deposit architecture and identify relationships between individual block-and-ash flow deposits.

References

A-Z

Abdurachman, E.K., Bourdier, J. and Voight, B. (2000). Nuées ardentes of 22 November 1994 at Merapi volcano, Java, Indonesia. *Journal of Volcanology and Geothermal Research* 100: 345-361.

Abich, H. (1882). Geologische Forschungen in den Kaukasischen Ländern (Geologie des Armenischen Hochlandes). Wien, Alfred Holde 2, 478 p.

Alexander, J. and Morris, S.A. (1994). Observations on experimental non-channelized turbidites: thickness variations around obstacles. *Journal of Sedimentary Petrology* 64: 899-909.

Allen, J.R. (1985). Principles of Physical Sedimentology. George Allen & Unwin, London: 272 pp.

Allen, S.R. and McPhie, J. (2003). Phenocryst fragments in rhyolitic lavas and lava domes. *Journal of Volcanology and Geothermal Research* 126: 263-283.

Amy, L.A, Hogg, A.J., Peakall, J. and Talling, P.J. (2005). Abrupt transitions in gravity currents. Journal of Geophysical Research 110: F03001, doi: 10.1029/2004JF000197.

Ancey, C. (2001). Snow avalanches. In Balmforth, N. and Provenzale, A. (eds) *Geomorphological Fluid Mechanics*. Lecture Notes in Physics 582 (Springer Verlag, Berlin): 319–338.

Anderson, T. and Flett, J.S. (1903). Report of the Soufriere in St. Vincent, in 1902, and on a visit to Montagne Pelée, in Martinique, Part 1. *Philosophical Transactions of the Royal Society, London* A200: 353-553.

Aramaki, S. (1957). The 1783 activity of Asama Volcano, Part II. *Japanese Journal of Geology and Geography* 28: 11-33.

Aramaki, S. and Ui, T. (1966). The Aira and Ata pyroclastic flows and related caldera depressions in southern Kyushu, Japan. *Bulletin Volcanologique* 29**:** 29-47.

Augé, A., Ousset, F., and Marco, O. (1995). "Effet d'une digue sur l'´ecoulement d'un aerosol". *Proceedings of Chamonix Symposium "The contribution of scientific research to safety with snow, ice and avalance":* 235-240.

Baas, J.H., McCaffrey, W.D., Haughton, P.D.W. and Choux, C. (2005). Coupling between suspended sediment distribution and turbulence structure in a laboratory turbidity current. *Journal of Geophysical Research* 110: C11015.

Baines, P.G. (1979). Observations of stratified flow over three-dimensional barriers. *Journal of Geophysical Research* 84: 7834-7838.

Baines, P.G. (1995). Topographic Effects in Stratified Flow. Cambridge University Press: 498 pp.

Barbolini, M., Biancardi, A., Cappabianca, F., Natale, L. and Pagliardi, M. (2005). Laboratory study of erosion processes in snow avalanches. *Cold Regions Science and Technology* 43: 1-9.

Bardintzeff, J.M. (1985). Les nuées ardentes: petrogenèse et volcanologie. Thèse d'Etat, Université Paris-Sud, Orsay.

Bareschino, P., T. Gravina, L. Lirer, A. Marzocchella, P. Petrosino, and P. Salatino (2007). Fluidization and de-aeration of pyroclastic mixtures: The influence of fines content, polydispersity and shear flow. *Journal of Volcanology and Geothermal Research* 164: 284-292.

Beghin, P. and Closet, J.-F. (1990). Effet d'une digue sur l'´ecoulemente l'avalanche poudreuse. *Note technique du Cemagref* 77, Grenoble.

Belousov, A.B. (1996). Pyroclastic deposits of March 30, 1956 directed blast at Bezymianny volcano. *Bulletin of Volcanology* 57: 649-662.

Boudon, G., Camus, G., Gourgand, A. and Lajoie, J. (1993). The 1984 nuée ardente deposits of Merapi Volcano, Central Java, Indonesia: stratigraphy, textural characteristics, and transport mechanisms. *Bulletin of Volcanology* 55: 327-342.

Bourdier, J.-L. and Abdurachman, E.K. (2001). Decoupling of small-volume pyroclastic flows and related hazards at Merapi volcano, Indonesia. *Bulletin of Volcanology* 63:309-325.

Branney, M.J. and Kokelaar, P. (1992). A reappraisal of ignimbrite emplacement: progressive aggradation and changes from particulate to non-particulate flow during emplacement of high-grade ignimbrite. *Bulletin of Volcanology* 54: 504-520.

Branney, M.J. and Kokelaar, P. (2002). Pyroclastic density currents and the sedimentation of ignimbrites. *Geological Society of London Memoirs 27:* 143 pp.

Brantley, S.R. and Waitt, R.B. (1988). Interrelations among pyroclastic surge, pyroclastic flow, and lahars in the Smith Creek valley during the first minutes of 18 May 1980 eruption of Mount St. Helens, USA. *Bulletin of Volcanology* 50: 304-326.

Bridge, J. and Demicco, R. (2008). Earth Surface Processes, Landforms and Sediment Deposits. Cambridge University Press: 815 pp.

Buckee, C., Kneller, B. and Peakall, J. (2001). Turbulence structure in steady, solute-driven gravity currents. In McCaffrey, W.D., Kneller, B.C. and Peakall, J. (eds.) Particulate Gravity Currents. *Special Publication of the International Association of Sedimentologists* 31: 173-187.

Buesch, D.C. (1992). Incorporation and redistribution of locally derived lithic fragments within a pyroclastic flow. *Geological Society of America Bulletin* 104: 1193-1207.

Bursik, M.I., and Woods, A.W. (1996). The dynamics and thermodynamics of large ash flows. *Bulletin of Volcanology* 58: 175-193.

Bursik, M., Patra, A., Pitman, E.B., Nichita, C., Macias, J.L., Saucedo, R. and Girina, O. (2005). Advances in studies of dense volcanic granular flows. *Reports on Progress in Physics* 68: 271-301.

Calder, E.S., Cole, P.D., Dade, W.B., Druitt, T.H., Hoblitt, R.P., Huppert, H.E., Ritchie, L., Sparks, R.S.J. and Young, S.R. (1999). Mobility of pyroclastic flows and surges at the Soufriere Hills volcano, Montserrat. *Geophysical Research Letters* 26: 537-540.

Calder, E.S., Sparks, R.S.J. and Gardeweg, M.C. (2000). Erosion, transport and segregation of pumice and lithic clasts in pyroclastic flows inferred from ignimbrite at Lascar Volcano, Chile. *Journal of Volcanology and Geothermal Research* 104: 201-235.

Capra, L. and Macias, J.L. (2000). Pleistocene cohesive debris flows at Nevado de Toluca Volcano, central Mexico. *Journal of Volcanology and Geothermal Research* 102: 149-168.

Capra, L., Macías, J.L., Scott, K.M., Abrams, M. and Garduño-Monroy, V.H. (2002). Debris avalanches and debris flows transformed from collapses in the Trans-Mexican Volcanic Belt, Mexico - behavior, and implications for hazard assessment. *Journal of Volcanology and Geothermal Research* 113(1-2): 81-110.

Carrasco-Núñez, G. (1999). Holocene block-and-ash flows from summit dome activity of Citlaltépetl volcano, Eastern Mexico. *Journal of Volcanology and Geothermal Research* 88: 47-66.

Cas, R.A.F. and Wright, J.V. (1988). Volcanic successions, modern and ancient: a geological approach to processes, products, and successions. *Allen and Unwin, London*: 528 pp.

Castro, I.P. and Snyder, W.H. (1993). Experiments in wave breaking in stratified flow over obstacles. *Journal of Fluid Mechanics* 255: 195-211.

Charbonnier, S.J. and Gertisser, R. (2008). Field observations and surface characteristics of pristine block-and-ash flow deposits from the 2006 eruption of Merapi Volcano, Java, Indonesia. *Journal of Volcanology and Geothermal Research* 177: 971-982.

Choux, C.M. and Druitt, T.H. (2002). Analogue study of particle segregation in pyroclastic density currents, with implications for the emplacement mechanisms of large ignimbrites. *Sedimentology* 49: 907-928.

Chun, S.S. and Chough, S.K. (1992). Depositional sequences from highconcentration turbidity currents, Cretaceous Uhangri Formation (SW Korea). *Sedimentary Geology* 77: 225-233.

Cioni, R., Marianelli, R., Santacroce, P. and Sbrana, A. (2000). Plinian and Subplinian eruptions. In: Sigurdsson, H., Houghton, B., McNutt, S.R., Rymer, H. and Stix, J. (eds) Encyclopedia of Volcanoes. Academic Press: 477-495.

Clark, J.D. and Pickering, K.T. (1996). Architectural Elements and Growth Patterns of Submarine Channels: Applications to Hydrocarbon Exploration. *AAPG Bulletin* 80: 194-221.

Clavero, J.E., Sparks, R.S.J., Pringle, M.S., Polanco, E. and Gardeweg, M.C. (2004). Evolution and volcanic hazards of Taapaca Volcano Complex, Central Andes of Northern Chile. *Journal of the Geological Society of London* 161: 603-618.

Cole, J.W. (1966). Tarawera Volcanic Complex. PhD thesis. Victoria University of Auckland, New Zealand.

Cole, J.W. (1970a). Structure and eruptive history of the Tarawera Volcanic Complex. *New Zealand Journal of Geology and Geophysics 13*: 879-902.

Cole, J.W. (1970b). Petrography of the rhyolite lavas of Tarawera Volcanic Complex. *New Zealand Journal of Geology and Geophysics* 13: 903-924.

Cole, J.W. (1970c). Petrology of the basic rocks of the Tarawera Volcanic Complex. *New Zealand Journal of Geology and Geophysics* 13: 925-936.

Cole, P.D., Guest, J.E. and Duncan, A.M. (1993). The emplacement of intermediate volume ignimbrites: a case study from Roccamonfina Volcano, southern Italy. *Bulletin of Volcanology* 55, 467-480.

Cole, P.D. and Scarpati, C. (1993). A facies interpretation of the eruption and emplacement mechanisms of the upper part of the Neapolitan Yellow Tuff, Campi-Flegrei, Southern Italy. *Bulletin of Volcanology* 55: 311-326.

Cole, P., Calder, E.S., Druitt, T.H., Hoblitt, R., Robertson, R., Sparks, R.S.J. and Young, S.R. (1998). Pyroclastic flows generated by gravitational instability of the

1996-97 lava dome of Soufriere Hills Volcano, Montserrat. *Geophysical Research Letters* 25(18): 3425-3428.

Cole, P.D., Calder, E.S., Sparks, R.S. J., Clarke, A.B., Druitt, T.H., Young, S.R., Herd, R.A., Harford, C.L. and Norton, G.E. (2002). Deposits from dome-collapse and fountain-collapse pyroclastic flows at Soufriére Hills Volcano, Montserrat. In Druitt, T.H and Kokelaar, B.P. (eds) The Eruption of Soufriére Hills Volcano, Montserrat, from 1995 to 1999. *Geological Society of London Memoirs* 21**:** 231-262.

Cole, J.W., Spinks, K.D., Deering, C.D., Nairn, I.A. and Leonard, G.S. (2009). Volcanic and structural evolution of the Okataina Volcanic Centre; dominantly silicic volcanism associated with the Taupo Rift, New Zealand. *Journal of Volcanology and Geothermal Research* 131: 241-264.

Crow, B.M. and Fisher, R.V. (1973). Sedimentary structures in base-surge deposits with special reference to cross-bedding, Ubehebe Craters, Death Valley, California. *Geological Society of America Bulletin* 84: 663-682.

Dade, W.B. and Huppert, H.E. (1996). Emplacement of the Taupo Ignimbrite by a dilute, turbulent flow. *Nature* 381: 509-512.

Dade, W.B. and Huppert, H.E. (1998). Long-runout rockfalls. *Geology* 26(9): 803-806.

Dakyn, J.R. and Greenly, E. (1905). On the probable Peléan origin of the felsitic slates of Snowdon. *Geological Magazine* 2: 541-549.

Darragh, M., Cole, J., Nairn, I. and Shane, P. (2006). Pyroclastic stratigraphy and eruptive dynamics of the 21.9 Okareka and 17.6 Rerewhakaaitu eruption episodes from Tarawera Volcano, Okataina Volcanic Centre, New Zealand. *New Zealand Journal of Geology and Geophysics* 49: 309-328.

Dartevelle, S., Rose, W.I., Stix, J., Kelfoun, K. and Vallance, J.W. (2004). Numerical modeling of geophysical granular flows: 2. Computer simulations of Plinian clouds and pyroclastic flows and surges. *G-cubed* 5(8): Q08004. doi:10.1029/2003GC000637.

Dellino, P., Frazzetta, G. and La Volpe, L. (1990). Wet surge deposits at La Fossa di Vulcano: depositional and eruptive mechanisms. *Journal of Volcanology and Geothermal Research* 43: 215-233.

Denlinger, R.P. (1987). A model for generation of ash clouds by pyroclastic flows, with application to the 1980 eruptions at Mount St. Helens, Washington. *Journal of Geophysical Research 92* (B10): 10 284-10 298.

Denlinger, R.P., Iverson, R.M. (2004). Granular avalanches across irregular three-dimensional terrain: 1, Theory and computation. *Journal of Geophysical Research* 109: F01014. doi:10.1029/ 2003JF000085.

Dobbins, W.E. (1944). Effects of turbulence on sedimentation. *Transactions of the American Society of Civil Engineers* 2218: 629-678.

Dobran, F., Neri, A. and Macedonio, G. (1993). Numerical simulation of collapsing volcanic columns. Journlal of Geophysical Research 98: 4231-4259.

Doyle, E.E., Hogg, A.J., Mader, H.M. and Sparks, R.S.J. (2010). A two-layer model for the evolution and propagation of dense and dilute regions of pyroclastic currents. *Journal of Volcanology and Geothermal Research* 190: 365-378.

Druitt, T.H. (1992). Emplacement of the 18 May 1980 lateral blast deposit ENE of Mount St. Helens, Washington. *Bulletin of Volcanology* 54: 554-572.

Druitt, T.H. (1998). Pyroclastic density currents. In: Gilbert, J. and Sparks, R.S.J. (eds) The Physics of Explosive Volcanic Eruptions. *Geological Society of London. Special Publication* 145: 145-182.

Druitt, T.H. and Sparks, R.S.J. (1982). A proximal ignimbrite breccia facies on Santorini volcano, Greece. *Journal of Volcanology and Geothermal Research* 13: 147-171.

Druitt, T.H., Calder, E.S., Cole, P.D., Hoblitt, R.P., Loughlin, S.C., Norton, G.E., Ritchie, L.J., Sparks, R.S.J. and Voight, B. (2002). Small-volume, highly mobile pyroclastic flows formed by rapid sedimentation from pyroclastic surges at Soufrière Hills Volcano, Montserrat: an important volcanic hazard. In: Druitt, T.H. and Kokelaar, B.P. (Eds.) The Eruption of Soufrière Hills Volcano, Montserrat, from 1995 to 1999. *Geological Society of London Memoirs* 21: 263-279.

Dufek, J. and Bergantz, M. (2007). The suspended-load and bed-load transport of particle-laden gravity currents: insight from pyroclastic flows that traverse water. *Theoretical and Computational Fluid Dynamics* 21: 119-145.

Dufresne, A. (2009). The influence of runout path material on rock and debris avalanches: field evidence and analogue modelling. *Unpublished Ph.D. thesis*. Canterbury University, Christchurch, New Zealand.

Edwards, D.A. (1993) Turbidity currents: dynamics, deposits and reversals. *Lecture Notes of Earth Sciences* 44: 1-174.

Ellison, T. H. and J. S. Turner (1959). Turbulent entrainment in stratified flows. *Journal of Fluid Mechanics* 6: 423– 448.

Engelund, F. (1974). Flow and bed topography in channel bends. *Journal of the Hydraulics Division, American Society of Civil Engineers* 100: 1631-1648.

Escher, B.G. (1933). On a classification of central eruptions according to gas pressure of the magma and viscosity of the lavas. *Leids.Geol.Meded., Decl. VI, Afl. I.*: 50-58.

Felix, M. (2001). A two-dimensional numerical model for a turbidity current. In McCaffrey, W.D., Kneller, B.C. and Peakall, J. (eds) Paniculate Gravity Currents*. International Association of Sedimentologists, Special Publications* 31: 71-82.

Fenner, C.N. (1923). The origin and mode of emplacement of the great tuff deposits in the Valley of Ten Thousand Smokes. Natl. Geog. Soc. Contributed Tech. Papers, Katmai Series 1:1-74.

Fenner, C.N. (1937). Tuffs and other volcanic deposits of Katmai and Yellowstone Park. Amer.Geophys.Un.Trans., 18th Annual Meeting: 236-289.

Fenner, C.N. (1948). Incandescent tuff flows in southern Peru. *Geological Society of America Bulletin* 59: 879-893.

Fisher, R.V. (1966). Mechanism of deposition from pyroclastic flows. *American Journal of Science* 264: 350-363.

Fisher, R.V. (1977). Erosion by volcanic base-surge density currents: U-shaped channels. *Geological Society of America Bulletin* 88: 1287-1297.

Fisher, R.V. (1979). Models for pyroclastic surges and pyroclastic flows. *Journal of Volcanology and Geothermal Research* 6: 305-318.

Fisher, R.V. (1983). Flow transformations in sediment gravity flows. *Geology* 11: 273-274.

Fisher, R.V. (1990). Transport and deposition of a pyroclastic surge across an area of high relief- the 18 May 1980 eruption of Mount St. Helens, Washington. *Geological Society of America Bulletin* 102: 1038-1054.

Fisher, R.V. (1995). Decoupling of pyroclastic currents: hazard assessments. *Journal of Volcanology and Geothermal Research* 66: 257-263.

Fisher, R.V. and Heiken, G. (1982). Mt. Pelee, Martinique - May 8 and 20, 1902, pyroclastic flows and surges. *Journal of Volcanology and Geothermal Research* 13: 339-371.

Fisher, R.V. and Schmincke, H.-U. (1984). Pyroclastic rocks. *Springer Verlag, Berlin, Heidelberg, New York, Tokyo*: 472 pp.

Fisher, R.V., Orsi, G., Ort, M. and Heiken, G. (1993). Mobility of a large volume pyroclastic flow – emplacement of the Campanian ignimbrite, Italy. *Journal of Volcanology and Geothermal Research* 56: 205-220.

Fouqué, F. (1873). San Jorge et ses eruptions. *Revue Scientifique de la France et de l'ettranger* 2(51): 1198-1201.

Francis, P. (1993). Volcanoes – a planetary perspective. *Oxford University Press*: 536 pp.

Francis P.W., Roobol, M.J., Walker, G.P.L., Cobbold, P.R. and Coward, M. (1974). The San Pedro and San Pablo volcanoes of northern Chile and their hot avalanches deposits. *Geologische Rundschau* 63 (1): 357-389.

Freundt, A. (1999). Formation of high-grade ignimbrites - Part II. A pyroclastic suspension current model with implications also for low-grade ignimbrites. *Bulletin of Volcanology* 60**:** 545-576.

Freundt, A. (2003). Entrance of hot pyroclastic flows into the sea: experimental observations*. Bulletin of Volcanology* 65: 144-164.

Freundt, A. and Bursik, M.I. (1998) Pyroclastic flow transport mechanisms. In: Freundt, A. and Rosi, M. (eds) From Magma to Tephra, Modelling Physical Processes of Explosive Volcanic Eruptions*. Elsevier, Amsterdam*: 173-231.

Freundt, A. and Schmincke, H.-U. (1985). Lithic-enriched segregation bodies in pyroclastic flow deposits of Laacher See Volcano (East Eifel, Germany). *Journal of Volcanology and Geothermal Research* 25: 193-224.

Freundt, A., Wilson, C.J.N. and Carey, S. N. (2000). Ignimbrites and block-and- ash flow deposits, In Sigurdsson, H., Houghton, B. F., McNutt, S.R., Rymer, H. and Stix, J. (eds) Encyclopedia of Volcanoes. *Academic Press, London*: 581-600.

Fritsch, K.V. and Reiss, W. (1868). Geologische Beschreibung der Insel Tenerife: Winterthur. *Verlag von Wurster and Co.*: 494 pp.

Fujii, T. and Nakada, S. (1999). The 15 September 1991 pyroclastic flows at Unzen Volcano (Japan): a flow model for associated ash-cloud surges. *Journal of Volcanology and Geothermal Research* 89: 159-172.

Gauer, P. and Issler, D. (2004). Possible erosion mechanism in snow avalanches. *Annals of Glaciolog*y 38: 384-392.

Garcia, M. and Parker, G. (1993). Experiments on the entrainment of sediment into suspension by a dense bottom current. *Journal of Geophysical Research* 98: 4793-4807.

Giordano, G. and Dobran, F. (1994). Computer simulations of the Tuscolano Artemisio's second pyroclastic flow unit (Alban Hills, Latium, Italy). *Journal of Volcanology and Geothermal Research* 61: 69-94.

Gladstone, C., Ritchie, L.J., Sparks, R.S.J. and Woods, A.W. (2004). An experimental investigation of stratified inertial gravity currents. *Sedimentology* 51: 767-789.

Glangeaud, P. (1907). L'éruption du Vésuve en avril 1906. *Annales de Géographie, Année* 16(88): 289-295.

Gomez, C., Lavigne, F., Lespinasse, L., Hadmoko, D.S. and Wassmer, P. (2008). Longitudinal structure of pyroclastic-flow deposits, revealed by GPR survey, at Merapi Volcano, Java, Indonesia. *Journal of Volcanology and Geothermal Research*, doi:10.1016/j.jvolgeores.2008.04.012.

Gorshkov, G.S. (1959). Gigantic eruption of the volcano Bezymianny. *Bulletin of Volcanology* 20: 77-109.

Grange, L.I. (1929). A classification of soils at Rotorua Country: New Zealand *Journal of Science and Technology* 11: 219-228.

Gravina, T., Lirer, L., Marzocchella, A., Petrosino, P. and Salatino, P. (2004). Fluidization and attrition of pyroclastic granular solids. *Journal of Volcanology and Geothermal Research* 138: 27-42.

Gray, T.E., Alexander, J. and Leeder, M.R. (2005). Quantifying velocity and turbulence structure in depositing sustained turbidity currents across breaks in slope. *Sedimentology* 52: 467-488.

Griggs, R.F. (1922). The Valley of Ten Thousand Smokes. *Washington, National Geographic Society*: 341 pp.

Hákonardóttir, K.M., Hogg, A. and Batey, J. (2003). Flying avalanches. *Geophysical Research Letters* 30(23): 2191, doi:10.1029/2003GL018172.

Hall, B., Meiburg, E. and Kneller, B. (2008). Channel formation by turbidity currents: Navier-Stokes based linear stability analysis. *Journal of Fluid Mechanics* 615: 185-210.

Hallworth, M.A. and Huppert, H.E. (1998). Abrupt transitions in high- concentration, particle-driven gravity currents. *Physics of Fluids* 10: 1083-1087.

Hallworth, M.A., Huppert, H.E., Phillips, J.C. and Sparks, R.S.J. (1996). Entrainment into two-dimensional and axisymmetric turbulent gravity currents. *Journal of Fluid Mechanics* 308: 289-311.

Hampton, M.A. (1972). The role of subaqueous debris flow in generating turbidity currents. *Journal of Sedimentary Petrology* 42: 775-793.

Hay, A.E. (1987). Turbidity currents and submarine channel formation in Rupert inlet, British Columbia: I. Surge observations. *Journal of Geophysical Research* 92: 2875-2881.

Hayashi, J.N. and Self, S. (1992). A comparison of pyroclastic flow and debris avalanche mobility. *Journal of Geophysical Research* B97: 9063-9071.

Hermann, F. and Hutter, K. (1991). Laboratory experiments on the dynamics of powder-snow avalanches in the run-out zone. *Journal of Glaciology* 37(126): 281-295.

Hoblitt, R.P. (1986). Observations of the eruptions of July 22 and August 7, 1980, at Mount St. Helens, Washington. *US Geological Survey, Professional Paper* 1335: 1-44.

Hodgson, K.A. and Nairn, I.A. (2005). The c. AD 1315 syn-eruption and AD 1904 post-eruption breakout floods from Lake Tarawera, Haroharo caldera, North Island, New Zealand. *New Zealand Journal of Geology and Geophysics* 48: 491-506.

Hogg, A.G., Higham, T.F.G., Lowe, D.J., Palmer, J.G., Reimer, P.I. and Newnham, R.F. (2003). A wiggle-match date for Polynesian settlement of New Zealand. *Antiquity* 77: 116-125.

Hooker, M. (1965). The origin of the volcanological concept nuée ardente. *Isis* 56 (4): 401-407.

Hopfinger, E. J. and Tochon-Danguy, J.-C. (1977). A model of powder snow avalanches. *Journal of Glaciology* 19(81): 343-356.

Houghton, B.F. and Wilson, C.J.N. (1986). Explosive rhyolitic volcanism: the case studies of Mayor Island and Taupo volcanoes. In*:* B. F. Houghton and S. D. Weaver (eds): North Island Volcanism. *N.Z. Geological Survey,* Record 12: 33-100.

Howells, M.F., Campbell, S.D.G. and Reedman, A.J. (1985). Isolated pods of subaqueous welded ash-flow tuff: a distal facies of the Capel Curig volcanic formation (Ordovician), North Wales. *Geological Magazine* 122: 175-180.

Hsü, K.J. (1975). Catastrophic debris atreams (Sturzstroms) generated by rockfalls. *Geological Society of America Bulletin* 86(1): 129-140.

Hungr, O. and Evans, S.G. (2004). Entrainment of debris in rock avalanches: an analysis of a long run-out mechanism. *Geological Society of America Bulletin* 116(9/10): 1240-1252.

Hunt, J.C.R. and Snyder, W.H. (1980). Experiments on stably and neutrally stratified flow over a model three-dimensional hill. *Journal of Fluid Mechanics* 96: 671-704.

Huppert, H.E., Turner, J.S., Carey, S.N., Sparks, R.S.J. and Hallworth, M.A. (1986). A laboratory simulation of pyroclastic flows down slopes. *Journal of Volcanology and Geothermal Research* 30: 179-199.

Iddings, J.P. (1909). Igneous rocks, v. 1. *New York, John Wiley and Sons*: 464 pp.

Iverson, R.M. (1997). The physics of debris flows. *Reviews of Geophysics* 35(3): 245-296.

Iverson, M.I. and Denlinger, R.P. (2001). Flow of variably fluidized granular masses across three-dimensional terrain, 1. Coulomb mixture theory. *Journal of Geophysical Research* 106: 537-552.

Jenks, W.F. and Goldich, S.S. (1956). Rhyolitic tuff flows in southern Peru. *Journal of Geology* 64: 156-172.

Johnson, R.W. (1968). Volcanic globule rock from Mount Suswa, Kenya. *Geological Society of America Bulletin* 79: 647-652.

Kassem, A. and Inram, J. (2006). Three-dimensional modeling of density current. II. Flow in sinuous confined and unconfined channels. *Journal of Hydraulic Research* 42(6): 591-602.

Keevil, G.M., Peakall, J. and Best, J.L. (2007). Influence of scale, slope and channel geometry on submarine channel flow dynamics. *Marine and Petroleum Geology:* doi:10.1016/j.marpetgeo.2007.01.009.

Kelfoun, K., Legros, F. and Gourgaud, A., (2000). A statistical study of tree damage by the November 22, 1994 eruption of Merapi volcano (Java, Indonesia): relationships between ash-cloud surges and block-and-ash flows. *Journal of Volcanology and Geothermal Research* 100: 379-393.

Kelfoun, K., Samaniego, P., Palacios, P. and Barba, D. (2009). Testing the suitability of frictional behaviour for pyroclastic flow simulation by comparison with a well-constrained eruption at tungurahua volcano (Ecuador). *Bulletin of Volcanology* 71(9): 1057-1075.

Keller, S. and Issler, D. (1996). Staublawinen über Dämme und Mauern im Labor; Zusammenstellung aller Resultate und Auswertung. *Internal report of the*

Swiss Federal Institute for Snow and Avalanche, Research 697, Davos (Switzerland).

Kieffer, S.W. (1981). Fluid dynamics of the May 18 blast at Mount St. Helens. In: Lipman, P.W., Mullineaux, D.R. (Eds.), The 1980 eruptions of Mount St. Helens, Washington. *U.S. Geological Survey Professional Papers* 1250: 379-400.

Kieffer, S.W. and Sturtevant, B. (1988). Erosional furrows formed during the lateral blast at Mount St. Helens, May 18, 1980. *Journal of Geophysical Research* 93: 14793-14816.

Kneller, B.C. and Buckee, C. (2000). The structure and fluid mechanics of turbidity currents; a review of some recent studies and their geological implications. *Sedimentology* 47: 62-94.

Kneller, B.C. and McCaffrey, W.D. (1999). Depositional effects of flow nonuniformity and stratification within turbidity currents approaching a bounding slope>: deflection, reflection and facies variation. *Journal of Sedimentary Research* 69: 980-991.

Kokelaar, B.P. (1982). Fluidization of wet sediment during the emplacement and cooling of various igneous bodies. *Journal of the Geological Society of London* 139: 21-33.

LaBerge, R., Giodarno, G., Cas, R.A.F. and Ailleres, L. (2006). Syn-depositional substrate deformation produced by the shear force of a pyroclastic density current: An example from the Pleistocene ignimbrite at Monte Cimino, northern Lazio, Italy. *Journal of Volcanology and Geothermal Research* 158: 307-320.

Lacroix, A. (1904). Montagne Pelée et ses eruptions. *Masson et Cie, Paris*: 662 pp.

Lacroix, A. (1930). Remarques sur les matériaux de projection des volcans et sur la genese des roches pyroclastiques qu'ils constituents. *Livre Jubilaire de Centenaire Societé Geologique de France* 2: 431-472.

Lane-Serff, B.L.M. and Hadfield, T.D. (1995). Gravity current over obstacles. *Journal of Fluid Mechanics* 292: 39-53.

Legros, F. (2002). The mobility of long-runout landslides. *Engineering Geology* 63: 301-331.

Legros F. and Kelfoun, K. (2000). On the ability of pyroclastic flows to scale topographic obstacles. *Journal of Volcanology and Geothermal Research* 98: 235-241.

Leonard, G.S. (1999). Magmatic Processes Associated with the V650 BP Kaharoa Eruption, Tarawera Volcanic Complex, New Zealand. *Unpubl. B.Sc. Hons. Project, University of Canterbury, Christchurch*: 157 pp.

Leonard, G.S., Cole, J.W., Nairn, I.A. and Self, S. (2002). Basalt triggering of the AD 1305 Kaharoa rhyolite eruption episode, Tarawera Volcanic Complex, New Zealand. *Journal of Volcanology and Geothermal Research* 115: 461-486.

Levine, A.H. and Kieffer, S.W. (1991). Hydraulics of the August 7, 1980, pyroclastic flow at Mount St. Helens, Washington. *Geology* 19: 1121-1124.

Lide, D.L., Baysinger, G., Berger, L.I., Goldberg, R.N., Kehiaian, H.V., Kuchitsu, K., Lin, C.C., Rosenblatt, G. and Smith, A.L. (2004). (eds.) CRC Handbook of Chemistry and Physics, 84th Edition. Available online (*http://www.hbcpnetbase.com/).*

Lipman, P.W. and Mullineaux, D.R. (1981) (eds). The 1980 Eruptions of Mount St. Helens, Washington. *U.S. Geological Survey Professional Paper 1250*: 872 pp.

Locardi, E. and Mittempergher, M. (1967). On the genesis of ignimbrites: how ignimbrites and other pyroclastic products originate from a flowing melt. *Bulletin of Volcanology* 31: 131-152.

Lorenz, V. (1985). Maars and diatremes of phreatomagmatic origin: a review. *Transactions of the Geological Society of South Afric*a 88: 459-470.

Loughlin, S.C., Calder, E.S., Clarke, A., Cole, P.D., Luckett, R., Mangan, M.T., Pyle, D.M., Sparks, R.S.J., Voight, B. and Watts, R.B. (2002). Pyroclastic flows and surges generated by the 25 June 1997 dome collapse, Soufrière Hills Volcano, Montserrat. In: Druitt, T.H. and Kokelaar, B.P. (Eds.) The Eruption of Soufrière Hills Volcano, Montserrat, from 1995 to 1999. *Geological Society of London Memoirs* 21: 191-210.

Lube, G., Cronin, S.J., Platz, T., Freundt, A., Procter, J.N., Henderson, C. and Sheridan, M.F. (2007). Flow and deposition of pyroclastic granular flows: A type example from the 1975 Ngauruhoe eruption, New Zealand. *Journal of Volcanology and Geothermal Research* 161: 165-186.

Luthi, S. (1981). Experiments on non-channelized turbidity currents. Marine *Geology* 40: M59–M68, doi: 10.1016/0025–3227(81)90139–0.

MacDonald, G.A. (1972). Volcanoes. *Prentice-Hall, Inc., Englewood Cliffs*: 510 pp.

Macgregor, A.G. (1952). Eruptive mechanisms - Mt.Pelée, the Soufrière of St.Vincent (West Indies) and the Valley of Ten Thousand Smokes (Alaska). *Bulletin of Volcanology* 12:49-74.

Macgregor, A.G. (1955). Classification of nuée ardente eruptions. *Bulletin of Volcanology* 16: 7-11.

Macías, J.L., Espíndola, J.M., Bursik, M., and Sheridan, M.F. (1998). Development of lithic-breccias in the 1982 pyroclastic flow deposits of El Chichón Volcano, Mexico. *Journal of Volcanology and Geothermal Research* 83: 173-196.

Major, J.J. and Pierson, T.C. (1992). Debris flow rheology: Experimental analysis of fine-grained slurries. *Water Resources Research* 28: 841-857.

Maleyev, E.F. (1965). Genetic types of clastolavas and their distinction from ignimbrites. *New Zealand Geological Survey Paleontological Bulletin* 65: 719-722.

Malin, M. C. and Sheridan, M. F. (1982). Computer- assisted mapping of pyroclastic surges. *Science* 217: 637-640.

Marr, J.G., Harff, P.A., Shanmugam, G. and Parker, G. (2001). Experiments on subaqueous sandy gravity flows: the role of clay and water content in the flow dynamics and depositional structures. *Geological Society of America Bulletin* 113, 1377-1386.

Marshall, P. (1935). Acid rocks of Taupo-Rotorua volcanic district. *Transactions and Proceedings of the Royal Society of New Zealand* 64(3): 323-366.

Martí, J. and Ernst, G.G.J. (2005). Volcanoes and the environment. *Cambridge University Press*: 471 pp.

Matumoto, T. (1943). The four gigantic caldera volcanoes of Kyusyu. *Japanese Journal of Geology and Geography* 19, Spec.No.: 57 pp.

McCall, G.J.H. (1964). Froth flows in Kenya. *Geologische Rundschau* 54: 1148-1195.

Meiburg, E. and Kneller, B. (2010). Turbidity currents and their deposits. *Annual Review of Fluid Mechanics* 42: 135-56.

Mellors, R.A., Waitt, W.B. and Swanson, D.A. (1988). Generation of pyroclastic flows and surges by hot-rock avalanches from the dome of Mount St. Helens volcano, USA. *Bulletin of Volcanology* 50: 14-25.

Michol, K.A., Russel, J.K. and Andrews, G.D.M. (2008). Welded block and ash flow deposits from Mount Meager, British Columbia, Canada. *Journal of Volcanology and Geothermal Research* 169: 121-144.

Middleton, G.V. (1966*)*. Small-scale models of turbidity currents and the criterion for auto-suspension. *Journal of Sedimentary Petrology* 36: 202-208.

Middleton, G.V. (1993). Sediment deposition from turbidity currents. *Annual Review of Earth and Planetary Sciences* 21: 89-114.

Miyabuchi, Y. (1999). Deposits associated with the 1990-1995 eruption of Unzen volcano, Japan. *Journal of Volcanology and Geothermal Research* 89: 139-158.

Mohrig, D., Whipple, K.X., Midhat, H., Ellis, C. and Parker, G. (1998). Hydroplaning of subaqueous debris flows. *Geological Society of America Bulletin* 110: 387-394.

Moore, B.N. (1934). Deposits of Possible Nuée Ardente Origin in the Crater Lake Region, Oregon. *The Journal of Geology* 42(4): 358-375.

Moore, J.G. (1967). Base surge in recent volcanic eruptions. *Bulletin of Volcanology* 30: 337-363.

Moore, J.G. and Melson, W.G. (1969). Nueés ardentes of the 1968 eruption of Mayon volcano, Philippines. *Bulletin Volcanologique* 33: 600-620.

Morris, S.A. and Alexander, J. (2003). Changes in flow direction at a point caused by obstacles during passage of a density current. *Journal of Sedimentary Research* 73(4): 621-629.

Morrissey, M., Zimanowski, B., Wohletz, K. and Buettner, R. (2000). Phreatomagmatic fragmentation. In: Sigurdsson, H., Houghton, B., McNutt, S.R., Rymer, H. and Stix, J. (eds) *Encyclopedia of Volcanoes. Academic Press*: 431-447.

Muck, M.T. and Underwood, M.B. (1990). Upslope flow of turbidity currents-a comparison among field observations, theory, and laboratory models. *Geology* 18: 54-57.

Murai, I. (1961). A study of the textural characteristics of pyroclastic flow deposits in Japan. *Tokyo University Earthquake Research Institute Bulletin* 39: 133-248.

Naaim, M. and Gurer, I. (1998). Two-phase Numerical Model of Powder Avalanche: Theory and Application. *Natural Hazards* 117**:** 129-145.

Naaim-Bouvet, F., Naaim, M., Bacher, M. and Heiligenstein, L. (2002). Physical modelling of the interaction between powder avalanches and defence structures. *Natural Hazards Earth System Science* 2: 193-202.

Nairn, I.A. (1981). Some studies of the geology, volcanic history, and geothermal resources of the Okataina volcanic centre. *Unpublished PhD thesis, Victoria University of Wellington, New Zealand*.

Nairn, I.A. (1989). Geological Map of New Zealand: Sheet V16AC Tarawera, with notes. *Department of Scientific and Industrial Research, Wellington*.

Nairn, I.A. (1992). The Te Rere and Okareka eruptive episodes — Okataina Volcanic centre, Taupo Volcanic Zone, New Zealand. *New Zealand Journal of Geology and Geophysics* 35: 93-108.

Nairn, I. A. and Self, S. (1978). Explosive eruptions and pyroclastic avalanches from Ngauruhoe in February 1975. *Journal of Volcanology and Geothermal Research* 3: 39-60.

Nairn, I.A., Self, S., Cole, J.W., Leonard G.S. and Scutter, C.R. (2001). Distribution, stratigraphy, and history of proximal deposits from the c. AD1305 Kaharoa eruptive episode at Tarawera volcano, New Zealand. *New Zealand Journal of Geology and Geophysics* 44(3): 467-484.

Nairn, I.A., Shane, P.R., Cole, J.W., Leonard, G.S., Self, S. and Pearson, N. (2004). Rhyolite magma processes of the ~AD 1315 Kaharoa eruption episode, Tarawera volcano, New Zealand. *Journal of Volcanology and Geothermal Research* 131: 265-294.

Nakada, S. and Fujii, T. (1993). Preliminary report on the activity at Unzen Volcano (Japan), November 1990 – November 1991: Dacite lava domes and pyroclastic flows. *Journal of Volcanology and Geothermal Research* 54: 319-333.

Nelson, J.M. and Smith, J.D. (1989). Evolution and stability of erodible channel bends. In: Ikeda, S. and Parker, G. (Eds.), *River Meandering. AGU*: 321–377.

Nemeth, K., Martin, U. and Harangi, S.Z. (2001). Miocene phreatomagmatic volcanism at Tihany (Pannonian Basin, Hungary). *Journal of Volcanology and Geothermal Research* 111: 111-135.

Neri, A., Esposti Ongaro, T., Macedonio, G. and Gidaspow, D. (2003). Multiparticle simulation of collapsing volcanic columns and pyroclastic flow. Journal of Geophysical Research 108(B4): 2202, doi: 10.1029/2001JB000508.

Neumann Van Padang, M. (1933). De uitbarsting van den Merapi (Midden Java) in de jaren 1930-1931. *Ned Indies, Dienst Mijnbouwk. vulkan, seism. Mededel* 12: 1-135.

Nir, A. and Acrivos, A. (1990). Sedimentation and sediment flow on inclined surfaces. *Journal of Fluid Mechanics* 212: 139-153.

Owen, G. (2003). Load structures: gravity-driven sediment mobilization in the shallow subsurface. In: Van Rensbergen, P., Hillis, R.R., Maltman, A.J. and Morley, C.K. (eds) Subsurface Sediment Mobilization. *Geological Society of London Special Publications* 216: 21-35.

Palladino, D.M. and Valentine, G.A. (1995). Coarse-tail vertical and lateral grading in pyroclastic flow deposits of the Latera Volcanic Complex (Vulsini, Central Italy): origin and implications for flow dynamics. *Journal of Volcanology and Geothermal Research* 69: 343-364.

Panto, G. (1962). The role of ignimbrites in the volcanism of Hungary. *Acta Geologica Budapest* 6: 307-331.

Parker, G., Garcia, M., Fukushima, Y. and Yu, W. (1987). Experiments on turbidity currents over an erodible bed. *Journal of Hydraulic Engineering* 52: 123-47.

Peakall, J., McCaffrey, W.D. and Kneller, B.C. (2000). A process model for the evolution, morphology and architecture of sinuous submarine channels. *Journal of Sedimentary Research* 70: 434-448.

Peakall, J., Amos, K.J., Keevil, G.M., Bradbury, P.W. and Gupta, S. (2007). Flow processes and sedimentation in submarine channel bends. *Marine and Petroleum Geology* 24: 470-486.

Perret, F.A. (1937). The eruption of Mt. Pelée 1929-1932. *Carnegie Institute of Washington Publications* 458: 1-126.

Pichór, W. and Janiec, A. (2009). Thermal stability of expanded perlite modified by mullite. *Ceramics International* 35: 527-530.

Pittari, A. and Cas, R.A.F. (2004). Sole Marks at the base of the late Pleistocene Abrigo Ignimbrite, Tenerife: implications for transport and depositional processes at the base of pyroclastic flows. *Bulletin of Volcanology* 66: 356-363.

Piper, D.J.W., and Normark, W.R., 1983. Turbidite depositional patterns and flow characteristics, Navy Submarine Fan, California Borderland. *Sedimentology* 30: 681-694.

Pirmez, C. and Imran, J. (2003). Reconstruction of turbidity currents in Amazon Channel. *Marine and Petroleum Geology* 20: 823-849.

Primus, M., Naaim-Bouvet, F., Naaim, M. and Faug, T. (2004). Physical modeling of the interaction between mounds or deflecting dams and powder snow avalanches. *Cold Regions Science and Technology* 39: 257-267.

Ritchie, L.J., Cole, P.D. and Sparks, R.S J. (2002). Sedimentology of deposits from the pyroclastic density current of 26 December 1997 at Soufriere Hills Volcano, Montserrat. In: Druitt, T.H. and Kokelaar, B.P. (eds) The Eruption of Soufriere Hills Volcano, Montserrat, from 1995 to 1999. *Geological Society of London Memoirs* 21: 435-456

Rittmann, A. (1931). Vulkanische Glutwolken und Glutlawinen. *Naturwissenschaften* 51: 1017-1020.

Rittmann, A. (1944). Vulcani attivita et genesi-Napoli-Editrice Politecnica.

Rose, W.I., Jr., Pearson, T. and Bonis, S. (1977). Nuee ardente eruption from the foot of a dacite lava flow, Santiaguito volcano, Guatemala. *Bulletin of Volcanology* 40: 1-16.

Rottman, J. W., and J. E. Simpson (1983). Gravity currents produced by instantaneous releases of heavy fluid in a rectangular channel. *Journal of Fluid Mechanics* 135: 95-110.

Rottman, J.W., Simpson, J.E. and Hunt, J.C.R. (1985). Unsteady gravity currents flows over obstacles: some observations and analysis related to Phase II trials. *Journal of Hazardous Materials* 11: 325-340.

Sable, J.E., Houghton, B.F., Wilson, C.J.N. and Carey, R.J. (2006). Complex proximal sedimentation from Plinian plumes: the example from Tarawera 1886. *Bulletin of Volcanology* 69: 89-103.

Sahetapy-Engel, S.T., Nairn, I.A. and Self, S. (2000). Kaharoa pyroclastic fall distribution. *IAVCEI General Assembly 2000, Bali, Abstr. Addresses:* 247pp.

Sampl, P., Naaim-Bouvet, F and Naaim, M. (2004). Interaction between dams and powder avalanches: determination of simple friction laws for shallow water avalanches models. *Cold Regions Sciences and Technology* 39: 114-131.

Saucedo, R., Macias, J.L., Bursik, M.I., Mora, J.C., Gavilanes, J.C. and Cortes, A. (2002). Emplacement of pyroclastic flows during the 1998-1999 eruption of Volcán de Colima, Mexico. *Journal of Volcanology and Geothermal Research* 117: 129-153.

Saucedo, R., Macias, J.L. and Bursik, M. (2004). Pyroclastic flow deposits of the 1991 eruption of Volcan de Colima, Mexico. *Bulletin of Volcanology* 66: 291-306.

Saucedo, R., Macias, J.L., Sheridan, M.F., Bursik, M.I. and Komorowski, J.C. (2005). Modeling of pyroclastic flows of Colima Volcano, Mexico: implications for hazard assessment. *Journal of Volcanology and Geothermal Research* 139: 103-115.

Scarth, A. (2002). La Catastrophe: The Eruption of Mount Pelée, the Worst Volcanic Disaster of the 20th Century. *Oxford University Press*: 256 pp.

Schaflinger, U., Acrivos, A. and Zhang, K. (1990). Viscous resuspension of a sediment within a laminar and stratified flow. *International Journal of Multiphase Flow* 16: 567-578.

Schmincke, H.-U. (2003). Vulkanismus. *Springer Verlag, Germany*. 351 pp.

Schneider, J.-L. and Fisher, R.V. (1998). Transport and emplacement mechanisms of large volcanic debris avalanches: evidence from the northwest sector of Cantal Volcano (France). *Journal of Volcanology and Geothermal Research* 83: 141-165.

Scolamacchia, T., Macias, J.L., Sheridan, M.F. and Hughes, S.R. (2005). Morphology of ash aggregates from wet pyroclastic surges of the 1982 eruption of El Chich ´on Volcano, Mexico. *Bulletin of Volcanology* 68: 171-200.

Scott, K.M. (1988). Origins, behavior, and sedimentology of lahars and lahar-runout flows in the Toutle-Cowlitz River system. *U.S. Geological Survey Professional Paper* 1447-A: 76 pp.

Shane, P., Martin, S.B., Smith, V.C., Beggs, K.F., Darragh, M.B., Cole, J.W. and Nairn, I.A. (2007a). Multiple rhyolite magmas and basalt injection in the 17.7 ka Rerewhakaaitu eruption episode from Tarawera volcanic complex, New Zealand. *Journal of Volcanology and Geothermal Research* 164: 1-26.

Shane, P., Nairn, I.A., Smith, V.C., Darragh, M., Beggs, K. and Cole, J.W. (2007b). Silicic recharge of multiple rhyolite magmas by basaltic intrusion during the 22.6 ka Okareka Eruption Episode, New Zealand. *Lithos* doi: 10.1016/j.lithos.2007.11.002.

Sheridan, M.F. (1979). Emplacement of pyroclastic flows: a review. In: Chapin, C. E. and Elston, W. E. (eds) Ash-flow Tuffs. *Geological Society of America Special Paper* 180: 125-136.

Sheridan, M.F. and Malin, M.C. (1983). Application of computer-assisted mapping to volcanic hazard evaluation of surge eruptions: Vulcano, Lipari, and Vesuvius. *Journal of Volcanology and Geothermal Research* 17: 187-202.

Sheridan, M.F. and Wohletz, K.H. (1983). Hydrovolcanism: basic considerations and reviews. *Journal of Volcanology and Geothermal Research* 17(1–4): 1-29.

Sigurdsson, H., Houghton, B., McNutt, S.R., Rymer, H., and Stix, J. (2000). Encyclopedia of volcanoes. *Academic Press*: 1417 pp.

Simpson, J.E. and Britter, R.E. (1979). The dynamics of the head of a gravity current advancing over a horizontal surface. *Journal of Fluid Mechanics* 94: 477-495.

Simpson, J. E. (1997). Gravity Currents in the Environment and the Laboratory. 2nd ed. *Cambridge Univ. Press, New York*: 244 pp.

Sisson, T.W. (1995). Blast ashfall deposit of May 18, 1980 at Mount St Helens, Washington. *Journal of Volcanology and Geothermal Research* 66: 203-216.

Smith, R.L. (1960). Ash flows. *Geological Society of America Bulletin* 71: 795-842.

Smith, A.L. and Robool, M.J. (1982). Andesite pyroclastic flows. In Thorpe, R.S., ed., Andesites. *John Wiley and Sons, New York*: 415-433.

Snyder, W.H., Thompson, R.S., Eskridge, R.E., Lawson, R.E., Castro, I.P., Lee, J.T., Hunt, J.C.R. and Ogawa, Y. (1985). The structure of strongly stratified flow over hills: dividing streamline concept. *Journal of Fluid Mechanics* 152: 249-288.

Sparks, R.S.J. (1976). Grain size variations in ignimbrites and implications for the transport of pyroclastic flows. *Sedimentology* 23: 147-188.

Sparks, R.S.J., Self, S. and Walker, G.P.L. (1973). Products of ignimbrite eruptions. *Geology* 1: 115-118.

Sparks, R.S.J. and Walker, G.P.L. (1973). The ground surge deposit: a third type of pyroclastic rock. *Nature* 241: 62-64.

Sparks, R.S.J. and Wilson, L. (1976). A model for the formation of ignimbrite by gravitational column collapse. Geological Society of London 132: 441-451.

Sparks. R.S.J., Wilson, L. and Hulme, G. (1978). Theoretical modeling of the generation, movement and emplacement of pyroclastic flows by column collapse. *Journal of Geophysical Research* 83: 1727-1739.

Sparks, R.S.J., Francis, P.W., Hamer, R.D., Pankhurst, R.J., O'Callaghan, L.O., Thorpe, R.S. and Page, R. (1985). Ignimbrites of the Cerro Galan Caldera, NW Argentina. *Journal of Volcanology and Geothermal Research* 24: 205-248.

Sparks, R.S.J., Bursik, M.I., Carey, S.N., Gilbert, J.S., Glaze, L., Sigurdsson, H. and Woods, A.W. (1997a). Volcanic plumes. *John Wiley, Chichester*: 590 pp.

Sparks, R.S.J., Gardeweg, M.C., Calder, E.S. and Matthews, S.J. (1997b). Erosion by pyroclastic flows on Lascar volcano, Chile. *Bulletin of Volcanology* 58(7): 557-565.

Speed, J., Shane, P. and Nairn, I.A. (2002). Volcanic stratigraphy and phase chemistry of the 11,900 yr BP Waiohau eruptive episode, Tarawera Volcanic Complex, New Zealand. *New Zealand Journal of Geology and Geophysics* 45: 395-410.

Stinton, A. (2007). Effects of valley geomorphology on the behavior of volcanic mass- flows. *Ph.D. Thesis, State University of New York at Buffalo, Buffalo, United States.*

Stinton, A.J. and Sheridan, M.F. (2008). Implications of long-term changes in valley geomorphology on the behavior of small-volume pyroclastic flows. *Journal of Volcanology and Geothermal Research* 176: 134-140.

Stix, J. (2001). Flow evolution of experimental gravity currents: Implications for pyroclastic flows at volcanoes. *The Journal of Geology* 109: 381-398.

Straub, K.M. (2007). Quantifying turbidity current interactions with topography. Unpublished PhD thesis. Department of Earth, Atmospheric and Planetary Science. *The Pennsylvannia State University*: 205 pp.

Sulpizio, R., De Rosa, R. and Donato, P. (2008). The influence of variable topography on the depositional behaviour of pyroclastic density currents: The examples of the Upper Pollara eruption (Salina Island, southern Italy). *Journal of Volcanology and Geothermal Research* 175: 367-385.

Suzuki-Kamata, K. and Ui, T. (1982). Grain orientation and depositional ramps as flow direction indicators of a large scale pyroclastic flow deposit in Japan. *Geology* 10: 429-432.

Takahashi, T. (2001). Mechanics and simulation of snow avalanches, pyroclastic flows and debris flows. In McCaffrey, W.D., Kneller, B.C. and Peakall, J. (eds) Particulate Gravity Currents. *International Association of Sedimentologists, Special Publication* 31: 11-43.

Takahashi, T. and Tsujimoto, H. (2000). A mechanical model for Merapi-type pyroclastic flow*. Journal of Volcanology and Geothermal Research* 98: 91-115.

Taneda, S. (1954). Geological and petrological studies on the "Shirasu" in south Kyushu, Japan, Part I, Preliminary note. *Kyushu Univ. Fac. Sci. Mem., ser. D, Geology* 4(2): 167-177.

Tanguy, J.-C., Ribière, Ch., Scarth, A. and Tjetjep, W.S. (1998). Victims from volcanic eruptions: a revised database. *Bulletin of Volcanology* 60: 137-144.

Taylor, G.A. (1958). The 1951 eruption of Mount Lamington, Papua. *Australian Bureau of Mineral Resources, Geology and Geophysics Bulletin* 38: 117 pp.

Thornburg, T.M., Kulm, L.D. and Hussong, D.M. (1990). Submarine-fan development in the southern Chile Trench: a dynamic interplay of tectonics and sedimentation. *Geological Society of America Bulletin* 102: 1658-1680.

Tilling, R. (2005). Volcanic hazards. In Marti, J. and Ernst, G.G.J. (eds). Volcanoes and the environment. *Cambridge University Press*: 55-89.

Torres, R. C., Self, S. and Martinez, M. L. (1996). Secondary pyroclastic flows from the June 15, 1991, ignimbrite of Mount Pinatubo. *In:* Newhall, C. G. and Punongbayan, S. (eds) *Fire and Mud: Eruptions of Mount Pinatubo, Philippines.* Philippine Institute of Volcanology and Seismology, Quezon City, University of Washington Press, Seattle: 665-678.

Ui, T., Matsuwo, N., Sumita, M. and Fujinawa, A. (1999). Generation of block and ash flows during the 1990-1995 eruption of Unzen volcano, Japan. *Journal of Volcanology and Geothermal Research* 89: 123-137.

Valentine, G.A. (1987). Stratified flow in pyroclastic surges. *Bulletin of Volcanology* 49: 616-630.

Valentine, G.A., Wohletz, K. and Kieffer, S.W. (1991). Sources of unsteady column dynamics in pyroclastic flow eruptions. *Journal of Geophysical Research* 96: 21887-21892.

Vallance, J.W. (2000). Lahars. In Sigurdsson, H., Houghton, B.F., McNutt, S.R., Rymer, H. and Stix, J. (eds) *Encyclopedia of Volcanoes, Academic Press*: 601-616.

Vallance, J.W., Siebert, L., Rose Jr, W.I., Girón, J.R. and Banks, N.G. (1995). Edifice collapse and related hazards in Guatemala. *Journal of Volcanology and Geothermal Research* 66(1-4): 337-355.

Van Bemmelen, R.W. (1949). The geology of Indonesia. *General Geology. Govt. Printing Office, The Hague* 1A: 1-732.

Van Loon, A.J. and Brodzikowski, K. (1987). Problems and progress in the research on soft-sediment deformations. *Sedimentary Geology* 50: 167-193.

Voight, B., Constantine, E.K., Siswowidjoyo, S. and Torley, R. (2000). Historical eruptions of Merapi Volcano, Central Java, Indonesia, 1768–1998. *Journal of Volcanology and Geothermal Research* 100: 69-138.

Vrolijk, P.J. and Southard, J.B. (1998). Experiments on rapid deposition of sand from high-velocity flows. *Geoscience Canada* 24: 45-54.

Walker, G.P.L., 1972. Crystal concentration in ignimbrites. *Contributions to Mineralogy and Petrology* 36: 135-146.

Walker, G.P.L., Self, S. and Wilson, L. (1984). Tarawera 1886, New Zealand: a basaltic plinian fissure eruption. *Journal of Volcanology and Geothermal Research* 21: 61-78

Weyl, R. (1954). Beiträge zur Geologie El Salvadors, V. Die Schmelztuffe der Balsamkette. *Neues Jahrbuch für Geologie und Paläontologie - Abhandlungen* 99(1): 1-32.

Williams, H. (1957). Glowing avalanche deposits of the Sudbury Basin. *Rept. Ontario Dept. Mines* 65: 57-89.

Williams, H. and McBirney, A.R. (1979). Volcanology. *Freeman, Cooper and Co, San Francisco*: 1-397.

Wilson, C.J.N. (1985). The Taupo eruption, New-Zealand: II. The Taupo ignimbrite. *Philosophical Transactions of the Royal Society of London Series A* 314: 229-310.

Wilson, C.J.N. and Walker G.P.L. (1985). The Taupo eruption, New Zealand. General aspects. *Philosophical Transactions of the Royal Society of London A* 314: 199-228.

Wohletz, K.H. (1998). Pyroclastic surges and compressible two-phase flow. In: Freundt, A. and Rosi, M. (eds.) From Magma to Tephra*: Modelling Physical Processes of Explosive Volcanic Eruptions. Elsevier, Amsterdam*: 47-312.

Wohletz, K.H. (2001). Pyroclastic surges and compressible two-phase flow. In: Freundt A and Rosi M. (eds) From magma to tephra: modeling physical processes of explosive volcanic eruptions. *Elsevier, Amsterdam*: 247-312.

Woods, A.W. and Bursik, M.I. (1994). A laboratory study of ash flows. *Journal of Geophysical Research* 99: 4375-4394.

Woods, A.W., Bursik, M.I. and Kurbatov, A.V. (1998). The interaction of ash flows with ridges. *Bulletin of Volcanology* 60: 38-51.

Wright, J.V., Smith, A.L. and Self, S. (1980). A working terminology of pyroclastic deposits. *Journal of Volcanology and Geothermal Research* 8: 315-336.

Wynn, R.B., Weaver, P.P.E., Masson, D.G. and Stowe, D.A.V. (2002). Turbidite depositional architecture across three inter-connected deep-water basins on the Northwest African Margin. *Sedimentology* 49: 669-695.

Yamamoto, T., Takarada, S. and Suto, S. (1993). Pyroclastic flows from the 1991 eruption of Unzen Volcano, Japan. *Bulletin of Volcanology* 55: 166-175.

Yamasaki, N. (1911). The condition of the eruption of Mt.Asama in 1783. *Report Earthquake Inv. Comm.* 73: 20-28 (in Japanese).

Yarnold, J.C. and Lombard, J.P. (1989). Facies model for large rock avalanche deposits formed in dry climates. In: Colburn, I. P., Abbott P. L. and Minch J. (eds) Field Trip Guidebook - Pacific Section, *Society of Economic Paleontologists and Mineralogists* 62: 9-31.

Internet pages

"The Destruction of Pompeii, 79 AD," EyeWitness to History
http://www.eyewitnesstohistory.com/pompeii.htm

Figure 1.2: http://www.mount-pelee.com/en/the-pioneers/ 2001-2009.

List of Appendices

Appendix A -1

- **Grain size distribution of block-and-ash flow deposits at Tarawera Volcano, corresponding to Graphs presented in Chapter 3**
- **Grain size distribution of detached ash cloud surge layer, discussed in Chapter 4**

Appendix A-2

- **Tarawera Volcano - Sample location map, including selected location pictures**

Appendix A-3

- **Formulas used for calculating flow parameters for analogue experiments**

Appendix A-4

- **Pictures taken by High-Speed video camera for each test run presented in Chapter 5 (Folder Appendix A-4)**
- **Quick-time movies of each of the test runs presented in Chapter 5 (Folder Appendix A-4)**

Appendix A-5

- **List of all conducted analogue experiments with setting descriptions**